Harnessing additional metabolic energy during fermentation processes: will the proton-motive force be with you?

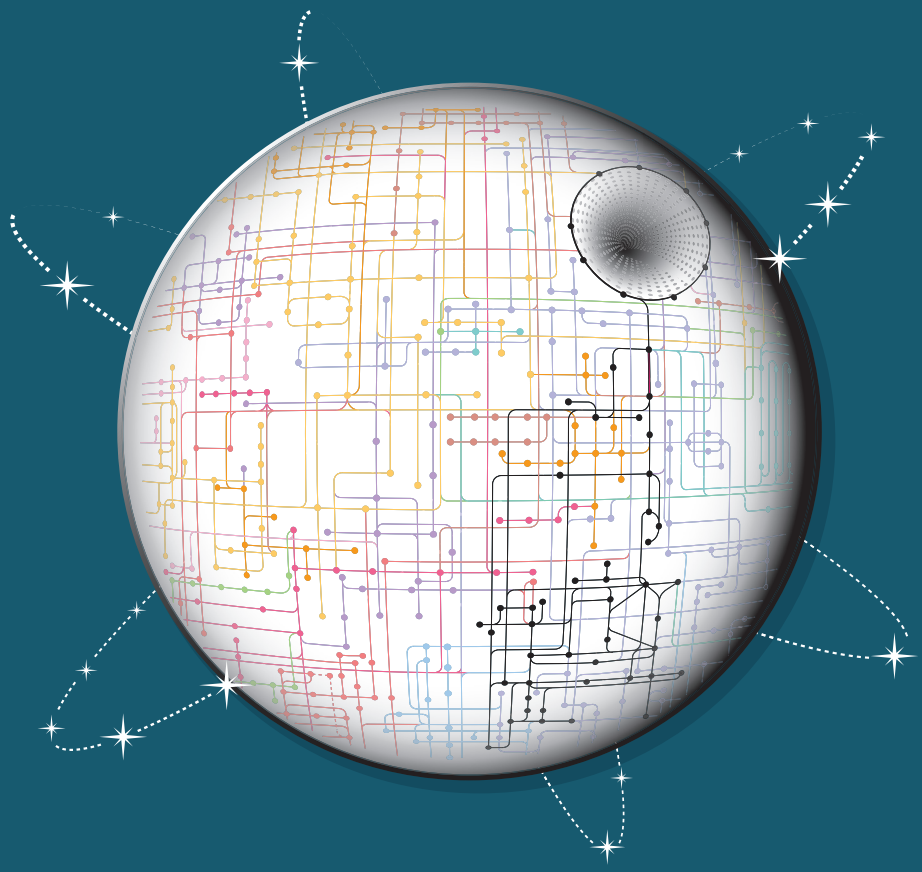

Pauline L. Folch

Propositions

1. Non-canonical redox cofactors are the step forward in designing the next microbial cell factories.
   (this thesis)

2. Fermentative production of low-cost chemicals by energetically efficient microbial cell factories can compete with petrochemical-based processes.
   (this thesis)

3. In science, expectations lead to biased results.

4. Reducing the level of complexity of an intricate idea is harder than making a simple concept complex.

5. Besides anticipated advantages, social media have a negative impact on the emotional health and well-being of its users.

6. An opinion should not be accepted as an alternative truth.

Propositions belonging to the thesis, entitled

Harnessing additional metabolic energy during fermentation processes: will the proton-motive force be with you?

Pauline L. Folch

Wageningen, 09 April 2021

Harnessing additional metabolic energy during fermentation processes:

will the proton-motive force be with you?

Pauline L. Folch

Thesis committee

Promotors

Prof. Dr Ruud A. Weusthuis

Personal chair at the Bioprocess Engineering Group

Wageningen University & Research

Prof. Dr Gerrit Eggink

Special professor, Industrial Biotechnology

Wageningen University & Research

Other members

Prof. Dr Richard van Kranenburg, Wageningen University & Research

Prof. Dr Pascale Daran-Lapujade, TU Delft

Prof. Dr Ir Henk Noorman, TU Delft and DSM, Delft

Dr Maria Suarez-Diez, Wageningen University & Research

This research was conducted under the auspices of Graduate School VLAG (Advanced studies in Food Technology, Agrobiotechnology, Nutrition and Health Sciences).

Harnessing additional metabolic energy during fermentation processes: will the proton-motive force be with you?

Pauline L. Folch

Thesis

submitted in fulfilment of the requirements for the degree of doctor

at Wageningen University

by the authority of the Rector Magnificus,

Prof. Dr A.P.J. Mol,

in the presence of the

Thesis Committee appointed by the Academic Board

to be defended in public

on Friday 9 April

at 1.30 p.m. in the Aula.

Pauline L. Folch

Harnessing additional metabolic energy during fermentation processes: will the proton-motive force be with you?

302 pages.

PhD thesis, Wageningen University, Wageningen, The Netherlands (2021)

With references, with summary in English

ISBN: 978-94-6395-665-9

DOI: https://doi.org/10.18174/537859

Table of contents

Chapter 1

General introduction and thesis outlines

1.1. Microbial bioconversion

Microbial bioconversion is an ancient technique that has gained interest in the last decades as alternative to petrochemical-based processes. These microbial processes are now used for the production of a wide range of compounds including bulk chemicals, food ingredients and pharmaceutical compounds (Hermann, 2003; Song and Lee, 2006; Papagianni, 2007; Lee *et al.*, 2011; Huang *et al.*, 2012; Zhao *et al.*, 2013b; Weusthuis *et al.*, 2017).

Microbial cell factories can realize complex sets of reactions with high selectivity and high catalytic efficiency under relatively mild conditions. The availability of whole-genome sequencing and omics techniques has increased in the last decades allowing a deeper understanding of microbial metabolism and providing new targets for metabolic engineering (Hermann, 2003; Pel *et al.*, 2007). *Escherichia coli* is the most studied bacterium and is applied for the production of many compounds like succinate, 1,4-butanediol, 2-fucosyl lactose, enzymes, etc (Sahdev *et al.*, 2008; Yim *et al.*, 2011; Huang *et al.*, 2012; Lee *et al.*, 2012; Thakker *et al.*, 2012; Du *et al.*, 2019). It was one of the first microorganisms to have its genome fully sequenced. Consequently, it was used as model organism for genetic tool development. The emergence of synthetic biology and new genome-editing techniques such as CRISPR-Cas9 (Jiang *et al.*, 2015; Mans *et al.*, 2015) have contributed to the fast development of new microbial cell factories through metabolic engineering and broaden the range of products that can be formed (Lee *et al.*, 2008; Keasling, 2010; Yim *et al.*, 2011; Li *et al.*, 2015; Pérez-García and Wendisch, 2018; Wang *et al.*, 2018).

1.2. Yield

Microbial production of low-cost chemicals such as biofuels and bulk chemicals requires a high titer, rate and especially yield (TRY) to be able to compete with petrochemical-based processes.

The maximum theoretical yield of product formation (Y^E) represents the maximum amount of product that can be formed from a specific substrate. This Y^E can be determined based on the ratio of the degree of reduction of substrate and product (Cueto-Rojas *et al.*, 2015; Vuoristo *et al.*, 2016). The degree of reduction (γ) corresponds to the number of electrons in a molecule available for chemical reactions. For instance, Y^E of ethanol from glucose is 24/12 = 2 mol/mol as $\gamma_{ethanol}$ is 12 and $\gamma_{glucose}$ is 24.

Substrate is converted into a product by a combination of metabolic pathways or a metabolic network. The pathway yield (Y^P) depends on the metabolic reactions involved and how cofactors are regenerated. To reach Y^P equals Y^E, the metabolic pathway(s) involved in product formation should be redox-balanced to ensure that all electrons present in the substrate end up in the product (Weusthuis *et al.*, 2011).

The conversion of sugars into bulk chemicals and fuels often have a negative Gibbs free energy change (ΔG'). Ideally, the metabolic network used should not dissipate all this energy but should conserve a part of it in a metabolically available form which can be used to sustain growth and maintenance. In this way the use of auxiliary energy-producing pathways, that require additional substrate input and as such lower the yield, can be avoided.

In the past, before genome-editing techniques became available, industrial microbial biotechnology often depended on native pathways in microorganisms with an innate ability to produce the desired compounds. In some cases – the production of e.g. ethanol and lactic acid – the pathways were redox-balanced and conserved energy, resulting in high yields. This type of metabolism is called fermentation. More often however, these pathways were not redox-balanced and/or did not conserve metabolic energy, e.g. for the production of citrate, fumarate, L-glutamate and L-lysine. In those cases, aerobic respiration was used to fulfil the energetic requirements of the cells and to balance the cofactors involved in product formation. Nevertheless, aerobic processes achieve lower productivities than anaerobic fermentations due to the limiting oxygen transfer

rate in the reactors (Garcia-Ochoa and Gomez, 2009). These processes generate a large amount of heat and therefore require high cooling capacity which makes them more cost-intensive than anaerobic fermentations. Electrons are transferred from substrate to oxygen, allowing the full oxidation of substrate to CO_2, resulting in decreased yields. This allows the synthesis of ATP, which is used for biomass formation also called assimilation. Both phenomena – full oxidation of substrate and biomass formation – reduce the availability of substrate for product formation and thereby decrease the overall product yield. Respiration should therefore be prevented, and fermentation processes are the preferred option to reach high yield and productivity for the microbial production of chemicals (Weusthuis *et al.*, 2011).

1.3. Energy conservation

During fermentations, the conversion of substrates into products has a negative Gibbs free energy ΔG_0' by definition. The energy available is for a small part used to generate metabolic energy and largely dissipated to avoid chemical equilibrium ((Cueto-Rojas *et al.*, 2015), **Table 1**).

Increasing the amount of metabolic energy conserved would – in principle – allow microorganisms to reach a higher biomass yield and grow under conditions leading to high maintenance requirement. Increasing energy efficiency is also beneficial for product formation. Three situations can be considered (**Figure 1**): 1) processes with a positive ΔG_0', requiring the input of metabolic energy, 2) processes with a negative ΔG_0', where the energy is partly used to synthetize ATP for maintenance and growth and in which the rest is dissipated to avoid chemical equilibrium and 3) processes with a negative ΔG_0', where the metabolic energy is dissipated and not harvested (metabolic energy-neutral processes).

Table 1. Energy fate in redox-neutral microbial bioconversions. The Gibbs free energy ΔG_m' values were calculated with eQuilibrator 2.2 using 1 mM concentrations for the species involved. The compounds were taken as aqueous for the calculations (Flamholz *et al.*, 2012; Noor *et al.*, 2012; Noor *et al.*, 2013; Noor *et al.*, 2014). EMP: Embden-Meyerhof-Parnas pathway, ED: Entner-Doudoroff pathway, PDC: pyruvate decarboxylase, ADH: alcohol dehydrogenase, PEP carboxylase: phosphoenolpyruvate carboxylase, OGOR: 2-oxoglutarate: ferredoxin oxidoreductase.

Conversion	Pathway	ΔG_m' dissipated (kJ/mol glucose)	ΔG_m' conserved (kJ/mol glucose)
Glucose = 2 Ethanol + 2 CO_2	EMP, PDC, ADH[1]	-178	87
	ED, PDC, ADH[2]	-222	44
Glucose + 2 CO_2 = 2 Fumarate + 2 H_2O	EMP, PEP carboxylase, reductive TCA branch	-136	0
Glucose + 2 CO_2 = 4/3 Citrate + 2/3 H_2O	EMP, reductive and oxidative TCA branches including OGOR	-163	0

1. As occurs in *S. cerevisiae*
2. As occurs in *Z. mobilis*

In the first case, substrate is burnt to generate the energy required for product formation. Examples of such a situation are the synthesis of proteins and vitamins. Increasing the energetic efficiency would therefore allow the microorganisms to synthetize higher amounts of these compounds. In the second situation, a higher energetic efficiency could be advantageous when microorganisms are exposed to conditions leading to high maintenance requirements such as high cell density cultivations and high product titers. In the third case, the harvest of additional metabolic energy during product formation would be beneficial since it will lower the fraction of substrate converted by other processes such as respiration to fulfil the energetic requirement of the cells for maintenance and growth.

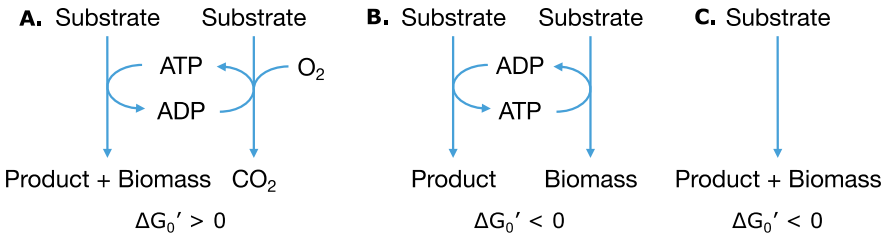

Figure 1. Three situations for microbial product formation. (A) Energy-requiring pathway for product formation. **(B)** Pathway for product formation with a negative ΔG_0' where the metabolic energy generated is used for cell growth and maintenance. **(C)** Product pathway with a negative ΔG_0' where energy is dissipated.

1.3.1. Conservation of metabolic energy for fermentative product formation

Harvesting additional metabolic energy is therefore a promising strategy to increase product formation and product yield. However, the energetic efficiency of a microbial conversion varies with the metabolic pathways used. Therefore, the following challenge arises: how can we harvest the Gibbs free energy in the form of metabolic energy (ATP)?

This requires a thorough understanding of the mechanisms used by microorganisms to conserve energy. Ideally, we aim at using a generally applicable mechanism to harvest the Gibbs free energy and not a product-specific process so that it can be applied to a wide range of products.

In **Chapter 2**, we provide an overview of the different mechanisms available in microorganisms to harvest the Gibbs free energy as metabolic energy during fermentative product formation from glucose. A brief description of the glycolytic and fermentative pathways that bacteria can employ is given with respects to ATP synthesis and cofactor regeneration. The main energy-generating mechanisms – substrate-level phosphorylation and generation of an ion-motive force – are described, as well as energy-conserving systems. The suitability and application of these mechanisms for the microbial production of chemicals are discussed.

Microorganisms can generate metabolic energy via two different mechanisms depending on the energy available in a reaction: direct ATP synthesis via substrate-level phosphorylation or generation of an ion-motive force (Decker *et al.*, 1970). During microbial fermentation processes all reactions involved in the conversion of substrate into product contribute to the overall Gibbs free energy. However, only a few reactions have a sufficient low Gibbs free energy to harvest it as metabolic energy. Direct ATP synthesis requires ΔG' around 40 kJ/mol and generation of an ion-motive force around 20-30 kJ/mol (100-150 mV).

Substrate-level phosphorylation (SLP) allows direct ATP synthesis by coupling a chemical reaction to the phosphorylation of ADP. This mechanism requires the reaction to have a Gibbs free energy ΔG' equal or lower than the energy necessary to form a molecule of ATP (-44 ± 1 kJ/mol, value for ATP synthesis from ADP and Pi). An example of such reaction is the conversion of acetyl-phosphate and ADP to acetate and ATP by the acetate kinase.

Although some reactions contributing to SLP can be a generally applicable mechanism e.g. the reaction catalyzed by glyceraldehyde-3-phosphate dehydrogenase (GAPDH), most of them are specific to certain pathways or products. Consequently, other methods that can be applied to a wider range of products should be considered.

1.3.2. Redox cofactors: NADH and NADPH

The use of the energy difference of redox cofactor couples is a promising option as they are widely used across the different metabolic networks. For instance, some acetogenic bacteria conserve metabolic energy using the Rnf complex. This membrane-bound enzyme couples the oxidation of reduced ferredoxin to the reduction of NAD^+ and uses the difference in redox potential of the two redox couples to create an ion gradient across the membrane (Herrmann *et al.*, 2008). This transmembrane ion gradient is then used by an ATP synthase to phosphorylate ADP.

Cofactors such as NAD^+ and $NADP^+$ have a central role in microbial metabolism where they act as electron carriers. Therefore, they are generally applicable options to harvest metabolic energy. Both cofactors fulfil very distinct functions in the cells and are involved in different sets of reactions albeit their chemical structures only differ from a phosphate group. NAD^+ is essentially used in oxidation reactions and is regenerated via fermentation or respiration. While NAD^+ is used for both anabolic and catabolic processes, NADPH is primarily involved in anabolic reactions for reduction reactions. NADPH is regenerated in the oxidative part of the pentose phosphate pathway (PPPox) and in the TCA cycle by the isocitrate dehydrogenase.

Although NAD^+/NADH and $NADP^+$/NADPH have identical standard redox potentials (E_0' = -320 mV), their actual redox potential in the cells varies substantially due to their distinct functions. NAD^+/NADH is maintained in an oxidized state while $NADP^+$/NADPH is in a reduced state (Harold, 1986; Spaans *et al.*, 2015; Weusthuis *et al.*, 2020). The values of these ratios vary greatly between organisms and growth conditions (Andersen and von Meyenburg, 1977; Thauer *et al.*, 1977; Bennett *et al.*, 2009; Amador-Noguez *et al.*, 2011). For instance, NAD^+/NADH values range from 3.74 to 1820 while $NADP^+$/NADPH values range from 0.017 to 0.95 (Spaans *et al.*, 2015). Considering the extreme ratios of both cofactors, the difference in redox potential corresponds to a $\Delta G'$ of –30 ± 1 kJ/mol. The Gibbs free energy is sufficient to capture energy in the metabolic pathways in the form of an ion-motive force.

1.4. Aim

The aim of this thesis is to develop an *Escherichia coli* strain with increased energetic efficiency during fermentative growth on glucose.

1.5. Strategy

Substrates used in microbial fermentations mostly utilize the metabolic pathways of the central carbon metabolism. Consequently, we will focus on these pathways to harvest additional metabolic energy.

The conversion of glucose into ethanol and CO_2 has a Gibbs free energy $\Delta G_m'$ of -265 ± 13 kJ/mol. Part of the energy available in this conversion is harvested in the reaction catalyzed by the glyceraldehyde-3-phosphate dehydrogenase (GAPDH), which allows the formation of 2 ATP per glucose by the phosphoglycerate kinase. The rest of the energy available (-178 ± 13 kJ/mol, **Table 1**) is dissipated. To harvest additional metabolic energy, we first need to identify reactions involved in the pathway that exhibit a sufficient low Gibbs free energy.

In **Chapter 2**, the conversion of pyruvate into acetyl-CoA catalyzed by the pyruvate dehydrogenase (PDH) complex was found to be a good candidate to capture metabolic energy as it presents a very negative $\Delta G_m'$ of -40 ± 3 kJ/mol. This reaction is part of the central metabolism of *E. coli* and acetyl-CoA is a precursor of numerous metabolites in the cells. So, coupling this reaction to energy conservation would benefit a wide range of products. The ΔG of this reaction is however insufficient to directly generate ATP via SLP and no ADP-dependent enzyme was reported in literature to catalyze this reaction. Energy should therefore be harvested in the form of an ion-motive force (IMF).

As such the natural PDH complex of *E. coli* cannot be used to generate an IMF. Several steps are therefore required to achieve a strategy in which the energy present in the reaction catalyzed by PDH is converted to metabolic energy. Here, we propose to change the cofactor dependency of PDH from NAD^+ to $NADP^+$ in *E. coli*. A high flux through the $NADP^+$-dependent PDH could potentially increase further the difference in redox potential between NAD^+/NADH and $NADP^+$/NADPH in the cells as it would increase the NADPH/$NADP^+$ ratio and decrease the NADH/NAD^+ ratio. If electrons are transferred from the relatively low redox potential of $NADP^+$/NADPH to the

relatively high redox potential of NAD^+/NADH, and the difference between their redox potentials is lower than the 100-150 mV of the membrane potential, the released energy could be harvested as an IMF. In this scenario, metabolic energy would be conserved by forcing NADPH reoxidation through the membrane-bound transhydrogenase PntAB. This enzyme couples the conversion of $NADP^+$ and NADH into NADPH and NAD^+ to an inward proton-motive force under physiological conditions. The reverse action of this enzyme would allow NADPH reoxidation as well as an outward proton translocation, which could be, in turn, used by the ATP synthase for ATP synthesis. The proposed strategy is described in **Figure 2**.

First, the cofactor dependency of the PDH complex must be changed from NAD^+ to $NADP^+$ as described in **Chapter 3**. The multienzyme PDH complex is encoded by three genes: *aceE*, *aceF* and *lpd* (Guest *et al.*, 1989). The single copy *lpd* gene encodes the dihydrolipoyl dehydrogenase (LPD) where the NAD^+ and NADH binding sites are located. Bocanegra *et al.* (1993) reported the change of cofactor specificity of the PDH complex from NAD^+ to $NADP^+$ by introducing seven amino acid mutations in the *lpd* gene.

Aerobically, PDH is a key enzyme in the central carbon metabolism of *E. coli* however it exhibits limited or no activity anaerobically due to NADH inhibition (Schmincke-Ott and Bisswanger, 1981; Wilkinson and Williams, 1981; Sahlman and Williams, 1989). Introduction of an amino acid mutation in *lpd* was shown to reduce NADH inhibition and allowed anaerobic activity of the complex (Kim *et al.*, 2008). As we aim at expressing the $NADP^+$-dependent PDH complex anaerobically, mutations will be introduced in the *lpd* gene to lower its sensitivity towards NADH. Characterization of the different $NADP^+$-dependent PDH complexes will be realized by enzymatic assays – including inhibition assays – as well as by performing aerobic and anaerobic fermentations.

During anaerobic growth of *E. coli*, pyruvate formate-lyase (PFL) takes over the role of PDH and catalyzes the conversion of pyruvate to acetyl-CoA, coproducing formate (Knappe *et al.*, 1974; Clark, 1989; Knappe and Sawers,

1990). The gene encoding PFL (*pflB*) must be knocked out to ensure that PDH is the only enzyme responsible for the reaction. In **Chapter 4**, the impact of an $NADP^+$-dependent PDH complex on the anaerobic metabolism of *E. coli* is investigated by disrupting the *pflB* gene encoding PFL. Growth and product formation are investigated under both aerobic and anaerobic conditions. In addition, a genome-scale metabolic model is used to predict the behavior of the mutant strains and to compare the results to the fermentation data.

To achieve the desired scenario, the excess NADPH – produced during the reaction catalyzed by the $NADP^+$-dependent PDH complex – must be converted into a proton gradient via the sole action of the membrane-bound transhydrogenase PntAB. *E. coli* is one of the few microorganisms to possess two transhydrogenases: an energy-independent soluble transhydrogenase (STH) and a membrane-bound, proton-translocating transhydrogenase (PntAB) (Clarke and Bragg, 1985a; Clarke *et al.*, 1986; Boonstra *et al.*, 1999). STH is known to convert NADPH and NAD^+ into $NADP^+$ and NADH during growth of *E. coli* on glucose (Sauer *et al.*, 2004) and therefore must be knocked out to force NADPH reoxidation through PntAB. In **Chapter 5**, we describe the behavior of an *E. coli* strain lacking both *pflB* and *sthA* genes and carrying an $NADP^+$-dependent PDH complex under aerobic and anaerobic conditions. Under fermentative conditions, *E. coli* can convert glucose to lactate by the action of the lactate dehydrogenase (LDH) as its formation allows regeneration of the cofactors consumed in glycolysis. Lactate formation would therefore circumvent flux through the $NADP^+$-PDH. In this chapter, another strain will be created carrying the additional *ldhA* knock-out to force the carbon flux through the PDH complex. Growth and metabolites profile of the resulting *E. coli* Δ*lpd* Δ*pflB* Δ*sthA* Δ*ldhA* strain exhibiting an $NADP^+$-dependent DH will be characterized under aerobic, anaerobic and oxygen-limited conditions. The data will be compared to the predictions of a genome-scale metabolic model for all strains.

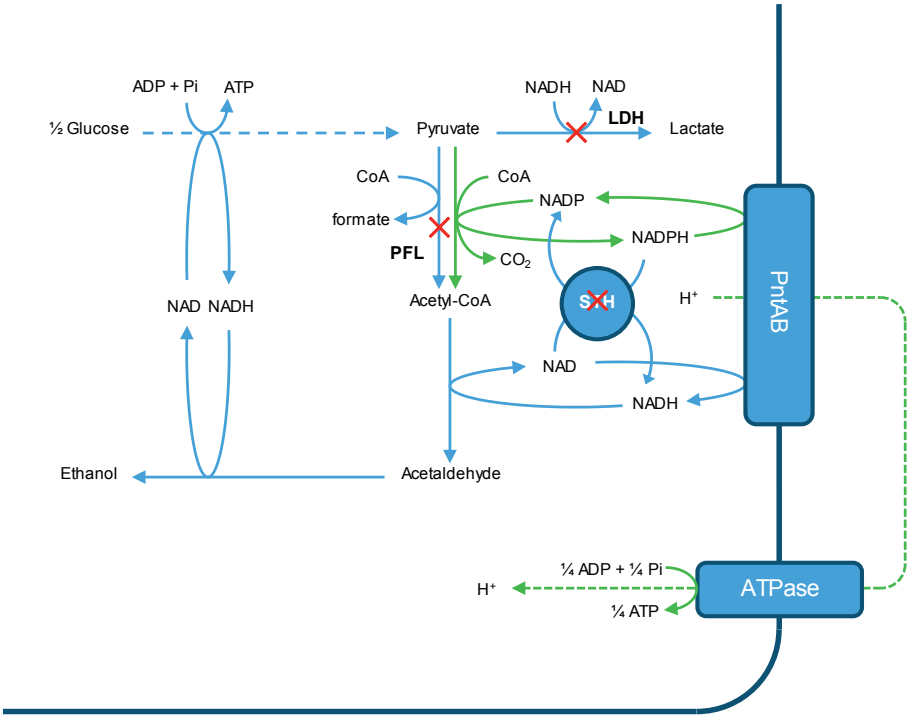

Figure 2. Proposed strategy for the generation of metabolic energy by forcing NADPH reoxidation through the membrane-bound transhydrogenase PntAB in *E. coli*. Here, the cofactor dependency of PDH (green) is modified to function with $NADP^+$. NADPH produced during this reaction is reoxidized through PntAB, which translocates one proton per NADPH reoxidized. The electrochemical proton gradient can in turn be used by the ATP synthase to drive ATP synthesis (green dotted line). Competing enzymes e.g. pyruvate formate-lyase (PFL), soluble transhydrogenase (STH) and lactate dehydrogenase (LDH) must be knocked out (red cross) to realize this scenario. The light blue dashed lines represent reactions sequence.

The strategy described in this thesis would theoretically allow the conservation of an additional 0.5 mol ATP per mol glucose. In *E. coli*, ethanol formation from glucose leads to the production of 2 moles of ATP per mole of glucose. Implementation of this strategy would increase the ATP yield – and analogously the biomass yield – by 25% under anaerobic conditions. Under aerobic conditions this improvement is relatively smaller as respiration generates 36-38 moles ATP per mole glucose.

1.6. Non-canonical redox cofactors

Successful implementation of this strategy would allow the capture of metabolic energy in the central carbon metabolism and could be used for the production of acetyl-CoA-based products. However, this approach relies on the use of redox cofactors – NAD(H) and NADP(H). These cofactors do not only transfer electron from substrate to product but to hundreds of other reactions. This might prevent us from reaching the maximum theoretical yield of product formation Y^E. Nicotinamide mononucleotide (NMN) and nicotinamide cytosine dinucleotide (NCD) can be used as non-canonical redox cofactors (NRC). Using such molecules as redox cofactors would prevent the unwanted diffuse distribution of electrons over the whole metabolic network and as such, allow us to approach the maximum theoretical yield of product formation Y^E.

In **Chapter 6**, we propose to improve the yield of microbial processes by applying non-canonical redox cofactors in metabolic pathways. We provide an introduction to synthetic cofactors and describe how their implementation can enhance significantly microbial product formation.

Finally, **Chapter 7** summarizes the main results obtained in this work and addresses the next engineering steps required to successfully achieve the goal scenario. Furthermore, we provide an overview of the future challenges and perspectives regarding both the approach considered in this thesis as well as microbial fermentation in general.

Chapter 2

Metabolic energy conservation for fermentative product formation

This chapter has been published as:
Folch, P.L., Bisschops, M.M.M. and Weusthuis, R.A. (2021). Metabolic energy conservation for fermentative product formation. *Microbial Biotechnology*

Summary

Microbial production of bulk chemicals and biofuels from carbohydrates competes with low-cost fossil-based production. To limit production costs, high titers, productivities and especially high yields are required. This necessitates metabolic networks involved in product formation to be redox-neutral and conserve metabolic energy to sustain growth and maintenance. Here, we review the mechanisms available to conserve energy and to prevent unnecessary energy expenditure. First, an overview of ATP production in existing sugar-based fermentation processes is presented. Substrate-level phosphorylation (SLP) and the involved kinase reactions are described. Based on the thermodynamics of these reactions, we explore whether other kinase-catalyzed reactions can be applied for SLP. Generation of ion-motive force is another means to conserve metabolic energy. We provide examples how its generation is supported by carbon-carbon double bond reduction, decarboxylation and electron transfer between redox cofactors. In a wider perspective, the relationship between redox potential and energy conservation is discussed. We describe how the energy input required for coenzyme A (CoA) and CO_2 binding can be reduced by applying CoA-transferases and transcarboxylases. The transport of sugars and fermentation products may require metabolic energy input, but alternative transport systems can be used to minimize this. Finally, we show that energy contained in glycosidic bonds and the phosphate-phosphate bond of pyrophosphate can be conserved. This review can be used as a reference to design energetically efficient microbial cell factories and enhance product yield.

Keywords

Energy conservation, fermentation, metabolic energy, metabolic networks, product yield

2.1. Introduction

Metabolic engineering has been extensively used in the past decades to improve the production of chemicals by microorganisms (Atsumi *et al.*, 2008; Keasling, 2010; Singh *et al.*, 2011; Zhao *et al.*, 2013a; Vuoristo *et al.*, 2015). Recent advances in omics and genetic techniques have allowed fast and efficient modifications of microorganisms (Datsenko and Wanner, 2000; Mans *et al.*, 2015), broadening the spectrum of both substrates and products (Zhang *et al.*, 2008; Jung *et al.*, 2010; Lindberg *et al.*, 2010; Yim *et al.*, 2011).

Fermentation is a well-studied metabolic concept in which a substrate is oxidized to an intermediate – resulting in the reduction of redox cofactors – after which the intermediate is reduced – regenerating the oxidized cofactors. Microbial fermentation has been used to produce biofuels and bulk chemicals (Bennett and San, 2001; Bechthold *et al.*, 2008; Abdel-Rahman *et al.*, 2013; Wang *et al.*, 2016). These chemicals compete with petrochemical-derived compounds; therefore, their manufacture requires high targets for productivity, titer and – most importantly – substrate efficiency. In microbial processes, the carbon and energy-source is generally used for maintenance, growth and product formation. To maximize product yield, growth must be minimized, and product formation should ideally conserve sufficient metabolic energy to fulfil the energy requirements of the cells (**Figure 1**). If not, a part of the substrate is dissimilated to CO_2 and H_2O by respiration to fulfil the energy requirement of the cell. In addition, the yield of the metabolic pathway (Y^P) designed to convert substrate into product should be equal or very close to the maximum theoretical yield (Y^E). The Y^E can be determined based on the ratio of the degree of reduction of substrate and product (Cueto-Rojas *et al.*, 2015; Vuoristo *et al.*, 2016). The degree of reduction represents the number of electrons in a molecule available for chemical reactions. To reach Y^E, metabolic pathways should be designed such that all electrons present in the substrate end up in the product and therefore be redox-neutral. The use of external electron acceptors, like in respiration, deviates electrons away from the product and is therefore a less

preferred option because it decreases the network yield (Weusthuis *et al.*, 2020).

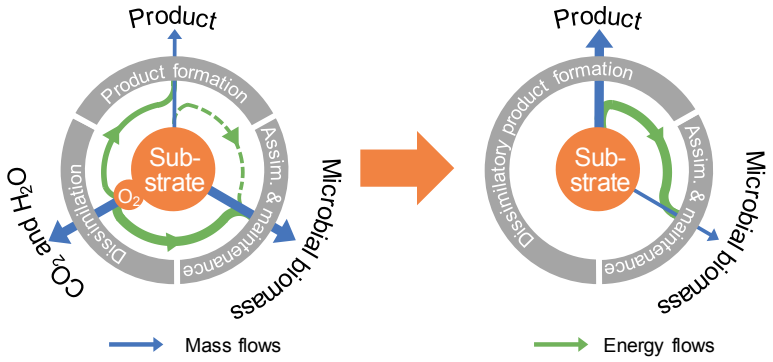

Figure 1. Conservation of additional metabolic energy in the product pathway to improve product yield. On the **left**, classical aerobic bioconversion where part of the substrate is diverted away from product formation by dissimilation to fulfil the cells energy requirement. On the **right**, improved product formation by capturing metabolic energy in the product-forming pathways.

Ethanol and lactic acid are synthesized from glucose by redox-neutral pathways that generate ATP, explaining why their practical yields approach Y^E. It is not straightforward to find such pathways for other substrate/product combinations. Obtaining redox balance often requires a metabolic network consisting of at least two pathways – one resulting in cofactor reduction, the other resulting in cofactor oxidation – that together act in a redox-balanced way. For instance, two parallel pathways combining oxidative and non-oxidative glycolysis have been implemented in *Corynebacterium glutamicum* to create a near redox-neutral metabolic network for the production of L-glutamate (Chinen *et al.*, 2007). This approach allowed to reach a practical yield of 90% of the maximum theoretical yield on glucose. Another example is the redox-neutral combination of oxidative and reductive branches of TCA cycle for the production of succinate, citrate, itaconate (Sánchez *et al.*, 2005; Vuoristo *et al.*, 2016) and 1,4-butanediol (Yim *et al.*, 2011).

These metabolic networks ideally should also provide energy for maintenance and growth. **Table 1** shows the chemical conversion equations and thermodynamics of the previously described metabolic networks. The Gibbs free energy $\Delta G_0'$ of these reactions is comparable to the ones of ethanol and lactic acid production from glucose (**Table 1**). These negative $\Delta G_0'$ values show that – in principle – sufficient free energy is liberated to be conserved as metabolic energy (Cueto-Rojas *et al.*, 2015). Metabolic reactions, however, in which energy can be conserved, are not common. Consequently, it is not straightforward to realize net ATP formation in these metabolic networks. In these cases, respiration is used to conserve metabolic energy, which has negative consequences for yield and productivity (Weusthuis *et al.*, 2011).

This review focuses on the available mechanisms for the conservation of metabolic energy, – excluding those involved in respiration – and how unnecessary metabolic energy expenditure can be avoided, as well as how to implement them into product-forming metabolic networks based on carbohydrates.

Table 1. Thermodynamics of microbial processes using redox-neutral pathways. The ΔG_0' were calculated using eQuilibrator 2.2 with CO_2 as gas (g) and aqueous (aq) for all other compounds (Flamholz *et al.*, 2012; Noor *et al.*, 2012; Noor *et al.*, 2013; Noor *et al.*, 2014). For ATP formation, the EMP pathway and energy-neutral substrate uptake and product efflux were used.

Overall conversions	ATP[a]	ΔG_0' (kJ/mol glucose)
Redox-neutral fermentation processes		
Glucose(aq) + 2 CO_2(g) = 4/3 Citrate(aq) + 2/3 H_2O	-2/3 to 0[b]	-175 ± 12
Glucose(aq) = 12/11 1,4-Butanediol(aq) + 18/11 CO_2(g) + 6/11 H_2O	-8/11[c]	-216 ± 10[d]
Glucose(aq) + 6/7 CO_2(g) = 12/7 succinate(ag) + 6/7 H_2O	4/7[e]	-257 ± 8
ATP generation in existing fermentation processes		
Glucose(aq) = 2 Ethanol(aq) + 2 CO_2(g)	2	-230 ± 13
Glucose(aq) = 2 Lactate(aq)	2	-187 ± 4
Glucose(aq) + H_2O = Acetate(aq) + Ethanol(aq) + 2 Formate(aq)	3	-211 ± 6
Glucose(aq) = Butyrate(aq) + 2 CO_2(g) + 2 H_2(g)	3	-266 ± 18
Glucose(aq) + CO_2(g) = Succinate(aq) + Formate(aq) + Acetate(aq)	3	-249 ± 8
Glucose(aq) + 2 NH_3(aq) = 2 Alanine(aq) + 2 H_2O	2	-209 ± 4

a. Amount of ATP produced (positive sign) or consumed (negative sign).
b. Calculated as described by Vuoristo *et al.* (2016). The –2/3 ATP was obtained by using the reversed glyoxylate cycle, the 0 ATP was obtained by combining the reductive and oxidative TCA shunts to reach redox-neutral conversion.
c. Calculated using the pathway described by Yim *et al.* (2011) assuming that both reductive and oxidative TCA shunts were applied to obtain redox-neutral conversion and that the acetate formed was recovered to acetyl-CoA by means of an acetyl-CoA synthase at the expense of two ATP equivalents.
d. The eQuilibrator database does not contain data on 1,4-butanediol. The Gibbs free energy was estimated by using the value for (*S,S*)-butane-2,3-diol instead.
e. Calculated with a combined reductive and oxidative TCA shunts to reach redox-neutral conversion. The same result was obtained with a combined reductive TCA cycle and glyoxylate cycle.

2.2. Energy in a biological context

Organisms convert carbon and energy-sources into the desired products to conserve energy for growth and maintenance purposes. This conversion has – by definition – a negative Gibbs free energy. A part of the Gibbs free energy can be conserved as metabolically available energy, and a part is dissipated to avoid chemical equilibrium.

The overall conversion is performed by a vast number of chemical reactions. Again, by definition, these reactions have negative Gibbs free energies under physiological conditions, with prevalent concentrations of substrates, products, intermediates and cofactors. The exact concentrations are mostly unknown, and the Gibbs free energy is therefore often expressed under normalized conditions. For product/substrate combinations ΔG_0' is most convenient, using 1 M concentrations for solutes, and 1 bar concentrations for gasses at pH 7.0. The actual concentrations of metabolic intermediates are however often much lower and therefore ΔG_m' is often applied for single reactions, using 1 mM concentrations for solutes instead (Flamholz *et al.*, 2012; Noor *et al.*, 2012; Noor *et al.*, 2013; Noor *et al.*, 2014). Expressing the Gibbs free energy as either ΔG_0' or ΔG_m' may result in positive values for reactions actually running under physiological conditions. Redox reactions can be expressed using either ΔG or the redox potential E'. The relationship between ΔG' and E' is 19.4 kJ/100 mV when 2 electrons are transferred. The redox potential E' can be expressed as E_0' normalized for 1 M concentrations of solutes and 1 bar concentrations for gasses or as E_m' normalized for 1 mM concentrations of solutes.

Energy can be conserved in two interchangeable forms: as energy-rich bonds (for example via substrate-level phosphorylation, SLP) or as electrochemical gradients over membranes (via ion-motive force, IMF) (Decker *et al.*, 1970).

Phosphate bonds used in e.g. ATP, GTP and polyphosphates are an important class of energy-rich bonds available in cells. **Table 2** lists the ΔG_m' values for the hydrolysis of the phosphate-phosphate bonds in a number of energy carriers.

Table 2. Hydrolysis of phosphate-phosphate bonds of different energy carriers.

Reactions	ΔG_m' (kJ/mol)
ATP + H_2O = ADP + Pi	-44 ± 1
ATP + H_2O = AMP + PPi	-52 ± 1
ATP + 2 H_2O = AMP + 2 Pi	-85 ± 1
ADP + H_2O = AMP + Pi	-41 ± 1
GTP + H_2O = GDP + Pi	-41 ± 3
PPi + H_2O = 2 Pi	-33 ± 0

The electrochemical gradient often exists in the form of a proton-motive force or a sodium ion-motive force. Its energy level is expressed as redox potential (E' (volt)). Typical values for the IMF of fermenting microorganisms are between -40 and -170 mV (Kashket and Wilson, 1974; Marty-Teysset *et al.*, 1996; Salema *et al.*, 1996; Trchounian *et al.*, 2013). Ion-motive force (IMF) is generated from the energy released by the difference in redox potentials of the compounds involved or the hydrolysis of phosphate-phosphate bonds. Bacteria use IMF for chemical conversions (e.g. drive endergonic ADP phosphorylation to ATP), for osmotic work (e.g. active transport of molecules across the membrane) and mechanical work (e.g. cell motility).

IMF consists of a chemical gradient Δp_X (difference in intracellular and extracellular ion concentrations) and an electrical gradient $\Delta\Psi$ (membrane potential), and it involves the transfer of protons (proton-motive force, PMF) or sodium ions (Na^+ ion-motive force) across the membrane (**Equation 1**).

$$\Delta\mu_{X^+} = -\frac{2.3RT}{nF}\Delta p_X + \Delta\Psi \qquad \textbf{(Equation 1)}$$

In this equation, $\Delta\mu$ represents the ion-motive force, X^+ the cation (H^+ or Na^+), Δp_X the chemical concentration gradient of cations over the membrane, $\Delta\Psi$ the membrane potential (V), n the charge of the species translocated (e.g. n=1 for a proton), F the Faraday constant, T the temperature (K) and R the gas constant.

The energy contained in an IMF can be used to create phosphate-phosphate bonds by ATP synthase. This form of phosphorylation is called electron transport phosphorylation (ETP). Redox reactions with a redox potential larger than 43.5/19.4x100 = 224 mV have therefore sufficient Gibbs free energy to phosphorylate ADP to ATP.

Although all reactions are contributing to the overall ΔG', only a few reactions have a sufficiently negative Gibbs free energy to harvest it in a metabolically available form: more than ~40 kJ/mol for ATP synthesis and ~100-150 mV (equals ~ 20-30 kJ/mol) for ion-motive force.

2.3. ATP generation in existing fermentation processes

Table 1 gives a non-exhaustive overview of product formation from glucose by fermentation processes and their ΔG_0' values. The ΔG_0' values are between -187 and -266 kJ/mol glucose, and sufficient to deliver the ΔG_m' necessary to create energy-rich phosphate-phosphate bonds once, twice or even three times.

2.3.1. Glycolytic pathways

The process in which C6 sugars are converted into oxidized intermediates is called glycolysis. Several different glycolytic pathways are used by fermenting microorganisms to generate metabolic energy. The pathways can be characterized by the way they split sugar phosphates and differ with respect to the amount of energy harvested and reduced redox cofactors produced (**Figure 2**). Thereby these pathways provide options for metabolic engineers to realize production of a certain compound. Below, we describe them in order of most to least ATP generation.

The pentose-phosphate pathway (PPP) is essentially an anabolic pathway able to generate NADPH and building blocks for biosynthetic purposes (Kruger and von Schaewen, 2003). In the PPP ribulose-5-phosphate is split and $^7/_3$ ATP

generated per glucose. The co-production of CO_2 results in more reduced $NAD(P)^+$ than from other glycolytic pathways. This limits its function as glycolytic pathway for fermentation processes to reduced products.

The Embden-Meyerhof-Parnas (EMP) pathway (Kresge *et al.*, 2005) is characterized by the split of fructose-1,6-bisphosphate into dihydroxyacetone-phosphate and D-glyceraldehyde-3-phosphate. It generates 2 ATP per glucose with the concomitant reduction of 2 NAD^+.

The Entner-Doudoroff (ED) pathway is characterized by the cleavage of 2-keto-3-deoxy-6-phosphogluconate into pyruvate and D-glyceraldehyde-3-phosphate. It generates 1 ATP per glucose. Instead of reducing 2 NAD^+, it is also able to reduce 1 $NADP^+$ and 1 NAD^+ (Conway, 1992).

In the heterolactic pathway xylulose-5-phosphate is split into acetyl-phosphate and D-glyceraldehyde-3-phosphate, which is subsequently oxidized to pyruvate (Burma and Horecker, 1958; Heath *et al.*, 1958; Hurwitz, 1958). It produces 1 ATP per glucose and reduces 3 $NAD(P)^+$. The acetyl-phosphate can be converted into acetyl-CoA and – as such – be used for the synthesis of other compounds. This has e.g. been applied to produce L-glutamate by *Corynebacterium glutamicum* (Chinen *et al.*, 2007).

The Bifidobacterium shunt (de Vries *et al.*, 1967) is hallmarked by splitting fructose-6-phosphate and xylulose-5-phosphate. The final products are acetyl-phosphate and pyruvate, with the concomitant synthesis of 1 ATP and 1 NADH per glucose.

A glycolytic pathway we dubbed the “Calvin shunt” is a modification of the pentose-phosphate pathway in which two enzymes of the Calvin cycle are included: phosphoribulokinase and ribulose-1,5-bisphosphate carboxylase. It is not generating ATP and as such its application in fermentation processes is limited. It has been used to replace the pentose-phosphate cycle, to prevent glycerol production in *Saccharomyces cerevisiae*, resulting in increased ethanol formation (Guadalupe-Medina *et al.*, 2013).

Non-oxidative glycolysis (NOG) is an artificial pathway based on the Bifidobacterium shunt but has only acetyl-phosphate as product (Bogorad *et al.*, 2013). It has been developed especially for its excellent carbon yield (1 Cmol/Cmol). It however requires ATP input and can therefore only be used in combination with other ATP-generating glycolytic pathways or ATP-generating product pathways (Lin *et al.*, 2018).

In *Pseudomonas putida* the D-glyceraldehyde-3-phosphate produced by the ED pathway can be converted back to glucose-6-phosphate by gluconeogenesis (Nikel *et al.*, 2015). This ED-EMP cycle requires ATP input and generates NAD(P)H.

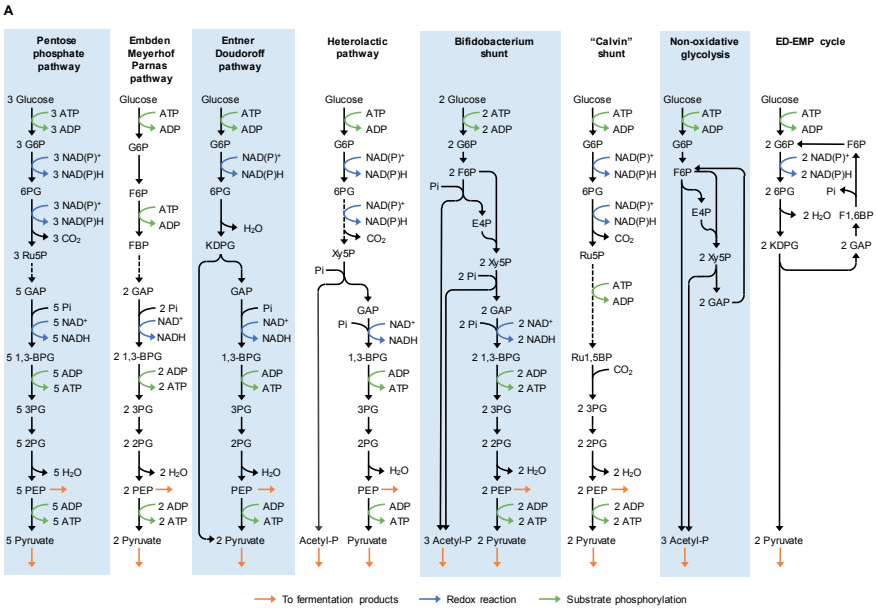

B

Pentose phosphate pathway:	Glucose + $^{7}/_{3}$ ADP + $^{7}/_{3}$ Pi + 2 NADP + $^{5}/_{3}$ NAD = $^{5}/_{3}$ Pyruvate + $^{7}/_{3}$ ATP + 2 NADPH + $^{5}/_{3}$ NADH + CO_2
Embden Meyerhof Parnas pathway:	Glucose + 2 ADP + 2 Pi + 2 NAD = 2 Pyruvate + 2 H_2O + 2 ATP + 2 NADH
Entner Doudoroff pathway:	Glucose + ADP + Pi + NAD + NAD(P) = 2 Pyruvate + H_2O + ATP + NAD + NAD(P)H
Heterolactic pathway:	Glucose + ADP + 2 Pi + 2 NAD(P) + NAD = Pyruvate + Acetyl-P + CO_2 + ATP + 2 NAD(P)H + NADH + H_2O
Bifidobacterium shunt:	Glucose + ADP + 2.5 Pi + NAD = Pyruvate + 1.5 Acetyl-P + ATP + NADH + 2.5 H_2O
"Calvin" shunt:	Glucose + 2 NAD(P) = 2 Pyruvate + 2 NAD(P)H
Non-oxidative glycolysis:	Glucose + ATP + 2 Pi = 3 Acetyl-P + ADP
ED-EMP cycle:	Glucose + ATP + 2 $NAD(P)^+$ = 2 Pyruvate + ADP + Pi + NAD(P)H

Figure 2. Microbial glycolytic pathways (A) and their overall reaction equations (B).

All the glycolytic pathways lead to the formation of the fermentation intermediates acetyl-phosphate, phospho-enol-pyruvate and/or pyruvate.

2.3.2. Fermentation pathways

Glycolysis is followed by reactions that convert phospho-enol-pyruvate (PEP), pyruvate and/or acetyl-phosphate into the final fermentation products (**Figure 3**). Product formation has to regenerate the redox cofactors used in glycolysis. The redox reactions are either the reduction of oxo-groups to hydroxy groups (acetaldehyde to ethanol, pyruvate to lactate, acetoacetyl-CoA to 3-hydroxybutyryl-CoA, oxaloacetate to malate), the reduction of 2-oxoacids into amino acids (e.g. pyruvate into alanine) or the reduction of carbon-carbon double bonds (fumarate to succinate, crotonyl-CoA to butyryl-CoA).

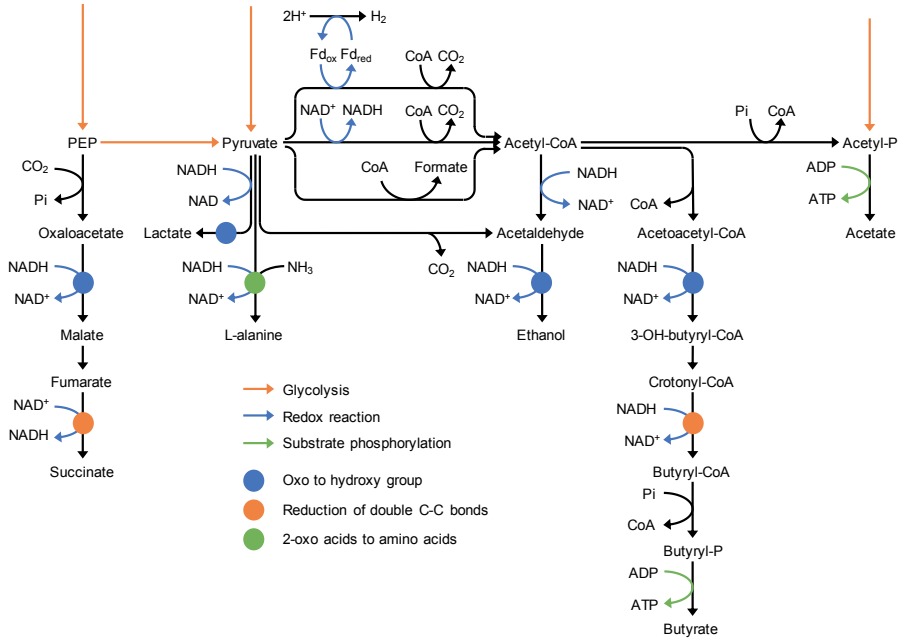

Figure 3. Conversion of PEP, pyruvate and acetyl-phosphate into final products of fermentation processes.

In the fermentation pathways, two mechanisms are available to conserve additional metabolic energy. The reduction of carbon-carbon double bonds can be coupled to harvesting additional metabolic energy in the form of IMF (Kröger,

1978; Graf *et al.*, 1985; Herrmann *et al.*, 2008; Li *et al.*, 2008) and the conversions of acetyl-phosphate and butyryl-phosphate into respectively acetate and butyrate are coupled to SLP and therefore generate ATP.

The harvesting of metabolic energy in these cases is connected to the production of a specific compound and therefore – as such – cannot be used for the production of other compounds. We therefore studied the mechanisms behind these cases of energy conservation to find out whether they can also be applied for harvesting metabolic energy in the production of other chemicals.

2.4. Substrate-level phosphorylation (SLP)

2.4.1. Reactions involved in substrate-level phosphorylation

2.4.1.1. 1,3-bisphosphoglycerate + ADP = 3-phosphoglycerate + ATP, ΔG_m' = -19 ± 1 kJ/mol

This reaction is catalyzed by phosphoglycerate kinase (EC 2.7.2.3). It harvests the energy released in the oxidation of D-glyceraldehyde-3-phosphate to 3-phosphoglycerate (**Figure 4A**). This redox couple has an E_m' of -524 mV and its electrons are transferred to NAD^+/NADH with a redox potential E' of -300 mV. The difference in redox potential between this redox couple and NAD^+/NADH is 224 mV, just sufficient to produce ATP. Harvesting of ATP is realized in two sub reactions. In the oxidation reaction, D-glyceraldehyde-3-phosphate is converted into 1,3-bisphosphoglycerate by glyceraldehyde 3-phosphate dehydrogenase (GAPDH, EC 1.2.1.12). First, the aldehyde group of glyceraldehyde-3P is oxidized to a carboxyl group and NAD^+ is reduced to NADH. This reaction involves the formation of a high-energy thioester intermediate, which allows attachment of a phosphate group to D-glyceraldehyde-3-phosphate creating 1,3-bisphosphoglycerate. The latter is subsequently converted into 3P-glycerate, forming ATP by transferring a phosphate group to ADP.

This reaction is the only one that truly generates ATP in the glycolytic pathways. This reaction is upstream of pyruvate, PEP and acetyl-phosphate – and is

therefore the main contributor to ATP production in existing and new fermentation processes.

2.4.1.2. PEP + ADP = pyruvate + ATP, ΔG_m' = -28 ± 1 kJ/mol

Although the conversion of PEP to pyruvate via pyruvate kinase (EC 2.7.1.40) is mentioned as part of SLP, this reaction does not actually lead to *de novo* ATP synthesis. In fact, the reaction enables the recovery of previously invested energy during phosphorylation of sugar to fructose-1,6-bisphosphate (**Figure 4B**).

2.4.1.3. Carbamoyl-phosphate + ADP = carbamate + ATP, ΔG_m' = -17 ± 4 kJ/mol

This reaction is catalyzed by carbamate kinase (EC 2.7.2.2). It harvests the energy released during the degradation of L-arginine into L-ornithine, CO_2 and ammonium (**Figure 4C**). Three sub reactions are used to harvest the energy.

First, L-arginine is hydrolyzed into L-citrulline and ammonia by arginine deiminase (EC 3.5.3.6). This reaction has a ΔG_m' of -52 ± 7 kJ/mol and the energy released is used to drive the following reaction. Ornithine carbamoyltransferase (EC 2.1.3.3) catalyzes the phosphoroclastic cleavage of L-citrulline into L-ornithine and carbamoyl-phosphate (ΔG_m' of 29 ± 6 kJ/mol). Then, carbamate kinase cleaves the thioester bond in the energy-rich carbamoyl-phosphate and releases the energy necessary to form ATP from ADP. Carbamate is usually spontaneously converted into CO_2 and ammonium.

Using this reaction for ATP production aiming to synthesize products other than L-ornithine is limited as it leads to CO_2 and ammonium.

Carbamoyl-phosphate is – to our knowledge – also produced in two other reactions: the conversion of oxalureate into oxamate by carbamoyl-phosphate:oxamate carbamoyltransferase (EC 2.1.3.5) (Vander Wauven *et al.*, 1986) and the hydrolysis of glutamine to glutamate by carbamoyl-phosphate synthase (EC 6.3.5.5) (Thoden *et al.*, 1999). Both reactions seem not easily applicable for the production of chemicals or fuels.

2.4.1.4. N^{10}-formyl THF + ADP + Pi = formate + THF + ATP, $\Delta G_m'$ = +5 ± 1 kJ/mol

This reaction is catalyzed by formyltetrahydrofolate synthetase (EC 6.3.4.3). This enzyme is found in numerous bacteria in which it however functions in the ATP-consuming direction, forming N^{10}-formyltetrahydrofolate. The positive $\Delta G_m'$ indicates that high substrate concentrations and low product concentrations are required to make SLP possible. To date, this reaction has only been mentioned to contribute to SLP in *Clostridium cylindrosporum* growing on purines (Curthoys *et al.*, 1972). Consequently, it is not a suitable general option for conservation of metabolic energy using more conventional substrates.

2.4.1.5. Adenylyl sulfate + PPi = sulfate + ATP, $\Delta G_m'$ = -47 ± 2 kJ/mol

This reaction is catalyzed by sulfate adenylyltransferase (EC 2.7.7.4). Energy is harvested during the oxidation of sulfite to sulfate.

First, the adenylyl-sulfate reductase (EC 1.8.99.2) catalyzes the AMP-dependent oxidation of sulfite to adenylyl sulfate. Electrons from sulfite are transferred to a cofactor, however the nature of the cofactor remains elusive. Then, sulfate adenylyltransferase cleaves adenylyl sulfate forming sulfate and AMP. The energy released in the reaction is used to attach a PPi group to AMP and form ATP (Krämer and Cypionka, 1989). In most bacteria, this system is used in sulfate activation for sulfonation, using oxygen as electron acceptor and consuming ATP (Gregory and Robbins, 1960). This reaction should therefore not be considered as a strategy for energy conservation for microbial production processes.

2.4.1.6. Acyl-phosphate + ADP = fatty acid + ATP

The reactions listed in **Table 3** fall in this category.

Table 3. Reactions coupling the conversion of an acyl-phosphate to a fatty acid to ADP phosphorylation to ATP. The values for ΔG_m' were calculated using eQuilibrator 2.2.

Reactions	Enzymes	ΔG_m' (kJ/mol)
Enzyme activities contributing to SLP		
Acetyl-phosphate + ADP = Acetate + ATP	Acetate kinase (EC 2.7.2.1) Propionate/acetate kinase	-13 ± 1
Propionyl-phosphate + ADP = Propionate + ATP	Propionate/acetate kinase Butyrate kinase	-32 ± 6
Butyryl-phosphate + ADP = Butyrate + ATP	Butyrate kinase	-29 ± 7
Isovaleryl-phosphate + ADP = Isovalerate + ATP	Branched-chain fatty acid kinase Butyrate kinase	n.a.
2-methylbutyryl-phosphate + ADP = 2-methylbutyrate + ATP	Branched-chain fatty acid kinase	n.a.
Isobutyryl-phosphate + ADP = Isobutyrate + ATP	Branched-chain fatty acid kinase Butyrate kinase	n.a.
Additional enzyme activities		
Valeryl-phosphate + ADP = Valerate + ATP	Butyrate kinase	n.a.
Vinyl-acetyl-phosphate + ADP = Vinyl-acetate + ATP	Butyrate kinase	n.a.
Isopropionyl-phosphate + ADP = Isopropionate + ATP	Branched-chain fatty acid kinase	n.a.

n.a. = not available

Acetate kinase

The reaction catalyzed by acetate kinase (EC 2.7.2.1) is member of a reaction sequence that harvests part of the energy released in the conversion of pyruvate into acetate (**Figure 4D**). Two options are available in the cells: by oxidative decarboxylation or by co-production of formate. The latter is not discussed here because electrons end up in the by-product formate and not in the desired product.

The pyruvate/acetate redox couple has an E_m' of -785 mV. The electrons can be transferred to the NAD^+/NADH redox couple with E' around -300 mV or to the Fd_{ox}/Fd_{red} redox couple with E_m' around -418 mV. The difference in redox potential between pyruvate/acetate and NAD^+/NADH or Fd_{ox}/Fd_{red} is 485 mV and 367 mV, respectively, both of which are larger than the 224 mV required to phosphorylate ADP to ATP.

Harvesting energy is realized in three sub reactions. During the oxidation reaction (dehydrogenation reaction), electrons from pyruvate are transferred to either NAD^+ catalyzed by the pyruvate dehydrogenase (PDH) complex, or $ferredoxin_{ox}$ catalyzed by pyruvate:ferredoxin oxidoreductase (PFOR, EC 1.2.7.1). CO_2 is released, and CoA is bound to create acetyl-CoA. The energy released in this reaction is stored in the energy-rich compound acetyl-CoA. Then, phosphate acetyltransferase (PTA, EC 2.3.1.8) catalyzes the exchange of CoA with a phosphate group to form acetyl-phosphate. Finally, acetyl-P is converted into acetate, transferring the phosphate group to ADP, forming ATP.

This reaction results in one specific fermentation product – acetate – and its contribution to SLP can therefore not be used to produce other compounds.

Propionate/acetate kinase

The reaction catalyzed by propionate/acetate kinase (EC 2.7.2.15) harvests the energy generated by the conversion of L-threonine into propionate (ΔG_m' of -102 ± 7 kJ/mol, **Figure 4E**). L-threonine is deaminated to 2-ketobutyrate, which is concomitantly converted into propionyl-CoA and formate by a pyruvate formate-lyase type of enzyme. The propionyl-CoA is converted into propionyl-phosphate, which donates its phosphate group to convert ADP into ATP (Heßlinger *et al.*, 1998).

This reaction depends on a non-conventional substrate – L-threonine – and can only be applied for the production of propionate. Application of this reaction to generate ATP in other fermentation processes is therefore unlikely.

Butyrate kinase

The reaction catalyzed by butyrate kinase (EC 2.7.2.7) harvests the energy released in the oxidation of 2 pyruvate into butyrate, 2 CO_2 and 2 H_2 (**Figure 4G**). The E_m' of the 2 pyruvate + 4 e- / butyrate + 2 CO_2 + 2 H_2 redox couple is 35 ± 37 mV. The difference in redox potentials with NAD^+/NADH is sufficient to harvest energy in the form of ATP. The reduction reactions are performed by acetoacetyl-CoA reductase (EC 1.1.1.36) and butyryl-CoA dehydrogenase (EC 1.3.8.1). The energy released in the reduction reaction is harvested by a sequence of reactions in which butyryl-CoA is first converted into butyryl-phosphate, which is concomitantly used for the phosphorylation of ADP, producing butyrate.

Butyrate kinase is an example of an enzyme involved in SLP with broad substrate specificity. It is also able to produce isobutyrate, valerate, isovalerate, propionate or vinyl-acetate (Twarog and Wolfe, 1963; Hartmanis, 1987).

Branched-chain fatty acid kinase

The reactions carried out in *Spirocheata sp.* by the branched-chain fatty acid kinase (EC 2.7.2.14) harvest the energy generated by the oxidative decarboxylation of a 2-keto organic acid into an organic acid, e.g. 2-ketoisocaproic acid into isovaleric acid, similar to the case described below for succinyl-CoA. During starvation, this organism conserves the energy required for its maintenance by fermenting branched-chain amino acids e.g. L-valine, L-leucine and L-isoleucine (although these compounds are not utilized as growth substrates) (Harwood and Canale-Parola, 1981a; Harwood and Canale-Parola, 1981b). ATP is formed via SLP using branched-chain fatty acid kinase. The branched-chain fatty acid kinase has been shown to accept a wide range of compounds such as 2-methylpropionyl-phosphate, 2-methylbutyryl-phosphate, butyryl-phosphate, valeryl-phosphate, propionyl-phosphate as well as different NTP (ATP, GTP, CTP) (Harwood and Canale-Parola, 1982).

2.4.1.7. Acyl-CoA + ADP + Pi = fatty acid + CoA + ATP

The reactions mentioned in **Table 4** fall into this category.

Table 4. Reactions coupling conversion of an acyl-CoA to a fatty acid to ADP phosphorylation to ATP. The values for ΔG_m' were calculated using eQuilibrator 2.2. ACS, acetyl-CoA synthetase; SCS, succinyl-CoA synthetase.

Reactions	Enzymes	ΔG_m' (kJ/mol)
Enzyme activities contributing to SLP		
Acetyl-CoA + ADP + Pi = Acetate + CoA + ATP	ACS	-4 ± 1
Succinyl-CoA + ADP + Pi = Succinate + CoA + ATP	SCS	-2 ± 3
Additional enzyme activities		
Itaconyl-CoA + ADP + Pi = Itaconate + CoA + ATP	SCS	5 ± 15
3-sulfinopropionyl-CoA + ADP + Pi = 3-sulfinopropionate + CoA + ATP	SCS	n.a.
Oxalyl-CoA + ADP + Pi = Oxalate + CoA + ATP	SCS	11 ± 7
Propionyl-CoA + ADP + Pi = Propionate + CoA + ATP	SCS	-14 ± 6
Butyryl-CoA + ADP + Pi = Butyrate + CoA + ATP	SCS	-8 ± 16
Adipyl-CoA + ADP + Pi = Adipate + CoA + ATP	SCS	5 ± 15
Glutaryl-CoA + ADP + Pi = Glutarate + CoA +ATP	SCS	5 ± 3

n.a. = not available

Acetyl-CoA synthetase (EC 6.2.1.13) combines the actions of phosphotransacetylase and acetate kinase (Labes and Schönheit, 2001). It also shows activity for propionate, (iso)butanoate, (iso)pentanoate, hexanoate, octanoate, imidazole-4-acetate, phenyl acetate, succinate and thioglycolate (Musfeldt *et al.*, 1999; Jones and Ingram-Smith, 2014). The reaction catalyzed by succinyl-CoA synthetase (EC 6.2.1.5) harvests the energy generated by the oxidative decarboxylation of 2-oxoglutarate to succinate (**Figure 4F**). This redox couple has an E_m' of -715 mV. Electrons are either transferred to the NAD^+/NADH or Fd_{ox}/Fd_{red} redox couples. The differences in redox potential between the redox couples are large enough to allow ATP synthesis.

Two sub reactions are used to harvest the energy. In an oxidation reaction, CoA is bound to form succinyl-CoA. This reaction is an oxidative decarboxylation that

can be catalyzed by either by the 2-oxoglutarate dehydrogenase complex (ODH) or the 2-oxoglutarate: ferredoxin oxidoreductase (OGOR). Succinyl-CoA is used as an energy-rich intermediate, and cleavage of the thioester bond releases the energy required to drive ADP phosphorylation to form ATP (catalyzed by the succinyl-CoA synthetase).

This reaction is part of the citric acid cycle. Fermentative product formation relying on intermediates of the TCA cycle – between succinyl-CoA and oxaloacetate – can therefore benefit from this reaction to generate ATP.

Succinyl-CoA synthetase (EC 6.2.1.5) is able to catalyze the ADP-forming conversion of succinate analogues such as itaconate or 3-sulfinopropionate (Schürmann *et al.*, 2011). Shikata *et al.* (2007) demonstrated that *Thermococcus kodakarensis* possesses an ADP-forming succinyl-CoA synthetase able to convert oxalate, propionate, butyrate, adipate and glutarate. It has not been proven that these additional reactions can contribute to SLP. The ΔG_m' values of the reactions involving itaconate, adipate and glutarate are relatively high indicating that substrate concentrations and low product concentration are required to contribute to SLP.

2.4.1.8. Acetyl-CoA + oxaloacetate + H_2O + ADP + Pi = citrate + CoA + ATP, ΔG_m' = +9 ± 1 kJ/mol

This reaction is catalyzed by ATP citrate synthase (EC 2.3.3.8 formerly EC 4.1.3.8). This enzyme usually works in the other direction: e.g. in oleaginous yeasts to make cytosolic acetyl-CoA available (Liu *et al.*, 2013; Dulermo *et al.*, 2015). Möller *et al.* (1987) have reported the ATP-harvesting action of this enzyme in *Desulfobacter postgatei*. The high ΔG_m' indicates that high substrate concentrations and low product concentrations are required to make SLP possible. The energy-conserving action is the oxidation of acetate to 2 CO_2 (acetate + 2 H_2O = 2 CO_2 + 8 e^-; E_0' = -272 ± 16 mV, **Figure 4H**) and concomitant transfer of the electrons to $NADP^+$ and ferredoxin.

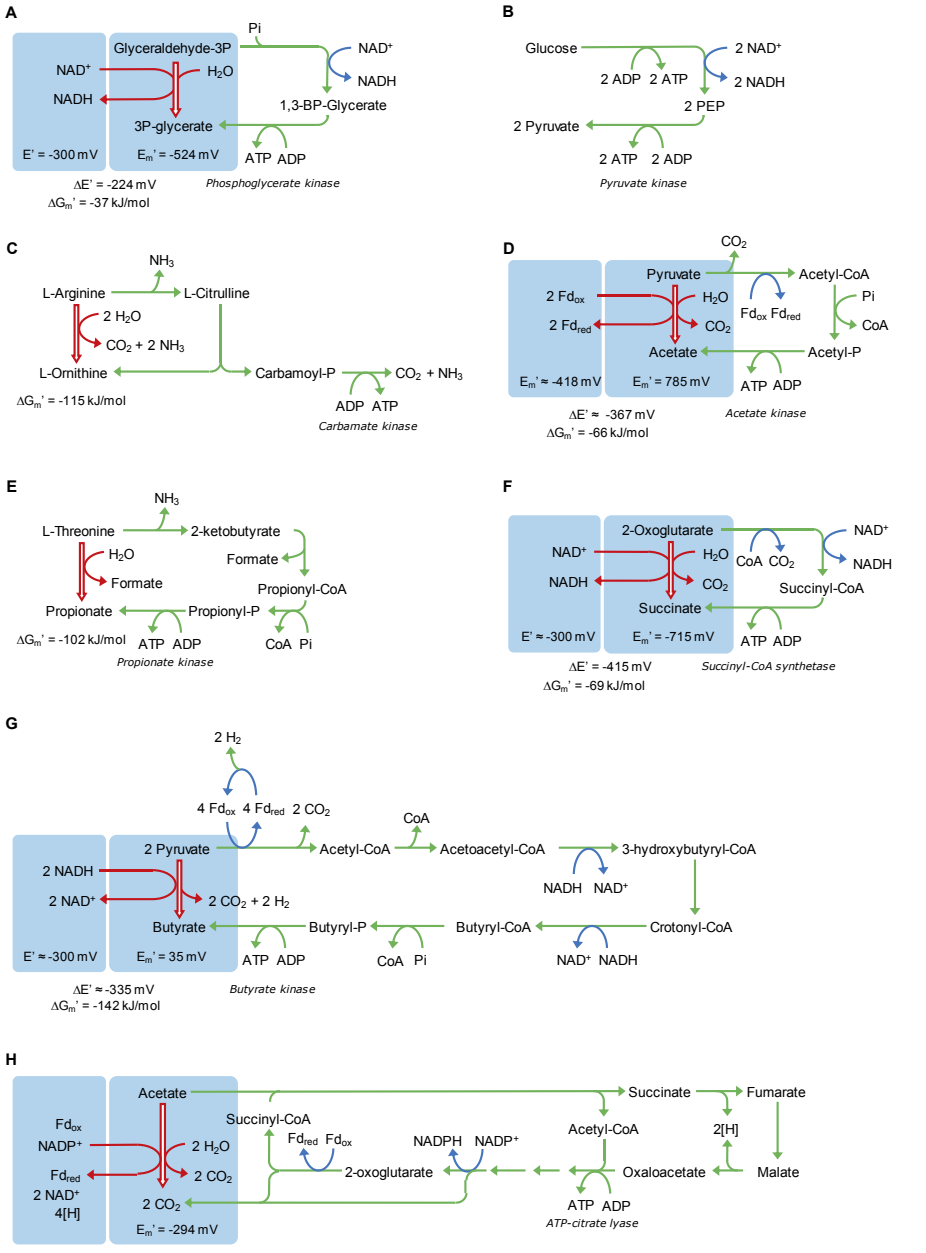

Figure 4. Reactions contributing to energy formation via substrate-level phosphorylation. Red arrows: reactions with strong negative ΔG_0', green arrows: reaction sequences to harvest ATP; blue arrows: electron transfer. Blue boxes: overall conversions involving redox cofactors.

The conversion of oxaloacetate and acetyl-CoA into citrate is a metabolic step used in the production of citrate, itaconate, L-glutamate and other compounds that depend on the oxidative TCA cycle. Application of ATP citrate synthase instead of citrate synthase could enhance the ATP yield in these processes.

2.4.2. Thermodynamic constraints to SLP

As indicated above, some of the enzymes involved in SLP reactions are able to catalyze a range of additional reactions. It can be envisaged that this range can be increased further by protein engineering. The question remains whether these reactions can also contribute to SLP. **Figure 5** shows the thermodynamic analysis of the hydrolysis of acyl-CoAs and carboxy-acyl-CoAs. It indicates that the hydrolysis of acetyl-CoA, propionyl-CoA and butyryl-CoA has a sufficiently low ΔG_m' to phosphorylate ADP, and that the reaction catalyzed by succinyl-CoA synthetase is on the verge of thermodynamic feasibility.

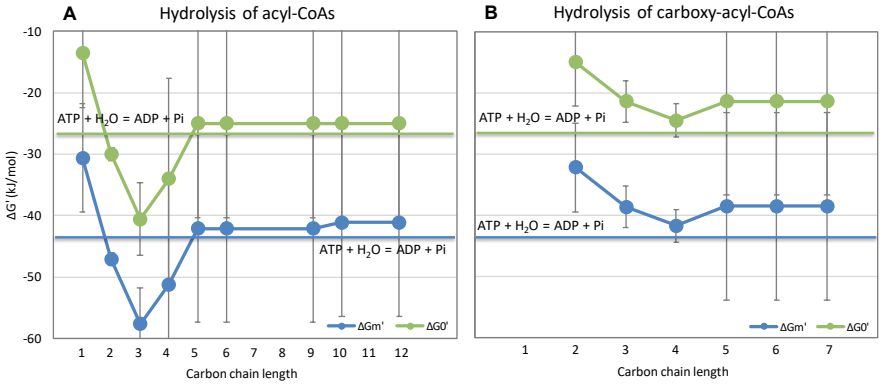

Figure 5. Gibbs free energy (ΔG_m') of hydrolysis of (A) acyl-CoA and (B) carboxy-acyl-CoA molecules of different carbon lengths. (A) C1: formyl-CoA + H_2O = formate + CoA; C2: acetyl-CoA + H_2O = acetate + CoA; C3: propionyl-CoA + H_2O = propionate + CoA; C4: butyryl-CoA + H_2O = butyrate + CoA; C5: valeryl-CoA + H_2O = valerate + CoA; C6: hexanoyl-CoA + H_2O = hexanoate + CoA; C9: nonanoyl-CoA + H_2O = nonanoate + CoA; C10: decanoyl-CoA + H_2O = decanoate + CoA. **(B)** C2: oxalyl-CoA + H_2O = oxalate + CoA; C3: malonyl-CoA + H_2O = malonate + CoA; C4: Succinyl-CoA + H_2O = succinate + CoA; C5: glutaryl-CoA + H_2O = glutarate + CoA; C6: Adipyl-CoA + H_2O = adipate + CoA; C7: pimeloyl-CoA + H_2O = pimelate + CoA. The green lines show the ΔG_m' required to create phosphate-phosphate bonds to convert ADP into ATP and 2 Pi into PPi. The values for ΔG_0' and ΔG_m' were calculated using eQuilibrator 2.2.

The graph shows that SLP using ADP/ATP may not be feasible for other acyl-CoAs and dicarboxyl-CoAs, although it is difficult to draw a clear conclusion due to the large standard deviations of the ΔG_m' values. SLP based on pyrophosphate instead seems to be feasible for all carbon lengths and is worth investigating.

2.5. Generation of an ion-motive force

Reactions coupled to ion translocation over cellular membranes comprise decarboxylation reactions, reduction of carbon-carbon double bonds and transfer of electrons between redox cofactors.

2.5.1. Reduction of carbon-carbon double bonds

The redox potential of reactions in which carbon-carbon double bonds are reduced is between +70 and -40 mV (**Table 5**). The redox potential difference with other redox couples as NADH is in most cases sufficiently large to enable electron transport phosphorylation (ETP). Experimental values are also given in **Table 5** as the values calculated using the group component contribution present large standard deviations.

Table 5. Reactions involving the reduction of a carbon-carbon double bond and their redox potential. The non-referenced E_m' values are derived from eQuilibrator based on component contribution. The referenced values were determined experimentally.

Redox reactions	E_m' (mV)
Acrylyl-CoA + 2 e- = Propionyl-CoA	-14 ± 87 +69 (Sato *et al.*, 1999)
Fumarate + 2 e- = Succinate	-5 ± 21 +33 (Thauer *et al.*, 1977)
Crotonyl-CoA + 2 e- = Butyryl-CoA	-37 ± 83 -13 (Sato *et al.*, 1999)
Caffeoyl-CoA + 2 e- = 1,3-dehydrocaffeoyl-CoA	n.a.

n.a. = not available

2.5.1.1. Reduction of fumarate to succinate

Due to the relatively high redox potential of the fumarate/succinate couple (ca. +30 mV), several electron donors can be used to oxidize fumarate e.g. H_2, NADH, lactate, formate, malate and glycerol-1-phosphate (Hirsch *et al.*, 1963; Thauer *et al.*, 1977; Kröger, 1978; Tran *et al.*, 1997). The two electrons released during these reactions are transferred to electron carriers e.g. menaquinone or demethylmenaquinone, which are reduced to menaquinol or demethylmenaquinol, respectively (Spencer and Guest, 1973; Lambden and Guest, 1976; Kröger, 1978; Wissenbach *et al.*, 1990). The reduced electron carriers transfer electrons to fumarate reductase (EC 1.3.5.1; EC 1.3.5.4), allowing reduction of fumarate to succinate. *Escherichia coli* the electron transfer from NADH to fumarate is coupled to the formation of a transmembrane proton gradient by NADH dehydrogenase I (also called NDH-I or Complex I of the ETC), which is then used to synthetize ATP by ADP synthase (Tran *et al.*, 1997) (**Figure 6A**).

The number of protons translocated per electron by NDH-I has been proposed to be between 1.5 and 2 (Bogachev *et al.*, 1996; Wikström and Hummer, 2012). Assuming that the ATP synthase requires an inward translocation of 4 protons per ATP, fumarate reduction using NDH-I allows the synthesis of 0.75 to 1 mol ATP per mol succinate formed.

This way of energy conservation can be applied for the production of succinate and succinate-derived chemicals such as 1,4-butanediol (Yim *et al.*, 2011).

2.5.1.2. Reduction of crotonyl-CoA to butyryl-CoA

During butyrate fermentation, ATP is produced via SLP in a chain of reactions from pyruvate to butyrate using butyrate kinase (see SLP section). However, additional energy can be harvested in the reaction catalyzed by butyryl-CoA dehydrogenase in which the carbon-carbon double bonds of crotonyl-CoA are reduced to form butyryl-CoA. This redox couple has an E_m' of -37 ± 83 mV. The difference with the redox potential of NAD^+/NADH is large enough to capture additional metabolic energy. In some bacteria such as Clostridia cytoplasmic

butyryl-CoA dehydrogenase/electron-transferring flavoprotein (Bcd/Etf; EC 1.3.1.109) couples the reduction of crotonyl-CoA and ferredoxin with the oxidation of NADH (Herrmann *et al.*, 2008; Li *et al.*, 2008; Seedorf *et al.*, 2008). In this reaction the Bcd/Etf complex transfers electrons from NADH (E_0'= -320 mV) to crotonyl-CoA (E_0'= -10 mV), and the difference in redox potential is used to drive the reduction of ferredoxin (E_0'= ca -400 mV) by a second NADH. This coupled electron transfer reaction is an example of electron bifurcation (Herrmann *et al.*, 2008; Li *et al.*, 2008; Buckel and Thauer, 2013; Buckel and Thauer, 2018a). The reduced ferredoxin is then used to reduce NAD^+ by a membrane-bound NAD^+:ferredoxin oxidoreductase (or Rnf complex) (Herrmann *et al.*, 2008) contributing to the generation of IMF (**Figure 6B**). Reduction of crotonyl-CoA to butyryl-CoA via Bcd/Etf in combination with Rnf complex can lead up to 0.5 ATP formed per butyryl-CoA formed.

2.5.1.3. Reduction of caffeyl-CoA to dihydrocaffeyl-CoA

The anaerobic acetogenic bacterium *Acetobacterium woodii* conserves energy during caffeate respiration via the reduction of caffeate to hydrocaffeate using H_2 as electron donor (Tschech and Pfennig, 1984; Hansen *et al.*, 1988). During caffeate respiration in *A. woodii*, caffeate is activated to caffeyl-CoA prior being reduced (Hess *et al.*, 2011). Once caffeate respiration reaches steady state, caffeate activation is replaced by caffeate CoA-transferase (CarA, EC 2.8.3.23) which transfers a CoA moiety from hydrocaffeyl-CoA to caffeate forming caffeyl-CoA (Hess *et al.*, 2013a). The electron-bifurcating caffeyl-CoA reductase (CarCDE) reduces caffeyl-CoA and ferredoxin with NADH (Bertsch *et al.*, 2013). The reduced ferredoxin is then used to reduce NAD^+ via the Rnf complex with the concomitant transfer of Na^+ ions across the membrane (Hess *et al.*, 2013b). In caffeate respiration, the electron-bifurcating hydrogenase HydABC uses H_2 as electron donor to reduce Fd_{ox} and NAD^+. The reduced ferredoxin produced in this reaction can in turn be used by the Na^+-dependent Rnf complex (**Figure 6C**). The conversion of caffeate to hydrocaffeate leads to the production of 0.9 mol ATP per mol caffeate reduced (Bertsch *et al.*, 2013).

2.5.1.4. Reduction of acrylyl-CoA to propionyl-CoA

Not all carbon-carbon reduction reactions result in the creation of an IMF. An example is the reduction of acrylyl-CoA to propionyl-CoA (Baldwin and Milligan, 1964; Seeliger *et al.*, 2002). Bacteria can ferment lactate to acetate and propionate via the succinate pathway (methylmalonyl-CoA) or via the acrylate pathway (acrylyl-CoA). The latter involves the reduction of acrylyl-CoA to propionyl-CoA catalyzed by a non-bifurcating EtfAB-propionyl-CoA dehydrogenase (also called acrylyl-CoA reductase) (Hetzel *et al.*, 2003). This reaction – which is present in anaerobic bacteria such as *Clostridium homopropionicum* – is not coupled to energy generation via IMF (Baldwin and Milligan, 1964; Seeliger *et al.*, 2002). According to Sato *et al.* (1999), this is due to the relatively low redox potential of this redox couple (see **Table 5**). For more information, see Seeliger *et al.* (2002) and Buckel and Thauer (2018a).

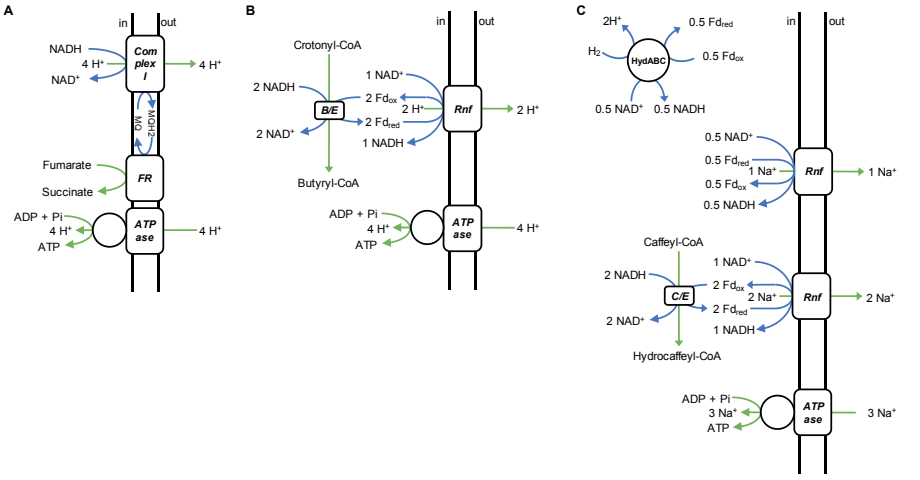

Figure 6. Examples of carbon-carbon double bond reductions. (A) Fumarate reduction in *E. coli* using NADH dehydrogenase I as electron donor, **(B)** Reduction of crotonyl-CoA to butyryl-CoA in *Clostridium kluyveri* and **(C)** Reduction of caffeyl-CoA to hydrocaffeyl-CoA in *Acetobacterium woodii* using H_2 as electron donor.

2.5.2. Decarboxylation phosphorylation

Oxidative decarboxylation reactions contribute to energy production via SLP; due to the large negative value of their ΔG_m'. Non-oxidative decarboxylation reactions have a less negative ΔG_m' (**Table 6**). These reactions can however

also be coupled to the generation of IMF as the energy released during such steps is comparable to the one required for generating an ion-motive force (~20-30 kJ/mol, equivalent to 100-150 mV). This mechanism is called decarboxylation phosphorylation (Dimroth, 1997; Buckel, 2001; Dimroth and von Ballmoos, 2007) and can be used for ATP formation or transport of molecules across the membrane against concentration gradients. The transport of molecules across the membrane can be realized electrogenically, where a net charge is translocated, or electroneutrally, where no net charge is translocated, depending on the carrier.

Table 6. Reactions involved in decarboxylation phosphorylation. The ΔG_m' values were calculated using eQuilibrator 2.2 with aqueous for all compounds and do not take into account the translocation of ions across the membrane.

Reactions	Enzymes	ΔG_m' (kJ/mol)	Ion translocated
Oxaloacetate + H^+ = Pyruvate + CO_2	Oxaloacetate decarboxylase (EC 7.2.4.2)	-34 ± 6	2 Na^+
(S)-methylmalonyl-CoA + H^+ = Propionyl-CoA + CO_2	Methylmalonyl-CoA decarboxylase (EC 7.2.4.3)	-37 ± 12	1 Na^+
Glutaconyl-CoA + H^+ = Crotonyl-CoA + CO_2	Glutaconyl-CoA decarboxylase (EC 7.2.4.5)	-36 ± 17	1 Na^+
Malonate + H^+ = Acetate + CO_2	Malonate decarboxylase (EC 7.2.4.4)	-44 ± 7	1 Na^+

Several anaerobic bacteria produce ATP exclusively through this mechanism such as *Propionigenium modestum* and *Malonomonas rubra* (Dimroth and Hilbi, 1997). In this process, the energy released during decarboxylation reactions is converted into a Na^+ electrochemical gradient, which is later used to drive ADP phosphorylation via ATP synthase. These Na^+-translocating decarboxylases are protein complexes consisting of soluble and membrane-bound subunits. They are biotin-dependent enzymes found in a limited number of microorganisms

grown under anaerobic conditions (Galivan and Allen, 1968; Dimroth, 1981; Buckel and Semmler, 1982; Dimroth, 1982b; Hilpert and Dimroth, 1982). Decarboxylases shown to contribute to decarboxylation phosphorylation are oxaloacetate decarboxylase, methylmalonyl-CoA decarboxylase, glutaconyl-CoA decarboxylase and malonate decarboxylase (**Table 6**).

These decarboxylations are two-step processes. First, the carboxyl group from the substrate is transferred to biotin in an Na^+-independent manner, forming products and carboxybiotin. The latter is then decarboxylated to biotin, and Na^+ ions are translocated across the membrane. Malonate decarboxylation differs slightly from the three other decarboxylations because malonate needs to be activated prior decarboxylation under physiological conditions. Therefore, malonate decarboxylase carries a transferase that forms the thiol ester bond. For more details about the structures and mechanisms of Na^+-translocating decarboxylases, see Dimroth and Hilbi (1997), Buckel (2001), Dimroth *et al.* (2001), Dimroth and von Ballmoos (2007) and references therein.

2.5.2.1. Oxaloacetate decarboxylase

Oxaloacetate decarboxylase has been characterized in citrate-fermenting *Klebsiella aerogenes* and *Klebsiella pneumoniae* (Dimroth, 1980; Dimroth, 1982a; Dimroth, 1982b; Schwarz *et al.*, 1988) as well as in citrate- and tartrate-fermenting *Salmonella typhymurium* (Wifling and Dimroth, 1989; Woehlke *et al.*, 1992; Woehlke and Dimroth, 1994). During citrate fermentation in *K. pneumoniae*, citrate uptake is realized by Na^+-dependent citrate carrier CitS. Citrate is subsequently cleaved into acetate and oxaloacetate by citrate lyase. Then, Na^+-pumping oxaloacetate decarboxylase converts oxaloacetate to pyruvate and CO_2, and the free energy from this decarboxylation reaction is used to translocate 2 Na^+ ions outside the cells. Pyruvate is cleaved into acetyl-CoA and formate by pyruvate formate-lyase. Formate hydrogen-lyase converts formate into H_2 and CO_2. Acetyl-CoA is further converted into acetate via phosphotransacetylase (PTA) and acetate kinase (AK). Citrate fermentation leads to the production of 1 mol ATP per mol citrate by SLP during acetate formation and to a Na^+ ion-motive force. The Na^+ ions gradient is used for the

electroneutral uptake of citrate using CitS (Pos and Dimroth, 1996) while the electrical component of the Na^+ ion-motive force is presumed to contribute to ATP synthesis by ATP synthase.

2.5.2.2. Methylmalonyl-CoA decarboxylase

Methylmalonyl-CoA decarboxylase activity has been demonstrated in bacteria such as *E. coli* (Benning *et al.*, 2000), lactate-fermenting *Veillonella parvula* (Hilpert and Dimroth, 1983; Hilpert *et al.*, 1984) or succinate-fermenting *Propionigenium modestum* (Hilpert *et al.*, 1984; Bott *et al.*, 1997). Decarboxylation of methylmalonyl-CoA is a vital step in succinate fermentation for *P. modestum* as it allows the organism to conserve the energy required for growth (Schink and Pfennig, 1982; Dimroth and Schink, 1998). During succinate fermentation in *P. modestum* (Dimroth and Schink, 1998), succinate propionyl-CoA transferase transfers a CoA group from propionyl-CoA to succinate leading to succinyl-CoA and propionate ($\Delta G_m' = -16 \pm 6$ kJ/mol). Succinyl-CoA is then converted into (*R*)-methylmalonyl-CoA by methylmalonyl-CoA mutase, and further isomerized to (*S*)-methylmalonyl-CoA by methylmalonyl-CoA isomerase. Methylmalonyl-CoA decarboxylase catalyzes the decarboxylation of (*S*)-methylmalonyl-CoA to propionyl-CoA and CO_2 and transfers 2 Na^+ ions across the membrane – one electrogenically and one electroneutrally (Hilpert and Dimroth, 1991; Di Berardino and Dimroth, 1996). The membrane potential of this Na^+ ion-motive force is then used by a Na^+-dependent ATP synthase to drive ADP phosphorylation (Laubinger and Dimroth, 1988; Dimroth *et al.*, 2000). The Na^+-dependent F_0F_1 ATP synthase of *P. modestum* requires the inward translocation of 3.3 Na^+ ions to synthetize 1 molecule of ATP (Stahlberg *et al.*, 2001; Dimroth and Cook, 2004).

2.5.2.3. Glutaconyl-CoA decarboxylase

Glutaconyl-CoA decarboxylase catalyzes a key reaction for energy conservation during L-glutamate fermentation (via (*R*)-2-hydroxyglutarate) in several anaerobic bacteria including *Acidaminococcus fermentans* (Buckel and Semmler, 1982; Bendrat and Buckel, 1993; Braune *et al.*, 1999), *Fusobacterium nucleatum* (Beatrix *et al.*, 1990) and *Clostridium symbiosum* (Buckel and

Semmler, 1983) and during glutarate degradation in *Pelospora glutarica* (Matthies and Schink, 1992a; Matthies and Schink, 1992b; Matthies *et al.*, 2000).

During glutarate degradation, glutarate is first activated to glutaryl-CoA by glutaconate CoA-transferase which transfers CoA from acetyl-CoA to glutarate. Glutaryl-CoA is converted to glutaconyl-CoA by glutaryl-CoA dehydrogenase/Etf. Subsequently, glutaconyl-CoA decarboxylase catalyzes the decarboxylation of glutaconyl-CoA to crotonyl-CoA with the concomitant transfer of Na^+ ions across the membrane. Crotonyl-CoA is further reduced to butyryl-CoA with NADH, allowing regeneration of the NAD^+ used in the conversion of glutaryl-CoA to glutaconyl-CoA. Then, acetate CoA-transferase transfers the CoA moiety from butyryl-CoA to acetate thereby forming acetyl-CoA, which is required for glutarate activation.

In *A. fermentans*, 5 L-glutamate are converted to 5 ammonia, 5 CO_2, H_2, 6 acetate and 2 butyrate (Buckel and Thauer, 2013). L-glutamate is first converted to 2-oxoglutarate by NAD^+-dependent glutamate dehydrogenase. The latter is then reduced to (*R*)-2-hydroxyglutarate by 2-oxoglutarate reductase. (*R*)-2-hydroxyglutarate CoA-transferase transfers a CoA moiety from acetyl-CoA to (*R*)-2-hydroxyglutarate, forming (*R*)-2-hydroxyglutaryl-CoA and acetate. Then, (*R*)-2-hydroxyglutaryl-CoA dehydratase catalyzes the conversion of (*R*)-2-hydroxyglutaryl-CoA to glutaconyl-CoA. Glutaconyl-CoA decarboxylase couples the decarboxylation of glutaconyl-CoA to crotonyl-CoA to the translocation of 2 Na^+ ions across the membrane (Buckel, 2001). Of each five crotonyl-CoA formed from five L-glutamate by *A. fermentans*, two are converted to butyrate via butyryl-CoA and three are converted to acetate via (*S*)-3-hydroxybutyryl-CoA, acetoacetyl-CoA and acetyl-CoA. In this latter pathway, the NADH formed during the conversion of (*S*)-3-hydroxybutyryl-CoA to acetoacetyl-CoA are used in the reduction of crotonyl-CoA to butyryl-CoA. Furthermore, 1 ATP is generated per crotonyl-CoA converted to acetate by the action of acetate-CoA ligase (ADP-forming). In *A. fermentans*, Bcd/Etf catalyze the conversion of crotonyl-CoA to butyryl-CoA (See section 5.1.2). The reduced ferredoxin

produced in this reaction is partly reoxidized by the Rnf complex and thereby contributing to the generation of an ion-motive force (Herrmann *et al.*, 2008). The remaining reduced ferredoxin is converted to H_2 by the action of a hydrogenase. Finally, acetate CoA-transferase transfers the CoA moiety from butyryl-CoA to acetate thereby forming acetyl-CoA and butyrate. The Na^+ ions translocated outside the cell can either be used for ATP synthesis or to take up L-glutamate by a sodium-glutamate symporter (Chang *et al.*, 2010). Buckel and Thauer (2013) calculated that 0.95 ATP can be formed per L-glutamate consumed in *A. fermentans*.

2.5.2.4. Malonate decarboxylase system

Malonate decarboxylation has been shown to be the sole energy-conserving route for anaerobic growth of some bacteria such as *Malonomonas rubra* and *Sporomusa malonica* (Dehning and Schink, 1989; Dehning *et al.*, 1989). The malonate decarboxylase system consists of several enzymes catalyzing distinct reactions to ultimately convert malonate into acetate and CO_2 with the concomitant generation of a sodium electrochemical gradient.

During malonate fermentation, malonate uptake is realized by a Na^+-dependent symporter (MadL-MadM) (Schaffitzel *et al.*, 1998). Prior to decarboxylation, malonate is activated by one of the malonate decarboxylase system modules that transfers an acyl carrier protein (ACP) moiety from acetate to malonate thereby generating acetate and malonyl-ACP (Hilbi *et al.*, 1992; Berg *et al.*, 1996; Berg *et al.*, 1997; Dimroth and Hilbi, 1997). The free carboxyl group of malonyl-ACP is then transferred to a biotin protein, allowing regeneration of acetyl-ACP for activation of malonate (Berg and Dimroth, 1998). Subsequently, a membrane-bound decarboxylase couples the decarboxylation of carboxybiotin to the outward translocation of 2 Na^+ ions. In this reaction, one Na^+ is transported electroneutrally and one Na^+ is translocated electrogenically. The electrogenic export of Na^+ ions can be used for ATP synthesis. During malonate fermentation in *M. rubra*, around three decarboxylation reactions are necessary to synthetize 1 mol of ATP (Dimroth and von Ballmoos, 2007).

2.5.3. Electron transfer between redox cofactors

2.5.3.1. Transfer of electrons between NAD^+/NADH and $ferredoxin_{ox}$/$ferredoxin_{red}$

The NAD^+/NADH redox couple is generally kept in an oxidized form, and therefore the E' is usually higher than the E_m'. The actual value depends on organism and growth conditions and may vary between -310 and -240 mV. Ferredoxins are a class of redox cofactor with a wide range of redox potentials. The ones used in fermentative metabolism have a lower redox potential than NAD^+/NADH. eQuilibrator uses an E_m' for $ferredoxin_{ox}$/$ferredoxin_{red}$ of -418 mV. The difference in redox potential between both redox cofactors is sufficient to translocate protons or sodium ions over the cell membrane and as such contribute to the formation of an IMF, which in turn can be used to drive ADP phosphorylation by ATP synthase. The Rnf complex most likely translocates one H^+ or Na^+ per electron (Buckel and Thauer, 2018b). Association of Bcd/Etf complex and Rnf complex to produce ATP (see **Figure 6B**) has been demonstrated during ethanol-acetate fermentation by *Clostridium kluyveri* (PMF) (Li *et al.*, 2008; Seedorf *et al.*, 2008) and during L-glutamate fermentation to butyrate and acetate in *Clostridium tetanomorphum* and *Acidaminococcus fermentans* (Na^+ ion-motive force) (Boiangiu *et al.*, 2005; Herrmann *et al.*, 2008; Jayamani and Buckel, 2008; Chowdhury *et al.*, 2016). For more details, see Buckel and Thauer (2013), Buckel and Thauer (2018a) and references therein.

2.5.3.2. Transfer of electrons between NAD^+/NADH and $NADP^+$/NADPH

Although NAD^+/NADH and $NADP^+$/NADPH have identical E_0' values, their actual redox potentials differ considerably. NAD^+/NADH is kept in the oxidized state to perform oxidation reactions for catabolic and anabolic purposes while $NADP^+$/NADPH is kept in the reduced state to perform reduction reactions (Spaans *et al.*, 2015; Weusthuis *et al.*, 2020) in biosynthetic pathways. Values reported for NAD^+/NADH ratios range from 3.74 to 1820, whereas $NADP^+$/NADPH ratios range from 0.017 to 0.95 (Spaans *et al.*, 2015). At the mentioned extreme ratios, the redox potential difference between both cofactors is 149 mV (-240 mV for NAD^+/NADH and -389 mV for $NADP^+$/NADPH, which in

principle is sufficient to contribute to the build-up of an IMF). Several reactions of central metabolism are able to generate NADPH (**Table 7**). Their redox potentials are lower than the 100-150 mV of the membrane potential, and therefore in principal low enough to contribute to the generation of IMF.

Table 7. Reactions involved in NADPH regeneration.

Reaction	Enzyme	E_0' (mV)
Pyruvate + CO_2 + 2 e^- = Malate	Malic enzyme	-379 ± 10
Ribose-5-phosphate + CO_2 + 2 e^- = 6-phosphogluconate	6-phosphogluconate dehydrogenase	-404 ± 12
2-oxoglutarate + CO_2 + 2 e^- = Isocitrate	Isocitrate dehydrogenase	-419 ± 10
6-phosphogluconate + 2 e^- = Glucose-6-phosphate + H_2O	Glucose-6-phosphate dehydrogenase	-458 ± 11
3-phosphoglycerate + 2 e^- = D-glyceraldehyde-3-phosphate	Glyceraldehyde-3-phosphate dehydrogenase (non-phosphorylating)	-425 ± 7
Pyruvate + CoA + 2 e^- = Acetyl-CoA + CO_2	Pyruvate dehydrogenase ($NADP^+$-dependent)	-541 ± 16

Many anaerobic bacteria such as *Clostridium kluyveri* and *Moorella thermoacetica* can transfer electrons from NADPH to oxidized ferredoxin and NAD^+ via an NAD^+-dependent ferredoxin NADPH oxidoreductase (Nfn). This enzyme couples the reversible reduction of 2 ferredoxin with 2 NADPH to the reduction of 1 NAD^+ (Wang *et al.*, 2010). The reduced ferredoxin can subsequently be used by the Rnf complex to generate NADH and an electrochemical Na^+ ion gradient over the membrane. Such a mechanism leads to the overall conversion of 2 NADPH and 2 NAD^+ into 2 $NADP^+$, 2 NADH and the translocation of 2 Na^+ ions.

Microorganisms can use a membrane-bound proton-translocating transhydrogenase to transfer electrons from NADH to NADPH. The enzyme uses the electrochemical proton gradient across the membrane to drive the following reaction: $NADH + NADP^+ + H^+_{out} = NAD^+ + NADPH + H^+_{in}$. The reaction was shown to be reversible *in vitro* (Van de Stadt *et al.*, 1971; Earle and Fisher, 1980; Vandock *et al.*, 2011). The reversed *in vivo* action of the transhydrogenase would result in proton translocation over the cytoplasmic membrane which could in turn be used for ATP formation via ATP synthase. Nonetheless, this mechanism for energy conservation is purely theoretical, it has not been observed yet.

2.5.4. End-product efflux

The group of Konings (Otto *et al.*, 1980; Otto *et al.*, 1982; Konings, 1985; ten Brink *et al.*, 1985) has shown that *Streptococcus cremoris* is able to generate an IMF by end-product efflux. The gradient of the end-product lactic acid over the plasma membrane was used as driving force by means of a lactate-proton symporter. Consequentially, the intracellular lactate concentration has to be larger than the extracellular concentration. van Maris *et al.* (2004) calculated that the intracellular concentration has to be approximately thousand times higher at pH 7, and about a million times higher at pH 2, to drive the translocation of one proton per lactate ion. This shows that although build-up of an IMF by means of product efflux may have benefits in natural habitats with low product concentration, this mechanism seems irrelevant for industrial application at high product concentrations.

2.5.5. ATPase: converting IMF into ATP and vice versa

Microorganisms with a fermentative metabolism can convert ATP into IMF and vice versa by means of membrane-bound ATPases. Based on structure and physiological role, these ion-pumping ATPases can be divided into three categories, the rotary F-type and V-type ATPases that consist of multiple subunits and the much simpler P-type ATPases. Structurally, the F-type and V-type ATPases have several similarities and may share a common evolutionary

origin with archaeal (A-type) ATPases (Grüber *et al.*, 2001). Their function, in general, is however opposite. F-type ATPases, found in eukaryotes and prokaryotes, mostly produce ATP. In contrast, the V-type ATPases, mainly located in organellar membranes such as the vacuolar membrane, couple ATP hydrolysis to proton pumping across the membrane (Beyenbach and Wieczorek, 2006). Similarly, the P-type plasma membrane H^+/ATPase of plants and fungi is mostly involved in proton extrusion at the expense of ATP (recently reviewed by Palmgren and Morsomme (2019)). As such, the V-type and plasma-membrane P-type H^+/ATPases are mostly involved in generation of IMF used to transport substrates or ions over the plasma or organellar membrane, respectively (Russnak *et al.*, 2001; Beyenbach and Wieczorek, 2006; Cyert and Philpott, 2013; Deprez *et al.*, 2018). Together they are vital for the regulation of intracellular and intra-organellar pH (Deprez *et al.*, 2018). Seen the importance of the V- and P-type ATPase activity for several biological processes in eukaryotes, there seems little room for engineering opportunities with respect to energy conservation. The biological role of the F-type ATPases is, as mentioned before, overall different and mostly in ATP synthesis from IMF. These ATPases are found in the plasma membrane of prokaryotes, the inner-mitochondrial membrane or thylakoid membranes. The F_0F_1-types H^+/ATPases of prokaryotes were recently reviewed by Neupane *et al.* (2019). The H^+/ATP ratio is of importance, as it shows how efficiently both forms of energy can be interconverted. The H^+/ATP stoichiometries of the F_0F_1-ATPase in *E. coli* is between 3 and 4 (Jiang *et al.*, 2001b; Arechaga *et al.*, 2002). For yeasts and chloroplasts, the H^+/ATP rate was found to differ with nearly one proton per ATP: for yeast mitochondrial F-ATPase the ratio was 3, for spinach chloroplasts this ratio was 4 (Petersen *et al.*, 2012). Such differences in ratio for F-type ATP synthases are mostly attributed to differences in subunit stoichiometry and may offer an opportunity to alter metabolic energy conservation from IMF (Tomashek and Brusilow, 2000; Petersen *et al.*, 2012). For V-type ATPases the H^+/ATP ratio is established at 2 protons extruded per ATP hydrolyzed (Grabe *et al.*, 2000; Tomashek and Brusilow, 2000) whereas the ratio for plasma-membrane P-type H^+/ATPase is even lower at 1 (Serrano, 1991; Burgstaller, 1997). These

lower H^+/ATPase ratios are directly coupled to their biological function as proton extrusion mechanisms against a chemical gradient.

2.6. Relationship between redox potential and energy generation

The redox potentials of most redox couples mentioned in this manuscript are plotted in **Figure 7** and – as such – offer the opportunity to reflect on SLP and IMF build-up based on redox potentials. The redox couples can be subdivided into several chemical categories based on their redox potential.

The oxidative decarboxylation of 2-oxoacids – pyruvate and 2-oxoglutarate to acetate and succinate respectively – represents the redox couples with the lowest redox potentials. The redox potential difference with NAD^+/NADH is larger than the 224 mV required for SLP. SLP is realized by binding CoA, the exchange of CoA with inorganic phosphate (Pi) and the concomitant phosphorylation of ADP (See section 4). Even when the reactions are combined with binding CoA, for instance, oxidizing pyruvate and 2-oxoglutarate to acetyl-CoA and succinyl-CoA respectively, there is still a sufficient redox potential difference with NAD^+/NADH. The difference may not be enough to support SLP, but certainly sufficient to potentially contribute to the build-up of an IMF. An example is the fermentation of L-glutamate (Herrmann *et al.*, 2008). The reduced ferredoxin formed during this process can be used to reduce NAD^+ and generate a Na^+ ion-motive force. Recently, Orsi *et al.* (2020) inferred that Rnf is involved at high substrate concentration while it is not necessary at concentrations below 1 mM as the reaction becomes more exergonic.

The next group represents the organic acid/aldehyde redox couples. The ones with the lowest redox potential – acetate/acetaldehyde, butyrate/butyraldehyde and 3-phospho-glycerate/glyceraldehyde-3-phosphate – support SLP. When these oxidations involve binding CoA or Pi, so resulting in the formation of acetyl-CoA, butyryl-CoA or 1,3-bisphosphoglycerate respectively, the redox

potential difference with NAD^+/NADH becomes too small to contribute to the generation of additional IMF. The redox potentials of gluconate/glucose and 6-phosphogluconate/glucose-6-phosphate are relatively high for this class of redox couples and these therefore not contribute to either SLP or the build-up of IMF but can reduce $NADP^+$.

The next group represents the oxidative decarboxylation of organic acids without an oxo-group on the 2-carbon position. The redox potential difference with NAD^+/NADH is not enough to support SLP. The redox potential is however low enough to regenerate NADPH.

The redox cofactors NAD^+/NADH, $NADP^+$/NADPH and Fd_{ox}/Fd_{red} represent a group with intermediate redox potentials. The redox potential difference between Fd_{ox}/Fd_{red} and NAD^+/NADH is sufficient to contribute to generating an IMF. The redox potential difference between $NADP^+$/NADPH and NAD^+/NADH could in theory be sufficient to support IMF generation, but this has not been shown yet (See section 5).

The groups representing the reduction of aldehydes to alcohols and 2-oxoacids to amino acids are able to receive electrons from NAD^+/NADH. The redox potential difference E_m' of some redox couples with NAD^+/NADH seems to be large enough to support the build-up of an IMF but, in reality, this does – as far as we know – not occur. This may be caused by the fact that the alcohols and amino acids are often end products at high concentrations, which rises the redox potential.

The reduction of carbon-carbon double bonds is the class with the highest redox potential. The E_m' difference with the redox cofactors is sufficient to support SLP, but this is not described in literature. Instead, the transfer of electrons from NAD^+/NADH to this class of redox couples is used to contribute to IMF build-up.

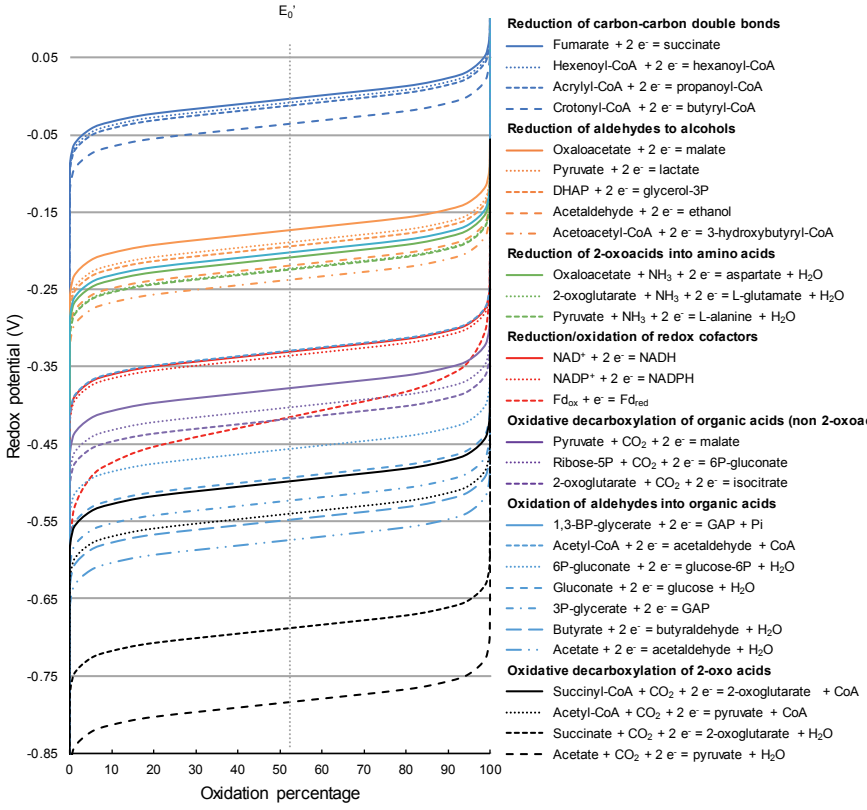

Figure 7. Redox potential profile of various couples as a function of the oxidation percentage. The colors depict the type of chemical reaction in the redox couples. Dark blue: reduction of carbon-carbon double bonds, orange: reduction of aldehydes to alcohols, green: reduction of 2-oxo acids into amino acids, red: reduction and oxidation of redox cofactors, purple: oxidative decarboxylation of organic acids, light blue: oxidation of aldehydes into organic acids and black: oxidative decarboxylation of 2-oxo acids. The graph is limited to a maximum redox potential of 0.1 V since redox couples with higher potentials are involved in respiration. The values were calculated using eQuilibrator 2.2.

These observations with respect to redox potential of classes of redox couples and the mechanism of energy conservation they support, are a valuable tool for the design of metabolic networks for product formation.

2.7. Energy-saving systems

Increasing energy efficiency of cells can be achieved by implementing energy-conserving reactions as mentioned in SLP and IMF sections. On the other hand, preventing loss of energy during energy-requiring processes is equally important. Energy-intensive reactions are, for instance, binding of CoA and Pi, carboxylation reactions and transport of solutes inside and outside the cells.

2.7.1. Preventing energy input for binding of CoA and CO_2

The energy released during hydrolysis of CoA and Pi bonds can be used for ATP formation by the action of a kinase. However, creation of such bonds requires the input of energy. For instance, conversions of acetate to acetyl-CoA and propionate to propionyl-CoA have a very high ΔG_m' of 47 ± 1 and 58 ± 6 kJ/mol, respectively, and therefore require the input of ATP. Preventing energy input to bind CoA is a viable strategy to increase energy efficiency in cells. Enzymes such as CoA-transferases can be implemented in the product pathway to conserve energy.

2.7.1.1. Saving energy input for CoA binding using CoA-transferases

CoA-transferases can limit the energy input as they catalyse the reversible transfer of a CoA moiety from an acyl-CoA thioester to a free carboxylic acid. These reactions do not require any cofactor nor activation of the carboxylic acid. CoA-transferases are usually divided in three classes based on substrate specificity, acyl transfer mechanisms and sequences. The Class I CoA-transferases consist of enzymes found primarily in fatty acid metabolism that act on 3-oxo acids, short-chain fatty acids and (*E*)-gluconate and use succinyl-CoA and acetyl-CoA as primary CoA donors. The Class II only comprises two enzymes: acetyl-CoA:citrate CoA-transferase (EC 2.8.3.10) and acetyl-CoA:citramalate CoA-transferase (EC 2.8.3.11). These enzymes are the homodimeric α subunits of citrate and citramalate lyases (EC 4.1.3.6 and EC 4.1.3.22), respectively. The Class III enzymes transfer CoA in a highly substrate-, stereo-specific manner. They are found in the 3-hydroxypropionate cycle of CO_2 fixation and in the metabolism of oxalate, toluene, carnitine and other

aromatic compounds. A non-exhaustive list of the reactions catalyzed by CoA-transferases is given in **Table 8**. These enzymes are able to catalyze more reactions than given in the table with various levels of activities. More details can be found in the Brenda database based on the EC number of the enzymes. Protein engineering can be employed to increase activities of enzymes towards certain reactions and also low activities are therefore of interest for cell factory design.

Table 8. Non-exhaustive list of reactions catalyzed by CoA-transferases. More substrates have been tested for the different CoA-transferases with different level of activities. For more information about the substrates that have been tested with the different CoA-transferases, see Brenda database.

EC #	Enzymes	Reactions
2.8.3.1	Propionate CoA-transferase	Acetyl-CoA + Propionate = Acetate + Propionyl-CoA Propionyl-CoA + (*R*)-lactate = Propionate + (*R*)-lactoyl-CoA Propionyl-CoA + (*S*)-lactate = Propionate + (*S*)-lactoyl-CoA Butyryl-CoA + Acetate = Butyrate + Acetyl-CoA Acetyl-CoA + (*S*)-lactate = Acetate + (*S*)-lactoyl-CoA Acetyl-CoA + (*R*)-lactate = Acetate + (*R*)-lactoyl-CoA
2.8.3.10	Citrate CoA-transferase	Acetyl-CoA + Citrate = Acetate + (3*S*)-citryl-CoA Acetyl-dephospho-CoA + Citrate = Acetate + (3*S*)-citryl-dephospho-CoA Acetyl-[acyl-carrier protein] + Citrate = Acetate + (3*S*)-citryl-[acyl-carrier protein]
2.8.3.11	Citramalate CoA-transferase	Acetyl-CoA + (*S*)-citramalate = Acetate + (*S*)-citramalyl-CoA Acetyl-[acyl-carrier protein] + Citramalate = Acetate + Citramalyl-[acyl-carrier protein] Succinate + (3*S*)-citramalyl-CoA = Succinyl-CoA + citramalate
2.8.3.12	Glutaconate CoA-transferase	Acetyl-CoA + *trans*-gluconate = Acetate + (2*E*)-glutaconyl-CoA Acetyl-CoA + Glutarate = Acetate + Glutaryl-CoA Acetyl-CoA + (*R*)-2-hydroxyglutarate = Acetate + (*R*)-2-hydroxyglutaryl-CoA Acetyl-CoA + Propenoate = Acetate + Propenoyl-CoA Acetyl-CoA + Propionate = Acetate + Propionyl-CoA
2.8.3.13	Succinate-hydroxymethylglutarate CoA-transferase	Succinyl-CoA + 3-hydroxy-3-methylglutarate = Succinate + (3S)-hydroxy-3-methylglutaryl-CoA Malonyl-CoA + 3-hydroxy-3-methylglutarate = Malonate + (3*S*)-hydroxy-3-methylglutaryl-CoA
2.8.3.14	5-hydroxypentanoate CoA-transferase	Acetyl-CoA + 5-hydroxypentanoate = Acetate + 5-hydroxy-pentanoyl-CoA
2.8.3.15	Succinyl-CoA:(*R*)-benzylsuccinate CoA-transferase	Succinyl-CoA + (*R*)-2-benzylsuccinate = Succinate + (*R*)-2-benzylsuccinyl-CoA
2.8.3.15	Succinyl-CoA:(*R*)-benzylsuccinate CoA-transferase	Succinyl-CoA + (*R*)-2-benzylsuccinate = Succinate + (*R*)-2-benzylsuccinyl-CoA

2.8.3.16	Formyl-CoA transferase	Formyl-CoA + Oxalate = Formate + Oxalyl-CoA Formyl-CoA + Succinate = Formate + Succinyl-CoA
2.8.3.17	Cinnamoyl-CoA:phenyllactate CoA-transferase	(*E*)-cinnamoyl-CoA + (*R*)-3-phenyllactate = *trans*-cinnamate + (*R*)-3-phenoyllactoyl-CoA (2*R*)-2-hydroxy-3-(4-hydroxyphenyl)propionate + (*E*)-4-coumaroyl-CoA = *trans*-4-coumarate + (*R*)-3-(4-hydroxyphenyl)lactoyl-CoA (*E*)-3-(indol-3-yl)acryloyl-CoA + (*R*)-3-(indol-3-yl)lactate = (*E*)-3-(indol-3-yl)acrylate + (*R*)-3-(indol-3-yl)lactoyl-CoA (*E*)-cinnamoyl-CoA + 3-phenylpropionate = (*E*)-cinnamate + 3-phenoylpropionate
2.8.3.18	Succinyl-CoA:acetate CoA-transferase	Succinyl-CoA + Acetate = Succinate + Acetyl-CoA
2.8.3.19	CoA:oxalate CoA-transferase	Acetyl-CoA + Oxalate = Acetate + Oxalyl-CoA Formyl-CoA + Acetate = Formate + Acetyl-CoA Formyl-CoA + Oxalate = Formate + Oxalyl-CoA
2.8.3.2	Oxaloate CoA-transferase	Succinyl-CoA + Oxalate = Succinate + Oxalyl-CoA
2.8.3.20	Succinyl-CoA-D-citramalate CoA-transferase	Succinyl-CoA + (3*R*)-citramalate = Succinate + (3*R*)-citramalyl-CoA Succinyl-CoA + (*R*)-malate = Succinate + (*R*)-malyl-CoA Succinyl-CoA + Itaconate = Succinate + Itaconyl-CoA
2.8.3.21	L-carnitine CoA-transferase	γ-butyrobetainyl-CoA + (R)-carnitine = 4-(trimethylamino)butyrate + (R)-carnitinyl-CoA Crotonobetainyl-CoA + (R)-carnitine = Crotonobetaine + (R)-carnitinyl-CoA
2.8.3.22	Succinyl-CoA-L-malate CoA-transferase	Succinyl-CoA + (S)-malate = Succinate + (S)-malyl-CoA Succinyl-CoA + Itaconate = Succinate + Itaconate Succinyl-CoA + (3S)-citramalate = Succinate + (3S)-citramalyl-CoA
2.3.3.23	Caffeate CoA-transferase	Hydrocaffeyl-CoA + (E)-caffeate = 3-(3,4-dihydroxyphenyl)propionate + (E)-caffeyl-CoA Hydrocaffeyl-CoA + 4-coumarate = 3-(3,4-dihydroxyphenyl)propionate + 4-coumaroyl-CoA Hydrocaffeyl-CoA + Ferulate = 3-(3,4-dihydroxyphenyl)propionate + Feruloyl-CoA

2.8.3.24	(*R*)-2-hydroxy-4-methylpentanoate CoA-transferase	4-methylpentanoyl-CoA + (*R*)-2-hydroxy-4-methylpentanoate = 4-methylpentanoate + (*R*)-2-hydroxy-4-methylpentanoyl-CoA
2.8.3.25	Bile acid CoA-transferase	Lithocholoyl-CoA + Cholate = Litocholate + Choloyl-CoA Deoxycholoyl-CoA + Cholate = Deoxycholate + Choloyl-CoA
2.8.3.3	Malonate CoA-transferase	Acetyl-CoA + Malonate + Acetate + Malonyl-CoA
2.8.3.5	3-oxoacid CoA-transferase	Succinyl-CoA + a 3-oxoacid = Succinate + a 3-oxoacyl-CoA Succinyl-CoA + Acetoacetate = Succinate + Acetoacetyl-CoA Succinyl-CoA + 3-oxopropionate = Succinate + 3-oxopropionyl-CoA Succinyl-CoA + 3-oxopentanoate = Succinate + 3-oxopentanoyl-CoA Succinyl-CoA + 3-oxo-4-methylpentanoate = Succinate + 3-oxo-4-methylpentanoyl-CoA Succinyl-CoA + 3-oxohexanoate = Succinate + 3-oxohexanoyl-CoA
2.8.3.6	3-oxoadipate CoA-transferase	Succinyl-CoA + 3-oxoadipate = Succinate + 3-oxoadipyl-CoA
2.8.3.8	Acetate CoA-transferase	Acyl-CoA + Acetate = a fatty acid anion + Acetyl-CoA Butyryl-CoA + Acetate = Butyrate + Acetyl-CoA Pentanoyl-CoA + Acetate = Pentanoate + Acetyl-CoA Succinate + Acetyl-CoA = Succinyl-CoA + Acetate
2.8.3.9	Butyrate-acetoacetate CoA-transferase	Butyryl-CoA + Acetoacetate = Butyrate + Acetoacetyl-CoA
2.8.3.B1	(*R*)-2-hydroxyisocaproate CoA-transferase	4-methylpent-2-enoyl-CoA + (*R*)-2-hydroxy-4-methylpentanoate = 4-methylpent-2-enoate + (*R*)-2-hydroxy-4-methylpentanoyl-CoA
2.8.3.B3	Mesaconate CoA-transferase	Succinyl-CoA + Mesaconate = Succinate + 2-methylfumaryl-CoA

Implementation of CoA-transferases in product pathways has been used to increase product titer, rate and yield (Yang *et al.*, 2010; Lee *et al.*, 2012; Deng *et al.*, 2015; Wang *et al.*, 2015b; Yu *et al.*, 2015; Chen *et al.*, 2018). Deng *et al.* (2015) replaced the native butyryl-CoA:acetate CoA transferase of *Thermobifida fusca* by an exogenous one with higher activity to increase butyrate titers. Yang *et al.* (2010) successfully engineered *E. coli* to produce polylactic acid (PLA) by expressing a heterologous pathway containing propionyl-CoA transferase from *Clostridium propionicum* and polyhydroxyalkanoate (PHA) synthase 1 from *Pseudomonas* sp. MBEL6-19. The enzyme activities were further enhanced by random and directed mutagenesis.

Some CoA-transferases have been shown to transfer CoA to a wide range of substrates from various CoA donors *in vitro*. These enzymes could therefore be used to increase pathway yield and conserve energy for other reactions than the ones they perform *in vivo*. Nevertheless, CoA-transferases show different levels of activity depending on the substrates used. Mutagenesis and adaptive laboratory evolution (ALE) could be used to increase their expression and activity.

2.7.1.2. Preventing energy input for binding CO_2 to increase energy efficiency of microorganisms – examples of fatty acid synthesis

Fatty acid synthesis (**Figure 8A**) from sugars is thermodynamically feasible without energy input as indicated by a ΔG_0' of the conversion of glucose into dodecanoate of -856 ± 31 kJ/mol dodecanoate. However, at a metabolic level ATP input is required. Glycolysis yields one ATP per fatty acid elongation, but the activation of acetyl-CoA to malonyl-CoA and the conversion of NADH produced in glycolysis to NADPH used in fatty acids synthesis requires a total input of 2 ATP. The breakdown pathway of fatty acids, β-oxidation, is very similar to the fatty acid synthesis pathway (**Figure 8B**). The algae *Euglena gracilis* is able to reverse this β-oxidation pathway to convert paramylon into wax esters, so in the fatty acid synthesis direction. It is able to do so because it uses an NADH-dependent enoyl-CoA reductase instead of a combination of acyl-CoA dehydrogenase and Etf. This reverse β-oxidation pathway is able to use acetyl-

CoA instead of malonyl-CoA, bypassing an ATP-requiring carboxylation step (Inui *et al.*, 1984a) (**Figure 8C**). Dellomonaco *et al.* (2011) have applied reverse β-oxidation successfully in *E. coli* and production of fatty acids has improved over the last years (Mehrer *et al.*, 2018). In general, this shows that biosynthetic pathways, like the fatty acid synthesis, are not necessarily operating at the highest energetic efficiency, and that more efficient pathways can be designed for product formation.

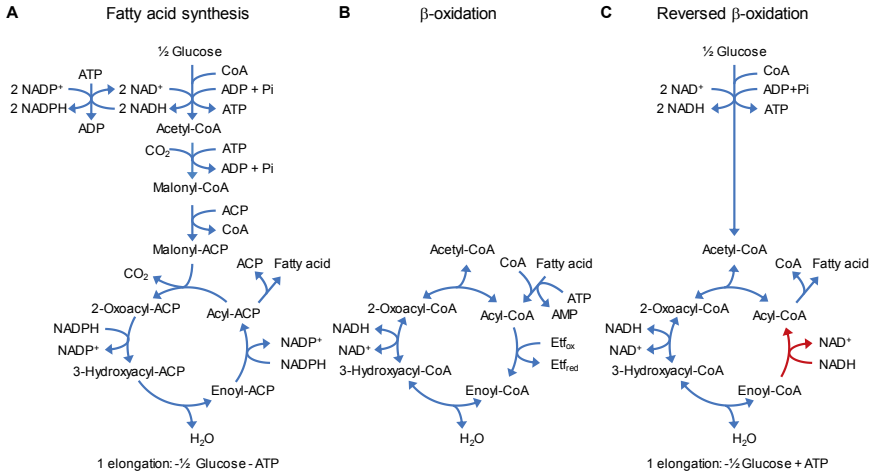

Figure 8. Fatty acid synthesis pathways. (A) Fatty acid chain elongation by the fatty acid synthesis pathway requires ATP input in the conversion of acetyl-CoA into malonyl-CoA and for the upgrade of NADH produced in glycolysis to NADPH required for fatty acid synthesis. **(B)** The β-oxidation pathway is chemically very similar. The acyl-CoA dehydrogenase/Etf determine the direction of the cycle towards fatty acid breakdown. **(C)** Reversal of the β-oxidation pathway is possible by introducing an NADH-dependent trans-enoyl-CoA reductase (red arrow) and results in a pathway that generates 1 ATP per chain elongation.

2.7.2. Energy conservation by transcarboxylation

Carboxylation reactions are often considered bottlenecks in metabolic pathways as they require energy input. This is of particular importance in CO_2-fixing bacteria such as Clostridia. Most of these reactions are coupled – directly or indirectly – to ATP hydrolysis, which provides the energy necessary for the

carboxylation step (Bar-Even *et al.*, 2012). The energy loss during such conversions can be avoided using transcarboxylases.

Transcarboxylases or carboxyl transferases transfer a carboxyl group between compounds, allowing the reactions to run near equilibrium and preventing high energy input. Replacing carboxylases by transcarboxylases would reduce the energetic cost of such reaction and allow microorganisms to dedicate a higher amount of ATP for other purposes. Such an example is the fermentation of lactate to propionate.

Propionibacteria convert lactate into propionate and acetate. The conversion of lactate into acetate yields one ATP, but also results in net reduction of NAD^+. The conversion of lactate into propionate is used to regenerate NAD^+. The pathway used can conserve metabolic energy via proton translocation at the reduction of succinate to fumarate (see paragraph 2.5.1.1). It also requires the carboxylation of pyruvate to oxaloacetate and the decarboxylation of (*S*)-methyl-malonyl-CoA to propionyl-CoA. If these reactions would be performed separately by pyruvate carboxylase (EC 6.4.1.1) and methylmalonyl-CoA decarboxylase (EC 7.2.4.3) this would require the input of ATP, severely reducing the overall energy yield (**Figure 9A**). Instead, the carboxylation of pyruvate to oxaloacetate is coupled to the decarboxylation of (*S*)-methyl-malonyl-CoA to propionyl-CoA (**Figure 9A**). This transcarboxylation reaction, performed by methylmalonyl-CoA carboxytransferase (EC 2.1.3.1), has a $\Delta G_0'$ of -2 ± 10 kJ/mol, close to equilibrium. This enzyme has a relaxed specificity as it is also able to perform the following transcarboxylations: acetoacetyl-CoA + oxaloacetate = 3-oxoglutaryl-CoA + pyruvate; acetyl-CoA + oxaloacetate = malonyl-CoA + pyruvate and butyryl-CoA + oxaloacetate = ethylmalonyl-CoA + pyruvate (Swick and Wood, 1960). As far as we are aware this way of energy conservation has not been used to design efficient metabolic networks for product formation yet.

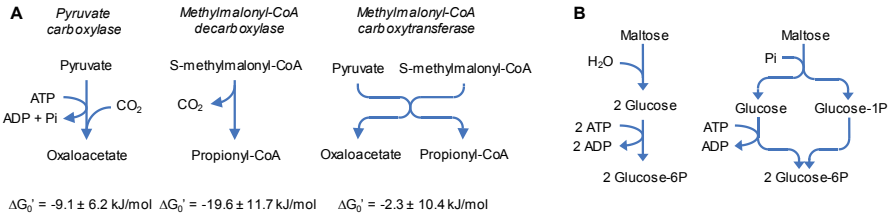

Figure 9. (A) Hydrolysis and phosphorylation of sugars. **(B)** Conversion of pyruvate to propionyl-CoA via either a combination of pyruvate decarboxylase and methylmalonyl-CoA decarboxylase or via methylmalonyl-CoA carboxytransferase.

2.7.3. Preventing energy input for extracellular transport (nutrient uptake and product excretion)

Transport of substrates and products over the microbial plasma membrane is an integral part of fermentation processes. In many studies homologous and heterologous transporters have been expressed to modify substrate specificity, growth and product formation (Zaslavskaia *et al.*, 2001; Hernández-Montalvo *et al.*, 2003; Wieczorke *et al.*, 2003; De Anda *et al.*, 2006; Doebbe *et al.*, 2007; Subtil and Boles, 2011; Young *et al.*, 2011; Wang *et al.*, 2015a; Shin *et al.*, 2018). Several transport mechanisms are available which differ with respect to the requirement of metabolic energy input (Jahreis *et al.*, 2008). Equipping the microbial cell factories with energy-independent transport systems is evidently important if fermentation processes have a negative ΔG', but the metabolic network is unable to harvest this energy.

2.7.3.1. Substrate influx

The substrate concentration in fermentation processes can be controlled by applying fed-batch or chemostat cultivation and by limiting concentrations of nutrients other than the carbon source. The substrate concentration can then be high enough to use its concentration gradient over the membrane as driving force. Input of metabolic energy is in such case not necessary.

Proton and Na^+ ion symporters use the ion-motive force to drive solute transport. Weusthuis *et al.* (1993) determined the ATP costs of proton symport of maltose in *S. cerevisiae*, in comparison with glucose transported by means of facilitated

diffusion. Proton symport required the input of 1 ATP per maltose. ATP-binding-cassette transporters (ABC-transporters) also require the input of ATP. ATP/substrate stoichiometries from 1 to 50 have been reported (Patzlaff *et al.*, 2003). Both mechanisms are therefore able to drive solute translocation against the concentration gradient, but at the expense of metabolic energy.

Facilitated sugar transporters (Barrett *et al.*, 1999; Jahreis *et al.*, 2008; Leandro *et al.*, 2011) use the concentration gradient of the solute over the plasma membrane as driving force, and therefore do not require the input of metabolic energy. Phosphoenolpyruvate:sugar phosphotransferase systems (PTS) use the energy released in the conversion of phosphoenolpyruvate to pyruvate to phosphorylate sugars and simultaneously import the sugar (Jahreis *et al.*, 2008). PTS systems are classified as active transport systems (Saier, 1977; Jeckelmann and Erni, 2019), but do not require energy that would be otherwise available for metabolism. Instead, energy that would be dissipated as heat is used to transport the sugar.

Facilitated sugar transporters and PTS are therefore the mechanisms of choice to engineer fermentation processes with net ATP output. Because PTS systems require the conversion of phosphoenolpyruvate into pyruvate, their application for products relying on phosphoenolpyruvate but not pyruvate is limited (Floras *et al.*, 1996; Hernández-Montalvo *et al.*, 2003; Nakamura and Whited, 2003; De Anda *et al.*, 2006; Shin *et al.*, 2018; Yang *et al.*, 2018). Sugar facilitator transporters have been identified in mammals, yeasts and bacteria (Wieczorke *et al.*, 2003; Jahreis *et al.*, 2008; Leandro *et al.*, 2011). Several groups have successfully expressed the glucose facilitator of *Zymomonas mobilis* in *E. coli* strains (Snoep *et al.*, 1994; Parker *et al.*, 1995; Weisser *et al.*, 1995) and human glucose facilitators in *S. cerevisiae* (Wieczorke *et al.*, 2003).

PTS systems occur in eubacteria, a few archaebacteria but not in plants and animals (Jeckelmann and Erni, 2019). They consist of two cytoplasmic phosphotransferase proteins (EI and HPr) and a variable number of sugar specific enzyme II complexes. Thompson *et al.* (2001) and Pikis *et al.* (2006)

have introduced homologous enzymes II proteins to change the substrate specificity of *Klebsiella pneumoniae* and *E. coli*, respectively.

2.7.3.2. Product efflux

Efflux systems in bacteria and their metabolic engineering applications have recently been reviewed by Jones *et al.* (2015) and Kell *et al.* (2015). They play a critical role in alleviating feedback inhibition and product toxicity. Overexpression of the transporters generally results in titer improvements (Jones *et al.*, 2015), also in fungi (Steiger *et al.*, 2019). Most of these studies however cover aerobic production systems in which sufficient metabolic energy is available to use active transport systems. The role of efflux systems in fermentative metabolism has received less attention.

The selling price of a product is inversely correlated with the final titer of a product (Hoek *et al.*, 2003). Fermentation processes often aim at the production of low value, bulk products. The desired final titer is therefore high and is generally between 50 and 200 g/L. This implies that the intracellular concentration is even higher when facilitated diffusion is used. Active forms of transport will be able to maintain lower intracellular concentrations and as such could alleviate product inhibition and toxicity. To date however identification of all exporters involved in organic acids excretion remains challenging as illustrated by the work of Mans *et al.* (2017) on lactic acid excretion in yeasts.

Table 1 shows that in natural fermentation processes in general 1 ATP is generated per mole of product. Consequently, product efflux has to rely on mechanisms that require substantially less than 1 mol ATP to transport 1 mol of product. Diffusion of small uncharged molecules or facilitated diffusion and symporters are therefore the mechanisms of choice.

The relationship between the input of Gibbs free energy and the gradient of product that can be reached over the plasma membrane has been assessed by van Maris *et al.* (2004) for the production of lactic acid and 3-hydroxypropionic acid in *S. cerevisiae*.

2.7.4. Using the energy available in glycosidic bonds

Disaccharides and oligosaccharides belong to the main sugar sources used in biotechnological applications. The $\Delta G_0'$ of the hydrolysis of the glycosidic bonds connecting the constituent monosaccharides is about -22 to -38 kJ/mol. Microorganisms like *Saccharomyces cerevisiae* and *E. coli* typically apply sugar hydrolases in order to use these carbon sources, and the ΔG' is dissipated as heat (**Figure 9B**). The monosaccharides are subsequently phosphorylated, e.g. by hexokinase, glucokinase or the PTS system, requiring the input of ATP. Other microorganisms are able to use sugar phosphorylases: e.g. maltose is converted into glucose-1-P and glucose by incorporation of inorganic phosphate. This reaction has a $\Delta G_0'$ of -8 ± 2 kJ/mol. The glucose-1-phosphate is subsequently isomerized to glucose-6-phosphate by phosphoglucomutase (**Figure 9B**). Consequently, the $\Delta G_0'$ available in the glycosidic bond is used to phosphorylate the sugar and as such reduces the input of ATP. This has been realized for cellobiose (Sadie *et al.*, 2011; Ha *et al.*, 2013), maltose (de Kok et al., 2011), and sucrose (Marques et al., 2018) in *Saccharomyces cerevisiae* as well as for maltodextrin and cellodextrin (Puchart, 2015). The increased energetic efficiency was reflected by higher biomass yields obtained under anaerobic conditions in the maltose and sucrose cases.

2.7.5. Pyrophosphate

Pyrophosphate (PPi) is released in the production of DNA, RNA, proteins, membrane lipids, etc. (Gutiérrez-Luna *et al.*, 2018). It is concomitantly hydrolyzed to inorganic phosphate by inorganic pyrophosphatase, rendering the PPi-releasing reactions virtually irreversible (Kornberg, 1957). The phosphate-phosphate bond of PPi is energy-rich (**Table 2**). If product formation involves the release of PPi, conservation of this energy may proof to be beneficial.

Two types of inorganic pyrophosphatases have been recognized: soluble and membrane-bound versions (Gutiérrez-Luna *et al.*, 2018). The membrane-bound versions translocate protons or Na^+ ions over the membrane, generating an IMF, and could as such contribute to conserving energy **(Figure 10A**). Such a step

is present during caffeate respiration in *A. woodii*. Prior being reduced, caffeate is first activated to caffeyl-CoA by AMP-, PPi-forming caffeyl-CoA synthetase (Hess *et al.*, 2011). Then, PPi is hydrolyzed by a membrane-bound pyrophosphatase which couples the hydrolysis to Na^+ ions translocation (Biegel and Müller, 2011).

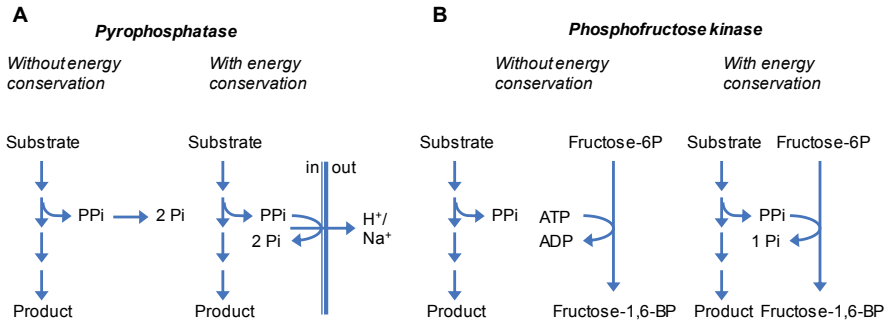

Figure 10. Energy conservation using PPi hydrolysis by **(A)** membrane-bound pyrophosphatases and **(B)** PPi-dependent phosphofructokinases.

In some microorganisms PPi is a central energy carrier (Bielen *et al.*, 2010). They harbor a pyrophosphate-dependent phosphofructokinase. This opens another energy-conserving option: if product formation involves PPi release, PPi can serve instead of ATP to phosphorylate fructose-6-phosphate (See **Figure 10B**).

A third option is the reaction catalyzed by pyruvate phosphate dikinase (PPDK), converting phosphoenolpyruvate and AMP with pyrophosphate into pyruvate and ATP (Cui *et al.*, 2020). Sufficient AMP should be present in the cell in order to conserve the energy in PPi by the PPDK reaction. A way to generate this required amount of AMP is by employing the enzyme adenylate kinase (EC 2.7.4.3).

Consequently, the soluble pyrophosphatase activity must be low or absent in order for these two energy-conserving options to be successful.

2.8. Concluding remarks and future perspectives

Conservation of metabolic energy is one of the limiting factors during fermentative product formation. Here, we reviewed the mechanisms available in microorganisms to conserve energy as well as to reduce unnecessary energy expenditure. We distinguished general and product-specific methods to conserve metabolic energy. General methods like energy-independent transporters, mechanisms that use the difference in redox potential between redox couples or using disaccharides are the most interesting because they can be applied in many fermentation processes regardless the product of interest. Substrate-level phosphorylation is one of the main sources of energy under fermentative conditions. It is however usually a product-specific method (with the exception of the reaction catalyzed by phosphorylating glyceraldehyde-3-phosphate dehydrogenase) and therefore cannot be applied in general. Some enzymes contributing to SLP have a broad substrate specificity *in vitro* and appear to be a good option. However, the thermodynamics of such reactions may not allow SLP to function under physiological conditions and should therefore be considered carefully.

The options to increase energy conservation described in this review should not be applied to maximize energy conservation *per se* but be used to optimize product formation. Just as too little energy conservation has detrimental effect on product formation, the same holds for too much energy conservation, as it moves the overall reaction to a thermodynamical equilibrium and may result in decreased product yield caused by excess biomass formation.

Nowadays, a lot of research is directed towards improving product titer, productivity and yield by either overexpressing enzymes involved in product pathways, knocking out competing pathways or using redox neutral metabolic networks. However, little research is done on using metabolic energy in a more efficient way. Energy conservation is a means to achieve high titer, productivity and yield during microbial processes. Understanding and applying the various

mechanisms available in microorganisms to conserve energy is therefore a key step towards improving fermentative product formation.

Chapter 3

Changing the cofactor dependency of dihydrolipoyl dehydrogenase and its impact on *Escherichia coli* metabolism

Pauline L. Folch, Coen Besseling, Lorena Tejada Garcia, Gerrit Eggink, Ruud A. Weusthuis

Abstract

Biosynthesis of various industrially relevant compounds such as terpenoids or amino acids requires the input of NADPH. Sufficient NADPH supply can be challenging as its regeneration capacity is low in the cells. Different strategies have been applied in the past to increase NADPH production such as redirecting the flux towards NADPH-producing pathways or engineering $NADP^+$-dependent enzymes. The dihydrolipoyl dehydrogenase (LPD) contributes significantly to NAD^+ reduction under aerobic conditions therefore engineering its cofactor specificity towards $NADP^+$ is a valuable strategy for the production of NADPH-requiring compounds.

In this study, we introduced modifications in *lpd* gene of *E. coli* to change the cofactor specificity of PDH and ODH from NAD^+ to $NADP^+$. The modified PDH complex showed a 7.6-fold higher apparent activity with $NADP^+$ than NAD^+ but showed to be inhibited by NADPH and – to a lesser extent – NADH. Therefore, another mutation (E354K) was introduced in the *lpd* gene to overcome NAD(P)H limitation. The resulting LPD enzyme showed to be less sensitive to both NADH and NADPH. After successful engineering of the LPD specificity, fermentations were performed to assess the impact of changing cofactor specificity on *E. coli* metabolism. Anaerobically, no differences were observed as the pyruvate formate-lyase (PFL) was active. However, under aerobic conditions *E. coli* strains carrying an $NADP^+$-dependent PDH complex were able to grow albeit they showed lower growth rates than strains carrying an NAD^+-dependent PDH and accumulated pyruvate. Our results indicate that introduction of an $NADP^+$-dependent PDH caused a surplus of NADPH and there is insufficient regeneration of $NADP^+$.

3.1. Introduction

NAD^+, $NADP^+$ and their reduced forms have a crucial role in the metabolism of microorganisms by acting as electron carriers. Even though they have a similar chemical structure, they have divergent functions. In heterotrophic microorganisms, NAD^+ is primarily involved in oxidation reactions – for both anabolic and catabolic processes - and is regenerated by respiration or fermentation. NADPH is used for reduction reactions – primarily, but not exclusively – in anabolic reactions. NADPH is mainly regenerated by the oxidative part of the pentose phosphate pathway (PPPox), by the TCA cycle enzyme isocitrate dehydrogenase and transhydrogenases (Sauer *et al.*, 2004). $NADP^+$ can be produced from NAD^+ by NAD^+ kinase (Kawai *et al.*, 2001).

Various natural products formed during biosynthetic processes such as terpenoids, amino acids, antibiotics and polymers are of industrial importance (Kabus *et al.*, 2007; Park *et al.*, 2014; Kim *et al.*, 2015). Their synthesis often relies on NADPH-dependent enzymes. Moreover, the efficiency of microbial production of such compounds depends on the availability of precursors and cofactors. The anabolic NADPH regeneration capacity is however relatively low compared to the catabolic capacity to reduce NAD^+. Therefore, enhancing NADPH availability in microorganisms has gained interest (Lee *et al.*, 2013; Wang *et al.*, 2013c; Spaans *et al.*, 2015; Han and Liang, 2018). Many groups have reported successful increase in NADPH production by either diverting the flux through the oxidative PPP (Lim *et al.*, 2002; Chemler *et al.*, 2010; Lee *et al.*, 2010), by changing the cofactor dependency of NAD^+-dependent enzymes towards $NADP^+$ (Bocanegra *et al.*, 1993; Martínez *et al.*, 2008; Wang *et al.*, 2013a) or by engineering/overexpressing enzymes involved in cofactor regeneration and synthesis, *e.g.* transhydrogenases and NAD^+ kinase (Canonaco *et al.*, 2001; Kabus *et al.*, 2007; Li *et al.*, 2009; Lee *et al.*, 2010; Bastian *et al.*, 2011). For example, Martínez *et al.* (2008) replaced the native GAPDH of *E. coli* by an $NADP^+$-GAPDH from *C. acetobutylicum* and successfully increased the production of lycopene and ε–caprolactone.

Dihydrolipoyl dehydrogenase (LPD) catalyzes NAD^+ reduction in the pyruvate dehydrogenase complex (PDH) and the oxoglutarate dehydrogenase complex (ODH) (Pettit and Reed, 1967; Guest and Creaghan, 1972; Guest and Creaghan, 1973). PDH catalyzes the irreversible conversion of pyruvate and CoA into acetyl-CoA and CO_2 while reducing NAD^+ to NADH. ODH catalyzes a similar oxidative decarboxylation reaction, converting 2-oxoglutarate into succinyl-CoA. PDH and ODH are multi-enzyme complexes consisting of three catalytic subunits: pyruvate or 2-oxoglutarate dehydrogenase (E1), dihydrolipoyllysine-residue acetyltransferase or succinyltransferase (E2) and LPD (E3).

LPD carries the NAD^+ binding site and is subjected to allosteric NADH inhibition (Schmincke-Ott and Bisswanger, 1981; Wilkinson and Williams, 1981; Sahlman and Williams, 1989) with a K_i of 0.009-0.016mM in case of the PDH complex (Schmincke-Ott and Bisswanger, 1981). As a consequence, PDH and ODH are highly expressed and active under aerobic conditions. Under anaerobic conditions the NADH concentration is higher, resulting in diminished PDH and ODH activities. Anaerobically, the role of the PDH complex is taken over by pyruvate formate-lyase (PFL) (Clark, 1989; Snoep *et al.*, 1993a; Quail *et al.*, 1994; Kim *et al.*, 2008). ODH is repressed and succinyl-CoA synthetase generates succinyl-CoA from succinate for anabolic reactions (Amarasingham and Davis, 1965; Gray *et al.*, 1966; Guest *et al.*, 1992).

Under aerobic conditions LPD contributes significantly to the reduction of NAD^+. Changing the cofactor dependency of LPD towards $NADP^+$ is therefore a viable strategy for enhancing NADPH bioavailability in the cells. Bocanegra *et al.* (1993) successfully created an $NADP^+$-dependent LPD by introducing 7 amino acid mutations in the *lpd* gene: G185A, G189A, E203V, M204R, F205K, D206H, P210R. However, they did not characterize the impact of such a change on *E. coli* metabolism. Furthermore, Kim *et al.* (2008) lowered the NADH sensitivity by introducing a single E354K mutation in the *lpd* gene. This change resulted in a 10-times higher *Ki*, allowing the PDH complex to be more active under anaerobic conditions. As NADH and NADPH have very similar structures, it

cannot be excluded that the PDH complex is also inhibited by NADPH and that the same E354K mutation could potentially reduce this NADPH sensitivity.

In this study, we investigated the impact of an $NADP^+$-dependent LPD on *E. coli* metabolism under both aerobic and anaerobic conditions. To this end, we first created and introduced different *lpd* variants in *E. coli* Δ*lpd* to change the cofactor dependency and lower the sensitivity of PDH towards NADH. We performed enzymatic assays to confirm that the introduced mutations resulted in a change of cofactor specificity. Moreover, NADH and NADPH inhibition assays were conducted to assess if an $NADP^+$-dependent PDH complex was subjected to either NADH or NADPH inhibition. Finally, we analyzed the impact of an $NADP^+$-dependent LPD on growth and formation of fermentation products by cultivating the strains under aerobic and anaerobic conditions on minimal medium.

3.2. Material and methods

3.2.1. Bacterial strains and plasmids

The bacterial strains and plasmids used in this study are listed in **Table 1**. All strains are derivatives of wild-type *E. coli* BW25113.

Table 1. Strains and plasmids used in this study.

Strains and plasmids	Characteristics[b]	References
Strains		
BW25113	F-, Δ*(araD-araB)567*, Δ*lacZ4787(::rrnB-3), λ*$^-$, *rph-1*, Δ*(rhaD-rhaB)568*,*hsdR514*	CGSC[a]
Δ*lpd*	BW25113 Δ*lpd*-734::*kan*	CGSC[a]
Δ*pflB*	BW25113 Δ*pflB*727::*kan*	CGSC[a]
Δ*ldhA* Δ*lpd*	BW25113 Δ*pflB* Δ*sthA* Δ*ldhA* Δ*lpd* marker free	This study
BW25113 (DE3)	BW25113 DE3 T7 RNA polymerase	Vuoristo *et al.* (2014)
BW25113 (DE3) Δ*ldhA*	BW25113 Δ*ldhA* DE3 T7 RNA polymerase marker free	This study
Plasmids		
pBbA2k-RFP	*p15A, P_{tet} - kan, tet, mRFP1*	Lee *et al.* (2011)
pBbA2k empty	*p15A, P_{tet} - kan, tet*	This study
pBbA2k WT-*lpd*	pBbA2k empty derivative, *P_{lpd} - lpd, T_{lpd}*	This study
pBbA2k $LPD_{low\ inhib}$	pBbA2k empty derivative, *P_{lpd} - lpd 1AA, T_{lpd}*	This study
pBbA2k LPD_{NADP}	pBbA2k empty derivative, *P_{lpd} - lpd 17A, T_{lpd}*	This study
pBbA2k $LPD_{NADP+low\ inhib}$	pBbA2k empty derivative, *P_{lpd} - lpd 8AA, T_{lpd}*	This study
pKD13	*oriR6K gamma, tL3LAM, bla, rrnB, kan, FRT*	CGSC[a]
pKD46	*repA101*(Ts), *P_{araB}-gam-bet-exo, oriR101, bla, araC*	CGSC[a]
pCP20	*repA101*(Ts), *bla*, *cm*, *flp*	CGSC[a]
pCas9	*repA101*(Ts) *kan P_{cas}-cas9 P_{araB}-gam-bet-exo lacI^q P_{trc}-sgRNA-pMB1*	Jiang *et al.* (2015)
pTargetF-*lpd*	*pMB1, spec, gRNA* scaffold, target for *lpd* gene, 200 bp flanking *lpd*	This study
pTargetF-*ldhA*	*pMB1, spec, gRNA* scaffold, target for *ldhA* gene, 200 bp flanking *ldhA*	This study

[a]Coli Genetic Stock Centre

[b]*kan*: kanamycin resistance gene; *tet*: tetracycline resistance gene; *bla*: ampicillin resistance gene; *cm*: chloramphenicol resistance gene; *spec*: spectinomycin resistance gene; Ts: temperature sensitive; *P_{araB}-gam-bet-exo:* Lambda-Red recombinase gene under arabinose inducible promoter; FRT: flippase recognition site; *flp*: flippase gene under thermal induction.

3.2.2. Creation of knock-out strains

The *sthA* gene encoding the soluble transhydrogenase was knocked out using the Lambda-Red mediated recombination according to the protocol described by Datsenko and Wanner (2000).

E. coli BW25113 Δ*pflB* (Baba *et al.*, 2006) was transformed with the pKD46 plasmid and cultured in the presence of 10 mM L-arabinose to induce Lambda-

Red recombinase expression. The gene of interest *sthA* was then replaced by a cassette containing a kanamycin resistance gene flanked by two flippase recognition sites (FRT). To do so, the cassette was PCR amplified from pKD13 using Phusion high-fidelity DNA polymerase (Thermo Scientific) and primers including 50 bp homologous flanking regions of the *sthA* gene and 20 bp of the FRT site. The cells were then electroporated with the deletion cassette and transformants were screened by applying kanamycin selection pressure and performing colony PCR using DreamTaq DNA polymerase (Thermo Scientific). The colonies harboring the correct genotype were subsequently transformed with pCP20, plasmid encoding the flippase recombinase gene, to remove the kanamycin resistance gene. The temperature sensitive plasmid pCP20 was cured by culturing the strains on liquid LB medium at 42°C overnight. The strain was checked by sequencing. The sequences used to disrupt the *sthA* gene are listed in **Table S1**.

The genes encoding lactate dehydrogenase (*ldhA*) and lipoamide dehydrogenase (*lpd*) were knocked out using the method previously described by Jiang *et al.* (2015). The pCas and pTargetF plasmids were a gift from Sheng Yang (Addgene plasmid #62225 and #62226) (Jiang *et al.*, 2015). The flanking regions used for deletion of *ldhA* and *lpd* are listed in **Table S1**.

All steps were carried out at 30°C unless stated otherwise to maintain the temperature sensitive plasmid pCas9. *E. coli* BW25113 Δ*pflB* Δ*sthA* was transformed with temperature sensitive pCas9 plasmid. The strain harboring pCas9 was subsequently transformed with pTargetF-*ldhA* plasmid carrying an *ldhA* knock-out specific cassette. The cassette consisting of *SpeI* promoter, target sequence, gRNA and 200 bp flanking regions of the *ldhA* gene was synthesized as gBlock (IDT) and assembled with pTargetF using Hifi DNA Assembly kit (NEB). Cells were screened by selecting for kanamycin and spectinomycin resistances and by colony PCR using DreamTaq DNA polymerase (Thermo Scientific) and primers targeting the flanking regions of the *ldhA* gene. The pTargetF-*ldhA* plasmid was then cured by plating the correct transformants on kanamycin plate containing 0.5 mM IPTG. *E. coli* BW25113

Δ*pflB* Δ*sthA* Δ*ldhA* pCas9 was transformed with pTargetF-*lpd* plasmid to knock out *lpd* gene according the same protocol. *E. coli* BW25113 Δ*pflB* Δ*sthA* Δ*ldhA* pCas9 and *E. coli* BW25113 Δ*pflB* Δ*sthA* Δ*ldhA* Δ*lpd* pCas9 were cultured at 42°C in liquid LB medium to cure pCas9. Both strains were verified by PCR for loss of the plasmid and sequenced for all knock-outs introduced. The target sequences used for targeting *ldhA* and *lpd* genes are 5'-CGATCCGTATCCAAGTGCAG-3' and 5'-GCGATTGTCGGTACTAACGG-3', respectively. In both cases, we used 200 bp flanking regions upstream and downstream the genes for recombination.

3.2.3. Plasmid construction

The expression vector pBbA2k-RFP was a gift from Jay Keasling (Addgene plasmid # 35327) (Lee *et al.*, 2011). The expression vector pBbA2k-RFP was used to express the four different versions of the *lpd* gene under the native *lpd* promoter, P_{lpd}, and terminator of *E. coli*. The four versions of the gene include: native *lpd* gene from *E. coli* BW25113, *lpd* carrying one amino acid mutation E354K (Kim *et al.*, 2008), *lpd* carrying 7 amino acid mutations G185A, G189A, E203V, M204R, F205K, D206H, P210R (Bocanegra *et al.*, 1993) and *lpd* carrying 8 amino acid mutations E354K, G185A, G189A, E203V, M204R, F205K, D206H, P210R. All cassettes including promoter, *lpd* gene and terminator were synthesized by GenScript, USA. The cassettes were PCR amplified to introduce *EcoRI* and *XhoI* restriction sites using a forward primer 5'-GCCTGAGAATTCTAGACAAATCGGTTGCCGTTTGTTG-3' and a reverse primer 5'-GCCATCCTCGAGTTACTTCTTCTTCGCTTTCGGGTTC-3', respectively. Cassettes and pBbA2k-RFP plasmid were digested using FastDigest enzymes *EcoRI* and *XhoI* (Thermo Scientific) and ligated using T4 DNA ligase (Thermo Scientific). The ligated plasmids were checked by PCR and sequencing.

3.2.4. Culture media

For plasmid construction and gene expression analysis, *E. coli* strains were grown on Luria Bertani (LB) agar plates or liquid medium at either 30°C or 37°C.

All recombinant strains harboring temperature sensitive plasmids were grown at 30°C whereas curing of the pCP20 and pCas9 were performed at 42°C.

3.2.5. Cultivation in shake flasks and anaerobic flasks

All cultivations were performed in a Kuhner shaker at 37°C and agitation rate of 250 rpm. The strains were grown overnight in 50 mL LB medium supplemented with 50 µg/mL kanamycin if necessary. For aerobic cultivations, 5 mL of the overnight preculture was transferred to 45 mL M9 minimal medium in 250 mL Erlenmeyer flasks. For anaerobic cultivations, 5 mL of the overnight preculture was transferred to 95 mL M9 minimal medium in 250 mL Erlenmeyer flasks. The minimal medium (MM) contained: 1 x M9 salts, 50 mM glucose, 2 mM $MgSO_4$, 1 mM $CaCl_2$, 1 mL/L US^{Fe} trace elements (Bühler *et al.*, 2003) and 50 µg/mL kanamycin. The medium was buffered to a pH of 6.9 with 44 mM KH_2PO_4 and 47.5 mM Na_2HPO_4. The next day, cells were harvested by centrifugation at 4700 rpm for 5 min at room temperature and inoculated into 50 mL MM to an OD_{600nm} of 0.2 in either 250 mL shake flasks for aerobic cultivation or 200 mL serum bottle for anaerobic cultivation. The anaerobic serum bottles were previously flushed with nitrogen to ensure strict anaerobic conditions.

3.2.6. Cell free extract preparation

Biological duplicates were grown on LB medium and cells were harvested from exponentially growing shake flasks cultures by centrifugation at 4700 rpm for 10 min at 4°C and stored at -20°C. Prior cell free extract preparation, the pellets were thawed on ice and resuspended in ice-cold 50 mM potassium phosphate buffer pH 8.0, 100 mM NaCl, 1 mM EDTA and 1 mM dithiothreitol (prepared fresh). Cell free extracts were prepared using a tissue homogenizer (Precellys 24, Bertin Technologies) with 1 pulse of 30 sec at 6500 rpm in a 2 mL lysis Matrix E tube (MP Biomedicals). The extract obtained was centrifuged at 15,000 rpm for 10 min at 4°C to remove cells and debris. The supernatant was collected and used for protein determination and enzymatic assays.

3.2.7. Protein determination

Protein concentration of the cell free extracts was determined by using the Total Protein Kit, Micro Lowry, Onishi and Barr Modification (Sigma-Aldrich) according to manufacturer's instructions.

3.2.8. Pyruvate dehydrogenase activity assays and inhibition assays

Pyruvate dehydrogenase activity was measured at room temperature on an Infinite M200 microplate reader (Tecan) by monitoring the reduction of either NAD^+ or $NADP^+$ at 340 nm in a 100 µL reaction containing: 50 mM potassium phosphate buffer pH 8.0, 1 mM $MgCl_2$, 0.2 mM thiamine pyrophosphate, 2 mM dithiothreitol (prepared fresh), 0.2 mM coenzyme A, 2 mM L-cysteine (prepared fresh), 1.5 mM $NAD(P)^+$, 10 µL cell free extract (12.5 µg protein in reaction). The reaction was started by addition of 5 mM sodium pyruvate. The results shown are data from biological duplicates and technical triplicates. The activity of the pyruvate dehydrogenase complex was calculated using the linear initial rates of reactions. The pyruvate dehydrogenase activity is expressed as nmoles NAD(P)H produced per min per mg protein.

Inhibition assays were performed as described for the pyruvate dehydrogenase activity assays. Different concentrations of NADH or NADPH were added to the reaction mixtures to obtain NAD(P)H/$NAD(P)^+$ ratios of 0.005, 0.01, 0.02, 0.05, 0.1 and 0.2. NADH and NADPH sensitivity were assessed for both NAD^+- and $NADP^+$-dependent PDH complexes.

3.2.9. Analytical methods

The cell density was monitored by measuring the absorbance at 600 nm.

Glucose and organic acids concentrations were determined using an Agilent 1290 Infinity (U)HPLC equipped with a UV detector operated at 210 nm and a RI detector operated at 55°C. The samples were separated on a guard column (Security Guard Cartridge System, Phenomenex) and a Rezex ROA-Organic

acid H^+ (8%) column (Phenomenex) at 55°C, using 0.5 mL/min 0.005 M H_2SO_4 as eluent. 250 mM propionic acid was used as internal standard.

3.3. Results

3.3.1. Construction of the LPD variants

To create an $NADP^+$-dependent LPD, we introduced mutations for both changes in cofactor specificity and lower NADH sensitivity. To do so, we knocked out the genomic *lpd* gene from *E. coli* WT BW25513 and introduced the *lpd* variants on a pBbA2k expression vector. All versions of the gene were expressed on the plasmid under the native *lpd* promoter P_{lpd} and terminator. The *lpd* variants include: $LPD_{low\ inhib}$ carrying one amino acid mutation E354K reported by Kim *et al.* (2008) to reduce inhibition by NADH, LPD_{NADP} carrying 7 amino acid mutations G185A, G189A, E203V, M204R, F205K, D206H, P210R reported by Bocanegra *et al.* (1993) to change the cofactor dependency from NAD^+ to $NADP^+$ and $LPD_{NADP+low\ inhib}$ carrying the combined 8 amino acid mutations. Moreover, we also introduced the native *lpd* gene of *E. coli* WT BW25113 on the pBbA2k plasmid as a control (LPD_{WT}). The assembly of the plasmids was checked by PCR and sequencing prior and after transformation in *E. coli* Δ*lpd* strain. The *lpd* knock-out strain formed smaller colonies on LB plates than the wild-type strain. Strains carrying the plasmid-based NAD^+-dependent LPD variants grew like wild-type strains on LB plates, whereas the $NADP^+$-dependent ones showed intermediate behavior (data not shown).

3.3.2. Testing the cofactor dependency and reduced inhibition to NAD(P)H of the LPD variants

After successful transformation of the four strains, enzymatic assays were performed to assess if the mutations introduced in the *lpd* gene resulted in the correct properties. Cell-free extracts (CFE) obtained from shake flask cultures with LB medium were tested in presence of $NAD(P)^+$ and pyruvate. Controls without cells, sodium pyruvate or $NAD(P)^+$ did not show any increase in

absorbance at 340 nm (data not shown). **Figure 1A** shows how the absorption at 340 nm, reflecting the increase in NAD(P)H concentration caused by PDH activity, develops during time. The absorbance with CFE of *E. coli* BW25113 maximally reached 0.07, and slowly decreased thereafter. The initial apparent PDH activity was around 350 nmol NADH.min^{-1}.mg protein^{-1} (**Figure 1C**). The apparent PDH activities in cell-free extracts obtained from the *lpd* knock-out strains *E. coli* Δ*lpd* and *E. coli* Δ*lpd* + empty pBbA2k were 20-fold lower.

Introducing *lpd* on a plasmid restored the apparent PDH activity to approximately 75% of the wild-type value (**Figure 1C**). With both CFEs similar maximal absorbances were reached, 0.071 ± 0.009 for WT and 0.073 ± 0.008 for PDH_{WT} (**Figure 1A**). The pBbA2k plasmid is a medium copy plasmid therefore more LPD subunits are expressed in LPD_{WT} than in BW25113. This increased number of LPD subunits does not entail more functional PDH complex as the two other subunits AceE and AceF were not overexpressed. Since the assays were performed with CFE, the amount of PDH present in LPD_{WT} was lower than in BW25113 for the same amount of total proteins: the increased number of LPD had a diluting effect, explaining the lower PDH activity. The initial apparent activity in the cell-free extract of *E. coli* Δ*lpd* + $LPD_{low\ inhib}$ was similar compared to that of *E. coli* Δ*lpd* + LPD_{WT} (**Figure 1C**), but 50% higher maximum absorbances were reached (**Figure 1A**).

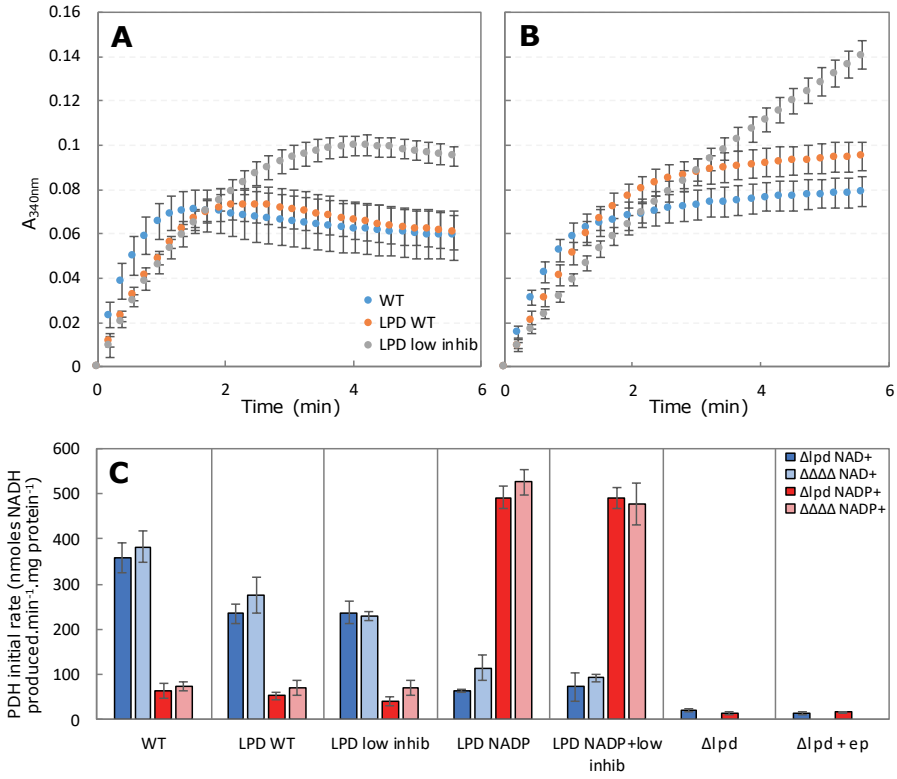

Figure 1. Absorbances profiles and activities of the PDH complexes. (A) Absorbances profiles of the PDH complexes at 340 nm using 12.5 µg proteins of *E. coli* WT BW25113, *E. coli* Δ*lpd* + LPD_{WT} and *E. coli* Δ*lpd* + $LPD_{low\ inhib}$. **(B)** Absorbances profiles of the PDH complexes at 340 nm using 10 µg proteins of *E. coli* Δ*ldhA* + pCas9 (WT), *E. coli* Δ*pflB* Δ*sthA* Δ*ldhA* Δ*lpd* + LPD_{WT} and *E. coli* Δ*pflB* Δ*sthA* Δ*ldhA* Δ*lpd* + $LPD_{low\ inhib}$. **(C)** PDH activities measured using 1.5 mM NAD^+ or $NADP^+$ as cofactor. The values are expressed as nmoles NAD(P)H produced.min^{-1}.mg $protein^{-1}$ and are calculated as the average of biological duplicates and technical triplicates. The error bars represent the standard deviations.

The CFE of *E. coli* WT BW25113 (WT), *E. coli* Δ*lpd* + LPD_{WT} and *E. coli* Δ*lpd* + $LPD_{low\ inhib}$ exhibited 5.6-, 4.5- and 5.8-times higher apparent PDH activity when NAD^+ was used as cofactor. *E. coli* Δ*lpd* + LPD_{NADP} and *E. coli* Δ*lpd* + $LPD_{NADP+low\ inhib}$ presented 7.6- and 6.7-times higher apparent PDH activity using $NADP^+$ as cofactor, respectively (**Figure 1C**). Moreover, both LPD_{NADP} and $LPD_{NADP+low\ inhib}$ showed higher apparent PDH activities than the NAD^+-dependent PDH complexes. Even though LPD_{WT} and $LPD_{low\ inhib}$ presented similar initial rates during the assays, the maximum A_{340nm} for $LPD_{low\ inhib}$ was

40% higher than the one for LPD_{WT} (**Figure 1A**). Enzymatic assays were also performed to test the cofactor dependency of the ODH complex and similar results were obtained (data not shown).

A decrease in absorbance was observed at the end of the assays (**Figure 1A**), suggesting the presence of enzymes consuming pyruvate and the NADH formed by PDH. This may have obscured the effect of lower NAD(P)H inhibition. To test the presence of an enzyme reducing pyruvate which could interfere with the NAD(P)H sensitivity assays, we performed an NAD(P)H consumption experiment in the presence of pyruvate. To do so, we used the CFE of our negative control strains *E. coli* Δ*lpd* and *E. coli* Δ*lpd* + empty pBbA2k which showed very low apparent PDH activity. A decrease in absorbance would therefore indicate that one or more other enzymes are using NAD(P)H and pyruvate.

With an initial NADH concentration of 0.3 mM NADH in the assay, the absorbance dropped from 1.1 to 0.2 (**Figure 2A**). This decrease demonstrates the presence of an NADH-utilizing enzyme in the CFE. The most likely candidate is lactate dehydrogenase (LDH) which catalyzes the conversion of pyruvate and NADH into lactate and NAD^+. On the other hand, only a small decrease in absorbance (0.05) was observed when adding NADPH to the reactions (**Figure 2B**). In *E. coli*, LDH can only function using NADH as cofactor (Tarmy and Kaplan, 1968; Clark, 1989). Therefore, this small decrease indicates the presence of other enzymes using NADPH.

For the reasons mentioned above, we decided to determine the apparent PDH activities of the LPD variants expressed in a Δ*ldhA* Δ*lpd* strain. The cultivation of these strains under anaerobic conditions did not result in lactate formation.

All the initial apparent PDH activities measured were not significantly different from the ones determined in *E. coli* Δ*lpd* strains (**Figure 1C**). However, differences in the final A_{340nm} were observed. For a same *lpd* variant, all curves obtained with strain Δ*ldhA* Δ*lpd* reached higher final A_{340nm} than the ones with *E. coli* Δ*lpd* strains and did not decrease thereafter (**Figure 1A** and **1B**).

Furthermore, the apparent activity of $LPD_{low\ inhib}$ did not show significant levelling off and exhibited a more linear absorbance increase in time (**Figure 1B**).

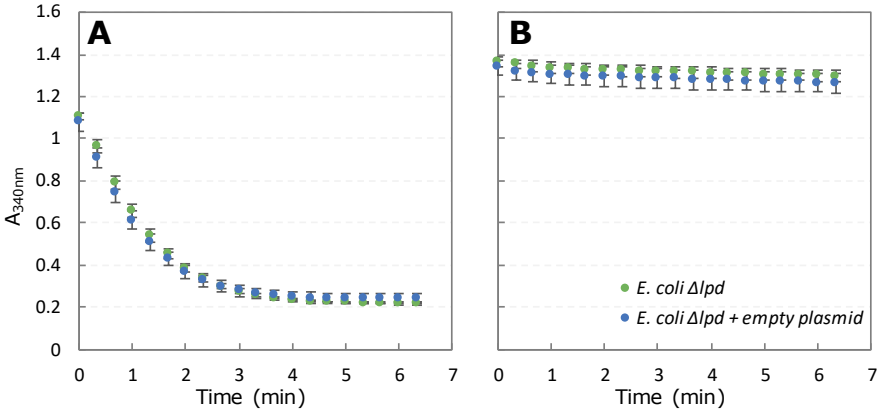

Figure 2. NADH (A) and NADPH (B) consumption profiles based on the absorbances measured at 340 nm. The assays were performed using 5 mM pyruvate, 1.5 mM NAD^+ and 0.3 mM NAD(P)H as substrates. The values shown represent the average of biological duplicates and technical triplicates with standard deviations.

3.3.3. NAD(P)H inhibition assays

The sensitivity towards NADH and NADPH of the mutated PDH complexes was determined using cell-free extract of aerobically grown *E. coli* Δ*ldhA* Δ*lpd,* 5 mM of sodium pyruvate, 1.5 mM of $NAD(P)^+$ and varying the concentration ratio of NADH and NADPH. The different ratios used were 0.005, 0.01, 0.02, 0.05, 0.1 and 0.2 (mol/mol). Moreover, we used the oxidized cofactor which proved to work during the PDH activity assays: NAD^+ for WT, LPD_{WT} and $LPD_{low\ inhib}$ and $NADP^+$ for LPD_{NADP} and $LPD_{NADP+low\ inhib}$. The results are shown in **Figure 3**, in which the change of absorbance in time is plotted. The experiments were performed using biological duplicates and technical triplicates. **Figure 3** shows the results without error bars, **Figure 1** and **Figure 2** of the **supplementary material** section show the results with error bars of the inhibition assays for NAD^+-dependent PDH and $NADP^+$-dependent PDH complex, respectively. WT and LPD_{WT} gave identical results, the WT results can be found in the **Figure S1.**

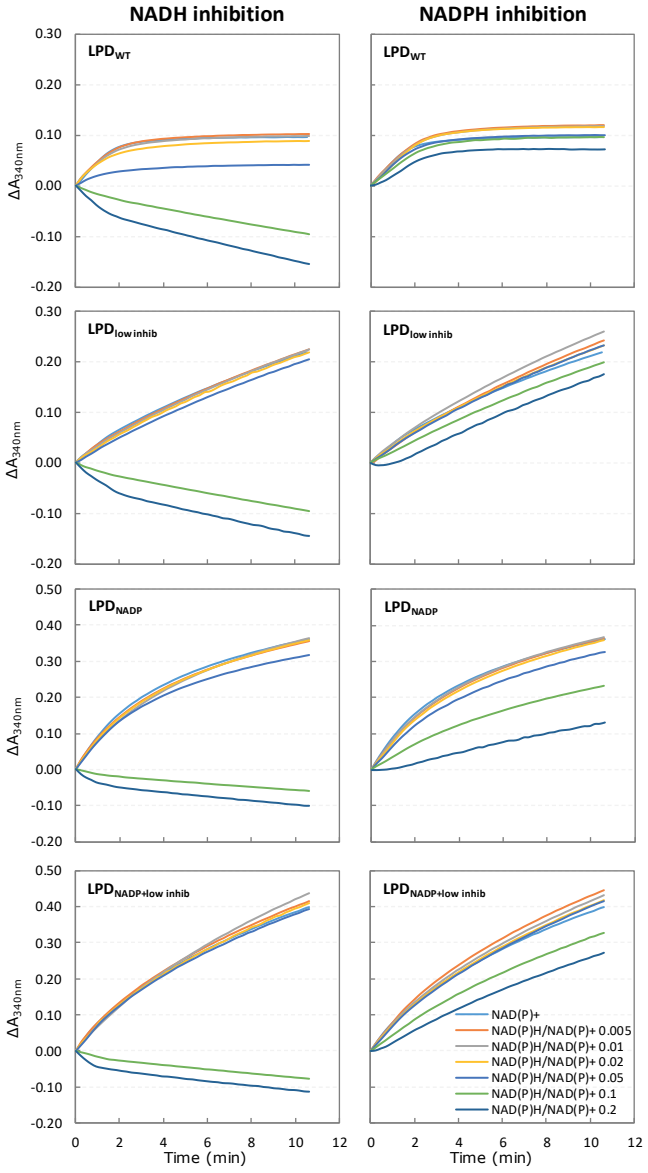

Figure 3. Inhibition assays for different NAD(P)H/NAD(P)$^+$ ratios. On the left, the graphs obtained during NADH inhibition assays and **on the right**, the graphs obtained during NADPH inhibition assays. NAD$^+$ was used as a cofactor for *E. coli* Δ*pflB* Δ*sthA* Δ*ldhA* Δ*lpd* + LPD$_{WT}$ and *E. coli* Δ*pflB* Δ*sth*A Δ*ldhA* Δ*lpd* + LPD$_{low\ inhib}$ whereas NADP$^+$ was used as cofactor for *E. coli* Δ*pflB* Δ*sthA* Δ*ldhA* Δ*lpd* + LPD$_{NADP}$ and *E. coli* Δ*pflB* Δ*sthA* Δ*ldhA* Δ*lpd* + LPD$_{NADP+low\ inhib}$. The values shown were corrected for the initial A$_{340nm}$ and expressed as ΔA$_{340nm}$. The same graphs with standard deviations can be found in **Figure S1** and **Figure S2**.

At NADH/NAD(P)$^+$ ratios 0.1 and 0.2, a decrease in absorbance (< 0.18) was visible for all CFE tested (**Figure 3**). However, NADH was consumed at a much lower rate than reported in **Figure 2**. Although the introduced knock-outs reduced the consumption of NADH significantly, one or more enzymes were still present and consumed the NADH formed by the NAD$^+$-dependent PDH complexes. $LPD_{low\ inhib}$ results showed less pronounced differences caused by the increasing initial NADH concentrations compared to LPD_{WT}: the conversions did not reach a plateau and higher absorbance differences were reached. Regarding NADPH inhibition assays, all strains exhibited apparent PDH activities even at NADPH/NAD(P)$^+$ ratios of 0.1 and 0.2. LPD_{WT} and $LPD_{low\ inhib}$ showed a similar behavior than the one observed with increased NADH concentrations but to a lesser extent. Surprisingly, at the lower NADPH concentrations significantly higher absorbance differences were reached.

Both LPD_{NADP} and $LPD_{NADP+low\ inhib}$ reached much higher absorbance differences than the NAD$^+$-dependent LPD during both assays. Regarding NADPH inhibition assays, LPD_{NADP} and $LPD_{NADP+low\ inhib}$ showed similar patterns as LPD_{WT} and $LPD_{low\ inhib}$ during NADH inhibition assays. Increased NADPH/NADP$^+$ ratios resulted in lower slopes and lower absorbance differences, but $LPD_{NADP+low\ inhib}$ was less affected.

3.3.4. Effect of LPD variants on *E. coli* metabolism during aerobic cultivations

During aerobic cultivation on M9 medium, both *E. coli* Δ*lpd* and *E. coli* Δ*lpd* + empty pBbA2k did not show any sign of growth (not shown), confirming that a functional LPD is indispensable for aerobic growth on mineral medium. Expressing the four *lpd* variants on a plasmid restored growth. *E. coli* WT BW25113 and *E. coli* Δ*lpd* + LPD_{WT} showed similar growth profiles and specific growth rates (**Figure 4A** and **4B**, and **Table 2**), indicating that expression of the *lpd* gene on a plasmid does not have consequences for aerobic growth of the strains. The strain carrying $LPD_{low\ inhib}$ showed similar growth profiles and growth rates to the strain expressing LPD_{WT}. On the other hand, both *E. coli* Δ*lpd* +

LPD_{NADP} (**Figure 4D**) and *E. coli* Δ*lpd* + $LPD_{NADP+low\ inhib}$ (**Figure 4E**) exhibited significantly lower growth rates than strains carrying an NAD^+-dependent LPD (**Table 2**).

Table 2. Specific growth rates (μ) for aerobic and anaerobic cultivations. The values are expressed in h^{-1} and represent the average of the specific growth rates calculated from two biological replicates with standard deviations.

Strain	Aerobic	Anaerobic
E. coli BW25113 WT	0.63 ± 0.00	0.36 ± 0.02
E. coli Δ*lpd*	NA[a]	0.28 ± 0.02
E. coli Δ*lpd* + empty plasmid	NA[a]	0.22 ± 0.00
E. coli Δ*lpd* + LPD_{WT}	0.60 ± 0.00	0.38 ± 0.01
E. coli Δ*lpd* + $LPD_{low\ inhib}$	0.61 ± 0.00	0.37 ± 0.01
E. coli Δ*lpd* + LPD_{NADP}	0.29 ± 0.01	0.37 ± 0.01
E. coli Δ*lpd* + $LPD_{NADP+low\ inhib}$	0.24 ± 0.01	0.38 ± 0.00

[a]NA, Not applicable.

Metabolite production by *E. coli* WT BW25113 and *E. coli* Δ*lpd* strains carrying either LPD_{WT}, $LPD_{low\ inhib}$, LPD_{NADP} or $LPD_{NADP+low\ inhib}$ was determined (**Figure 4**). The metabolite profiles of *E. coli* Δ*lpd* and *E. coli* Δ*lpd* + empty pBbA2k are not shown because the strains did not grow aerobically. The presence of fermentation products during aerobic cultivations in shake flasks such as ethanol, lactate and formate (**Figure 4**) indicates that oxygen limitation occurred in the aerobic cultivations.

As for growth, *E. coli* WT and *E. coli* Δ*lpd* + LPD_{WT} have very similar fermentation profiles. *E. coli* WT and *E. coli* Δ*lpd* + LPD_{WT} produced up to 22.2 and 21.2 mM of acetate and up to 5.7 mM and 4.1 mM of ethanol, respectively. On the other hand, *E. coli* Δ*lpd* + $LPD_{low\ inhib}$ produced less acetate (13.1 mM) and more ethanol (7.9 mM).

Both strains carrying an $NADP^+$-dependent LPD did not produce ethanol (or negligible) but produced acetate in much higher concentrations than their NAD^+-dependent counterparts. *E. coli* Δ*lpd* + LPD_{NADP} and *E. coli* Δ*lpd* + $LPD_{NADP+low\ inhib}$ produced 1.31- and 2-times more acetate than WT, respectively.

Furthermore, pyruvate accumulated up to 23 mM for *E. coli* Δ*lpd* + LPD_{NADP} and up to 41.1 mM for *E. coli* Δ*lpd* + $LPD_{NADP+low\ inhib}$, after which it was consumed. The same pattern can be seen for lactate, which *E. coli* Δ*lpd* + $LPD_{NADP+low\ inhib}$ accumulated up to 5.7 mM and consumed it completely. When glucose was completely consumed, all the pyruvate was converted into acetate. Formate was produced by all strains up to 10 mM (WT produced 10 mM formate whereas the other strains did not produce more than 6 mM). Finally, succinate was produced up to 1.2 mM for NAD^+-dependent LPD strains whereas $NADP^+$-dependent LPD strains showed no or little production.

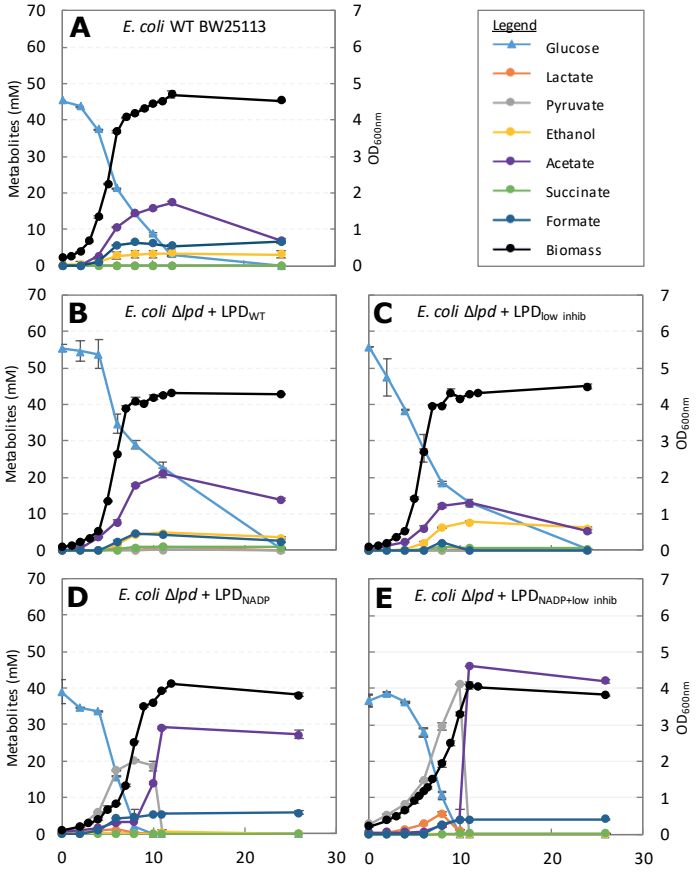

Figure 4. Aerobic cultivations on M9 medium. Both growth and fermentation profiles are shown per strain. The values represent the average of biological duplicates with standard deviations.

3.3.5. Effect of LPD variants on *E. coli* metabolism during anaerobic cultivations

Under anaerobic conditions, both *E. coli* Δ*lpd* and *E. coli* Δ*lpd* + empty plasmid strains presented a lower growth rate (**Table 2**) and reached lower final OD_{600nm} (**Figure 5F** and **5G**) than strains carrying an *lpd* variant. Furthermore, *E. coli* Δ*lpd* + empty plasmid presented a lower biomass concentration than *E. coli* Δ*lpd* which might reflect the cost of plasmid maintenance. All strains carrying an *lpd* gene presented similar growth profiles and growth rates, regardless whether the gene was expressed at genome level or on a plasmid.

Regarding fermentation products, all strains showed similar but not identical metabolite profiles (**Figure 5**). *E. coli* WT and *E. coli* Δ*lpd* + empty plasmid produced 38.4 mM and 38.2 mM formate, respectively. Strains carrying an *lpd* variant – regardless of the cofactor specificity – produced up to 28.4 mM formate. Moreover, *E. coli* WT produced up to 33.4 mM lactate and all the strains exhibiting a pBbA2k plasmid produced between 26.2 and 29.4 mM lactate. On the other hand, *E. coli* Δ*lpd* only produced 11.7 mM lactate. Furthermore, $LPD_{low\ inhib}$ produced up to 28.4 mM ethanol while all other strains produced around 20 mM ethanol. All strains produced about 20 mM of acetate. Traces of pyruvate up to 3.4 mM were detected after 12 h of cultivation and pyruvate was consumed again, except for *E. coli* Δ*lpd*.

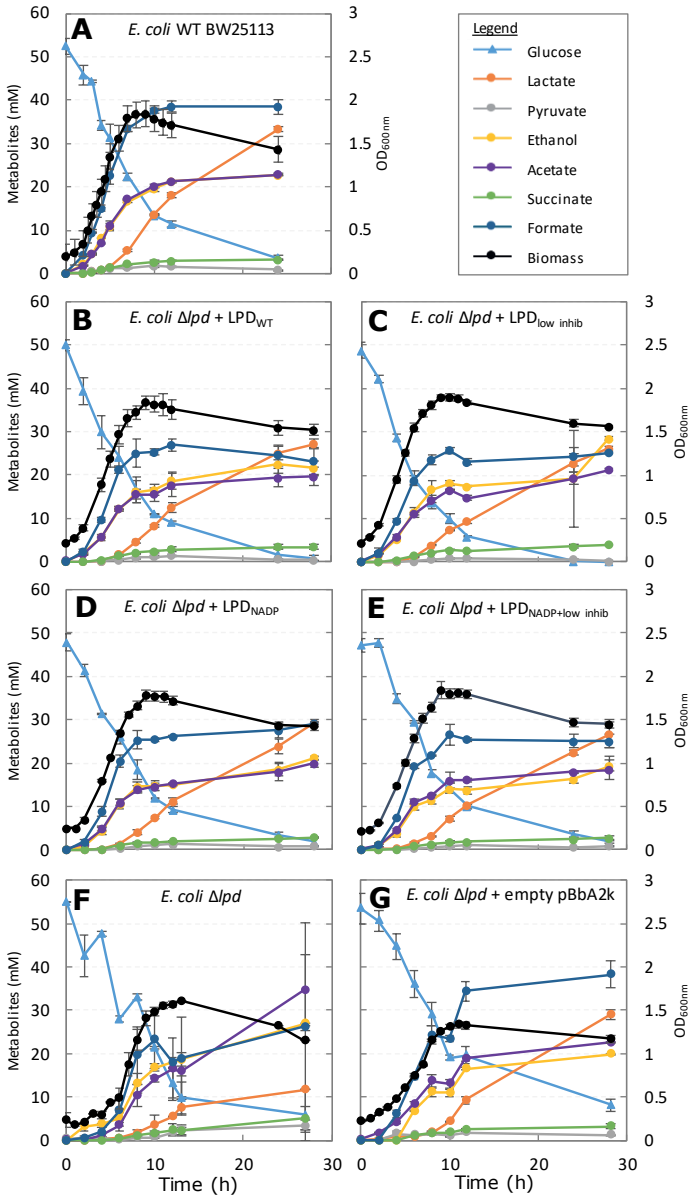

Figure 5. Anaerobic cultivations on M9 medium. Growth and fermentation profiles are presented per strain. The values shown represent the average of biological duplicates with standard deviations.

3.4. Discussion

The biotechnological production of many compounds requires reduction reactions in which NADPH is used as reducing cofactor. Several studies describe how the availability of NADPH can be increased by forcing the flux over the oxidative pentose phosphate pathway (Lim *et al.*, 2002; Lee *et al.*, 2007; Chemler *et al.*, 2010; Lee *et al.*, 2010), or by using an $NADP^+$-dependent GAPDH (Martínez *et al.*, 2008; Wang *et al.*, 2013c). LPD contributes significantly to the reduction of NAD^+, and could provide an alternative means to increase NADPH bioavailability if $NADP^+$ would be reduced. We replaced 7 amino acids in LPD to change the cofactor specificity from NAD^+ to $NADP^+$ based on Bocanegra *et al.* (1993). Furthermore, the PDH complex is known to be highly sensitive to NADH and therefore exhibits a very low activity under anaerobic conditions (Schmincke-Ott and Bisswanger, 1981; Wilkinson and Williams, 1981; Snoep *et al.*, 1993a). An $NADP^+$-specific LPD may be inhibited by NADH and presumably by NADPH as well, which is an undesired property. We therefore also introduced an E354K mutation reported to suppress the NADH inhibition of LPD (Kim *et al.*, 2008) and verified whether this also reduced putative NADPH inhibition.

To verify whether the mutations introduced in LPD result in the desired PDH properties, enzyme assays were performed using cell-free extracts of *E. coli* Δ*lpd* carrying the LPD variants. The presence of LDH made it difficult to identify putative inhibition by NAD(P)H, therefore Δ*ldhA* strains were used. We demonstrated that the seven amino acids introduced in the LPD result in a change of cofactor specificity from NAD^+ to $NADP^+$, confirming the results of Bocanegra *et al.* (1993). LPD_{WT} showed to be highly inhibited by NADH and – to a lesser extent – by NADPH. Our results confirmed that the E354K mutation results in lower NADH inhibition (Kim *et al.*, 2008), and also demonstrated lower NADPH inhibition. The *lpd* carrying the combined 8 amino acid replacements showed to be less sensitive to both NADH and NADPH. In *E. coli*, NADH inhibits LPD by competitive inhibition and by over-reducing the enzyme from a catalytically active state to an inactive state (Schmincke-Ott and Bisswanger,

1981; Wilkinson and Williams, 1981; Sahlman and Williams, 1989). Kim *et al.* (2008) showed that introduction of the E354K mutation reduced the apparent K_i of LPD for NADH by 10-fold. However, the AA at position 354 has not been identified as part of the NAD^+ binding site. It is located in the central domain of the enzyme. Therefore, Sun *et al.* (2012) proposed that the E354K mutation lowers NADH sensitivity of LPD by restraining NADH to reach the NAD^+ binding site. Following their hypothesis, the mutation could also act on NADPH by hindering its access to $NAD(P)^+$ binding site.

LPD is involved in three enzyme complexes: PDH, ODH and the glycine cleavage system (Pettit and Reed, 1967; Guest and Creaghan, 1973; Smith and Neidhardt, 1983; Steiert *et al.*, 1990). Changing the cofactor specificity of LPD will inevitably change the cofactor specificity of these enzyme complexes and this may affect growth. The glycine cleavage system is involved in the catabolism of glycine therefore we do not expect it to be affected under our growth conditions (Meedel and Pizer, 1974; Stauffer *et al.*, 1994). ODH is active under aerobic conditions as it catalyzes a key step of the TCA cycle and provides succinyl-CoA for amino acid synthesis (Guest *et al.*, 1992). Consequently, an $NADP^+$-dependent LPD is likely to contribute to NADPH generation during aerobic production of succinyl-CoA. Under anaerobic conditions, native ODH is severely repressed and succinyl-CoA synthetase takes over to supply succinyl-CoA from succinate (Amarasingham and Davis, 1965; Gray *et al.*, 1966; Guest *et al.*, 1992). The modified ODH are therefore not expected to play a role anaerobically.

To create *E. coli* strains with the various LPDs, the genomic *lpd* gene was knocked out and plasmid-based *lpd* genes were introduced. Expression of *lpd* on a plasmid did not result in phenotypic changes under aerobic and anaerobic conditions (**Table 2**).

E. coli Δ*lpd* was not able to grow on minimal medium under aerobic conditions, showing LPD activity is indispensable for aerobic growth. Under anaerobic conditions *E. coli* Δ*lpd* is able to grow because PFL is active (Knappe *et al.*,

1974; Sawers and Böck, 1989; Knappe and Sawers, 1990) and succinyl-CoA synthetase generates succinyl-CoA from succinate for anabolic processes (Buck *et al.*, 1986; Guest *et al.*, 1992). The growth rates are lower than wild-type rates though, showing that LPD does contribute to growth under anaerobic conditions. A functional PDH may allow increased flux for the conversion of pyruvate into acetyl-CoA and additionally the generated CO_2 may enable higher anaplerotic fluxes. This confirms previous studies that have reported that PDH is expressed and active under anaerobic conditions (Snoep *et al.*, 1993a; de Graef *et al.*, 1999). Remarkably, the strains carrying the low inhibition LPD variants did not show increased growth rates.

During aerobic cultivations, fermentation products such as lactate, ethanol and formate were formed indicating that the growth conditions became oxygen-limited. Therefore, enzymes such as LDH, PFL and alcohol dehydrogenase/aldehyde dehydrogenase (ADH) were slightly active. The presence of $LPD_{low\ inhib}$ resulted in lower formate concentrations compared to the PDH_{WT} strain indicating that $LPD_{low\ inhib}$ is indeed less susceptible to NADH inhibition. The higher flux through PDH and the accompanying increased reduction of NAD^+ to NADH may explain the shift from acetate production to ethanol production.

Changing the cofactor dependency of LPD has significant consequences under aerobic conditions. Introduction of an $NADP^+$-dependent LPD in an *E. coli* Δ*lpd* strain resulted in lower growth rates both on LB plates and in M9 shake flask cultures under aerobic conditions. In the shake flask cultures, slower growth was accompanied by accumulation of pyruvate, the substrate of PDH. Both phenomena suggest that the PDH activity was lower, but it was not supported by the enzyme assay studies which showed higher maximal activities for the $NADP^+$-dependent enzymes than the NAD^+-dependent enzymes. This suggests that changing the cofactor dependency of LPD has caused a surplus of NADPH. *E. coli* uses a soluble transhydrogenase to transfer electrons from $NADP^+$/NADPH to NAD^+/NADH (Canonaco *et al.*, 2001; Sauer *et al.*, 2004) and apparently its activity is not sufficient. This challenge to regenerate $NADP^+$ will

of course be less significant when NADPH-dependent product formation is applied.

The accumulated pyruvate was rapidly converted into acetate when glucose was depleted from the medium. Apparently, glucose depletion triggered the derepression or induction of the transhydrogenase or pyruvate oxidase (POX). POX catalyzes the oxidative decarboxylation of pyruvate into acetate and CO_2. It has been reported to significantly contribute to acetate formation when *E. coli* enters stationary phase (Dittrich *et al.*, 2005) and under oxygen-limited conditions where both PDH and PFL are less functional (Chang *et al.*, 1994). Consequently, POX is very likely to be responsible for the fast formation of acetate.

Both strains carrying an $NADP^+$-dependent LPD showed strongly reduced production of fermentation products. Formation of these compounds require input of NADH, and the availability of this cofactor may be limited under these conditions. This provides additional proof that the $NADP^+$-dependent complexes indeed have the cofactor specificity determined in the enzyme assays.

Under anaerobic conditions, less pronounced effects on growth and product formation were found. PDH is only carrying a small flux, as PFL is the main contributor to the conversion of pyruvate to acetyl-CoA under these conditions. Moreover, the flux to lactate and succinate bypasses PDH.

3.5. Conclusion

We were able to modify the LPD of *E. coli* in such a way that its cofactor specificity was changed from NAD^+ to $NADP^+$, and that it was less susceptible to NAD(P)H inhibition. The modified LPD was able to sustain growth, albeit at a lower growth rate and with concomitant accumulation of pyruvate. This indicates that the active $NADP^+$-dependent LPD creates an excess of NADPH in *E. coli* which the cells struggle to dissipate.

To further characterize the impact of an $NADP^+$-PDH complex on *E. coli* metabolism, a comparison of the redox flux going through each LPD would be of great interest. However, it was not possible to accurately determine such fluxes in this study. Aerobically, respiration occurs and the pathway leading to acetate production in the strains carrying an $NADP^+$-LPD is unknown. Anaerobically, presence of enzymes such as PFL and LDH do not allow proper estimation of the carbon flux going through PDH. Moreover, if NADPH excess cannot be recovered, production of lactate will occur in order to regenerate the NADH produced during glycolysis. Therefore, further work is needed to assess the impact of an $NADP^+$-dependent PDH on *E. coli* metabolism under anaerobic conditions. A first step would be the deletion of *pflB* gene encoding the pyruvate formate-lyase.

3.6. Supplementary material

Table S1. Sequences used for the disruption of the *sthA* gene using Lambda-Red recombination and flanking regions of *ldhA* and *lpd* genes for recombination after disruption using CRISPR-Cas9 system. The 50 bp flanking regions for disruption of *sthA* are underlined.

Names	Sequences (5' to 3')	Description	References
sthA H1P1*	TGTTACCATTCTGTTGCTTTTATGTATAAGAACAGGTAAGC CCTACCATGTGGTCCATATGAATATCCTC	50-bp flanking region upstream *sthA* gene + 20-bp for Cm^R gene	Baba *et al.* (2006)
sthA H2P2*	CAAGAATGGATGGCCATTTCGATAAAGTTTTAAAACAGGC GGTTTAAACCTGTAGGCTGGAGCTGCTTCG	50-bp flanking region downstream *sthA* gene + 20-bp for Cm^R gene	Baba *et al.* (2006)
lpd H1	CCGACGGATAGAACGACCCGGTGGTGGTTAGGGTATTACTT CACATACCCTATGGATTTCTGGGTGCAGCAAGGTAGCAAGC GCCAGAATCCCCAGGAGCTTACATAAGTAAGTGACTGGGGT GAGGGCGTGAAGCTAACGCCGCTGCGGCCTGAAAGACGAC GGGTATGACCGCCGGAGATAAATATATAGAGGTCATG	200-bp flanking region upstream *lpd* gene	This study
lpd H2	TTTTTCGTTTGCCGGAACATCCGGCAATTAAAAAAGCGGCTA ACCACGCCGCTTTTTTTACGTCTGCAATTTACCTTTCCAGTCT TCTTGCTCCACGTTCAGAGAGACGTTCGCATACTGCTGACCG TTGCTCGTTATTCAGCCTGACAGTATGGTTACTGTCGTTTAGA CGTTGTGGGCGGCTCTCCTGAACTTTCTCC	200-bp flanking region downstream *lpd* gene	This study
ldhA H1	TAATATCCTGATTTAGCGAAAAATTAAGCATTCAATACGGGTA TTGTGGCATGTTTAACCGTTCAGTTGAAGGTTGCGCCTACACT AAGCATAGTTGTTGATGAATTTTTCAATATCGCCATAGCTTTCA ATTAAATTTGAAATTTTGTAAAATATTTTTAGTAGCTTAAATGTG ATTCAACATCACTGGAGAAAGTCTT	200-bp flanking region upstream *ldhA* gene	This study
ldhA H2	TCTTGCCGCTCCCCTGCATTCCAGGGGAGCTGATTCAGATAAT CCCCAATGACCTTTCATCCTCTATTCTTAAAATAGTCCTGAGTC AGAAACTGTAATTGAGAACCACAATGAAGAAAGTAGCCGCGTT TGTTGCGCTAAGCCTGCTGATGGCGGGATGTGTAAGTAATGAC AAAATTGCTGTTACGCCAGAACAGCTA	200-bp flanking region downstream *ldhA* gene	This study

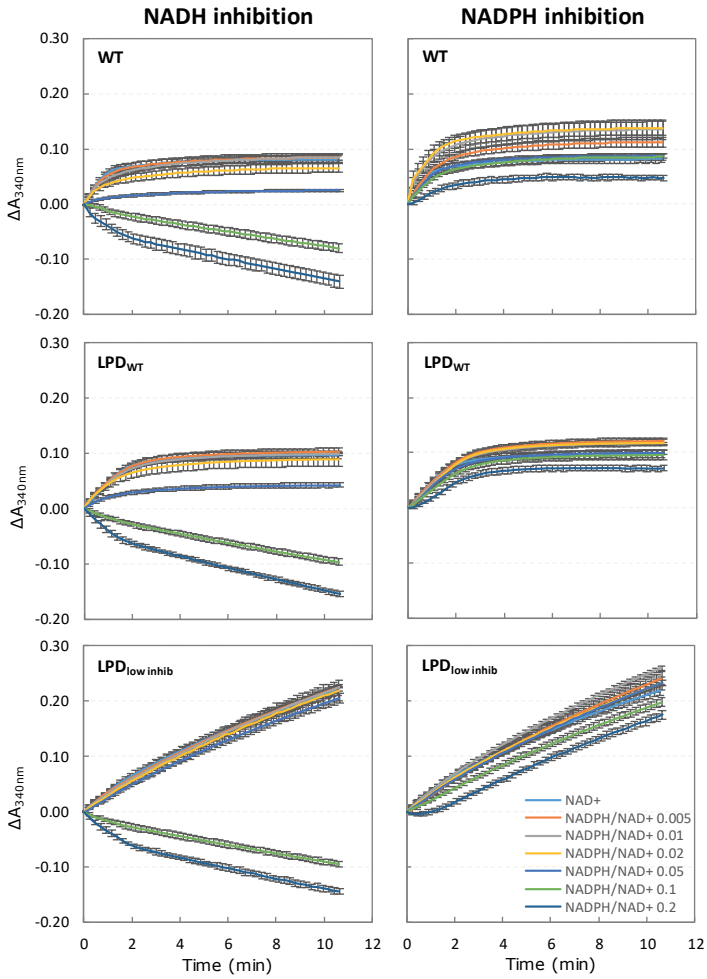

Figure S1. Inhibition assays for different NAD(P)H/NAD(P)$^+$ ratios on NAD$^+$-dependent PDH complexes with standard deviations. On the left, the graphs obtained during NADH inhibition assays and **on the right**, the graphs obtained during NADPH inhibition assays. NAD$^+$ was used as a cofactor for *E. coli* (DE3) Δ*ldhA* (WT), *E. coli* Δ*pflB* Δ*sthA* Δ*ldhA* Δ*lpd* + LPD_{WT} (LPD_{WT}) and *E. coli* Δ*pflB* Δ*sthA* Δ*ldhA* Δ*lpd* + $LPD_{low\ inhib}$ ($LPD_{low\ inhib}$). The values represent the average of biological duplicates and technical triplicates with standard deviations. The values shown were corrected for the initial A_{340nm} and expressed as ΔA_{340nm}.

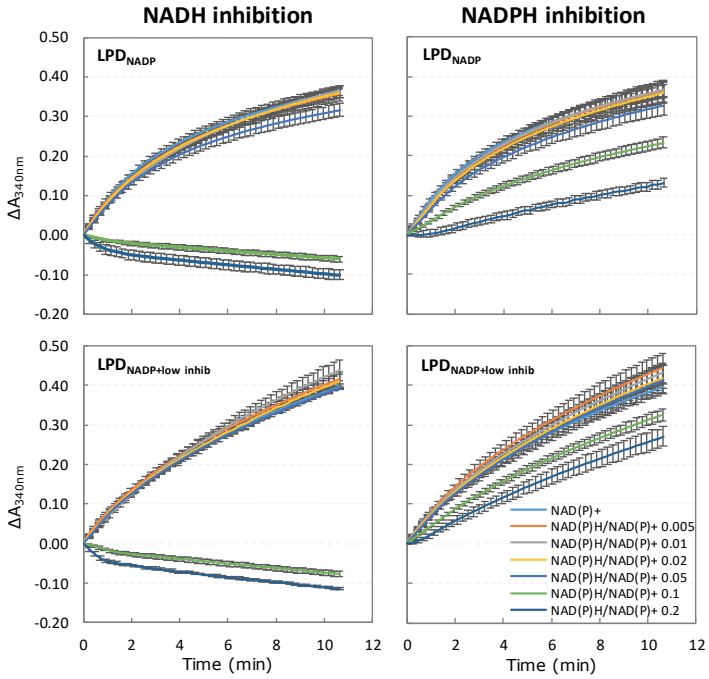

Figure S2. Inhibition assays for different NAD(P)H/NAD(P)$^+$ ratios on NADP$^+$-dependent PDH complexes with standard deviations. On the left, the graphs obtained during NADH inhibition assays and **on the right**, the graphs obtained during NADPH inhibition assays. NADP$^+$ was used as cofactor for both *E. coli* Δ*pflB* Δ*sthA* Δ*ldhA* Δ*lpd* + LPD$_{NADP}$ (LPD$_{NADP}$) and *E. coli* Δ*pflB* Δ*sthA* Δ*ldhA* Δ*lpd* + LPD$_{NADP+low\ inhib}$ (LPD$_{NADP+low\ inhib}$). The values represent the average of biological duplicates and technical triplicates with standard deviations. The values shown were corrected for the initial A$_{340nm}$ and expressed as ΔA$_{340nm}$.

Chapter 4

Effect of an $NADP^+$-dependent dihydrolipoyl dehydrogenase on the metabolism of *E. coli* lacking pyruvate formate-lyase

Pauline L. Folch, Vivienne Mol, Gerrit Eggink, Ruud A. Weusthuis

Abstract

Several industrially relevant compounds such as amino acids or fatty acids require NADPH for their synthesis. However, NADPH supply can be challenging as NADPH regeneration is limited in the cells. Various groups reported successful enhancement of NADPH bioavailability by either forcing the flux through the oxidative pentose phosphate pathway (oxPPP) or by expressing heterologous $NADP^+$-dependent enzymes. Another valuable strategy is changing the cofactor dependency of NAD^+-dependent enzymes towards $NADP^+$. Dihydrolipoyl dehydrogenase (LPD) is responsible for the reduction of NAD^+ in the pyruvate dehydrogenase (PDH) and 2-oxoglutarate dehydrogenase (ODH) complexes, and as such contributes significantly to the availability of NADH. Changing its cofactor specificity from NAD^+ to $NADP^+$ could enhance the NADPH regeneration capacity.

We previously engineered the cofactor specificity of LPD to reduce $NADP^+$, knocked out the genomic *lpd* gene and introduced the $NADP^+$-LPD variants on a medium copy plasmid. Aerobically, the strains accumulated pyruvate due to the surplus of NADPH produced. Anaerobically, no conclusions could be drawn as the pyruvate formate-lyase (PFL) was active, bypassing PDH to convert pyruvate into acetyl-CoA.

In this study, we knocked out both *lpd* and *pflB* genes of *E. coli* and introduced the different LPD variants. Aerobically, deletion of *pflB* had little influence and the results obtained for *E. coli* Δ*lpd* Δ*pflB* strains carrying the different *lpd* variants were similar to the ones reported in Chapter 3 of this thesis. Anaerobically, PDH was shown to support growth of a strain lacking a functional PFL – regardless of its cofactor specificity. However, the strains carrying an $NADP^+$-PDH exhibited poor growth and presented a high yield of lactate. Our results indicate that the cells struggle in regenerating the excess NADPH produced. We hypothesized that the activity of the soluble transhydrogenase was limited under this condition.

4.1. Introduction

Cofactors such as NAD^+ and $NADP^+$ have a central role in microbial metabolism. They act as electron carriers but are involved in distinct sets of reactions. NAD^+ is used in oxidation reactions and is regenerated by respiration or fermentation. NADPH is involved in anabolic reduction reactions and is mainly regenerated in the pentose phosphate pathway (PPP) and in the TCA cycle by isocitrate dehydrogenase. NADPH is required for the production of many compounds like amino acids or terpenoids (Wang *et al.*, 2013c; Park *et al.*, 2014; Kim *et al.*, 2015; Ng *et al.*, 2015). To improve product formation, the availability of NADPH fluxes has been increased by forcing the flux over the oxidative pentose phosphate pathway (Lim *et al.*, 2002; Chemler *et al.*, 2010; Lee *et al.*, 2010), or by applying an NADPH-dependent glyceraldehyde-3-phosphate dehydrogenase in the Embden-Meyerhoff-Parnass (EMP) pathway (Martínez *et al.*, 2008; Wang *et al.*, 2013a). Dihydrolipoyl dehydrogenase (LPD) is responsible for the reduction of NAD^+ in the pyruvate dehydrogenase (PDH) and 2-oxoglutarate dehydrogenase (ODH) complexes, and as such contributes significantly to the availability of NADH. Consequently, engineering the cofactor specificity of LPD to reduce $NADP^+$ would be beneficial for the production of these compounds whose synthesis requires NADPH input.

PDH catalyzes the irreversible conversion of pyruvate and CoA into acetyl-CoA and CO_2, using NAD^+ as cofactor. This complex consists of multiple copies of three catalytic subunits: pyruvate dehydrogenase (E1), dihydrolipoyllysine-residue acetyltransferase (E2) and lipoamide dehydrogenase (E3) encoded by *aceE*, *aceF* and *lpd*, respectively (Guest *et al.*, 1989). The promoter P_{ace} controls both *aceE* and *aceF* genes, whereas *lpd* is under the control of its own promoter P_{lpd}. All three genes are regulated by PdhR, which represses their transcription (Quail *et al.*, 1994; Quail and Guest, 1995). This regulator is inactivated in the presence of pyruvate, allowing expression of PDH (Quail *et al.*, 1994). Furthermore, the PDH complex is highly inhibited by NADH and this allosteric inhibition takes place on the LPD subunit (E3) (Hansen and Henning, 1966; Schmincke-Ott and Bisswanger, 1981; Wilkinson and Williams, 1981; Sahlman

and Williams, 1989), which is responsible for the transfer of electrons to the final acceptor NAD^+. The PDH complex is strongly expressed and active under aerobic conditions. Anaerobically however, as a result of NADH inhibition, it is considerably less active and its role is taken over by pyruvate formate-lyase (PFL) (Clark, 1989; de Graef *et al.*, 1999; Kim *et al.*, 2008).

PFL catalyzes the non-oxidative conversion of pyruvate and CoA into acetyl-CoA and formate (Knappe *et al.*, 1974; Clark, 1989; Knappe and Sawers, 1990). Unlike PDH, PFL does not require a cofactor such as NAD^+. PFL is composed of a PFL activating enzyme I and a formate acetyltransferase I encoded by *pflA* and *pflB*, respectively (Sawers and Böck, 1988). Both genes are controlled by several promoters (Sawers and Böck, 1989). PFL is induced at anaerobic conditions at both transcriptional and post-translational levels. At transcriptional level, the promoters are controlled by FNR and ArcA/ArcB system, resulting in a 12- to 15-fold increase when cells are subjected to anaerobiosis (Sawers and Böck, 1988; Sawers and Böck, 1989; Knappe and Sawers, 1990). Furthermore, the enzyme is active anaerobically since it requires an oxygen-sensitive radical for catalysis. As a consequence, the enzyme is interconverted between the active and inactive form in the absence or presence of oxygen, respectively (Knappe *et al.*, 1974; Knappe and Blaschkowski, 1975; Wagner *et al.*, 1992).

ODH catalyzes the irreversible conversion of 2-oxoglutarate, CoA and NAD^+ into succinyl-CoA, CO_2 and NADH (Guest and Creaghan, 1973; Smith and Neidhardt, 1983). The ODH complex consists of three subunits: 2-oxoglutarate dehydrogenase (E1), dihydrolipoyllysine-residue succinyltransferase (E2) and LPD (E3) encoded by *sucA*, *sucB* and *lpd* genes, respectively. Under aerobic conditions, ODH is highly active as it is a key step, rate-limiting enzyme of the TCA cycle. Anaerobically, ODH is repressed and succinyl-CoA transferase is switched on, providing succinyl-CoA from succinate for anabolic reactions (Amarasingham and Davis, 1965; Gray *et al.*, 1966; Guest *et al.*, 1992).

We previously engineered an *E. coli* strain carrying an $NADP^+$-dependent PDH complex by knocking out the native *lpd* gene and expressing $NADP^+$-dependent

lpd variants on a plasmid (Chapter 3 of thesis). The variants include a lower NAD(P)H sensitivity, a change of cofactor specificity from NAD^+ to $NADP^+$ and a combination of both ((Bocanegra *et al.*, 1993; Kim *et al.*, 2008), Chapter 3). Enzymatic assays confirmed that the changes introduced in the *lpd* gene resulted in the desired phenotype (Chapter 3). We studied the metabolic changes induced by these PDH variants under both aerobic and anaerobic conditions. However, no significant differences could be observed under anaerobic conditions as the *pflB* gene was still active.

In the present study, we introduced the different LPD variants on a plasmid in *lpd-pflB* knock-out strains. We performed fermentation studies under both aerobic and anaerobic conditions to assess the impact of the PDH variants on growth and product formation. A genome-scale metabolic model of *E. coli* was used to help explain how the change of cofactor specificity of LPD affects the strain metabolism, and more specifically, cofactor regeneration.

4.2. Material and methods

4.2.1. Bacterial strains and plasmids

The bacterial strains and plasmids used in this study are listed in **Table 1**. All strains are derived from wild-type *Escherichia coli* BW25113.

Table 2. Bacterial strains and plasmids used in this study.

Strains and plasmids	Characteristics	References
Strains		
BW25113	F-, Δ*(araD-araB)567,* ΔlacZ4787(::rrnB-3), *λ*-, *rph-1,* Δ*(rhaD-rhaB)568, hsdR514*	CGSC[a]
BW25113 Δ*lpd*	BW25113 Δ*lpd-734*::*kan*	CGSC[a]
BW25113 Δ*pflB*	BW25113 Δ*pflB727*::*kan*	CGSC[a]
BW25113 Δ*lpd* Δ*pflB*	BW25113 Δ*lpd* Δ*pflB* marker free	This study
Plasmids		
pBbA2k-RFP	*p15A, Ptet, kan, tet, mRFP1*	Lee *et al.* (2011)
pBbA2k empty	*p15A, Ptet, kan, tet*	Chapter 3
pBbA2k LPD_{WT}	pBbA2k empty derivative, P_{lpd}, native *lpd*, T_{lpd}	Chapter 3
pBbA2k $LPD_{low\ inhib}$	pBbA2k empty derivative, P_{lpd}, *lpd 1AA*, T_{lpd}	Chapter 3
pBbA2k LPD_{NADP}	pBbA2k empty derivative, P_{lpd}, *lpd 7A*, T_{lpd}	Chapter 3
pBbA2k $LPD_{NADP+low\ inhib}$	pBbA2k empty derivative, P_{lpd}, *lpd 8AA*, T_{lpd}	Chapter 3
pKD13	*oriR6K gamma, tL3LAM, bla, rrnB, kan, FRT*	CGSC[a]
pKD46	*repA101*(Ts), *ParaB-gam-bet-exo, oriR101, bla, araC*	CGSC[a]
pCP20	*repA101*(Ts), bla, cat, *flp*	CGSC[a]

[a]Coli Genetic Stock Centre

[b]*kan*: kanamycin resistance gene; *tet*: tetracyclin resistance gene; *bla*: ampicillin resistance gene; P_{araB}-*gam-bet-exo*: Lambda Red recombinase genes under arabinose induction; FRT; flippase recognition sites; *flp*: flippase gene under thermal induction

4.2.2. Deletion of pyruvate formate-lyase gene (*pflB*)

The gene encoding pyruvate formate-lyase (*pflB*) was knocked out by Lambda-Red-mediated recombination as described previously by Datsenko and Wanner (2000).

Briefly, *E. coli* BW25113 Δ*lpd* (Baba *et al.*, 2006) was transformed with the pKD46 plasmid and grown on LB medium containing 10 mM L-arabinose to induce the expression of Lambda-Red recombinase. Subsequently, the *pflB* gene was removed by introduction of a kanamycin resistance cassette flanked with flippase recognition sites (FRT). The cassette was amplified by PCR from

the pKD13 plasmid using Phusion high-fidelity DNA polymerase (Thermo Scientific) and primers including 20 bp of the FRT sites and 50 bp homologous flanking sites of the *pflB* gene. The knock-out cassette was introduced by electroporation into the cells and transformants were screened on kanamycin selective plates and colony PCR using DreamTaq DNA polymerase (Thermo Scientific). The kanamycin resistance cassette was subsequently removed from the colonies harboring the desired genotype using the pCP20 plasmid. Curing of the pCP20 plasmid was performed by growing cells on liquid LB at 42°C under 250 rpm agitation. The sequences for recombination, the primers used to check the insertion of the knock-out cassette and the loss of the kanamycin resistance cassette are given in **Table S1**.

4.2.3. Cultivation conditions

The cultivations were performed as described in Chapter 3 of this thesis. All fermentations were performed at 37°C in a Kuhner shaker with an agitation of 250 rpm. The medium was supplemented with 50 µg/mL kanamycin for all strains carrying pBbA2k plasmid. Precultures of all strains were performed overnight in 50 mL LB. 5 mL of the overnight preculture was transferred to either 45 mL or 95 mL M9 minimal medium in 250 mL shake flasks for aerobic and anaerobic conditions, respectively. The minimal medium (MM) contained: 1 x M9 salts, 50 mM glucose, 2 mM $MgSO_4$, 1 mM $CaCl_2$, 1 mL/L of US^{Fe} trace elements (Bühler *et al.*, 2002). The pH of the medium was buffered at 6.9 with 44 mM KH_2PO_4 and 47.5 mM Na_2HPO_4. The following day, cells were harvested by centrifugation at 4700 rpm for 5 min at room temperature and inoculated into 50 mL MM to an OD_{600nm} of 0.2. Aerobic cultivations were carried out in 250 mL Erlenmeyer flasks whereas anaerobic cultivations were performed in 200 mL serum bottles previously flushed with nitrogen.

4.2.4. Analytical methods

The analytical methods used to determine growth and metabolite production are the same as in Chapter 3 of this thesis. Growth was followed by measuring the absorbance at 600nm using a Hach Lange DR6000 spectrophotometer.

Glucose, ethanol and organic acid concentrations were analyzed on an Agilent 1290 Infinity (U)HPLC equipped with a UV detector (210 nm) and a RI detector (55°C). Separation of the samples was performed on a guard column (Security Guard Cartridge System, Phenomenex) and a Rezex ROA-Organic acid H^+ (8%) column (Phenomenex) operated at 55°C. 0.005 M sulphuric acid was used as eluent with a flow of 0.5 mL/min and 250 mM propionic acid was used as internal standard.

4.2.5. Carbon balances

Based on the fermentation and growth profiles, carbon recovery was determined during anaerobic cultivations. The carbon balances account for glucose, pyruvate, ethanol, lactate, acetate, succinate, formate, CO_2 and biomass. They are calculated based on the concentrations and number of carbons of each compound measured. We chose to express it as C-mmol present and not as a fraction of the glucose consumed to limit overestimations.

Aerobically, carbon balances cannot be determined since the cultivations were performed in shake flasks and the CO_2 produced could not be accounted for. Anaerobically, the CO_2 concentrations were estimated from the fermentation products according to **Equation 1**:

$$CO_{2\,produced} = ethanol_{\,produced} + acetate_{\,produced} - succinate_{\,produced} - formate_{\,produced}$$

(Equation 1)

The biomass was estimated from the OD_{600nm} measurements. Based on the elemental stoichiometry of *E. coli* (Folsom and Carlson, 2015), we determined the percentage of carbon present in the cells (g/g). Moreover, the correlation between *E. coli* cell dry weight and OD_{600nm} is 0.36 g/L (Ren *et al.*, 2013). With this information, the measured OD_{600nm} is translated into a cell concentration, according to **Equation 2**:

$$Biomass\ carbon\ present\ (mM) = \frac{OD_{600nm} * 0.36 * \text{carbon present in } E.coli}{MW_{carbon}} * 1000$$

(**Equation 2**)

Where the carbon present in *E. coli* is 0.504 g/g and the molecular weight of carbon is 12.01 g/mol.

The carbon balances can be found in **Table S2**. The strains were grown on M9 medium containing 50 mM glucose as sole carbon source therefore 300 C-mmol (50 mM * 6 carbon molecules per glucose) were introduced in the system. The carbon balances fluctuated between 277.1 ± 18.9 and 326.4 ± 0.4 C-mmol, which is within 10% deviation of 300 C-mmol. This indicates that the metabolites concentrations determined together with the estimations for biomass and CO_2 are accurate.

4.2.6. Yields

Yields of biomass and products formed on glucose were determined during anaerobic cultivations. Yields of fermentation products were calculated based on the HPLC measurements whereas yields of CO_2 and biomass formed on glucose were determined from the calculations mentioned above. All yields are expressed as mol product formed per mol glucose consumed. The values displayed in the results section represent the average yields of biological replicates with standard deviations.

4.2.7. Flux through PDH complex

Fluxes through the PDH complex (J_{PDH}, expressed in mM/h) were determined based on the metabolite profiles at the beginning of the stationary phase. Both the absolute flux through PDH (J_{PDH}) and the fraction of flux going through PDH versus the possible maximum flux J_{max} were calculated. J_{max} corresponds to the maximum flux resulting from a complete conversion of glucose into acetyl-CoA based products only.

The absolute flux going through PDH was calculated according to the **Equation 3**, assuming that PDH and PFL are the only two enzymes able to convert pyruvate into acetyl-CoA in *E. coli*. Moreover, we also assumed that all acetate was only produced from acetyl-CoA and that direct production of acetate from pyruvate was negligible.

$$J_{PDH} = \frac{\Delta[ethanol] + \Delta[acetate] - \Delta[formate]}{\Delta t} \qquad \textbf{(Equation 3)}$$

The relative fraction of the flux going through PDH was determined by calculating the total flux through the system based on the glucose consumption rate.

4.2.8. Genome-scale metabolic model

The iML1515 genome-scale metabolic model of *E. coli* K-12 *substr.* MG1655 was obtained from Monk *et al.* (2017). This model is suitable to predict the behavior of the strains used in this study because both are K-12 derivatives. This model is the most complete model for *E. coli* up to date and shows increased accuracy in predicting the effect of gene knock-outs. The model contains 1515 open reading frame, 2719 reactions and 1192 unique metabolites. It also includes three compartments – cytosol, periplasm and extracellular space – as well as gene-protein-reaction (GPR) relationships.

The iML1515 metabolic model was modified to understand the impact of an $NADP^+$-dependent LPD on *E. coli* Δ*lpd* Δ*pflB* metabolism under both aerobic and anaerobic conditions.

The *pflB* gene encoding the pyruvate formate-lyase (PFL) was knocked out by setting the upper and lower bounds of the PFL reaction to 0.

For *E. coli* Δ*lpd* Δ*pflB* carrying the native LPD gene, the bounds of the reactions catalyzed by PDH and ODH complexes were retained as default values [0; 1000].

To predict the behavior of *E. coli* Δ*lpd* Δ*pflB* carrying an $NADP^+$-dependent LPD, the reactions catalyzed by PDH and ODH complex were modified. Both cofactors NAD^+ and NADH were substituted for $NADP^+$ and NADPH, respectively. The default bounds remained unchanged as PDH and ODH reactions are irreversible.

The upper and lower bounds for the oxygen exchange reaction were set at -1000 and 0 mmol/g_{DW}/h, respectively to simulate aerobic conditions. Anaerobic conditions were enabled by changing the lower bound to 0.

The bounds for the glucose exchange reaction remained unchanged and were [-10; 1000].

Pyruvate production was included in the aerobic model by increasing the bounds of the pyruvate exchange reaction while keeping the glucose uptake rate at -10 mmol/g_{DW}/h.

In this modified iML1515 GEM, biomass formation was used as objective to maximize using flux balance analysis (FBA). Reactions involved in NADH and NADPH metabolisms were identified in *E. coli* Δ*pflB* carrying either NAD^+- or $NADP^+$-dependent PDH and ODH complexes.

4.3. Results and Discussion

4.3.1. *E. coli* Δ*pflB*

Prior to assessing the effect of changing the cofactor specificity of LPD on *E. coli* metabolism, we knocked out the *pflB* gene encoding pyruvate formate-lyase (PFL) and assessed the phenotype of the mutant strain under aerobic and anaerobic conditions. The aerobic cultures were oxygen-limited during a large period of the aerobic fermentation, as reported previously (Chapter 3). In *E. coli* WT BW25113 this resulted in the synthesis of fermentation products, including formate by PFL (Chapter 3, Figure 4A). Knocking out *pflB* reduced formate production by 70% (**Figure 1** and Chapter 3, Figure 4A). The inability to use PFL reduced the strains capacity to convert pyruvate into acetyl-CoA under these conditions, resulting in a 12.7% decrease of the specific aerobic growth rate (**Table 2**). The conversion of pyruvate to acetyl-CoA by the exclusive action of PDH increased the availability of NADH for energy generation by respiration and the availability of CO_2 for biomass formation, resulting in a 13.7% increase

in biomass concentration (**Figure 1A** and Chapter 3, Figure 4A) compared to *E. coli* WT BW25113.

Table 2. Specific growth rates μ determined during aerobic and anaerobic fermentations. The values are expressed in h^{-1} and correspond to the average of the specific growth rates determined for biological triplicates (or duplicates for *E. coli* Δ*pflB* grown aerobically and *E. coli* Δ*lpd* Δ*pflB* + $LPD_{NADP+low\ inhib}$ grown anaerobically).

Strains	Aerobic	Anaerobic	References
E. coli WT BW25113	0.63 ± 0.00	0.36 ± 0.02	Chapter 3
E. coli Δ*lpd*	NA[a]	0.28 ± 0.02	Chapter 3
E. coli Δ*lpd* + empty plasmid	NA[a]	0.22 ± 0.00	Chapter 3
E. coli Δ*lpd* + LPD_{WT}	0.60 ± 0.00	0.38 ± 0.01	Chapter 3
E. coli Δ*lpd* + $LPD_{low\ inhib}$	0.61 ± 0.00	0.37 ± 0.01	Chapter 3
E. coli Δ*lpd* + LPD_{NADP}	0.29 ± 0.01	0.37 ± 0.01	Chapter 3
E. coli Δ*lpd* + $LPD_{NADP+low\ inhib}$	0.24 ± 0.01	0.38 ± 0.00	Chapter 3
E. coli Δ*pflB*	0.55 ± 0.00	0.17 ± 0.00	This study
E. coli Δ*lpd* Δ*pflB*	NA[a]	NA[a]	This study
E. coli Δ*lpd* Δ*pflB* + empty plasmid	NA[a]	NA[a]	This study
E. coli Δ*lpd* Δ*pflB* + LPD_{WT}	0.53 ± 0.00	0.15 ± 0.00	This study
E. coli Δ*lpd* Δ*pflB* + $LPD_{low\ inhib}$	0.54 ± 0.00	0.15 ± 0.00	This study
E. coli Δ*lpd* Δ*pflB* + LPD_{NADP}	0.28 ± 0.01	0.11 ± 0.00	This study
E. coli Δ*lpd* Δ*pflB* + $LPD_{NADP+low\ inhib}$	0.35 ± 0.01	0.02 - 0.10 ± 0.00	This study

[a]NA, Not applicable. The strains did not grow under the cultivation condition tested.

Anaerobically, the strain grew without producing formate, which demonstrates that PDH is able to support anaerobic growth of *E. coli*. Previous research has shown that PDH activity of anaerobically grown *E. coli* cells was low or undetectable (Smith and Neidhardt, 1983; Snoep *et al.*, 1993a; de Graef *et al.*, 1999). Our result supports the findings of Murarka *et al.* (2010) where the native PDH was shown to support anaerobic growth of *E. coli* Δ*pflB* strains grown on minimal medium supplemented with glucuronate. They showed that knocking out *pflB* resulted in increased flux through PDH and transhydrogenases. They hypothesized that NADPH was regenerated from the excess NADH produced during the reaction catalyzed by PDH to be further used for synthesis of building

blocks. Moreover, a decrease in acetyl-CoA-based products such as acetate and ethanol was observed. Knocking out *pflB* reduced the production of acetate by a factor of 10. The presence of an active PFL makes it possible to coproduce acetate/ethanol/2 formate in redox balance, with a generation of 3 mol ATP/mol glucose. A redox-balanced production of acetate is not possible with PDH because – unlike PFL – it requires the reduction of NAD^+. Consequently, PDH can only be used to produce ethanol as a fermentation product. Ethanol production was however reduced 5-fold, indicating the low capacity of PDH under anaerobic conditions. Instead, inactivation of PFL resulted in a 2.5-fold increase in lactate production. Both ethanol and lactate production have an associated ATP yield of 2 mol ATP/mol glucose. The reduced ATP yield resulted in a 58% decrease in specific growth rate (**Table 2**) and 20.6% lower cell densities than *E. coli* WT BW25113 (**Figure 2A** and Chapter 3, Figure 5A). In comparison, deletion of *lpd* only resulted in a decrease in specific growth rate and biomass formation of 22% and 12.7%, respectively (**Table 2** and Chapter 3, Figure 5F and 5G).

4.3.2. *E. coli* Δ*lpd* Δ*pflB*

Prior to introducing the different LPD variants, we first knocked out the genomic *lpd* gene in *E. coli* Δ*pflB* and we determined the impact on *E. coli* metabolism aerobically and anaerobically on minimal medium. An overview of the changes introduced in the carbon metabolism of *E. coli* can be found in **Figure S1**. *E. coli* Δ*lpd* Δ*pflB* did not show any sign of growth on glucose under both aerobic and anaerobic conditions (**Figure S2**). However, the strain was able to form small colonies on LB plates when plated at the end of both experiments. The same phenomenon was observed for *E. coli* Δ*lpd* Δ*pflB* strain carrying the empty pBbA2k, demonstrating that the strains remained metabolically active albeit no growth was detected. As both strains lack functional PDH and PFL, no acetyl-CoA can be generated which results in a growth defect on minimal medium. Nevertheless, the strains consumed glucose and formed lactate as main fermentation product (**Figure S2**), allowing the generation of 2 mol ATP/mol glucose which can be used for maintenance. In addition, *E. coli* Δ*lpd* Δ*pflB* and

E. coli Δ*lpd* Δ*pflB* + empty pBbA2k grew on LB medium. LB is a rich medium in which the complex molecules can be used by the strains for growth and do not require the conversion of pyruvate to acetyl-CoA. However, the strains only formed small colonies since they rely on fermentation for energy generation and growth.

4.3.3. *E. coli* Δ*lpd* Δ*pflB* + LPD_{WT}

The native *lpd* gene of *E. coli* was introduced in *E. coli* Δ*lpd* Δ*pflB* strain on a medium copy plasmid (pBbA2k) under the control of its native promoter and terminator. This strain was used as a control for the expression of the modified *lpd* genes on plasmid.

Aerobically, *E. coli* Δ*lpd* Δ*pflB* + LPD_{WT} exhibited very similar growth profiles and growth rates as *E. coli* Δ*pflB* (**Figure 1** and **Table 2**). Furthermore, *E. coli* Δ*lpd* Δ*pflB* + LPD_{WT} and *E. coli* Δ*pflB* reached comparable biomass concentrations with 5.34 ± 0.08 and 5.10 ± 0.07 as maximum OD_{600nm} (**Figure 1A** and **1B**). The metabolite profiles obtained for both strains were also similar since they both accumulated up to 15.0 mM acetate and 7.1 mM lactate. Traces of pyruvate, succinate, ethanol and formate were also observed, with concentrations below 4.0 mM.

Under anaerobic conditions, *E. coli* Δ*lpd* Δ*pflB* + LPD_{WT} exhibited an 11.8% lower specific growth rate (**Table 2**) and 14.4% lower cell density than *E. coli* Δ*pflB* (**Figure 2A** and **2B**). This decrease in both growth rate and cell density most likely results from the cost of maintaining the plasmid in the cells. Moreover, it is likely that LPD subunits are overexpressed relative to the other PDH/ODH complex subunits, not contributing to PDH and ODH activity but adding to ATP costs. This phenomenon was not observed aerobically as higher amounts of metabolic energy (ATP) were available. As a consequence, *E. coli* Δ*lpd* Δ*pflB* + LPD_{WT} exhibited higher fluxes through PDH compared to *E. coli* Δ*pflB* with an increase of 34.8% and 42.1% in J_{PDH} and J_{PDH}/J_{max}, respectively (**Table 3**).

Although a higher flux through PDH is observed, PDH activity is still limited anaerobically due to NAD(P)H inhibition. Our results show that the flux going through PDH in this strain is mainly used for anabolic reactions, and not catabolism.

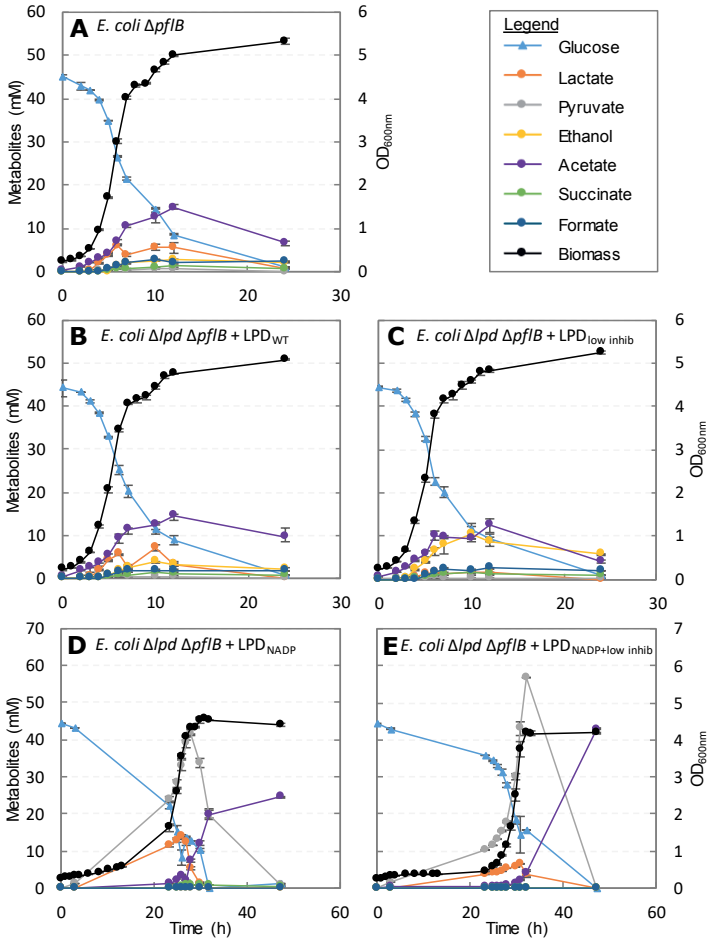

Figure 1. Aerobic fermentations on M9 medium. Growth and metabolites profiles are shown per strain. The values represent the average of biological triplicates (or duplicates for *E. coli* Δ*pflB*) with standard deviations.

4.3.4. *E. coli* Δ*lpd* Δ*pflB* + LPD$_{low\ inhib}$

As NADH inhibition restricts the anaerobic activity of LPD, an E354K mutation was introduced in the *lpd* gene of *E. coli* Δ*lpd* Δ*pflB* based on the findings of Kim *et al.* (2008). They reported that this mutation lowered the K_i for NADH by 10-

fold, allowing the PDH complex to be active anaerobically. Furthermore, we previously reported that this mutation not only reduces NADH inhibition but also NADPH inhibition in *E. coli* strains (Chapter 3, Figure 3).

The strain exhibiting a PDH complex with reduced inhibition by NAD(P)H presented similar specific growth rates to *E. coli* Δ*lpd* Δ*pflB* + LPD_{WT} under both aerobic and anaerobic conditions. However, *E. coli* Δ*lpd* Δ*pflB* + $LPD_{low\ inhib}$ showed 6.7% and 9.6% higher maximum OD_{600nm} under aerobic (**Figure 1B** and **1C**) and anaerobic conditions (**Figure 2B** and **2C**), respectively.

Aerobically, *E. coli* Δ*lpd* Δ*pflB* + $LPD_{low\ inhib}$ produced about 2.2 mM less acetate and 5.6 mM less lactate than *E. coli* Δ*lpd* Δ*pflB* + LPD_{WT}, and the ethanol concentration increased by 2.7-fold (**Figure 1C**). These data are in accordance with previous results reported in Chapter 3, Figure 4C. Introduction of the mutation for reduced NAD(P)H inhibition increased the production of ethanol under anaerobic conditions, at the expense of lactate production. *E. coli* Δ*lpd* Δ*pflB* + $LPD_{low\ inhib}$ exhibited about 2.5- and 4.6-times higher flux through its PDH than *E. coli* Δ*lpd* Δ*pflB* + LPD_{WT} and *E. coli* WT BW25113, respectively. Additionally, *E. coli* Δ*lpd* Δ*pflB* + $LPD_{low\ inhib}$ showed 3.7 times higher J_{PDH}/J_{max} than the one of *E. coli* WT BW25113 with 18.7 ± 0.6% (**Table 3**). The increased flux as well as the anaerobic fermentation profiles confirm the findings of Kim *et al.* (2008). The increased ethanol concentration indicates that the additional flux through PDH in this strain was used for catabolic as well as anabolic reactions. Nonetheless, *E. coli* Δ*lpd* Δ*pflB* + $LPD_{low\ inhib}$ still produced lactate as main fermentation product, demonstrating that the E354K mutation does not entirely relieve NAD(P)H inhibition and/or that inhibition is not the only factor limiting the anaerobic activity of PDH.

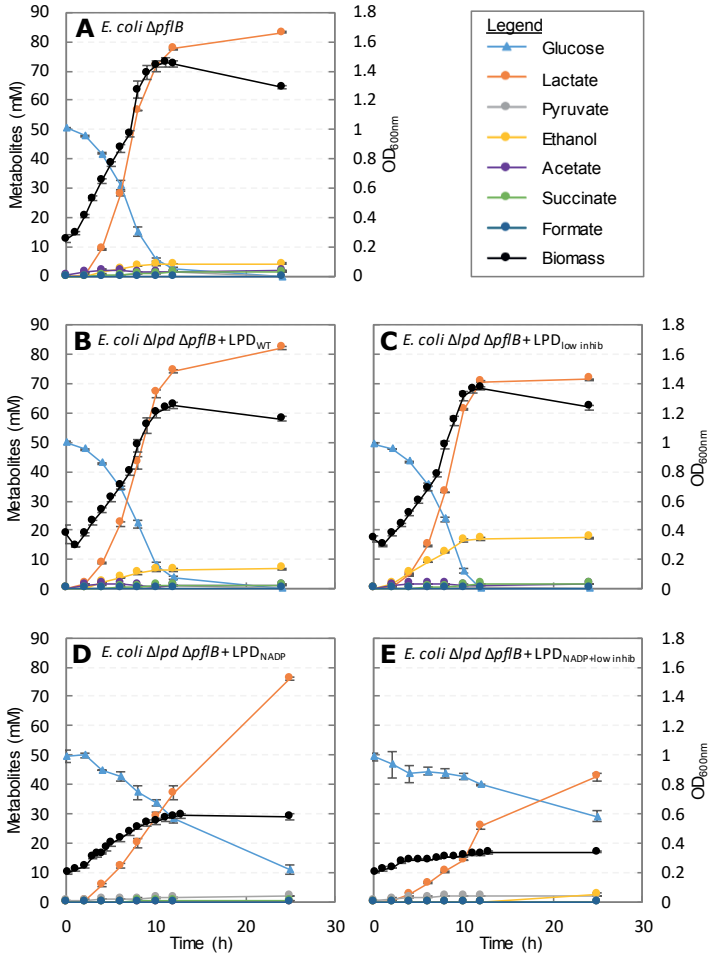

Figure 2. Anaerobic fermentations on M9 medium. Growth and metabolite profiles are shown per strain. The values represent the average of biological triplicates (or duplicates for *E. coli* Δ*lpd* Δ*pflB* + LPD_{NADP} and *E. coli* Δ*lpd* Δ*pflB* + $LPD_{NADP+low\ inhib}$) with standard deviations.

4.3.5. *E. coli* Δ*lpd* Δ*pflB* + LPD_{NADP}

In Chapter 3, *E. coli* Δ*lpd* + LPD_{NADP} showed reduced growth rate and biomass concentration compared to *E. coli* Δ*lpd* + LPD_{WT} under aerobic conditions (Chapter 3, Table 2 and Figure 4B and 4D). Furthermore, the strain accumulated pyruvate up to 20.1 ± 0.0 mM during growth on glucose. Once glucose was depleted from the medium, pyruvate was further converted to 29.1 ± 0.3 mM acetate, presumably by using pyruvate oxidase activity (Chapter 3 of this thesis,

Figure 4D). The results obtained in this study for *E. coli* Δ*lpd* Δ*pflB* + LPD_{NADP} (**Table 2**, **Figure 1D** and **2D**) are in accordance with the findings of Chapter 3, Figure 4D. However, no formate was detected in the cultures (**Figure 2D**).

Aerobically, *E. coli* Δ*lpd* Δ*pflB* + LPD_{NADP} exhibited a 1.9-fold lower growth rate than *E. coli* Δ*lpd* Δ*pflB* + LPD_{WT} (**Table 2**) and reached lower cell densities (**Figure 1D**). As the strain exhibits an $NADP^+$-PDH complex, pyruvate, CoA and $NADP^+$ are converted to acetyl-CoA, CO_2 and NADPH, which can be further used for anabolic processes such as growth. However, less NADH is produced in *E. coli* Δ*lpd* Δ*pflB* + LPD_{NADP} compared to a strain carrying an NAD^+-PDH. Consequently, less NADH is available for energy generation by respiration, which results in lower growth rates and biomass concentrations. In addition, the strain accumulated 41.4 ± 0.2 mM pyruvate and 13.8 ± 0.5 mM lactate during exponential growth on glucose. After entering the stationary phase, both metabolites were subsequently converted to 24.5 mM acetate (**Figure 1D**).

Accumulation of both pyruvate and lactate indicates that the change of cofactor specificity created a bottleneck at the PDH node since formation of both metabolites does not involve PDH. PDH_{NADP} was shown to have higher *in vitro* activity than PDH complexes using NAD^+ as cofactor (Chapter 3, Figure 1C). Consequently, it seems that cells have difficulty to regenerate $NADP^+$. In addition, formate and ethanol were not detected in the cultures and the strain presented a 13 h delay prior exponential growth which was not observed for *E. coli* Δ*lpd* + LPD_{NADP} (Chapter 3, Figure 4D). This longer lag phase must be a consequence of a lack of functional PFL at the beginning of the fermentations.

The impact of changing the cofactor specificity of PDH under anaerobic conditions could not be characterized well in Chapter 3 of this thesis since PFL was present and carried most of the flux for the conversion of pyruvate to acetyl-CoA. *E. coli* Δ*lpd* Δ*pflB* + LPD_{NADP} grew anaerobically demonstrating that an $NADP^+$-PDH complex supports anaerobic growth of an *E. coli* strain lacking a functional PFL. Although the strain exhibited a similar specific growth rate to strains carrying an NAD^+-dependent PDH (**Table 2**), it reached a 2.1-fold lower

maximum OD_{600nm} which corresponds to a 1.6-fold decrease in biomass yield on glucose (**Table 4**).

Table 3. Calculated catabolic fluxes through the PDH complex of all strains grown under anaerobic conditions. Absolute flux through PDH (J_{PDH}) and fraction of the flux through PDH compared to the total possible flux (J_{PDH}/J_{max}). The values shown are the average of biological triplicates (or duplicates for *E. coli* WT BW25113, *E. coli* Δ*pflB* and *E. coli* Δ*lpd* Δ*pflB* + $LPD_{NADP+low\ inhib}$) with standard deviations. The fluxes were not determined for *E. coli* Δ*lpd* Δ*pflB* and *E. coli* Δ*lpd* Δ*pflB* + empty plasmid since they did not grow.

Strains	J_{PDH} (mM pyruvate/h)	J_{PDH}/J_{max} (%)
E. coli WT BW25113	0.34 ± 0.10	5.0 ± 1.6
E. coli Δ*pflB*	0.46 ± 0.02	5.7 ± 0.2
E. coli Δ*lpd* Δ*pflB*	ND[a]	ND[a]
E. coli Δ*lpd* Δ*pflB* + empty plasmid	ND[a]	ND[a]
E. coli Δ*lpd* Δ*pflB* + LPD_{WT}	0.62 ± 0.04	8.1 ± 0.4
E. coli Δ*lpd* Δ*pflB* + $LPD_{low\ inhib}$	1.55 ± 0.05	18.7 ± 0.6
E. coli Δ*lpd* Δ*pflB* + LPD_{NADP}	0.00 ± 0.00	0.0 ± 0.0
E. coli Δ*lpd* Δ*pflB* + $LPD_{NADP+low\ inhib}$	0.00 ± 0.00	0.0 ± 0.0

[a]ND, Not determined. The strains did not grow.

Unlike strains exhibiting an NAD+-dependent PDH complex, *E. coli* Δ*lpd* Δ*pflB* + LPD_{NADP} did not consume all glucose in 24 h of cultivation. The strain produced lactate as main fermentation product with 76.3 ± 0.5 mM (**Figure 2D**). Even though the absolute amount of lactate is lower than the one reported for *E. coli* Δ*lpd* Δ*pflB* + LPD_{WT}, *E. coli* Δ*lpd* Δ*pflB* + LPD_{NADP} showed an increase in lactate yield on glucose of 18.8% (**Table 4**). *E. coli* Δ*lpd* Δ*pflB* + LPD_{NADP} did not produce any formate, ethanol or acetate but it did form traces of pyruvate up to 1.9 mM (**Figure 2D**). Deletion of the *pflB* gene led to an increase in the flux through PDH as it is the only enzyme available in the cells for acetyl-CoA formation. Nevertheless, no catabolic flux through the PDH complex of *E. coli* Δ*lpd* Δ*pflB* + LPD_{NADP} was observed anaerobically (**Table 3**) as the strain did not produce ethanol or acetate.

Table 4. Product yields formed on glucose (mol/mol) during anaerobic cultivations. The yields were calculated at 24 h and 25 h of cultivation for strains carrying an NAD^+-LPD and $NADP^+$-LPD, respectively. The values shown are the average of biological triplicates (or duplicates for *E. coli* Δ*lpd* Δ*pflB* + LPD_{NADP} and *E. coli* Δ*lpd* Δ*pflB* + $LPD_{NADP+low\ inhib}$) with standard deviations.

Strains	Lactate	Pyruvate	Ethanol	Acetate	Succinate	Formate	Biomass	CO_2
WT BW25113	0.68 ± 0.01	0.02 ± 0.00	0.47 ± 0.02	0.47 ± 0.01	0.07 ± 0.01	0.79 ± 0.02	0.38 ± 0.02	0.08 ± 0.03
Δ*pflB*	1.65 ± 0.01	0.00 ± 0.00	0.08 ± 0.01	0.03 ± 0.00	0.03 ± 0.00	0.00 ± 0.00	0.31 ± 0.01	0.09 ± 0.01
ΔΔ + LPD_{WT}	1.65 ± 0.02	0.00 ± 0.01	0.14 ± 0.00	0.02 ± 0.00	0.03 ± 0.00	0.00 ± 0.00	0.24 ± 0.02	0.13 ± 0.00
ΔΔ + $LPD_{low\ inhib}$	1.45 ± 0.01	0.00 ± 0.02	0.35 ± 0.00	0.03 ± 0.00	0.04 ± 0.00	0.00 ± 0.00	0.27 ± 0.01	0.35 ± 0.00
ΔΔ + LPD_{NADP}	1.96 ± 0.05	0.04 ± 0.00	0.00 ± 0.00	0.00 ± 0.00	0.01 ± 0.00	0.00 ± 0.00	0.15 ± 0.00	-0.01 ± 0.00
ΔΔ + $LPD_{NADP+low\ inhib}$	2.07 ± 0.00	0.08 ± 0.01	0.12 ± 0.03	0.00 ± 0.00	0.00 ± 0.00	0.00 ± 0.00	0.10 ± 0.01	0.12 0.03

4.3.6. *E. coli* Δ*lpd* Δ*pflB* + LPD$_{NADP+low\ inhib}$

A final *lpd* variant was introduced in *E. coli* Δ*lpd* Δ*pflB* which carries both changes of cofactor dependency of the PDH and reduced inhibition towards NAD(P)H.

Aerobically, *E. coli* Δ*lpd* Δ*pflB* + LPD$_{NADP+low\ inhib}$ reached a similar biomass concentration as *E. coli* Δ*lpd* Δ*pflB* + LPD$_{NADP}$ (**Figure 1E**) however it exhibited a 25% higher specific growth rate (**Table 2**). Remarkably, *E. coli* Δ*lpd* Δ*pflB* + LPD$_{NADP+low\ inhib}$ showed a 45.8% increased specific growth rate compared to its counterpart exhibiting a functional PFL (**Table 2**). The strain presented a delay prior exponential growth as reported earlier for *E. coli* Δ*lpd* Δ*pflB* + LPD$_{NADP}$ (**Figure 1E**). The strain carrying an NADP$^+$-PDH with reduced NADH inhibition showed comparable metabolite profiles to *E. coli* Δ*lpd* Δ*pflB* + LPD$_{NADP}$. Pyruvate and lactate accumulated during growth on glucose and were subsequently converted into acetate after entering the stationary phase. Nonetheless, *E. coli* Δ*lpd* Δ*pflB* + LPD$_{NADP+low\ inhib}$ produced less lactate and more pyruvate and acetate than *E. coli* Δ*lpd* Δ*pflB* + LPD$_{NADP}$ with 6.5 mM, 57 mM and 43 mM, respectively. The results obtained in this study are in accordance with the aerobic profiles obtained with *E. coli* Δ*lpd* + LPD$_{NADP+low\ inhib}$ (Chapter 3, Figure 4E).

Changing the cofactor dependency of LPD from NAD$^+$ to NADP$^+$ decreased the specific growth rate of the strain from 0.53 ± 0.00 h^{-1} (**Table 2**, *E. coli* Δ*lpd* Δ*pflB* + LPD$_{WT}$) to 0.28 ± 0.01 h^{-1} (**Table 2**, *E. coli* Δ*lpd* Δ*pflB* + LPD$_{NADP}$). Nevertheless, *E. coli* Δ*lpd* Δ*pflB* carrying an NADP$^+$-dependent LPD less sensitive to NAD(P)H inhibition showed a 25% increase in specific growth rate, which indicates that higher flux went through both PDH and ODH complexes.

Anaerobically, *E. coli* Δ*lpd* Δ*pflB* + LPD$_{NADP+low\ inhib}$ barely grew and only reached a final OD$_{600nm}$ of 0.34 ± 0.01 (**Figure 2E** and **Table 2**). Furthermore, the strain only consumed 20.5 ± 0.6 mM glucose within 28 h of cultivation and formed lactate as main fermentation metabolite with concentrations up to 42.5 ± 1.1 mM (**Figure 2E**). The lactate yield on glucose exhibited by *E. coli* Δ*lpd* Δ*pflB* +

$LPD_{NADP+low\ inhib}$ was 5.6% higher than the one obtained for *E. coli* Δ*lpd* Δ*pflB* + LPD_{NADP} (**Table 4**). As observed during anaerobic growth of *E. coli* Δ*lpd* Δ*pflB* + LPD_{NADP}, no formate, succinate or acetate were formed but traces of pyruvate were detected (**Figure 2E**). Both strains carrying an $NADP^+$-dependent LPD reduce $NADP^+$ instead of NAD^+ during the conversion of pyruvate to acetyl-CoA and CO_2. Because NAD^+ is now only reduced by glyceraldehyde-3-phosphate dehydrogenase, lactic acid production is the only redox-neutral way to regenerate NAD^+ under anaerobic conditions. Formation of other fermentation products like ethanol, acetate and succinate cannot be performed in a redox-neutral manner. In addition, the change of cofactor of LPD from NAD^+ to $NADP^+$ results in a higher availability of NADPH in the cells. $NADP^+$ cannot be regenerated by the dehydrogenases involved in the formation of fermentation products as they are all specific for NAD^+. $NADP^+$ regeneration therefore depends on NADPH-specific enzymes involved in anabolic reactions, or on transhydrogenases. *E. coli* possesses two transhydrogenases which transfer electrons between NADH and NADPH, allowing the cells to maintain viable NADH/NAD^+ and NADPH/$NADP^+$ ratios. The membrane-bound, energy-dependent transhydrogenase PntAB catalyzes the conversion of NADH and $NADP^+$ to NADPH and NAD^+ (Clarke and Bragg, 1985a; Clarke and Bragg, 1985b). This enzyme was reported to contribute to NADPH production during aerobic growth of *E. coli* on glucose (Clarke and Bragg, 1985a; Bizouarn *et al.*, 2000; Sauer *et al.*, 2004; Chou *et al.*, 2015). The second transhydrogenase (STH) is a soluble enzyme catalyzing the transfer of electrons from NADPH to NADH at physiological conditions in which the NADPH/$NADP^+$ ratio is high, and the NADH/NAD^+ ratio is low (Voordouw *et al.*, 1983; Canonaco *et al.*, 2001; Sauer *et al.*, 2004; Fuhrer and Sauer, 2009). Several studies reported that STH was required for growth under metabolic conditions leading to NADPH excess (Canonaco *et al.*, 2001; Sauer *et al.*, 2004; Zhao *et al.*, 2008; Fuhrer and Sauer, 2009). Overexpression of *sthA* encoding STH was shown to restore redox balance in strains overproducing NADPH (Boonstra *et al.*, 2000; Canonaco *et al.*, 2001; Qi *et al.*, 2014; Komati Reddy *et al.*, 2015). Lindner *et al.* (2018) reported aerobic growth of an NADPH-auxotrophic *E. coli* strain carrying an

$NADP^+$-dependent PDH on M9 medium supplemented with glucose. Therefore, introduction of an NADPH-requiring pathway should be sufficient to solve the redox balance problem.

$PDH_{NADP+low\ inhib}$ was reported to have high activity and reduced sensitivity towards both NADH and NADPH (Chapter 3, Figure 1C and Figure 3). Therefore, the complex is more likely to be active anaerobically in the cells than PDH_{NADP}. In this work, *E. coli* Δ*lpd* Δ*pflB* + $LPD_{NADP+low\ inhib}$ produced 2.5 + 0.6 mM ethanol at the end of the fermentations. Contrary to *E. coli* Δ*lpd* Δ*pflB* + LPD_{NADP}, the flux through $PDH_{NADP+low\ inhib}$ was not exclusively used for growth but for catabolic processes as well. Ethanol formation shows that higher flux went through $PDH_{NADP+low\ inhib}$ as a result of lower NAD(P)H inhibition and that NADPH was converted into NADH, probably by STH.

4.3.7. Genome-scale metabolic model iML1515

In a normal situation, *E. coli* produces NADPH via the pentose phosphate pathway and the isocitrate dehydrogenase present in the TCA cycle. Therefore, 1 NADPH is produced per processed acetyl-CoA. The change of cofactor dependency of both PDH and ODH in *E. coli* Δ*lpd* Δ*pflB* + LPD_{NADP} leads to the formation of 3 NADPH per processed acetyl-CoA. This increase probably exceeds the NADPH requirement for cell growth. Growth of *E. coli* Δ*lpd* Δ*pflB* + LPD_{NADP} on glucose indicates that there is flux through the PDH complex (and ODH complex) since the cells require acetyl-CoA for growth. Nevertheless, pyruvate accumulation suggests that the surplus of NADPH formed is not sufficiently reoxidized. Biomass formation requires a certain amount of ATP, NAD^+ and NADPH and, changing the cofactor dependency of LPD might upset the NADH/NADPH ratio in the cells. *E. coli* possesses a soluble transhydrogenase (STH) that is able to convert the excess NADPH into NADH to restore the balance. As the cultivations performed in this study were conducted in batch mode, accurate calculations for fluxes were not possible. Therefore, the modified iML1515 genome-scale metabolic model was used to understand how the change of cofactor specificity of LPD affected *E. coli* metabolism, and more specifically, identify enzymes involved in NADH and

NADPH metabolisms. To do so, two scenarios were tested in the model: *E. coli* Δ*pflB* carrying the native PDH and ODH complexes (NAD^+-dependent) and *E. coli* Δ*pflB* carrying $NADP^+$-dependent PDH and ODH complexes.

4.3.7.1. E. coli Δlpd ΔpflB + LPD$_{WT}$

A glucose uptake rate of 10 mmol/g_{DW}/h allowed *E. coli* Δ*lpd* Δ*pflB* + LPD_{WT} to reach a specific growth rate of 0.877 h^{-1} and 0.116 h^{-1} under aerobic and anaerobic conditions, respectively (**Table 5**). The model predicts the production of 17.8 mmol/g_{DW}/h of lactate as well as 0.493 mmol/g_{DW}/h of succinate under anaerobic conditions (**Table 5**). The enzymes predicted to be involved in NADH- and NADPH-dependent reactions under both aerobic and anaerobic conditions are presented in **Table 6**.

The model shows that NADPH is produced in the TCA cycle via isocitrate dehydrogenase (IDH) (55%) and the oxidative branch of the PPP (19%) (**Table 6**). The model predicted that 60% of the flux for NADPH consumption was carried out by the $NADP^+$-dependent glutamate dehydrogenase. This enzyme catalyzes the conversion of 2-oxoglutarate, ammonium and NADPH into glutamate and $NADP^+$ (Sakamoto *et al.*, 1975; Veronese *et al.*, 1975), and it is expressed during growth on glucose with excess ammonium (Vender and Rickenberg, 1964; Varricchio, 1969; Reitzer, 2004). Glutamate dehydrogenase (NADP) is predicted to carry such a high flux since L-glutamate has a central role in *E. coli* metabolism, being a major constituent of proteins, being a precursor for other amino acids (L-glutamine, L-proline, L-arginine) (Reitzer, 2003; Reitzer, 2004) and it regenerates L-glutamate used in transaminase reactions. Glyceraldehyde-3-phosphate dehydrogenase (GAPDH) carries most of the flux for NADH production with 41%. PDH, malate dehydrogenase (MDH) and ODH contribute to NADH formation by 23%, 17% and 14%, respectively. NADH is mainly consumed by the electron transport chain (ETC), allowing ATP generation. The model predicted that 91% of the flux for NADH consumption is carried by NADH dehydrogenase I – also known as complex I of the ETC.

Table 5. Solutions obtained with the modified iML1515 GEM for *E. coli* Δ*lpd* Δ*pflB* carrying either NAD$^+$- or NADP$^+$-dependent PDH and ODH complexes. The values for in and out fluxes are expressed in mmol/g_{DW}/h. The values for biomass correspond to the specific growth rates and are expressed in h^{-1}.

Fluxes	*E. coli* Δ*lpd* Δ*pflB* + LPD_{WT}		*E. coli* Δ*lpd* Δ*pflB* + LPD_{NADP}	
	Aerobic	**Anaerobic**	**Aerobic**	**Anaerobic**
In fluxes				
O_2	22.1	NA[a]	22	NA[a]
Glucose	10	10	10	10
NH_4^+	9.47	1.25	9.51	1.32
Pi	0.846	0.112	0.85	0.118
SO_4^{2-}	0.221	0.0292	0.222	0.0308
K^+	0.171	0.0226	0.172	0.0239
Fe^{2+}	0.0141	0.000956	0.0141	0.00101
Fe^{3+}	NA[a]	0.000905	NA[a]	0.000956
Mg^{2+}	0.00761	0.00101	0.00764	0.00106
Ca^{2+}	0.00456	0.000603	0.00458	0.000637
Cl^-	0.00456	0.000603	0.00458	0.000637
Cu^{2+}	0.000622	8.22E-05	0.000624	8.68E-05
Mn^{2+}	0.000606	8.01E-05	0.000609	8.46E-05
Zn^{2+}	0.000299	3.95E-05	0.0003	4.18E-05
Ni^{2+}	0.000283	3.74E-05	0.000284	3.96E-05
Out fluxes				
H_2O	47.2	3.55	47.1	3.76
CO_2	24	0.00121	23.8	0.973
H^+	8.06	19.8	8.09	18.8
Lactate	NA[a]	17.8	NA[a]	16.7
Succinate	NA[a]	0.493	NA[a]	0.521
Ethanol	NA[a]	NA[a]	NA[a]	0.972
Objective				
Biomass	0.877	0.116	0.881	0.122

[a]NA, Not applicable.

During anaerobic cultivation, the model predicts that NADPH is mainly produced by the membrane-bound transhydrogenase, which carries 86% of the NADPH flux and uses 7% of the NADH flux. The NADP$^+$-dependent glutamate dehydrogenase carries 60% of the flux. According to the model, GAPDH and PDH carry 97% and 2% of the flux for NADH formation, respectively. As lactate

is the main fermentation product formed under anaerobic conditions, lactate dehydrogenase is responsible for 87% of NADH consumption.

Differences between the predictions of the modified iML1515 genome-scale metabolic model and the experimental data obtained in this study can be observed. Aerobically, the model predicts a much higher specific growth rate than determined experimentally during aerobic cultivations. As the model maximizes for growth, no fermentation products were formed. However, in reality, *E. coli* Δ*lpd* Δ*pflB* + LPD_{WT} produced acetate as main fermentation product as well as lactate, formate, ethanol and succinate (**Figure 1B**). Production of fermentation products decreases the amount of glucose available for biomass formation and reduces the amount of ATP formed, therefore a lower specific growth rate was observed experimentally. Similarly, ethanol formation was not predicted anaerobically. Although the model is a powerful tool to understand the bacterium metabolism, it is limited as it does not take into account kinetics such as regulation and inhibition of enzymes.

4.3.7.2. E. coli Δlpd ΔpflB + LPD_{NADP}

Using the same glucose uptake rate of 10 mmol/g_{DW}/h, the model predicted that *E. coli* Δ*lpd* Δ*pflB* carrying $NADP^+$-dependent PDH and ODH complexes reaches slightly higher growth rates than a strain carrying native enzymes. The growth rates predicted for *E. coli* Δ*lpd* Δ*pflB* + LPD_{NADP} were 0.881 h^{-1} and 0.122 h^{-1} under aerobic and anaerobic conditions, respectively (**Table 5**).

Aerobically, similar solutions to the ones found for *E. coli* Δ*lpd* Δ*pflB* carrying native PDH and ODH were predicted by the model, and no fermentation products were formed. Under aerobic conditions, the model predicts that a strain carrying $NADP^+$-dependent PDH and ODH complexes produces NADPH mainly through the PDH complex (41%). The two TCA cycle enzymes – IDH and ODH – are carrying 30% and 26% of the flux, respectively. Contrary to *E. coli* Δ*lpd* Δ*pflB* + LPD_{WT}, no enzymes from the oxidative branch of the pentose phosphate pathway (oxPPP) were listed in the NADPH producing reactions, indicating that PDH and ODH – together with IDH - supply sufficient amount of NADPH for

anabolic reactions. Furthermore, *E. coli* Δ*lpd* Δ*pflB* + LPD_{NADP} requires the soluble transhydrogenase (STH) to regenerate NADH from NADPH, carrying 51% and 32% of the flux for NADPH consumption and NADH production, respectively. Experimentally, *E. coli* Δ*lpd* Δ*pflB* + LPD_{NADP} accumulated pyruvate under aerobic conditions. Pyruvate accumulation prevents the flux to go through the PDH complex and therefore decreases the amount of NADPH produced in the cells. These experimental results indicate that the strain is not able to convert NADPH into NADH by means of STH activity. Therefore, another simulation was performed using the modified iML1515 GEM in which the reaction catalyzed by STH was knocked out. The model however always found a solution by combining reactions in which NADPH was converted into NADH, mimicking transhydrogenase activity (data not shown). However, these reactions are not feasible *in vivo*.

Table 6. Enzymes predicted by the modified iML1515 GEM to contribute to NADH and NADPH metabolisms in *E. coli* Δ*lpd* Δ*pflB* carrying NAD$^+$-dependent PDH and ODH complexes. The fluxes are expressed as percentage of the total flux of NAD(P)H (%) as well as in mmol/gDW/h. In the model, reversible reactions are indicated with <=> and irreversible reactions with -->. Enzymes carrying less than 5% of the flux are not listed in this table but can be found in the supplementary material section, **Tables S3** and **S4**.

Reactions ID	Enzymes	Reactions	Aerobic		Anaerobic	
			%	Flux	%	Flux
NADPH producing reactions						
ICDHyr	Isocitrate dehydrogenase	isocitrate + NADP <=> 2-oxoglutarate + CO_2 + NADPH	55%	6.91	8%	0.125
G6PDH2r	Glucose 6-phosphate dehydrogenase	G6P + NADP <=> 6-phospho-D-glucono-1,5-lactone + NADPH + H^+	19%	2.36	NA[a]	NA[a]
GND	Phosphogluconate dehydrogenase	6-phospho-D-gluconate + CO_2 + NADP --> D-ribulose-5-phosphate + NADPH	19%	2.36	NA[a]	NA[a]
MTHFD	Methylenetetrahydrofolate dehydrogenase (NADP)	5,10-methyleneTHF + NADP <=> 5,10-methenylTHF + NADPH	7%	0.87	7%	0.12
THD2pp	Membrane-bound transhydrogenase PntAB	2 H^+_{out} + NADH + NADP --> 2 H^+_{in} + NAD + NADPH	NA[a]	NA[a]	86%	1.41
NADPH consuming reactions						
GLUDy	Glutamate dehydrogenase (NADP)	L-glutamate + H_2O + NADP <=> 2-oxoglutarate + NH_4^+ + NADPH	60%	7.5	60%	0.99
ASAD	Aspartate-semialdehyde dehydrogenase	L-aspartate 4-semialdehyde + NADP + Pi <=> 4-phospho-L-aspartate + NADPH + H^+	8%	0.94	8%	0.12
KARA1	Ketol-acid reductoisomerase	(R)-2,3-dihydroxy-3-methylbutanoate + NADP <=> (S)-2-acetolatate + NADPH + H^+	6%	0.77	6%	0.10
SULR	Sulfite reductase (NADPH2)	5 H^+ + 3 NADPH + SO_3 --> 3 H_2O + 3 NADP + H_2S	5%	0.65	5%	0.09
HSDy	Homoserine dehydrogenase (NADPH)	L-homoserine + NADP <=> L-aspartate 4-semialdehyde + NADPH + H^+	5%	0.61	5%	0.08
NADH producing reactions						
GAPD	Glyceraldehyde-3-phosphate dehydrogenase	G3P + NAD + Pi <=> 3-phospho-D-glyceroylphosphate + NADH + H^+	41%	17.1	97%	19.7
PDH	Pyruvate dehydrogenase (NAD)	pyruvate + CoA + NAD --> acetyl-CoA + CO_2 + NADH	23%	9.69	2%	0.49
MDH	Malate dehydrogenase	L-malate + NAD <=> oxaloacetate + NADH + H_+	17%	6.88	NA[a]	NA[a]
AKGDH	2-Oxoglutarate dehydrogenase (NAD)	2-oxoglutarate + CoA + NAD --> succinyl-CoA + CO_2 + NADH	14%	5.97	NA[a]	NA[a]
NADH consuming reactions						
NADH17pp	NADH dehydrogenase (menaquinone-8 & 3 H^+)	menaquinone-8 + 4 H^+_{in} + NADH --> menaquinol-8 + 3 H^+_{out} + NAD	91%	38	2%	0.45
FADRx	FAD reductase	FAD + NADH + H^+ --> $FADH_2$ + NAD	5%	1.92	1%	0.25
LDH_D	Lactate dehydrogenase	D-lactate + NAD <=> pyruvate + NADH + H^+	NA[a]	NA[a]	87%	17.8
THD2pp	Membrane-bound transhydrogenase PntAB	2 H^+_{out} + NADH + NADP --> 2 H^+_{in} + NAD + NADPH	NA[a]	NA[a]	7%	1.41

[a]NA, Not applicable. The enzymes were not found in the list of enzymes involved in NADH or NADPH metabolism under the cultivation condition tested.

Consequently, another simulation was performed in which the pyruvate production rate was increased gradually/stepwise (increase of 2 mmol/g_{DW}/h from 0 to 12 mmol/g_{DW}/h) for a given glucose uptake rate (10 mmol/g_{DW}/h). This allows the determination of the pyruvate production rate at which STH is not required anymore. Solutions for in and out fluxes as well as enzymes predicted by the model to contribute to NADH and NADPH metabolism can be found in **Table S7 and Table S8**.

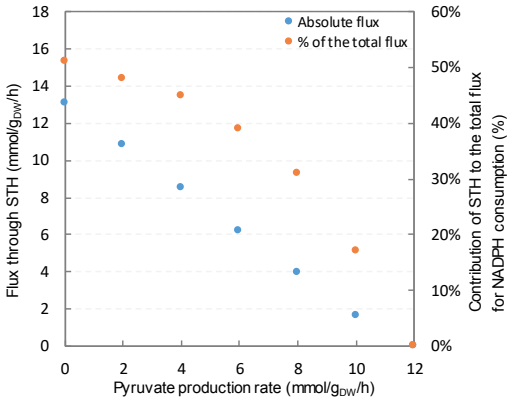

Figure 3. Impact of pyruvate accumulation on the contribution of the soluble transhydrogenase (STH) to the flux for NADPH consumption. The values shown are the solutions predicted by the modified iML1515 GEM.

The model predicts that increasing pyruvate production rate decreases the specific growth rates of the strain as less glucose is available for biomass formation (**Table S7**). For instance, production of 10 mmol/g_{DW}/h of pyruvate decreases the specific growth rate by 39.5% (0.533 h^{-1}). Furthermore, increasing pyruvate production rates decrease the total flux for NADPH metabolism (**Table S8**). As pyruvate accumulates, less absolute flux is going through PDH and other NADPH-producing enzymes thereby decreasing NADPH production. Consequently, STH contribution to NADPH-consuming reactions decreases gradually (**Figure 3**). The model predicted that STH was carrying 51% of the flux (13.1 mmol/g_{DW}/h) of the flux for NADPH consumption when no pyruvate was accumulated in the cells. However, this enzyme only carries 17% (1.6 mmol/g_{DW}/h) of the flux when applying a pyruvate production rate of 10 mmol/g_{DW}/h (**Table S8**). At 12 mmol/g_{DW}/h of pyruvate, the strain did

not require the presence of STH. In addition, *E. coli* Δ*lpd* Δ*pflB* carrying $NADP^+$-dependent PDH and ODH complexes requires the presence of enzymes from the oxPPP for NADPH production. This suggests that the amount of NADPH produced during the reactions catalyzed by PDH, IDH and ODH is not sufficient for anabolic processes. The predictions of the model regarding STH contribution with increasing pyruvate production rates support the hypothesis that the lower growth rate and pyruvate accumulation observed during aerobic cultivations on glucose for *E. coli* Δ*lpd* Δ*pflB* + LPD_{NADP} are a consequence of a lack of STH activity in the cells.

Anaerobically, the model predicted the formation of lactate and succinate with 16.7 and 0.521 mmol/g_{DW}/h, respectively (**Table 5**). Contrary to the strain carrying a native PDH, *E. coli* Δ*lpd* Δ*pflB* + LPD_{NADP} produces 0.972 mmol/g_{DW}/h of ethanol. Experimentally the strain did not show any ethanol production however its counterpart carrying an $NADP^+$-dependent PDH complex with reduced NAD(P)H inhibition did.

Under anaerobic conditions, the $NADP^+$-dependent PDH complex is now responsible for 86% of the flux for NADPH formation (**Table 7**), which was supported by the membrane-bound transhydrogenase PntAB in *E. coli* Δ*lpd* Δ*pflB* + LPD_{WT}. Therefore, PDH generates sufficient NADPH in the cells for growth. The isocitrate dehydrogenase (IDH) carries the same flux as reported for the strain carrying the native PDH and ODH complexes (8%). All NADPH produced is exclusively used for anabolism. Regarding NADH metabolism, GAPDH is supporting 99% of the flux for NADH formation, indicating that the flux which was previously carried by GAPDH and PDH in *E. coli* Δ*lpd* Δ*pflB* + LPD_{WT} is now solely carried by GAPDH. As reported for *E. coli* Δ*lpd* Δ*pflB* + LPD_{WT}, lactate dehydrogenase carries 84% of the flux for NADH consumption since lactate is the main fermentation product in *E. coli* Δ*lpd* Δ*pflB* + LPD_{NADP} as well. Both enzymes involved in ethanol formation – acetaldehyde dehydrogenase and alcohol dehydrogenase – carry 5% of the flux for NADH consumption.

Differences can be observed between the experimental data obtained in this study and the predictions of the model. During anaerobic cultivations, *E. coli* Δ*lpd* Δ*pflB* + LPD_{NADP} produced lactate as main fermentation product and traces of succinate and pyruvate were observed. However, the strain did not produce ethanol, which is the main difference predicted by the model between strains carrying a native PDH and an $NADP^+$-dependent PDH. Nevertheless, *E. coli* Δ*lpd* Δ*pflB* + $LPD_{NADP+low\ inhib}$ (**Figure 2E**) produced traces of ethanol, demonstrating that the differences observed between the model and reality can be partially explained by NADH inhibition of the PDH complex. As lactate is the main fermentation product, most of the carbon flux goes through the lactate dehydrogenase circumventing PDH.

Under aerobic conditions, a strain carrying an $NADP^+$-dependent LPD produces a large amount of NADPH compared to a wild-type strain. Two moles of NADPH per glucose can be produced by PDH, and four additional NADPH can be formed in the TCA cycle by IDH and ODH. As a consequence of the increasing NADPH concentration, cells limit NADPH production by accumulating pyruvate. Anaerobically, the same phenomenon occurs where *E. coli* Δ*lpd* Δ*pflB* + LPD_{NADP} prevents NADPH formation through PDH by producing lactate. The surplus NADPH produced under both cultivation conditions should be converted into NADH by the action of STH, as predicted by the model. Nevertheless, pyruvate accumulation and lactate production clearly demonstrate that STH is not active in our strains or that its activity is insufficient.

Table 7. Enzymes predicted by the modified iML1515 GEM to contribute to NADH and NADPH metabolisms in *E. coli* Δ*lpd* Δ*pflB* carrying NADP$^+$-dependent PDH and ODH complexes. The fluxes are expressed as percentage of the total flux of NAD(P)H (%) as well as in mmol/g_{DW}/h. In the model, reversible reactions are indicated with <=> and irreversible reactions with -->. Enzymes carrying less than 5% of the flux for NADPH and NADH are not listed in Table 7 but can be found in **Table S5** and **Table S6** of the Supplementary material section, respectively.

Reactions ID	Enzymes	Reactions	Aerobic		Anaerobic	
			%	Flux	%	Flux
NADPH producing reactions						
PDH	Pyruvate dehydrogenase (NADP)	pyruvate + CoA + NADP --> acetyl-CoA + CO_2 + NADPH	41%	10.4	86%	1.49
ICDHyr	Isocitrate dehydrogenase	isocitrate + NADP <=> 2-oxoglutarate + CO_2 + NADPH	30%	7.64	8%	0.13
AKGDH	2-oxoglutarate dehydrogenase (NADP)	2-oxoglutarate + CoA + NADP --> succinyl-CoA + CO_2 + NADPH	26%	6.7	NA[a]	NA[a]
MTHFD	Methylenetetrahydrofolate dehydrogenase (NADP)	5,10-methyleneTHF + NADP <=> 5,10-methenylTHF + NADPH	3%	0.87	7%	0.12
NADPH consuming reactions						
NADTRHD	Soluble transhydrogenase	NAD + NADPH --> NADH + NADP	51%	13.1	NA[a]	NA[a]
GLUDy	Glutamate dehydrogenase (NADP)	L-glutamate + H_2O + NADP <=> 2-oxoglutarate + NH_4^+ + NADPH	29%	7.53	60%	1.05
ASAD	Aspartate-semialdehyde dehydrogenase	L-aspartate 4-semialdehyde + NADP + Pi <=> 4-phospho-L-aspartate + NADPH + H^+	4%	0.94	8%	0.13
KARA1	Ketol-acid reductoisomerase	(R)-2,3-dihydroxy-3-methylbutanoate + NADP <=> (S)-2-acetolatate + NADPH + H^+	3%	0.77	6%	0.11
SULR	Sulfite reductase (NADPH2)	5 H^+ + 3 NADPH + SO_3 --> 3 H_2O + 3 NADP + H_2S	3%	0.65	5%	0.010
HSDy	Homoserine dehydrogenase (NADPH)	L-homoserine + NADP <=> L-aspartate 4-semialdehyde + NADPH + H^+	2%	0.62	5%	0.09
NADH producing reactions						
GAPD	Glyceraldehyde-3-phosphate dehydrogenase	G3P + NAD + Pi <=> 3-phospho-D-glyceroylphosphate + NADH + H^+	44%	17.9	99%	19.7
NADTRHD	Soluble transhydrogenase	NAD + NADPH --> NADH + NADP	32%	13.1	NA[a]	NA[a]
MDH	Malate dehydrogenase	L-malate + NAD <=> oxaloacetate + NADH + H^+	19%	7.62	NA[a]	NA[a]
NADH consuming reactions						
NADH17pp	NADH dehydrogenase (menaquinone-8 & 3 H^+)	menaquinone-8 + 4 H^+_{in} + NADH --> menaquinol-8 + 3 H^+_{out} + NAD	91%	36.9	2%	0.48
FADRx	FAD reductase	FAD + NADH + H^+ --> $FADH_2$ + NAD	5%	1.93	1%	0.27
LDH_D	Lactate dehydrogenase	D-lactate + NAD <=> pyurvate + NADH + H^+	NA[a]	NA[a]	84%	16.7
ACALD	Acetaldehyde dehydrogenase (acetylating)	acetaldehyde + CoA + NAD <=> acetyl-CoA + NADH + H^+	NA[a]	NA[a]	5%	0.97
ALCD2x	Alcohol dehydrogenase (ethanol)	ethanol + NAD <=> acetaldehyde + NADH + H^+	NA[a]	NA[a]	5%	0.97

[a]NA, Not applicable. The enzymes were not found in the list of enzymes involved in NADH and NADPH metabolisms under the conditions tested.

4.4. Conclusion

An *E. coli* strain lacking a functional PFL grew anaerobically on minimal medium, demonstrating that the PDH complex took over the conversion of pyruvate to acetyl-CoA. However, lactate was formed as main fermentation product, preventing high flux through PDH.

Introduction of an NADP+-dependent PDH complex in *E. coli* Δ*lpd* Δ*pflB* has the potential to produce a surplus of NADPH. However, because no sink for NADPH was available, the strain accumulated pyruvate and lactate whose formation circumvented the PDH complex. STH could have provided this sink to transfer the surplus of reducing power from NADPH to NADH under both cultivation conditions, so apparently its activity was insufficient in the cells. Anaerobically, the poor growth profile exhibited by *E. coli* Δ*lpd* Δ*pflB* + LPD_{NADP} likely results from a lack of STH activity as well as NAD(P)H inhibition. Introduction of $LPD_{NADP+low\ inhib}$ allowed the strain to redirect part of the flux for lactate formation to ethanol.

To fully assess the impact of an NADP+-dependent LPD on *E. coli* metabolism, further research is necessary to understand if the soluble transhydrogenase is the limiting factor for cofactor regeneration. Additionally, presence of the lactate dehydrogenase limits the carbon flux to go through the PDH complex under anaerobic conditions. Deletion of *ldhA* gene would be an option to force the flux through the PDH complex and deletion of *sthA* gene would give insights in the role of STH – as well as the activity – in our strains carrying an NADP+-dependent PDH complex.

4.5. Supplementary materials

Table S1. Primers used in this study to disrupt the *pflB* gene (H1P1 and H2P2) and to check for correct transformants. The 50 bp flanking regions of the *pflB* gene are underlined.

Names	Sequences	References
pflB H1P1	TTTTACTGTACGATTTCAGTCAAATCTAATTAC ATAGATTGAGTGAAGGTATTCCGGGGATCCGT CGACC	Baba *et al.* (2006)
pflB H2P2	CGAAGTACGCAGTAAATAAAAAATCCACTTAA GAAGGTAGGTGTTACATGTGTAGGCTGGAGC TGCTTCG	Baba *et al.* (2006)
pflB -156FW	GTGTTGGTGCGCAGCTCGAA	This study
pflB +151REV	CCTGATTCCGGTTACGATCG	This study

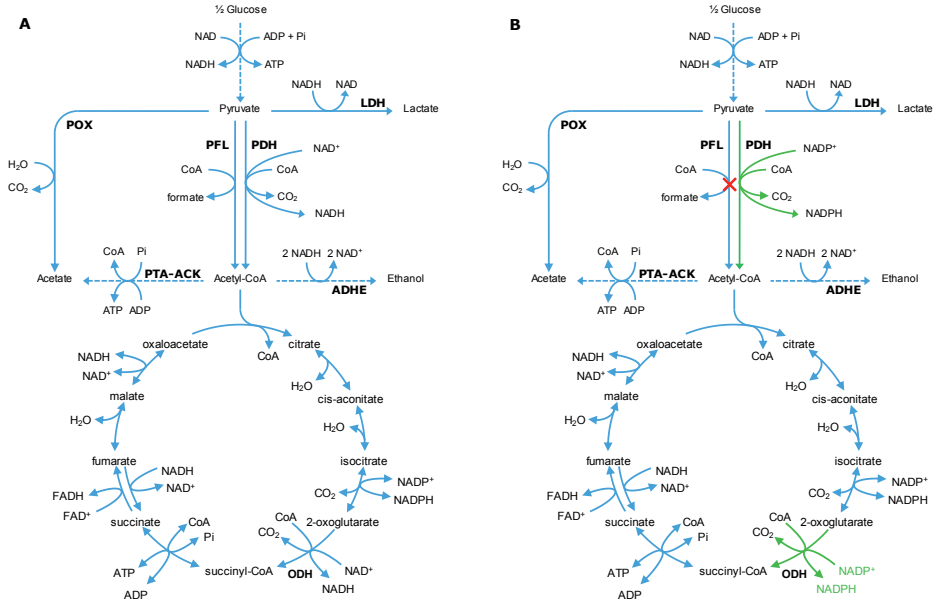

Figure S1. Carbon metabolism of (A) *E. coli* WT BW25113 and (B) after genetic engineering. Reactions impacted by the change of cofactor specificity of LPD are shown in green. Disruption of the *pflB* gene encoding the pyruvate formate-lyase (PFL) is shown with a red cross.

Table S2. Carbon balances determined during anaerobic cultivations on M9 medium. The values are expressed as C-mmol accumulated and represent the average of biological triplicates (or duplicates for *E. coli* Δ*lpd* Δ*pflB* + LPD_{NADP} and *E. coli* Δ*lpd* Δ*pflB* + $LPD_{NADP+low\ inhib}$) with standard deviations.

Time (h)	Δ*pflB*	LPD_{WT}	$LPD_{low\ inhib}$	LPD_{NADP}	$LPD_{NADP+low\ inhib}$
0	307.0 ± 0.8	301.2 ± 4.5	303.2 ± 0.8	301.7± 13.5	300.7 ± 7.3
2	300.1 ± 0.1	296.0 ± 2.8	302.7 ± 0.6	305.9 ± 5.7	287.4 ± 28.8
4	301.1 ± 0.3	296.8 ± 4.4	302.3 ± 0.6	292.6 ± 1.5	277.1 ± 18.9
6	295.8 ± 0.4	293.9 ± 4.4	300.4 ± 1.4	300.5 ± 11.7	294.7 ± 8.7
8	295.0 ± 1.6	289.1 ± 8.2	300.2 ± 1.0	294.2 ± 19.5	303.2 ± 11.2
10	294.1 ± 1.0	282.2 ± 11.2	296.3 ± 0.6	303.3 ± 10.0	308.2 ± 6.2
12	293.3 ± 0.5	282.0 ± 8.5	296.4 ± 2.1	295.5 ± 17.4	326.4 ± 0.4
24*	294.1 ± 0.9	281.4 ± 7.9	296.6 ± 0.6	308.7 ± 8.0	319.7 ± 5.6

*25 h of cultivation for *E. coli* Δ*lpd* Δ*pflB* + LPD_{NADP} and *E. coli* Δ*lpd* Δ*pflB* + $LPD_{NADP+low\ inhib}$.

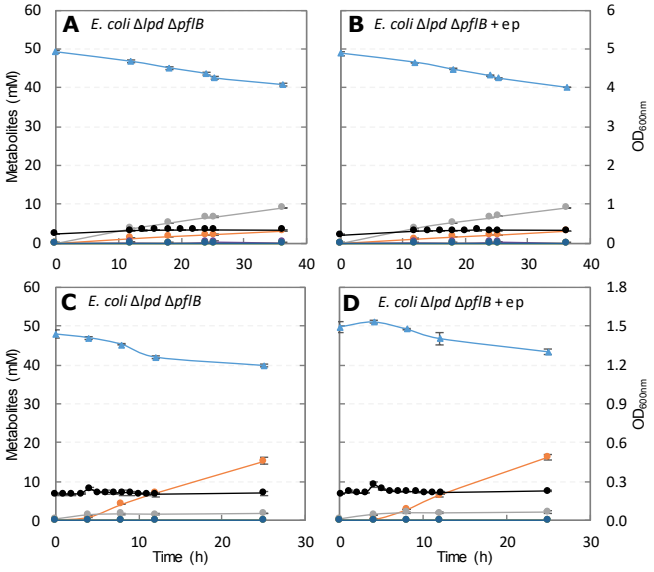

Figure S2. Aerobic (A and B) and anaerobic (C and D) fermentations profiles of *E. coli* Δ*lpd* Δ*pflB* with or without empty pBbA2k plasmid (ep). The values shown represent the average of biological triplicates with standard deviations. Light blue triangles: glucose, orange: lactate, grey: pyruvate, yellow: ethanol, purple: acetate, green: succinate, dark blue: formate and black: biomass.

Table S3. Enzymes predicted to contribute to NADPH metabolism in *E. coli* Δ*lpd* Δ*pflB* carrying NAD$^+$-dependent PDH and ODH complexes according to the modified iML1515 GEM. The fluxes are expressed in mmol/g_{DW}/h as well as in percentage of the total flux (%). In the model, reversible reactions are indicated with <=> and irreversible reaction are indicated with -->. G6P, D-glucose-6-phosphate; THF, tetrahydrofolate; DHAP, dihydroxyacetone phosphate.

Reactions ID	Enzymes	Reactions	Aerobic		Anaerobic	
			%	Flux	%	Flux
NADPH producing						
ICDHyr	Isocitrate dehydrogenase	isocitrate + NADP <=> 2-oxoglutarate + CO_2 + NADPH	55%	6.91	8%	0.125
G6PDH2r	Glucose 6-phosphate dehydrogenase	G6P + NADP <=> 6-phospho-D-glucono-1,5-lactone + NADPH + H^+	19%	2.36	NA[a]	NA[a]
GND	Phosphogluconate dehydrogenase	6-phospho-D-gluconate + CO_2 + NADP --> D-ribulose-5-phosphate + NADPH	19%	2.36	NA[a]	NA[a]
MTHFD	Methylenetetrahydrofolate dehydrogenase (NADP)	5,10-methyleneTHF + NADP <=> 5,10-methenylTHF + NADPH	7%	0.867	7%	0.115
THD2pp	Membrane-bound transhydrogenase PntAB	2 H^+_{out} + NADH + NADP --> 2 H^+_{in} + NAD + NADPH	NA[a]	NA[a]	86%	1.41
NADPH consuming						
GLUDy	Glutamate dehydrogenase (NADP)	L-glutamate + H_2O + NADP <=> 2-oxoglutarate + NH_4^+ + NADPH	60%	7.5	60%	0.991
ASAD	Aspartate-semialdehyde dehydrogenase	L-aspartate 4-semialdehyde + NADP + Pi <=> 4-phospho-L-aspartate + NADPH + H^+	8%	0.938	8%	0.124
KARA1	Ketol-acid reductoisomerase	(R)-2,3-dihydroxy-3-methylbutanoate + NADP <=> (S)-2-acetolatate + NADPH + H^+	6%	0.767	6%	0.101
SULR	Sulfite reductase (NADPH2)	5 H^+ + 3 NADPH + SO_3 --> 3 H_2O + 3 NADP + H_2S	5%	0.651	5%	0.086
HSDy	Homoserine dehydrogenase (NADPH)	L-homoserine + NADP <=> L-aspartate 4-semialdehyde + NADPH + H^+	5%	0.612	5%	0.0809
SHK3Dr	Shikimate dehydrogenase	3-dehydroshikimate + NADPH + H^+ <=> shikimate + NADP	3%	0.334	3%	0.0442
DHDPRy	Dihydrodipicolinate reductase (NADPH)	2,3-dihydrodipicolinate + NADPH + H^+ <=> 2,3,4,5-tetrahydrodipicolinate + NADP	3%	0.325	3%	0.043
AGPR	N-acetyl-g-glutamyl-phosphate reductase	N-acetyl-L-glutamyl 5-semialdehyde + NADP + Pi <=> N-acetyl-L-glutamyl 5-phosphate + NADPH + H^+	2%	0.259	2%	0.0343
KARA2	Ketol-acid reductoisomerase (2-Acetolactate)	(S)-2-aceto-2-hydroxybutanoate + NADPH + H^+ <=> (R)-2,3-dihydroxy-3-methyl-pentanoate + NADP	2%	0.255	2%	0.0337
TRDR	Thioredoxin reductase (NADPH)	oxidized thioredoxin + NADPH + H^+ --> reduced thioredoxin + NADP	2%	0.217	2%	0.0287
G5SD	Glutamate-5-semialdehyde dehydrogenase	L-glutamate 5-phosphate + NADPH + H^+ --> L-glutamate semialdehyde + NADP + Pi	2%	0.194	2%	0.0256
P5CR	Pyrroline-5-carboxylate reductase	1-pyrroline-5-carboxylate + 2 H^+ + NADPH --> L-proline + NADP	2%	0.194	2%	0.0256
G3PD2	Glycerol-3-phosphate dehydrogenase (NADP)	Glycerol-3-phosphate + NADP <=> DHAP + NADPH + H^+	1%	0.122	1%	0.0161

[a]NA, Not applicable. The enzymes were not listed as enzymes participating in NADPH metabolism under the cultivation condition tested.

Table S4. Enzymes predicted to contribute to NADH metabolism in *E. coli* Δ*lpd* Δ*pflB* carrying NAD$^+$-dependent PDH and ODH complexes according to the modified iML1515 GEM. The fluxes are expressed in mmol/g_{DW}/h as well as in percentage of the total flux (%). In the model, reversible reactions are indicated with <=> and irreversible reaction are indicated with -->. G3P, glyceraldehyde-3-phosphate.

Reactions ID	Enzymes	Reactions	Aerobic		Anaerobic	
			%	Flux	%	Flux
NADH producing						
GAPD	Glyceraldehyde-3-phosphate dehydrogenase	G3P + NAD + Pi <=> 3-phospho-D-glyceroylphosphate + NADH + H^+	41%	17.1	97%	19.7
PDH	Pyruvate dehydrogenase (NAD)	pyruvate + CoA + NAD --> acetyl-CoA + CO_2 + NADH	23%	9.69	2%	0.491
MDH	Malate dehydrogenase	L-malate + NAD <=> oxaloacetate + NADH + H^+	17%	6.88	NA[a]	NA[a]
AKGDH	2-Oxoglutarate dehydrogenase (NAD)	2-oxoglutarate + CoA + NAD --> succinyl-CoA + CO_2 + NADH	14%	5.97	NA[a]	NA[a]
PGCD	Phosphoglycerate dehydrogenase	3-phospho-D-glycerate + NAD --> 3-phosphohydroxypyruvate + NADH + H^+	4%	1.51	1%	0.199
IPMD	3-isopropylmalate dehydrogenase	3-carboxy-2-hydroxy-4-methylpentanoate + NAD --> 3-carboxy-4-hydroxy-2-oxopentanoate + NADH + H^+	1%	0.395	NA[a]	NA[a]
NADH consuming						
NADH17pp	NADH dehydrogenase (menaquinone-8 & 3 H^+)	menaquinone-8 + 4 H^+_{in} + NADH --> menaquinol-8 + 3 H^+_{out} + NAD	91%	38	2%	0.454
FADRx	FAD reductase	FAD + NADH + H^+ --> $FADH_2$ + NAD	5%	1.92	1%	0.253
LDH_D	Lactate dehydrogenase	D-lactate + NAD <=> pyruvate + NADH + H^+	NA[a]	NA[a]	87%	17.8
THD2pp	Membrane-bound transhydrogenase PntAB	2 H^+_{out} + NADH + NADP --> 2 H^+_{in} + NAD + NADPH	NA[a]	NA[a]	7%	1.41
MDH	Malate dehydrogenase	L-malate + NAD <=> oxaloacetate + NADH + H^+	NA[a]	NA[a]	2%	0.372

[a]NA, Not applicable. The enzymes were not listed as enzymes participating in NADH metabolism under the cultivation condition tested.

Table S5. Enzymes predicted to contribute to NADPH metabolism in *E. coli* Δ*lpd* Δ*pflB* carrying NADP$^+$-dependent PDH and ODH complexes according to the modified iML1515 GEM. The fluxes are expressed in mmol/g_{DW}/h as well as in percentage of the total flux (%). In the model, reversible reactions are indicated with <=> and irreversible reaction are indicated with -->. THF, tetrahydrofolate.

Reactions ID	Enzymes	Reactions	Aerobic		Anaerobic	
			%	Flux	%	Flux
NADPH producing						
PDH	Pyruvate dehydrogenase (NADP)	pyruvate + CoA + NADP --> acetyl-CoA + CO_2 + NADPH	41%	10.4	86%	1.49
ICDHyr	Isocitrate dehydrogenase	isocitrate + NADP <=> 2-oxoglutarate + CO_2 + NADPH	30%	7.64	8%	0.13
AKGDH	2-oxoglutarate dehydrogenase (NADP)	2-oxoglutarate + CoA + NADP --> succinyl-CoA + CO_2 + NADPH	26%	6.7	NA[a]	NA[a]
MTHFD	Methylenetetrahydrofolate dehydrogenase (NADP)	5,10-methyleneTHF + NADP <=> 5,10-methenylTHF + NADPH	3%	0.87	7%	0.12
NADPH consuming						
NADTRHD	Soluble transhydrogenase	NAD + NADPH --> NADH + NADP	51%	13.1	NA[a]	NA[a]
GLUDy	Glutamate dehydrogenase (NADP)	L-glutamate + H_2O + NADP <=> 2-oxoglutarate + NH_4^+ + NADPH	29%	7.53	60%	1.05
ASAD	Aspartate-semialdehyde dehydrogenase	L-aspartate 4-semialdehyde + NADP + Pi <=> 4-phospho-L-aspartate + NADPH + H^+	4%	0.94	8%	0.13
KARA1	Ketol-acid reductoisomerase	(R)-2,3-dihydroxy-3-methylbutanoate + NADP <=> (S)-2-acetolatate + NADPH + H^+	3%	0.77	6%	0.11
SULR	Sulfite reductase (NADPH2)	5 H^+ + 3 NADPH + SO_3 --> 3 H_2O + 3 NADP + H_2S	3%	0.65	5%	0.09
HSDy	Homoserine dehydrogenase (NADPH)	L-homoserine + NADP <=> L-aspartate 4-semialdehyde + NADPH + H^+	2%	0.62	5%	0.09
SHK3Dr	Shikimate dehydrogenase	3-dehydroshikimate + NADPH + H^+ <=> shikimate + NADP	1%	0.34	3%	0.05
DHDPRy	Dihydrodipicolinate reductase (NADPH)	2,3-dihydrodipicolinate + NADPH + H^+ <=> 2,3,4,5-tetrahydrodipicolinate + NADP	1%	0.33	3%	0.05
AGPR	N-acetyl-g-glutamyl-phosphate reductase	N-acetyl-L-glutamyl 5-semialdehyde + NADP + Pi <=> N-acetyl-L-glutamyl 5-phosphate + NADPH + H^+	1%	0.26	2%	0.04
KARA2	Ketol-acid reductoisomerase (2-Acetolactate)	(S)-2-aceto-2-hydroxybutanoate + NADPH + H+ <=> (R)-2,3-dihydroxy-3-methylpentanoate + NADP	1%	0.26	2%	0.04
TRDR	Thioredoxin reductase (NADPH)	oxidized thioredoxin + NADPH + H^+ --> reduced thioredoxin + NADP	1%	0.22	2%	0.03
G5SD	Glutamate-5-semialdehyde dehydrogenase	L-glutamate 5-phosphate + NADPH + H^+ --> L-glutamate semialdehyde + NADP + Pi	1%	0.20	2%	0.03
P5CR	Pyrroline-5-carboxylate reductase	1-pyrroline-5-carboxylate + 2 H^+ + NADPH --> L-proline + NADP	1%	0.20	2%	0.03
G3PD2	Glycerol-3-phosphate dehydrogenase (NADP)	Glycerol-3-phosphate + NADP <=> DHAP + NADPH + H^+	NA[a]	NA[a]	1%	0.017

[a]NA, Not applicable. The enzymes were not listed as enzymes participating in NADPH metabolism under the cultivation condition tested.

Table S6. Enzymes predicted to contribute to NADH metabolism in *E. coli* Δ*lpd* Δ*pflB* carrying NADP$^+$-dependent PDH and ODH complexes according to the modified iML1515 GEM. The fluxes are expressed in mmol/g_{DW}/h as well as in percentage of the total flux (%). In the model, reversible reactions are indicated with <=> and irreversible reaction are indicated with -->. G3P, glyceraldehyde-3-phosphate.

Reactions ID	Enzymes	Reactions	Aerobic		Anaerobic	
			%	Flux	%	Flux
NADH producing						
GAPD	Glyceraldehyde-3-phosphate dehydrogenase	G3P + NAD + Pi <=> 3-phospho-D-glyceroylphosphate + NADH + H^+	44%	17.9	99%	19.7
NADTRHD	Soluble transhydrogenase	NAD + NADPH --> NADH + NADP	32%	13.1	NA[a]	NA[a]
MDH	Malate dehydrogenase	L-malate + NAD <=> oxaloacetate + NADH + H^+	19%	7.62	NA[a]	NA[a]
PGCD	Phosphoglycerate dehydrogenase	3-phospho-D-glycerate + NAD --> 3-phosphohydroxypyruvate + NADH + H^+	4%	1.51	1%	0.21
IPMD	3-isopropylmalate dehydrogenase	3-carboxy-2-hydroxy-4-methylpentanoate + NAD --> 3-carboxy-4-hydroxy-2-oxopentanoate + NADH + H^+	1%	0.397	NA[a]	NA[a]
NADH consuming						
NADH17pp	NADH dehydrogenase (menaquinone-8 & 3 H^+)	menaquinone-8 + 4 H^+_{in} + NADH --> menaquinol-8 + 3 H^+_{out} + NAD	91%	36.9	2%	0.48
FADRx	FAD reductase	FAD + NADH + H^+ --> $FADH_2$ + NAD	5%	1.93	1%	0.27
LDH_D	Lactate dehydrogenase	D-lactate + NAD <=> pyruvate + NADH + H^+	NA[a]	NA[a]	84%	16.7
ACALD	Acetaldehyde dehydrogenase (acetylating)	acetaldehyde + CoA + NAD <=> acetyl-CoA + NADH + H^+	NA[a]	NA[a]	5%	0.97
ALCD2x	Alcohol dehydrogenase (ethanol)	ethanol + NAD <=> acetaldehyde + NADH + H^+	NA[a]	NA[a]	5%	0.97
MDH	Malate dehydrogenase	L-malate + NAD <=> oxaloacetate + NADH + H^+	NA[a]	NA[a]	2%	0.40

[a]NA, Not applicable. The enzymes were not listed as enzymes participating in NADH metabolism under the cultivation condition tested.

Table S7. Solutions predicted by the model for *E. coli* Δ*lpd* Δ*pflB* carrying $NADP^+$-dependent PDH and ODH complexes with increasing pyruvate production rates. The values for the in and out fluxes are given in mmol/g_{DW}/h. The values for biomass represent the specific growth rate of the strain and are expressed in h^{-1}.

	Fluxes (mmol/g_{DW}/h)						
Fixed parameters							
Glucose	10	10	10	10	10	10	10
Pyruvate	NA[a]	2	4	6	8	10	12
In fluxes							
O_2	22	20	18	16	14	12	10
NH_4^+	9.51	8.76	8.01	7.26	6.51	5.76	5
Pi	0.85	0.783	0.716	0.649	0.581	0.514	0.446
SO_4^{2-}	0.222	0.204	0.187	0.169	0.152	0.134	0.117
K^+	0.172	0.158	0.145	0.131	0.118	0.104	0.0903
Fe^{2+}	0.0141	0.013	0.0119	0.0108	0.00968	0.00857	0.00743
Mg^{2+}	0.00764	0.00704	0.00644	0.00583	0.00523	0.00463	0.00401
Ca^{2+}	0.00458	0.00422	0.00386	0.0035	0.00314	0.00278	0.00241
Cl^-	0.00458	0.00422	0.00386	0.0035	0.00314	0.00278	0.00241
Cu^{2+}	0.000624	0.000575	5.26E-04	0.000477	4.27E-04	0.000378	0.000328
Mn^{2+}	0.000609	0.000561	5.13E-04	0.000465	4.17E-04	0.000369	0.00032
Zn^{2+}	0.0003	0.000277	2.53E-04	0.000229	2.06E-04	0.000182	0.000158
Ni^{2+}	0.000284	0.000262	2.40E-04	0.000217	1.95E-04	0.000172	0.000149
Out fluxes							
H_2O	47.1	44.1	41.1	38.2	35.2	32.2	29.21
CO_2	23.8	20.7	17.6	14.4	11.3	8.11	5
H^+	8.09	9.45	10.8	12.2	13.5	14.9	16.3
Objective							
Biomass	0.881	0.811	0.742	0.672	0.603	0.533	0.463

[a]NA, Not applicable.

Table S8. Enzymes predicted to contribute to NADH and NADPH metabolisms in *E. coli* Δ*lpd* Δ*pflB* carrying NADP$^+$-dependent PDH and ODH complexes during pyruvate accumulation. The values for the fluxes are expressed in mmol/g_{DW}/h as well as percentage of the total flux for NADH or NADPH (%).

Reactions ID	Enzymes	Pyruvate production rate (mmol/g_{DW}/h)													
		0		2		4		6		8		10		12	
		%	Flux	%	Flux	%	Flux	%	Flux	%	Flux	%	Flux	%	Flux
NADPH producing reactions															
PDH	Pyruvate dehydrogenase (NADP)	41%	10.4	41%	9.19	42%	7.94	42%	6.7	44%	5.45	46%	4.21	42%	2.76
ICDHyr	Isocitrate dehydrogenase	30%	7.64	30%	6.62	29%	5.59	29%	4.57	28%	3.54	27%	2.52	20%	1.29
AKGDH	2-oxoglutarate dehydrogenase (NADP)	26%	6.7	26%	5.75	25%	4.8	24%	3.85	23%	2.9	21%	1.95	12%	0.80
MTHFD	Methylenetetrahydrofolate dehydrogenase (NADP)	3%	0.87	4%	0.80	4%	0.73	4%	0.66	5%	0.60	6%	0.53	7%	0.46
G6PDH2r	Glucose 6-phosphate dehydrogenase	NA[a]	NA[a]	NA[a]	NA[a]	NA[a]	NA[a]	NA[a]	NA[a]	NA[a]	NA[a]	NA[a]	NA[a]	10%	0.64
GND	Phosphogluconate dehydrogenase	NA[a]	NA[a]	NA[a]	NA[a]	NA[a]	NA[a]	NA[a]	NA[a]	NA[a]	NA[a]	NA[a]	NA[a]	10%	0.64
NADPH consuming reactions															
NADTRHD	Soluble transhydrogenase	51%	13.1	48%	10.8	45%	8.5	39%	6.2	31%	3.9	17%	1.6	NA[a]	NA[a]
GLUDy	Glutamate dehydrogenase (NADP)	29%	7.53	31%	6.94	33%	6.34	36%	5.75	41%	5.15	50%	4.56	60%	3.96
ASAD	Aspartate-semialdehyde dehydrogenase	4%	0.94	4%	0.87	4%	0.79	5%	0.72	5%	0.64	6%	0.57	8%	0.50
KARA1	Ketol-acid reductoisomerase (2,3-dihydroxy-3-methylbutanoate)	3%	0.77	3%	0.71	3%	0.65	4%	0.59	4%	0.53	5%	0.47	6%	0.41
SULR	Sulfite reductase (NADPH2)	3%	0.65	3%	0.60	3%	0.55	3%	0.50	4%	0.45	4%	0.40	5%	0.34
HSDy	Homoserine dehydrogenase (NADPH)	2%	0.62	3%	0.57	3%	0.52	3%	0.47	3%	0.42	4%	0.37	5%	0.32
SHK3Dr	Shikimate dehydrogenase	1%	0.34	1%	0.31	1%	0.28	2%	0.26	2%	0.23	2%	0.20	3%	0.18
DHDPRy	Dihydrodipicolinate reductase (NADPH)	1%	0.33	1%	0.30	1%	0.28	2%	0.25	2%	0.22	2%	0.20	3%	0.17
AGPR	N-acetyl-g-glutamyl-phosphate reductase	1%	0.26	1%	0.24	1%	0.22	1%	0.20	1%	0.18	2%	0.16	2%	0.14
KARA2	Ketol-acid reductoisomerase (2-Acetolactate)	1%	0.26	1%	0.24	1%	0.22	1%	0.20	1%	0.18	2%	0.16	2%	0.13
TRDR	Thioredoxin reductase (NADPH)	1%	0.22	1%	0.20	1%	0.18	1%	0.17	1%	0.15	1%	0.13	2%	0.12
G5SD	Glutamate-5-semialdehyde dehydrogenase	1%	0.20	1%	0.18	1%	0.16	1%	0.15	1%	0.13	1%	0.12	2%	0.10
P5CR	Pyrroline-5-carboxylate reductase	1%	0.20	1%	0.180	1%	0.16	1%	0.15	1%	0.13	1%	0.12	2%	0.10
G3PD2	Glycerol-3-phosphate dehydrogenase (NADP)	NA[a]	NA[a]	1%	0.11	1%	0.10	1%	0.09	1%	0.08	1%	0.07	1%	0.06

NADH producing reactions														
GAPD	Glyceraldehyde-3-phosphate dehydrogenase	44%	17.9	49%	18	54%	18.2	60%	18.4	68%	18.6	78%	18.7	89%	18.7
NADTRHD	Soluble transhydrogenase	32%	13.1	29%	10.8	25%	8.5	20%	6.2	14%	3.9	7%	1.6	NA[a]	NA[a]
MDH	Malate dehydrogenase	19%	7.62	18%	6.59	16%	5.57	15%	4.55	13%	3.52	10%	2.5	6%	1.28
PGCD	Phosphoglycerate dehydrogenase	4%	1.51	4%	1.39	4%	1.27	4%	1.15	4%	1.04	4%	0.92	4%	0.80
IPMD	3-isopropylmalate dehydrogenase	1%	0.40	1%	0.37	1%	0.33	1%	0.30	1%	0.27	1%	0.24	1%	0.21
NADH consuming reactions														
NADH17pp	NADH dehydrogenase (menaquinone-8 & 3 H^+)	91%	36.9	91%	33.9	91%	30.9	91%	27.9	91%	24.8	91%	21.8	91%	19.1
FADRx	FAD reductase	5%	1.93	5%	1.77	5%	1.62	5%	1.47	5%	1.32	5%	1.17	5%	1.01

Chapter 5

Impact of an $NADP^+$-dependent PDH complex on the metabolism of *E. coli* lacking pyruvate formate-lyase, soluble transhydrogenase and lactate dehydrogenase

Pauline L. Folch, Gerrit Eggink, Ruud A. Weusthuis

Abstract

During microbial conversions, substrates are converted into products to generate the metabolic energy required for the formation of microbial biomass. In dissimilation, the Gibbs free energy available is partly converted to metabolic energy for cell growth, and partly dissipated to avoid a chemical equilibrium. Microbial processes would benefit from capturing additional metabolic energy during product formation. A higher energetic efficiency would allow microorganisms to grow under more inhibitory conditions and reach higher biomass yield. In addition, it would also allow higher product yield in energy-neutral and energy-requiring product pathways. Harvesting extra metabolic energy should be realized in the product pathway to ensure the highest product yield possible.

Here, we propose a strategy to harvest additional energy during the anaerobic conversion of glucose to ethanol using an $NADP^+$-dependent pyruvate dehydrogenase (PDH) complex. The strategy aims at coupling the reoxidation of the NADPH produced by PDH to the formation of a transmembrane proton gradient via a membrane-bound transhydrogenase. The proton-motive force can then be used by the ATP synthase to synthetize ATP. This approach would theoretically allow the capture of 25% more ATP during ethanol formation from glucose. To realize this scenario, competing enzymes e.g. pyruvate formate-lyase, soluble transhydrogenase and lactate dehydrogenase must be knocked out.

We previously engineered the cofactor specificity of the PDH complex to reduce $NADP^+$ by introducing point mutations in the *lpd* gene encoding the dihydrolipoyl dehydrogenase (LPD), knocked out the genomic *lpd* and *pflB* genes and introduced the $NADP^+$-LPD variants on a plasmid. Aerobically, the additional NADPH produced led to pyruvate accumulation. Anaerobically, PDH was shown to support growth however the strains produced high amount of lactate and grew poorly. These results suggested that the cells struggled to reoxidize NADPH most likely due to low activity of the soluble transhydrogenase.

In this study, we knocked out *lpd*, *pflB*, *sthA* and *ldhA* genes and introduced the NADP$^+$-dependent LPD variants on a plasmid. Aerobically, the strains exhibiting an NADP$^+$-LPD did not accumulate any fermentation products and presented high biomass yield. Our results indicate that NADPH was reoxidized by the membrane-bound transhydrogenase PntAB although we cannot rule out that it was achieved by other mechanisms such as respiration. *E. coli* Δ*lpd* Δ*pflB* Δ*sthA* Δ*ldhA* strains carrying an NADP$^+$-PDH grew very poorly under both anaerobic and oxygen-limited conditions suggesting that PntAB was not able to regenerate the NADPH produced under these conditions. We hypothesized that the NADPH/NADP$^+$ ratio necessary for reversal of the PntAB was not met due to low expression of the PDH complex as well as NAD(P)H inhibition. However, the poor growth could also be caused by low expression of the PntAB anaerobically. We describe how both challenges can be tackled.

5.1. Introduction

Heterotrophic microorganisms use organic compounds as carbon and energy-source. A part of the organic compound is converted into microbial biomass, in a process named assimilation. This requires energy, which is generated by the breakdown of the remaining part of the organic compounds, a process called dissimilation. In dissimilation, the total energy available is partly used to generate metabolic energy (in the form of ATP or proton-motive force) and partly dissipated to avoid a chemical equilibrium. A classic example of dissimilation is the conversion of glucose into ethanol, which has a Gibbs free energy under standard conditions ($\Delta G_0'$) of -224 ± 6 kJ/mol glucose (**Table 1, reaction 1**). This conversion is realized by *Escherichia coli* via the Embden-Meyerhof-Parnas (EMP) pathway and used to generate ATP, resulting in a $\Delta G_0'$ of -171 ± 6 kJ/mol glucose (**Table 1, reaction 2**). In the hypothetical case that a cell would experience at the end of an ethanol production process 1 mM of glucose, 1 bar of CO_2, 100 mM concentrations of ATP, ADP and Pi and 17.2 M ethanol (pure ethanol), the $\Delta G'$ of this reaction is still -135 ± 13 kJ/mol glucose. This indicates that, from a bioengineering point of view, more energy is dissipated than required. Therefore, in principal, it would be possible to dissipate less energy and instead create more metabolic energy.

Metabolic energy is required for the synthesis of microbial biomass and for maintenance purposes. A higher efficiency of metabolic energy conservation would therefore result in a higher biomass yield and would enable microorganisms to grow under more inhibitory conditions in which the energy requirement of maintenance is high. A higher energy efficiency also affects microbial product formation. Three situations can be envisaged: 1) product formation generating metabolic energy, 2) metabolic energy neutral processes and 3) processes requiring the input of metabolic energy. In the first case a higher energy efficiency could either be detrimental because a higher ATP yield would deviate more substrate towards microbial biomass production, or beneficial at high maintenance conditions, e.g. when high product titers are reached. In the second case a more efficient energy generation would be

beneficial because product formation would result in the generation of metabolic energy and this could – partly – obviate the necessity to convert a part of the substrate by other energy-generating processes like respiration. The third case would benefit from the higher efficiency, comparable to microbial biomass production.

The energetic efficiency of a microbial conversion depends on the metabolic pathway used. In *E. coli* the conversion of glucose into ethanol is performed by the oxidation of glucose to pyruvate by the EMP pathway (**Table 1, reactions 3-12**), followed by the reduction of pyruvate to ethanol (**Table 1, reactions 13-15**). Metabolic energy is harvested at reactions 9 and 12. The challenge is to couple one of these other enzymatic activities to the conservation of additional energy. The uptake of glucose (**Table 1, reaction 3**) has in principle a sufficiently low $\Delta G_0'$ to increase the ATP yield. This reaction is catalyzed by the PTS and can apply the $\Delta G_0'$ surplus to transport glucose over the cell membrane against a concentration gradient. Reducing energy dissipation at this step could therefore impair glucose transport. The conversion of pyruvate into acetyl-CoA is either catalyzed by pyruvate formate-lyase (**Table 1, reaction 13a**) under anaerobic conditions, or by the pyruvate dehydrogenase complex (**Table 1, reaction 13b**) under aerobic conditions. The $\Delta G_0'$ value of this last reaction is -40 ± 3 kJ/mol and therefore also a potential candidate to increase the efficiency of energy conservation.

Recently we changed the cofactor dependency of the dihydrolipoyl dehydrogenase (LPD) from NAD^+ to $NADP^+$ and reduced the inhibition of this enzyme by high NAD(P)H concentrations. LPD is a subunit of both the pyruvate dehydrogenase (PDH) and 2-oxoglutarate dehydrogenase (ODH) complexes (see Chapter 3). *E. coli* strains expressing this modified LPD were able to grow under both aerobic and anaerobic conditions, indicating that both the $NADP^+$-dependent PDH and ODH complexes, which are essential for growth on mineral medium, carried flux.

Table 1. Reactions involved in the EMP pathway and associated Gibbs free energy (ΔG_0') release. The ΔG_0' values were calculated with eQuilibrator 2.2 (Flamholz *et al.*, 2012; Noor *et al.*, 2012; Noor *et al.*, 2013; Noor *et al.*, 2014) using CO_2 as gas and aqueous for all other compounds.

Reaction #	Reactions	ΔG_0' (kJ/mol)
1	Glucose = 2 Ethanol + 2 CO_2	-224 ± 6
2	Glucose + 2 ADP + 2 Pi = 2 Ethanol + 2 ATP + 2 CO_2	-171 ± 6
Enzymatic conversions involved in the EMP pathway		
3	Glucose + PEP = Glucose-6P + Pyruvate	-45 ± 1
4	Glucose-6P = Fructose-6P	3 ± 1
5	Fructose-6P + ATP = Fructose-1,6-BP + ADP	-13 ± 4
6	Fructose-1,6-BP = DHAP + GAP	18 ± 4
7	DHAP = GAP	6 ± 1
8	GAP + NAD^+ + Pi = 1,3-BP-glycerate + NADH	8 ± 1
9	1,3-BP-glycerate + ADP = 3P-glycerate + ATP	-19 ± 1
10	3P-glycerate = 2P-glycerate	4 ± 1
11	2P-glycerate = PEP + H_2O	-4 ± 1
12	PEP + ADP = Pyruvate + ATP	-28 ± 1
Enzymatic conversions of pyruvate to acetyl-CoA		
13a	Pyruvate + CoA = Acetyl-CoA + Formate	-21 ± 3
13b	Pyruvate + NAD^+ + CoA =Acetyl-CoA + NADH + CO_2	-40 ± 3
13c	Pyruvate + $NADP^+$ + CoA = Acetyl-CoA + NADPH + CO_2	-39 ± 3

NAD^+ and $NADP^+$ have divergent functions in the cells although their structure is similar. NAD^+ is primarily used for oxidation reactions and is regenerated via respiration or fermentation. NADPH is mostly involved in anabolic reactions where it provides reducing power. NADPH is regenerated in the oxidative pentose phosphate pathway (oxPPP) and by the TCA cycle enzyme isocitrate dehydrogenase. Due to their distinct roles, NAD^+/NADH is maintained in an oxidized state whereas $NADP^+$/NADPH is in its reduced form (Harold, 1986). The values of these ratios differ between organisms and growth conditions. For instance, $NADP^+$/NADPH ratios vary from 0.017 to 0.95 and NAD^+/NADH ratios vary from 3.74 to 1820 (Spaans *et al.*, 2015). Consequently, NAD(H) and NADP(H) have different redox potentials in the cells although their standard redox potentials are identical (E_0' = -320 mV). A high flux over the modified LPD

would increase the NADPH/NADP+ ratio, and decrease the NADH/NAD+ ratio, and as such could potentially increase the difference in redox potential between NAD+/NADH and NADP+/NADPH even further. If electrons were transferred from the relatively low redox potential of NADP+/NADPH to the relatively high redox potential of NAD+/NADH, the released energy could be harvested.

E. coli is carrying two transhydrogenases: STH and PntAB (Clarke and Bragg, 1985a; Clarke *et al.*, 1986; Boonstra *et al.*, 1999). Both enzymes catalyze *in vitro* the reversible transfer of electrons between the NAD+/NADH and NADP+/NADPH redox couples (Sweetman and Griffiths, 1971; Van de Stadt *et al.*, 1971; Hanson, 1979; Clarke and Bragg, 1985b; Boonstra *et al.*, 1999). STH is a soluble cytosolic enzyme, encoded by the *sthA* gene (Boonstra *et al.*, 1999). PntAB consists of two alpha and two beta subunits encoded by *pntA* and *pntB* genes, respectively (Clarke and Bragg, 1985a; Clarke and Bragg, 1985b; Clarke *et al.*, 1986). PntAB is a membrane-bound transhydrogenase that uses an electrochemical proton gradient to drive the reduction of NADP+ to NADPH by oxidizing NADH (Sweetman and Griffiths, 1971; Jackson, 2003). At the concentration ratios of the cofactors mentioned above, STH transfers electrons from NADP+/NADPH to NAD+/NADH, whereas PntAB uses the proton-motive force to transfer electrons in the opposite direction. One proton is translocated across the membrane per hydride transferred from NADH to NADP+ (Bizouarn *et al.*, 1996). Jan *et al.* (2013) reported that overexpression of *pntAB* genes reduced NADPH bioavailability in the cells, suggesting that the reaction is also reversible *in vivo*. But to date, the *in vivo* reversibility of the reaction catalyzed by PntAB remains a matter of controversy (Van de Stadt *et al.*, 1971; Hanson, 1979; Clarke and Bragg, 1985b; Pedersen *et al.*, 2008).

E. coli cells have a proton gradient over the cell membrane, designated as proton-motive force (PMF), of 150-180 mV (Kashket, 1983; Tran and Unden, 1998). An *in vivo* reversal of PntAB requires the transfer of protons over the plasma membrane, against this proton gradient. This would require a difference in redox potential between NAD+/NADH and NADP+/NADPH larger than the membrane potential. The ultimate concentration ratios of NAD+/NADH and

$NADP^+$/NADPH mentioned above are sufficient to realize the required redox potential. Under these conditions it could in principal contribute to the generation of the proton-motive force and as such result in the additional production of ATP via the plasma membrane ATPase. This would increase the energetic efficiency of sugar utilization (**Figure 1**).

The flux over the $NADP^+$-dependent LPD we constructed was however limited because glucose was largely converted into lactate and pyruvate. The flux over LPD was mainly limited to supply anabolic processes. Under anaerobic conditions however, some ethanol was produced, indicating that a transhydrogenase was transferring electrons from NADPH to NAD^+. Which transhydrogenase was involved remained unclear as the strain carried both STH and PntAB.

In this work, we report on the role of the membrane-bound transhydrogenase PntAB in NADH regeneration under NADPH excess conditions. Our aim was to determine if PntAB could function in the reverse direction and use the PMF to drive the reduction of NAD^+ to NADH by oxidizing NADPH (as well as to generate additional ATP via the ATP synthase). The LPD variants were expressed on a plasmid in *pflB-lpd-sthA* and *pflB-lpd-sthA-ldhA* knock-out backgrounds. The *sthA* gene encoding STH was disrupted to ensure that PntAB was the sole transhydrogenase able to regenerate NADH from NADPH in the cells. Furthermore, *ldhA* was knocked out since lactate formation was potentially masking the effect of the transhydrogenase under anaerobic conditions. Batch fermentations were performed under aerobic, anaerobic and oxygen-limited conditions. A genome-scale metabolic model was used to predict the behavior of the strains and compare the solutions obtained to the experimental data.

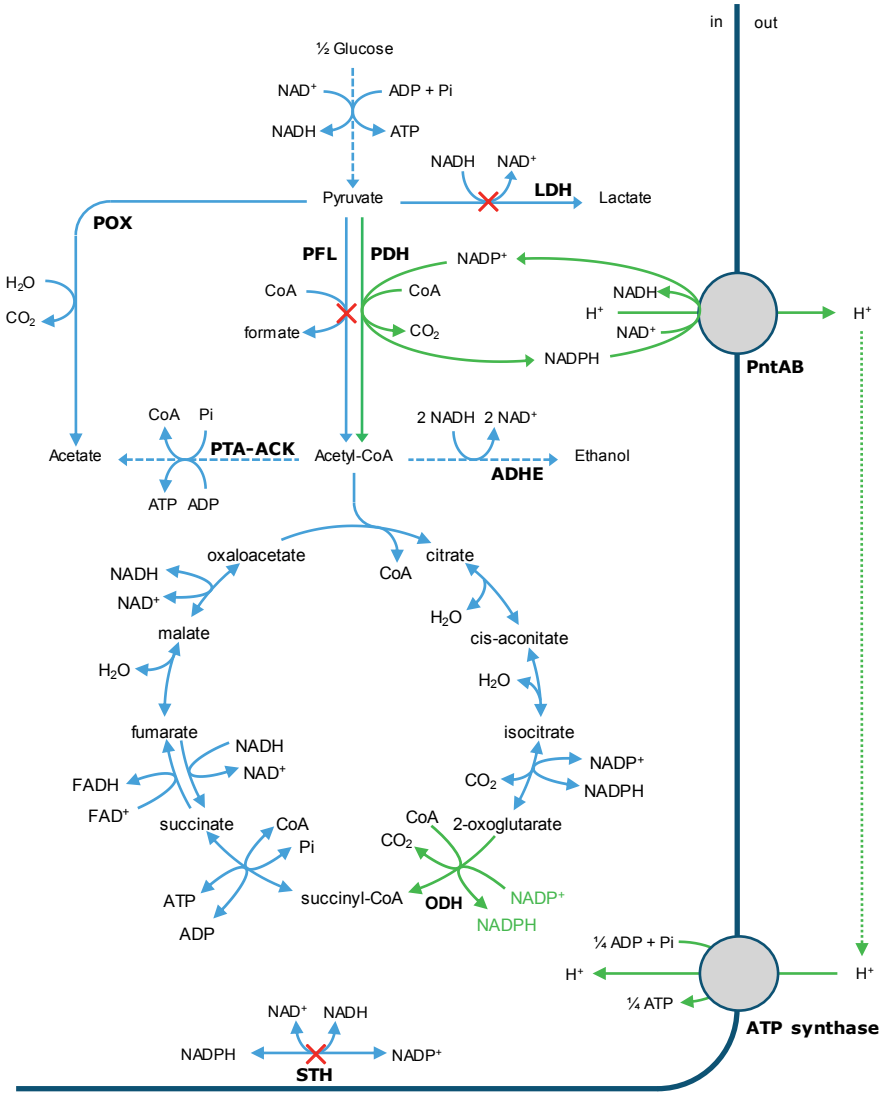

Figure 1. Strategy for additional energy conservation by forcing NADPH reoxidation through the membrane-bound transhydrogenase PntAB. Disrupted reactions are shown with a red cross (PFL, LDH and STH) and modified reactions and enzymes contributing to capture metabolic energy are depicted in green. LDH, lactate dehydrogenase; POX, pyruvate oxidase; PFL, pyruvate formate-lyase; PDH, pyruvate dehydrogenase complex; ADHE, acetaldehyde/alcohol dehydrogenase; PTA, phosphate acetyltransferase; ACK, acetate kinase, ODH, 2-oxoglutarate dehydrogenase complex; STH, soluble transhydrogenase.

5.2. Material and methods

5.2.1. Bacterial strains and plasmids

Wild-type *Escherichia coli* BW25113 was used as parental strain. Bacterial strains and plasmids used in this work are listed in **Table 2**.

Table 2. Strains and plasmids used in this study.

Strains and plasmids	Characteristics[b]	References
Strains		
BW25113	F-, Δ*(araD-araB)567*, Δ*lacZ4787(::rrnB-3)*, λ⁻, rph-1, Δ*(rhaD-rhaB)568*, hsdR514	CGSC[a]
Δ*pflB*	BW25113 Δ*pflB727::kan*	CGSC[a]
Δ*pflB* Δ*sthA*	BW25113 Δ*pflB* Δ*sthA::cm*	This study
Δ*pflB* Δ*sthA* Δ*lpd*	BW25113 Δ*pflB* Δ*sthA::cm* Δ*lpd*	This study
Δ*pflB* Δ*sthA* Δ*ldhA* Δ*lpd*	BW25113 Δ*pflB* Δ*sthA::cm* Δ*ldhA* Δ*lpd*	Chapter 3
Plasmids		
pBbA2k-RFP	*p15A, P_{tet}, kan, tet, mRFP1*	Lee *et al.* (2011)
pBbA2k empty	*p15A, P_{tet}, kan, tet*	Chapter 3
pBbA2k LPD_{WT}	pBbA2k empty derivative, P_{lpd}, native lpd	Chapter 3
pBbA2k $LPD_{low\ inhib}$	pBbA2k empty derivative, P_{lpd}, *lpd* 1AA	Chapter 3
pBbA2k LPD_{NADP}	pBbA2k empty derivative, P_{lpd}, *lpd* 7AA	Chapter 3
pBbA2k $LPD_{NADP+low\ inhib}$	pBbA2k empty derivative, P_{lpd}, *lpd* 8AA	Chapter 3
pKD3	*oriR6K gamma, tL3LAM, bla, rrnB, cm,* FRT	CGSC[a]
pKD46	*repA101(Ts), P_{araB}-gam-bet-exo, oriR101, bla, araC*	CGSC[a]
pCP20	*repA101(Ts), bla*, *cat*, *flp*	CGSC[a]
pCas9	*repA101(Ts), kan, P_{cas}-cas9, P_{araB}-gam-bet-exo, $lacI^q$, P_{trc}-sgRNA-pMB1*	Jiang *et al.* (2015)
pTargetF-*ldhA*	*pMB1, spec, gRNA* scaffold, target for *ldhA* gene, 200-nt flanking *ldhA*	Chapter 3
pTargetF-*lpd*	*pMB1, spec, gRNA* scaffold, target for *lpd* gene, 200-nt flanking *lpd*	Chapter 3

[a]CGSC, Coli Genetic Stock Center

[b]*kan*: kanamycin resistance gene; *cm*: chloramphenicol resistance gene; *tet*: tetracycline resistance gene; *bla*: ampicillin resistance gene; *spec*: spectinomycin resistance gene; Ts: temperature sensitive; *P_{araB}-gam-bet-exo*: Lambda-red recombinase genes under arabinose induction, FRT: flippase recognition site, *flp*: flippase gene under thermal induction

5.2.2. Creation of the knock-out strains

Escherichia coli Δ*pflB* was used as parental strain for creating the knock-out strains. The gene encoding the soluble transhydrogenase (*sthA*) was disrupted using the Lambda-Red recombination method as described by Datsenko and Wanner (2000). The sequences used for deletion of the *sthA* gene were taken from Baba *et al.* (2006) (see Table S1, Chapter 3).

The genes encoding the lactate dehydrogenase (*ldhA*) and the lipoamide dehydrogenase (*lpd*) were knocked out using the CRISPR-Cas9 system as described previously by Jiang *et al.* (2015). The pCas and pTargetF plasmids were a gift from Sheng Yang (Addgene plasmid #62225 and #62226). The flanking regions used for disrupting *ldhA* and *lpd* genes are listed in Chapter 3, Table S1.

5.2.3. Cultivation in shake flasks and serum bottles

Cultivations were performed under aerobic, anaerobic and oxygen-limited conditions. Both aerobic and anaerobic fermentations were performed as described in Chapters 3 and 4 of this thesis. All cultivations were carried out in a Kuhner shaker at 37°C with an agitation rate of 250 rpm. Strains carrying a pBbA2k plasmid were grown in the presence of 50 µg/mL kanamycin.

Briefly, a preculture on minimal medium was performed by transferring 5 mL of an overnight preculture on LB medium to either 45 mL or 95 mL M9 medium in 250 mL shake flasks for aerobic or anaerobic conditions, respectively. The M9 medium contained: 1 x M9 salts, 50 mM glucose, 2 mM $MgSO_4$, 1 mM $CaCl_2$, 1 mL/L of US^{Fe} trace elements (Bühler *et al.*, 2003). The pH was buffered at 6.9 using 47.5 mM Na_2HPO_4 and 44 mM KH_2PO_4. The next day, exponentially growing cells were harvested by centrifugation for 5 min at 4700 rpm at room temperature. The pellet was subsequently resuspended in 5 mL M9 medium and used to inoculate the minimal medium supplemented with glucose to a starting OD_{600nm} of 0.2. Aerobic and anaerobic fermentations were conducted in 50 mL M9 medium whereas oxygen-limited fermentations were performed using 150 mL M9 medium. In addition, cultivations were performed in 250 mL

Erlenmeyer whereas anaerobic and oxygen-limited cultivations were carried out in 200 mL serum bottles. The flasks for anaerobic fermentations were previously flushed with nitrogen to ensure complete anaerobiosis but not for the oxygen-limited conditions. Therefore, the oxygen-limited conditions were 50 mL of air which corresponds to 10.5 mL of oxygen in the serum bottles.

5.2.4. Analytical methods

The analytical methods used to characterize growth and metabolite profiles are the same as described in Chapters 3 and 4 of this thesis.

Growth was monitored by determining the absorbance at 600 nm using a Hach Lange spectrophotometer. Organic acids, glucose and ethanol concentrations were measured on an Agilent 1290 Infinity (U)HPLC. The UV and RI detectors were set at 210 nm and 55°C, respectively and 0.0005 M sulfuric acid was used as eluent with a flow of 0.5 mL/min. The internal standard used in this method was 250 mM propionic acid.

5.2.5. Carbon balances

Carbon balances and yields on glucose were calculated from the fermentation and growth profiles as described in Chapter 4.

Carbon recovery was determined for anaerobic and oxygen-limited fermentations. Aerobically, the presence of the pyruvate oxidase which catalyzes the direct decarboxylation of pyruvate to acetate does not allow us to accurately assess the CO_2 formed. The carbon balances are expressed in C-mmol present in the system.

Carbon recovery for *E. coli* Δ*pflB* Δ*sthA* and *E. coli* Δ*lpd* Δ*pflB* Δ*sthA* strains carrying the LPD variants grown anaerobically fluctuated between 285.3 ± 0.7 and 303.1 ± 0.7 C-mmol. These values are within 10% deviation indicating that the metabolites concentrations determined by HPLC as well as our estimations for biomass and CO_2 are accurate (**Table S3**). Regarding *E. coli* Δ*pflB* Δ*sthA* Δ*ldhA* Δ*lpd* strains carrying the different LPD variants, the carbon recovery

obtained during anaerobic and oxygen-limited growth were within 10% of deviation. The values can be found in **Table S6 and Table S7**, respectively.

5.2.6. Yields

As for the carbon recovery, yields of metabolites formed on glucose were determined from the HPLC measurements. Aerobically, the CO_2 yield on glucose is not included for the reasons mentioned above. The yields are expressed as mole of product formed per mole of glucose consumed. All yields can be found in the **supplementary material** section.

5.2.7. Flux through PDH complex

To further characterize the impact of the various LPD variants on the strains, fluxes through the PDH complexes were calculated from the metabolite profiles. Both the absolute flux through PDH (J_{PDH}) and the percentage of flux going through PDH against the possible maximum flux (J_{max}) were determined. J_{max} represents the maximum flux resulting from the complete glucose conversion into acetyl-CoA-based products. Both fluxes were calculated as previously described in Chapter 4.

5.2.8. Genome-scale metabolic model

The iML1515 genome-scale metabolic model from Monk *et al.* (2017) was modified to predict the behavior of *E. coli* Δ*lpd* Δ*pflB* Δ*sthA* Δ*ldhA* strain carrying an NADP+-dependent LPD. More specifically, the GEM was used to predict the consequences of replacing STH by PntAB for NADPH reoxidation. Therefore, another strain was tested in which STH was present and PntAB catalyzed the irreversible transfer of electrons from NADH to NADP+, forming NADPH.

First, the reactions catalyzed by PDH and ODH complexes were modified by substituting NAD+ and NADH for NADP+ and NADPH, respectively. As both PDH and ODH catalyze irreversible reactions, the upper and lower bounds remained unchanged ([0; 1000]).

The lactate exchange reaction was disrupted in both strains by setting the upper and lower bounds of the reaction to 0.

For *E. coli* Δ*lpd* Δ*pflB* Δ*sthA* Δ*ldhA* + LPD_{NADP}, the soluble transhydrogenase reaction was also disrupted by setting the upper and lower bounds to 0. In this strain, the reaction catalyzed by the membrane-bound transhydrogenase PntAB was made reversible by setting the upper and lower bounds to -100 and 1000, respectively. In addition, the reaction stoichiometry was changed to match the stoichiometry found in literature. The reaction used in our model was as follow: $NADH + NADP^+ + H^+_{out} = NAD^+ + NADPH + H^+_{in}$.

Aerobic conditions were enabled by setting the bounds of the oxygen uptake reaction to [-1000; 0]. To simulate anaerobic conditions, the lower bound of the reaction wat set to 0.

The default value for the glucose uptake rate fixed in the model at -10 $mmol/g_{DW}/h$ was used for both aerobic and anaerobic conditions.

Biomass and ATP maintenance requirement (ATPM) were used as objectives to maximize in the modified iML1515 GEM.

5.3. Results and Discussion

5.3.1. Genome-scale metabolic model

The modified LPD is active in both assimilation and dissimilation and predicting the consequences of increased ATP production is therefore not straightforward. Consequently, a modified iML1515 genome-scale metabolic model was used to predict the behavior of an *E. coli* strain carrying an $NADP^+$-dependent LPD (LPD_{NADP}) in which *pflB*, *sthA* and *ldhA* were knocked out. In addition, the reaction catalyzed by the membrane-bound transhydrogenase PntAB was made reversible to allow NADPH reoxidation through this enzyme. The model was also used to simulate the metabolism of *E. coli* Δ*lpd* Δ*pflB* Δ*ldhA* + LPD_{NADP} in which STH is active to understand the impact of replacing STH by PntAB for

NADPH reoxidation on the strain and ATP formation. Biomass formation and ATPM (ATP maintenance requirement) were used as objectives to maximize in the model (independently).

5.3.1.1. Maximizing for ATPM

Maximizing for ATPM allows the determination of the maximum theoretical yield of ATP formation on glucose under both aerobic and anaerobic conditions (**Table 3**).

Using a glucose uptake rate of 10 mmol/g_{DW}/h, the model predicts the formation of 235 and 20 mmol/g_{DW}/h of ATP in *E. coli* Δ*lpd* Δ*pflB* Δ*ldhA* + LPD_{NADP} under aerobic and anaerobic conditions, respectively.

Aerobically, the model predicts that *E. coli* Δ*lpd* Δ*pflB* Δ*ldhA* + LPD_{NADP} produces 79.6% of its ATP via the ATP synthase (**Table S1**). Succinyl-CoA synthetase, phosphoglycerate kinase and pyruvate kinase contribute to ATP formation by 8.2%, 8.2% and 4.1%, respectively.

Anaerobically, the model predicts an ATP yield on glucose of 2 mol/mol for *E. coli* Δ*lpd* Δ*pflB* Δ*ldhA* + LPD_{NADP}. ATP is produced during glycolysis – 66.7% ATP produced by the phosphoglycerate kinase (PGK) – and by the nucleoside-diphosphate kinase (ATP:dTDP) with 33.3%. The latter enzyme contributes to ATP formation by converting the dTTP produced during the conversion of PEP to pyruvate catalyzed by the dTDP-dependent pyruvate kinase.

On the other hand, disrupting the *sthA* gene and making PntAB reversible lead to an increase of the ATP production rate of 6.4% and 25% under aerobic and anaerobic conditions, respectively (**Table 3**). The model predicts that *E. coli* Δ*lpd* Δ*pflB* Δ*ldhA* Δ*sthA* + LPD_{NADP} can produce 2.5 ATP per glucose under anaerobic conditions. In this simulation, NADPH is exclusively reoxidized by PntAB while STH was responsible in the previous simulation. As for *E. coli* Δ*lpd* Δ*pflB* Δ*ldhA* + LPD_{NADP}, the phosphoglycerate kinase and nucleoside-diphosphate kinase (ATP:dTDP) are contributing to ATP formation. However, a third enzyme – ATP synthase – carries 14.3% of the flux for ATP production.

The reverse action of PntAB allows the production of 0.5 additional ATP per glucose using the ATP synthase (**Table S1**).

Table 3. Solutions for in and out fluxes predicted by the modified iML1515 genome-scale metabolic model when maximizing for ATP maintenance requirement (ATPM). The values are expressed in mmol/g_{DW}/h. Enzymes and reactions predicted to contribute to NADPH, NADH and ATP metabolism can be found in the **Table S1**. The model predicts that dihydroxyacetone phosphotransferase (DHAPT, which catalyzes the conversion of dihydroxyacetone and phosphoenolpyruvate into dihydroxyacetone phosphate and pyruvate) is carrying flux for pyruvate formation in *E. coli* Δ*lpd* Δ*pflB* Δ*ldhA* + LPD_{NADP} and *E. coli* Δ*lpd* Δ*pflB* Δ*ldhA* + LPD_{NADP} grown aerobically and anaerobically, respectively. DHAPT is known to be involved in glycerol degradation (Jin and Lin, 1984) and should be inactive under these conditions. Therefore, the upper and lower bounds of the reaction catalyzed by DHAPT were set to 0 (knock-out). Knocking out this reaction did not affect the final solutions described in this table.

Strains	**Δ*lpd* Δ*pflB* Δ*ldhA* + LPD_{NADP}**		**Δ*lpd* Δ*pflB* Δ*sthA* Δ*ldhA* + LPD_{NADP}**	
Parameters	**STH active PntAB irreversible**		**STH inactive PntAB reversible**	
Cultivations conditions	**Aerobic**	**Anaerobic**	**Aerobic**	**Anaerobic**
In fluxes				
Glucose	10	10	10	10
Oxygen	60	NA[a]	60	NA[a]
Out fluxes				
H_2O	60	NA[a]	60	NA[a]
CO_2	60	20	60	20
Ethanol	NA[a]	20	NA[a]	20
Objective				
ATPM	235	20	250	25

[a]NA, Not applicable. The model does not predict the production or consumption of the species.

Aerobically, the model predicts that *E. coli* Δ*lpd* Δ*pflB* Δ*ldhA* Δ*sthA* + LPD_{NADP} produces ATP thanks to the ATP synthase (80.8%), succinyl-CoA synthetase (7.7%), phosphoglycerate kinase (7.7%) and nucleoside-diphosphate kinase (ATP:GDP) (3.9%). The 6.4% augmentation observed in ATPM is due to the increase in flux through the ATP synthase.

5.3.1.2. Maximizing for biomass formation

Simulations were performed using biomass formation as an objective (**Table 4**). The model was used to predict fluxes over enzymes involved in NADH, NADPH and ATP metabolism.

For *E. coli* Δ*lpd* Δ*pflB* Δ*ldhA* + LPD_{NADP}, the model predicts specific growth rates of 0.881 h^{-1} and 0.122 h^{-1} under aerobic and anaerobic conditions, respectively (**Table 4**). No fermentation products are formed aerobically; 17.6 mmol/g_{DW}/h of ethanol is produced as well as 0.5 mmol/g_{DW}/h of succinate under anaerobic conditions.

Aerobically, the model predicts that PDH, isocitrate dehydrogenase (IDH) and ODH are responsible for 40.9%, 29.7% and 26% of the flux for NADPH production, respectively (**Table 5**). NADPH is mainly consumed by STH (43.4%) and by the $NADP^+$-dependent glutamate dehydrogenase (29.3%). NADH is produced during the reactions catalyzed by the glyceraldehyde phosphate dehydrogenase (GAPDH), STH and malate dehydrogenase (MDH) with 46.3%, 29% and 19.7%, respectively. The NADH dehydrogenase (NADH17pp) which is part of the electron transport chain (ETC) consumed most of the NADH produced in the cells. Under this cultivation condition, the model predicts that *E. coli* Δ*lpd* Δ*pflB* Δ*ldhA* + LPD_{NADP} mainly produces ATP thanks to the ATP synthase (72.5%), the phosphoglycerate kinase (18.7%) and the succinyl-CoA synthetase (6.5%).

Under anaerobic conditions, NADPH is exclusively produced during the reaction catalyzed by PDH and it is mainly consumed by STH (88.1%). Production of NADH is performed by GAPDH and STH, carrying 54.9% and 44.5% of the flux, respectively. The two enzymes involved in ethanol production – acetaldehyde dehydrogenase and alcohol dehydrogenase – are responsible for NADH consumption. Anaerobically, ATP is primarily produced by the phosphoglycerate kinase (70.9%) however the nucleotide-diphosphate kinase (ATP:dTDP) is responsible for 29.1% of the flux for ATP formation.

For *E. coli* Δ*lpd* Δ*pflB* Δ*ldhA* Δ*sthA* + LPD_{NADP}, the model predicts that the strain will exhibit a growth rate of 0.893 h^{-1} and 0.159 h^{-1} under aerobic and anaerobic conditions, respectively (**Table 4**). Replacing STH by PntAB for NADPH reoxidation therefore results in a 1.4% and 29.8% increase in growth rate – and biomass yield on glucose – under aerobic and anaerobic conditions, respectively (**Table 4**).

Table 4. Solutions for in and out fluxes predicted by the model when maximizing for biomass formation. The values for biomass are expressed in h^{-1} and the values for biomass yield on glucose are expressed in mol/mol. All the other values are given in mmol/g_{DW}/h.

Strains	**Δ*lpd* Δ*pflB* Δ*ldhA* + LPD_{NADP}**		**Δ*lpd* Δ*pflB* Δ*sthA* Δ*ldhA* + LPD_{NADP}**	
Parameters	**STH active PntAB irreversible**		**STH inactive PntAB reversible**	
Cultivations conditions	**Aerobic**	**Anaerobic**	**Aerobic**	**Anaerobic**
In fluxes				
Glucose	10	10	10	10
Oxygen	22.0	NA[a]	21.4	NA[a]
NH_4^+	9.5	1.3	9.6	1.7
Pi	0.8	NA[a]	0.9	NA[a]
Out fluxes				
H_2O	47.1	3.8	46.9	4.9
CO_2	23.8	17.6	23.4	16.9
H^+	8.1	2.2	8.2	2.8
Ethanol	NA[a]	17.6	NA[a]	16.9
Succinate	NA[a]	0.5	NA[a]	0.7
Objective				
Biomass (X)	0.881	0.122	0.893	0.159
Yield X/glc	0.088	0.012	0.089	0.016

[a]NA, Not applicable. The model does not predict the production or consumption of the species.

Table 5. Enzymes predicted to contribute to NADH, NADPH and ATP metabolisms when maximizing for biomass formation. The values are expressed in mmol/g_{DW}/h. Enzymes carrying 5% of flux or less can be found in **Table S2**.

Reactions ID	Enzymes	Reactions	*E. coli* ΔΔΔ + LPD_{NADP}				*E. coli* ΔΔΔΔ + LPD_{NADP}			
			Aerobic		Anaerobic		Aerobic*		Anaerobic*	
			%	Flux	%	Flux	%	Flux	%	Flux
NADPH producing reactions										
PDH	Pyruvate dehydrogenase (NADP)	pyruvate + CoA + NADP --> acetyl-CoA + CO_2 + NADPH	40.9	10.5	100	18.2	41.1	10.4	100	17.6
ICDHyr	Isocitrate dehydrogenase	isocitrate + NADP <=> 2-oxoglutarate + CO_2 + NADPH	29.7	7.6	NA[a]	NA[a]	29.6	7.5	NA[a]	NA[a]
AKGDH	2-oxoglutarate dehydrogenase (NADP)	2-oxoglutarate + CoA + NADP --> succinyl-CoA + CO_2 + NADPH	26.0	6.7	NA[a]	NA[a]	25.8	6.5	NA[a]	NA[a]
NADPH consuming reactions										
NADTRHD	Soluble transhydrogenase (STH)	NAD + NADPH --> NADH + NADP	43.4	11.2	88.1	16.0	NA[a]	NA[a]	NA[a]	NA[a]
THD2pp	Membrane-bound transhydrogenase (PntAB)	NADH + NADP + H^+_{out} --> NAD + NADPH + H^+_{in}	NA[a]	NA[a]	NA[a]	NA[a]	49.3	12.5	88.9	15.7
GLUDy	Glutamate dehydrogenase (NADP)	L-glutamate + H_2O + NADP <=> 2-oxoglutarate + NH_4^+ + NADPH	29.3	7.5	7.9	1.4	30.2	7.6	7.7	1.4
FADRx2	FAD reductase	FAD + NADPH + H^+ --> $FADH_2$ + NADP	7.5	1.9	1.5	0.3	NA[a]	NA[a]	NA[a]	NA[a]
NADH producing reactions										
GAPD	Glyceraldehyde-3-phosphate dehydrogenase	G3P + Pi + NAD <=> 3-phospho-D-glyceroylphosphate + NADH + H^+	46.3	17.9	54.9	19.7	45.0	17.9	55.2	19.6
NADTRHD	Soluble transhydrogenase (STH)	NAD + NADPH --> NADH + NADP	29.0	11.2	44.5	16.0	NA[a]	NA[a]	NA[a]	NA[a]
THD2pp	Membrane-bound transhydrogenase (PntAB)	NADH + NADP + H^+_{out} --> NAD + NADPH + H^+_{in}	NA[a]	NA[a]	NA[a]	NA[a]	31.4	12.5	44.1	15.7
MDH	Malate dehydrogenase	L-malate + NAD <=> oxaloacetate + NADH + H^+	19.7	7.6	NA[a]	NA[a]	18.8	7.4	NA[a]	NA[a]
NADH consuming reactions										
NADH17pp	NADH dehydrogenase (menaquinone-8 & 3 protons)	menaquinone-8 + NADH + 4 H^+_{in} --> menaquinol-8 + NAD + 3 H^+_{out}	95.7	36.9	1.3	0.5	90.9	36.1	NA[a]	NA[a]
ACALD	Acetaldehyde dehydrogenase (acetylating)	acetaldehyde + CoA + NAD <=> acetyl-CoA + NADH + H^+	NA[a]	NA[a]	49.1	17.6	NA[a]	NA[a]	47.6	16.9
ALCD2x	Alcohol dehydrogenase (ethanol)	ethanol + NAD <=> acetaldehyde + NADH + H^+	NA[a]	NA[a]	49.1	17.6	NA[a]	NA[a]	47.6	16.9
ATP producing reactions										
ATPS4rpp	ATP synthase (four protons for one ATP	ADP + Pi + 4 H^+_{out} <=> ATP + H_2O + 3 H^+_{in}	72.5	69.3	NA[a]	NA[a]	73.0	70.7	11.6	3.6
PGK	Phosphoglycerate kinase	3-phosphoglycerate + ATP <=> 1,3-bisphosphoglycerate + ADP	18.7	17.9	70.9	19.7	18.4	17.9	62.7	19.6
SUCOAS	Succinyl-CoA synthetase (ADP-forming)	succinate + CoA + ATP <=> succinyl-CoA + ADP + Pi	6.5	6.2	NA[a]	NA[a]	6.2	6.0	NA[a]	NA[a]
NDPK4	Nucleoside-diphosphate kinase (ATP:dTDP)	ATP + dTDP <=> ADP + dTTP	NA[a]	NA[a]	29.1	8.1	NA[a]	NA[a]	25.8	8.1
ATP consuming reactions										
BIOMASS	Biomass	0.000223 10fthf_c + 2.6e-05 2fe2s_c + 0.000223 ...	69.6	66.5	33.3	9.3	69.6	67.5	38.4	12.0
PFK	Phosphofructokinase	fructose-6-phosphate + ATP --> fructose-1,6-bisphosphate + ADP + H^+	9.7	9.2	NA[a]	NA[a]	9.5	9.2	31.5	9.9
ATPM	ATP maintenance requirement	ATP + H_2O --> ADP + Pi + H^+	7.2	6.9	24.7	6.9	7.1	6.9	21.9	6.9
PFK3	Phosphofructokinase (s7p)	sedoheptulose 7-phosphate + ATP <=> sedoheptulose 1,7-bisphosphate + ADP + H^+	NA[a]	NA[a]	35.6	9.9	NA[a]	NA[a]	NA[a]	NA[a]

[a]NA, Not applicable. The enzymes are not predicted to contribute to production or consumption of either NADH, NADPH or ATP.

Anaerobically, the predicted ethanol (16.9 mmol/g_{DW}/h) and succinate (0.7 mmol/g_{DW}/h) production rates are similar to the ones reported for a strain carrying an active STH.

Under aerobic conditions, PDH, IDH and ODH enzymes are responsible for NADPH production and carry similar fluxes than previously reported for *E. coli* Δ*lpd* Δ*pflB* Δ*ldhA* + LPD_{NADP} (**Table 5**).

Furthermore, the model predicts that the $NADP^+$-dependent glutamate dehydrogenase contributes to NADPH consumption by 30.2% while PntAB reoxidizes 49.3% of the NADPH produced. Consequently, PntAB is also responsible for 31.4% of the flux for NADH production. GAPDH carries most of the flux with 45% and the malate dehydrogenase (MDH) carries 18.8%. Respiration is the main NADH consuming process and the NADH dehydrogenase carries 90.9% of the flux. As for the strain carrying an active STH, the model predicts that both ATP synthase and PGK contributes to ATP formation, and in similar proportions. ATP is mainly consumed for biomass formation.

Anaerobically, NADPH is exclusively formed during the reaction catalyzed by PDH and it is mainly consumed by PntAB to regenerate NADH (88.9%). GAPDH and PntAB carry 55.2% and 44% of the flux for NADH production, respectively. As predicted for the strain carrying an active STH, acetaldehyde dehydrogenase and alcohol dehydrogenase are responsible for NADH consumption. While E*. coli* Δ*lpd* Δ*pflB* Δ*ldhA* + LPD_{NADP} synthetizes ATP via PGK and nucleoside-diphosphate kinase (ATP:dTDP), E*. coli* Δ*lpd* Δ*pflB* Δ*ldhA* Δ*sthA* + LPD_{NADP} also uses the ATP synthase which carries 11.6% of the total flux. the model predicts that this strain produces higher amount of ATP than its counterpart with an active STH. As biomass formation is the main ATP consuming process – and objective to maximize – the higher ATP production rate results in higher growth rate (**Table 4**).

The modified iML151 genome-scale metabolic model allowed us to predict flux in *E. coli* Δ*lpd* Δ*pflB* Δ*ldhA* + LPD_{NADP} under both aerobic and anaerobic

conditions. The model predicted that a strain using PntAB for NADPH reoxidation will produce additional ATP which will be used for biomass formation. Nevertheless, the augmentation of growth rate might not be seen *in vivo* as the capacity of the modified LPD may be limiting the growth rate. Instead, *E. coli* Δ*lpd* Δ*pflB* Δ*ldhA* + LPD_{NADP} can also show a 29.8% increase in biomass formed anaerobically.

5.3.2. *In vivo* characterization of *sthA* disruption in strains carrying an NADP+-dependent LPD

To force NADPH reoxidation through the membrane-bound transhydrogenase PntAB, the *sthA* gene was knocked out in *E. coli* Δ*lpd* Δ*pflB* strains carrying different LPD variants. Aerobic and anaerobic fermentations were performed to determine the effect of STH inactivation on the strains' metabolism.

E. coli Δ*lpd* Δ*pflB* Δ*sthA* did not grow on minimal medium supplemented with glucose under both aerobic and anaerobic conditions (data not shown), but introduction of an LPD variant restored growth (**Figure 2**). These observations fit the results reported previously in Chapter 3 and Chapter 4 of this thesis.

Disruption of *sthA* in *E. coli* Δ*lpd* Δ*pflB* strains carrying NAD^+-dependent LPDs resulted in minor differences in both growth and metabolite profiles under aerobic and anaerobic conditions (**Table 6**, **Table 7** and **Figure 2**, **A1-A3** and **Figure 2**, **B1-B3**). These observations are in accordance with the findings of Sauer *et al.* (2004) where wild-type *E. coli* and *sthA* mutant exhibited identical growth rates during aerobic growth on glucose. STH was reported to have a crucial role in NADPH reoxidation under conditions leading to NADPH excess (Sauer *et al.*, 2004). *E. coli* strains carrying NAD^+-LPD variants do not produce high amount of NADPH therefore knocking out *sthA* should not have any influence, as observed in this study.

Table 6. Specific growth rates μ for *E. coli* Δ*lpd* Δ*pflB* and *E. coli* Δ*lpd* Δ*pflB* Δ*sthA* strains harboring an LPD variant. The specific growth rates were calculated from the OD_{600nm} measurements under both aerobic and anaerobic conditions. The values represent the average of biological triplicates (or duplicates in the case of *E. coli* Δ*lpd* Δ*pflB* Δ*sthA* + LPD_{WT} grown anaerobically) with standard deviations. The values are expressed in h^{-1}.

Strains	Aerobic	Anaerobic	References
E. coli Δ*pflB*	0.55 ± 0.00	0.17 ± 0.00	Chapter 4
E. coli Δ*lpd* Δ*pflB*	NA[a]	NA[a]	Chapter 4
E. coli Δ*lpd* Δ*pflB* + empty pBbA2k	NA[a]	NA[a]	Chapter 4
E. coli Δ*lpd* Δ*pflB* + LPD_{WT}	0.53 ± 0.00	0.15 ± 0.00	Chapter 4
E. coli Δ*lpd* Δ*pflB* + $LPD_{low\ inhib}$	0.54 ± 0.00	0.15 ± 0.00	Chapter 4
E. coli Δ*lpd* Δ*pflB* + LPD_{NADP}	0.28 ± 0.01	0.11 ± 0.00	Chapter 4
E. coli Δ*lpd* Δ*pflB* + $LPD_{NADP+low\ inhib}$	0.35 ± 0.01	0.02-0.10 ± 0.00	Chapter 4
E. coli Δ*pflB* Δ*sthA*	0.55 ± 0.00	0.14 ± 0.00	This study
E. coli Δ*lpd* Δ*pflB* Δ*sthA*	NA[a]	NA[a]	This study
E. coli Δ*lpd* Δ*pflB* Δ*sthA* + empty pBbA2k	NA[a]	NA[a]	This study
E. coli Δ*lpd* Δ*pflB* Δ*sthA* + LPD_{WT}	0.52 ± 0.00	0.15 ± 0.00	This study
E. coli Δ*lpd* Δ*pflB* Δ*sthA* + $LPD_{low\ inhib}$	0.54 ± 0.00	0.16 ± 0.00	This study
E. coli Δ*lpd* Δ*pflB* Δ*sthA* + LPD_{NADP}	0.28 ± 0.00	0.10 ± 0.00	This study
E. coli Δ*lpd* Δ*pflB* Δ*sthA* + $LPD_{NADP+low\ inhib}$	0.32 ± 0.00	0.13 ± 0.00	This study

[a]NA, Not applicable. The strains did not show any sign of growth.

E. coli Δ*lpd* Δ*pflB* Δ*sthA* + $LPD_{NADP+low\ inhib}$ showed very similar growth and metabolite profiles to its counterpart exhibiting an active STH under both aerobic and anaerobic conditions (**Table 6**, **Table 7**, **Figure 2, A5** and **B5** and Chapter 4, Figures 1E and 2E). The lack of significant changes indicates that STH was not involved in NADPH reoxidation in the strain characterized in Chapter 4.

E. coli Δ*lpd* Δ*pflB* Δ*sthA* + LPD_{NADP} also showed minor differences with *E. coli* Δ*lpd* Δ*pflB* + LPD_{NADP} anaerobically (**Table 6** and **Figure 2, B4**), indicating that STH was not carrying flux under this condition. However, deletion of the *sthA* gene in *E. coli* Δ*lpd* Δ*pflB* + LPD_{NADP} led to major changes under aerobic

conditions (**Figure 2, A4**). Although it grew at the same specific growth rate (**Table 6**), *E. coli* Δ*lpd* Δ*pflB* Δ*sthA* + LPD_{NADP} showed an 18.6% increase in maximum OD_{600nm} and an apparent biomass yield on glucose of 2.08 ± 0.9 mol/mol (**Table S4**). Remarkably, the strain did not consume all glucose in 38h of cultivation. It did not accumulate pyruvate during its exponential phase of growth (**Figure 2, A4**) and produced little amounts of fermentation products; 5.6 ± 0.27 mM acetate, 2.50 ± 0.14 mM lactate and 2.50 ± 0.14 mM pyruvate.

Table 7. Fluxes through the PDH complex of *E. coli* strains grown anaerobically on M9 medium supplemented with 50mM glucose. Absolute flux through PDH (J_{PDH}) and fraction of the flux through PDH compared to the total possible flux (J_{PDH}/J_{max}) are given. The values correspond to the average of fluxes from biological triplicates with standard deviations.

Strains	J_{PDH} (mM pyruvate/h)	J_{PDH}/J_{max} (%)	References
E. coli Δ*pflB*	0.46 ± 0.02	5.7 ± 0.2	Chapter 4
E. coli Δ*pflB* Δ*sthA*	0.35 ± 0.02	5.0 ± 0.2	This study
E. coli Δ*lpd* Δ*pflB* Δ*sthA*	ND[a]	ND[a]	This study
E. coli Δ*lpd* Δ*pflB* Δ*sthA* + LPD_{WT}	0.62 ± 0.02	8.2 ± 0.2	This study
E. coli Δ*lpd* Δ*pflB* Δ*sthA* + $LPD_{low\ inhib}$	1.66 ± 0.05	20.1 ± 0.6	This study
E. coli Δ*lpd* Δ*pflB* Δ*sthA* + LPD_{NADP}	0.03 ± 0.01	2.3 ± 0.7	This study
E. coli Δ*lpd* Δ*pflB* Δ*sthA* + $LPD_{NADP+low\ inhib}$	0.04 ± 0.00	1.0 ± 0.0	This study

[a]ND, Not determined. The strain did not grow.

We reasoned that the apparent increased biomass formation as well as the lack of fermentation products exhibited by *E. coli* Δ*lpd* Δ*pflB* Δ*sthA* + LPD_{NADP} can be the consequence of NADPH reoxidation via the membrane-bound transhydrogenase PntAB or via respiration. As STH was knocked out in this strain, the NADPH produced during the conversions catalyzed by both PDH and ODH complexes can only be reoxidized in the reaction catalyzed by PntAB. Nevertheless, knocking out *sthA* in *E. coli* Δ*lpd* Δ*pflB* + $LPD_{NADP+low\ inhib}$ did not result in significant changes. $LPD_{NADP+low\ inhib}$ was shown to be less sensitive to NAD(P)H inhibition than LPD_{NADP} (Chapter 3, Figure 3). So, the strain carrying $LPD_{NADP+low\ inhib}$ potentially produced higher amount of NADPH in the same amount of time than a strain carrying LPD_{NADP}. We hypothesized that the

amount of NADPH generated in *E. coli* Δ*lpd* Δ*pflB* Δ*sthA* + $LPD_{NADP+low\ inhib}$ exceeded the capacity of PntAB and therefore the strain accumulated pyruvate instead (**Figure 2, A5**). However, we cannot rule out the possibility that NADPH could have been respired by the strain. Overproduction of NADPH could have led to point mutations in one of the genes encoding NADH dehydrogenase I (Complex I of the electron transport chain), thereby allowing the enzyme to oxidize NADPH. Auriol *et al.* (2011) demonstrated that an NADPH-overproducing strain was able to respire both NADH and NADPH after the apparition of an E183A point mutation in the NuoF enzyme. Thus, NADPH could be used to generate catabolic energy. This should however not result in an increased ATP production.

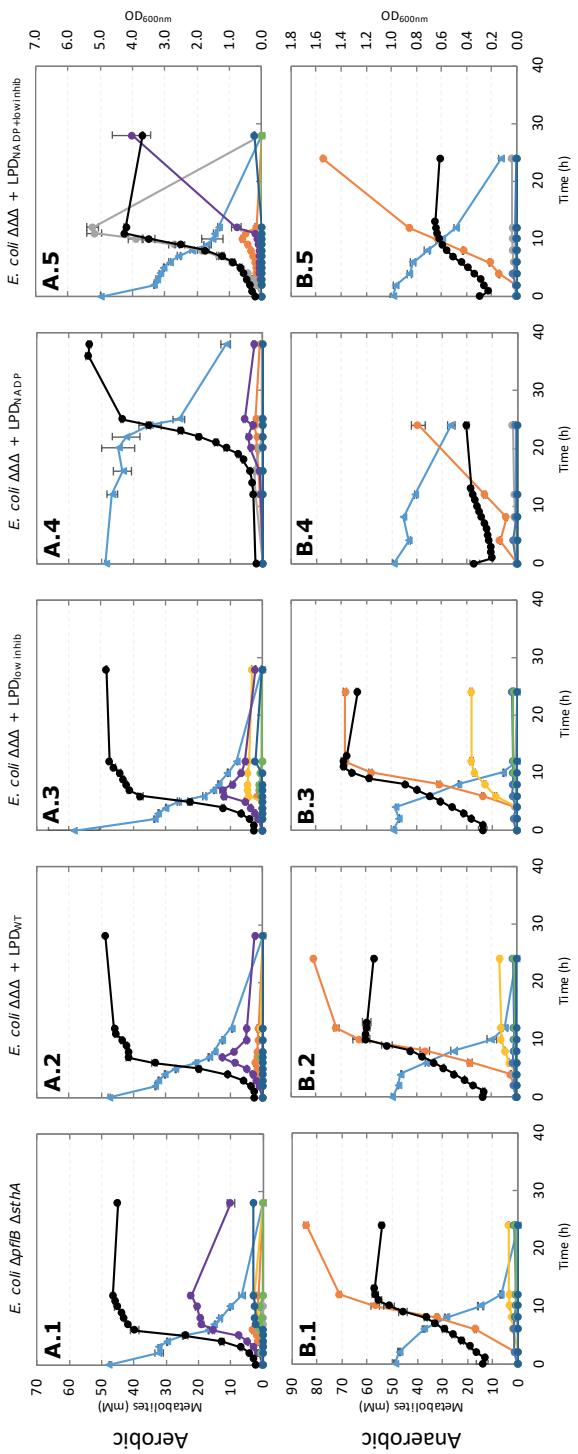

Figure 2. Growth and metabolite profiles of *E. coli* Δ*lpd* Δ*pflB* Δ*sthA* strains carrying an LPD variant under both aerobic and anaerobic conditions. The values represent the average of biological triplicates (or duplicates for *E. coli* Δ*lpd* Δ*pflB* Δ*sthA* + LPD_{WT} grown anaerobically) with standard deviations. Legend: glucose, lactate, pyruvate, ethanol, acetate, succinate, formate and biomass.

5.3.3. *In vivo* characterization of *ldhA* disruption in *E. coli* Δ*lpd* Δ*pflB* Δ*sthA* strains carrying LPD variants

During anaerobic fermentations of *E. coli* Δ*lpd* Δ*pflB* Δ*sthA* and *E. coli* Δ*lpd* Δ*pflB* Δ*sthA* strains, lactate was produced as main fermentation product (Chapter 4, Figure 2 and Figure 2, B1-B5), preventing most of the flux to go through the PDH complexes. Nonetheless, the strategy proposed in this work to reoxidize NADPH by the reverse action of PntAB – and capture additional metabolic energy – requires flux through the $NADP^+$-dependent PDH complex under anaerobic conditions. Consequently, the *ldhA* gene encoding the lactate dehydrogenase (LDH) was knocked out in *E. coli* Δ*lpd* Δ*pflB* Δ*sthA* strains carrying the LPD variants. Fermentations were conducted under aerobic, anaerobic and oxygen-limited conditions to assess the phenotype of the strains as well as the realization of the proposed strategy.

5.3.3.1. Aerobic fermentations

E. coli Δ*lpd* Δ*pflB* Δ*sthA* strains carrying either LPD_{WT}, $LPD_{low\ inhib}$, LPD_{NADP} or $LPD_{NADP+low\ inhib}$ (**Figure 2, A2-A5** and **Figure 3, A1-A4**) produced trace amounts of lactate under aerobic conditions. The additional knock out of *ldhA* reduced lactate production to zero.

Both strains carrying an NAD^+-dependent LPD exhibited lower specific growth rates (**Table 6** and **Table 8**) than their counterparts carrying the *ldhA* gene, but they reached higher maximum OD_{600nm} (**Figure 2, A2-A3** and **Figure 3, A1-A2**). Their apparent biomass yields on glucose also showed an increase of 32.2% and 55.8% for the quadruple mutant strains carrying LPD_{WT} and $LPD_{low\ inhib}$, respectively (**Table S4** and **Table S8**). Both strains accumulated between 12 and 14.5 mM acetate during their exponential phase of growth. After 7 h of cultivation, both strains started co-consumption of glucose and acetate and they exhibited linear growth.

Likewise, knocking out *ldhA* in *E. coli* Δ*lpd* Δ*pflB* Δ*sthA* + LPD_{NADP} led to an increase in apparent biomass yield (**Table S4** and **Table S8**) and maximum OD_{600nm} (**Figure 2, A4** and **Figure 3, A3**). The strain also exhibited a 14.3%

higher specific growth rate than *E. coli* Δ*lpd* Δ*pflB* Δ*sthA* + LPD_{NADP} (**Table 6** and **Table 8**). The absence of fermentation products, especially pyruvate, indicates that the NADPH produced during the reactions catalyzed by both PDH and ODH complexes was used to regenerate NADH, either by the intended reverse action of PntAB or by NADPH respiration.

Table 8. Specific growth rates μ determined for *E. coli* Δ*lpd* Δ*pflB* Δ*sthA* Δ*ldhA* strains grown under different conditions. The growth rates were determined from the OD_{600nm} measurements and are expressed in h^{-1}. The values determined during aerobic and anaerobic cultivations represent the average of specific growth rates calculated from three biological replicates with standard deviations. The values presented in the table for oxygen-limited cultivations were determined from biological duplicates with standard deviations.

Strains	Aerobic	Anaerobic	Oxygen-limited
E. coli Δ*pflB* Δ*sthA* Δ*ldhA* Δ*lpd*	NA[a]	NA[a]	NA[a]
E. coli Δ*pflB* Δ*sthA* Δ*ldhA* Δ*lpd* + empty pBbA2k	NA[a]	NA[a]	NA[a]
E. coli Δ*pflB* Δ*sthA* Δ*ldhA* Δ*lpd* + LPD_{WT}	0.48 ± 0.00	0.12 ± 0.01	0.43 ± 0.01
E. coli Δ*pflB* Δ*sthA* Δ*ldhA* Δ*lpd* + $LPD_{low\ inhib}$	0.49 ± 0.00	0.21 ± 0.01	0.40 ± 0.02
E. coli Δ*pflB* Δ*sthA* Δ*ldhA* Δ*lpd* + LPD_{NADP}	0.32 ± 0.00	0.05 ± 0.00	0.08 ± 0.00
E. coli Δ*pflB* Δ*sthA* Δ*ldhA* Δ*lpd* + $LPD_{NADP+low\ inhib}$	0.34 ± 0.00	0.12 ± 0.01	0.16 ± 0.00

[a]NA, Not applicable. The strains did not grow under the cultivation condition tested.

Unexpectedly, disruption of *ldhA* resulted in major changes in both growth and metabolite profiles for *E. coli* Δ*lpd* Δ*pflB* Δ*sthA* Δ*ldhA* + $LPD_{NADP+low\ inhib}$ (**Figure 2, A5** and **Figure 3, A4**). Nevertheless, these profiles are very similar to the ones obtained for *E. coli* Δ*lpd* Δ*pflB* Δ*sthA* + LPD_{NADP} and *E. coli* Δ*lpd* Δ*pflB* Δ*sthA* Δ*ldhA* + LPD_{NADP} (**Figure 2, A4** and **Figure 3, A3** and **A4**). *E. coli* Δ*lpd* Δ*pflB* Δ*sthA* Δ*ldhA* + $LPD_{NADP+low\ inhib}$ did not accumulate a high amount of pyruvate during exponential phase of growth. Instead, the strain produced up to 8.2 ± 0.3 mM acetate, 2.3 ± 0.1 mM pyruvate, 2.5 ± 1.4 mM formate, 2.1 ± 2.4 mM ethanol and traces of succinate (**Figure 3, A4**). As observed for the quadruple knock-out strains carrying an LPD variant, *E. coli* Δ*lpd* Δ*pflB* Δ*sthA* Δ*ldhA* + $LPD_{NADP+low\ inhib}$ reached a higher maximum OD_{600nm} (**Figure 2, A5** and

Figure 3, A4) and showed an 80% increase in apparent biomass yield on glucose (**Table S4** and **Table S8**).

Deleting LDH resulted in higher OD_{600nm} values and associated apparent biomass yields for all four strains. The final OD_{600nm} values were similar for strains carrying either NAD^+- or $NADP^+$- dependent LPDs. It can therefore not be concluded that using an $NADP^+$-dependent LPD in conjunction with proton-translocating transhydrogenase activity of PntAB caused this increase. We should take into consideration that OD measurements not only depends on biomass concentrations but also on cell morphology. We cannot exclude that the LDH knockout changed the cells morphology. This indicates that dry cell weight measurements have to be applied to assess the effect of the final strains.

5.3.3.2. Anaerobic fermentations

Although the anaerobic activity of PDH_{WT} was proven to support anabolic processes (growth) in a strain lacking a PFL (Chapter 4), lactate was formed as main fermentation product due to the high NADH inhibition of the PDH complex. Lactate formation allows maintenance of the glycolysis by regenerating NAD^+ in a strain exclusively using PDH for the anaerobic conversion of pyruvate to acetyl-CoA (Chapter 4). Cells carrying an active PDH and lacking a functional LDH cannot rely on lactate formation and should perform homofermentative production of ethanol to maintain glycolysis as well as regenerate NAD^+.

All *E. coli* Δ*lpd* Δ*pflB* Δ*sthA* Δ*ldhA* strains carrying an LPD variant consumed less than 5.0 mM glucose in 28 h of cultivations (**Figure 3, B1-B4**) and reached significantly lower maximum OD_{600nm} than strains carrying a functional LDH (**Figure 2, B1-B5** and **Figure 3, B1-B4**).

E. coli Δ*lpd* Δ*pflB* Δ*sthA* Δ*ldhA* carrying LPD_{WT}, $LPD_{low\ inhib}$, LPD_{NADP} and $LPD_{NADP+low\ inhib}$ reached 75.3%, 71.2%, 40.2% and 55.7% lower maximum OD_{600nm} than strains carrying a functional LDH, respectively. Furthermore, the strains produced little amounts of pyruvate and acetate with concentrations below 2.5 mM. All strains did not exhibit a lag phase and reached their maximum OD_{600nm} between 3 to 6 h of cultivation (**Figure 3, B1-B4**). Together with the

absence of fermentation products, this suggests that respiration occurred at the beginning of the cultivations, allowing the formation of small amount of biomass. Perhaps oxygen was introduced in the anaerobic flasks during inoculation as the inoculum were prepared aerobically.

Besides, the low acetate and pyruvate concentrations indicate that little flux went through the PDH complexes – regardless their cofactor specificity – probably due to NAD(P)H inhibition. This hypothesis is supported by the fact that both strains carrying either $LPD_{low\ inhib}$ and $LPD_{NADP+low\ inhib}$ reached higher maximum OD_{600nm} than strains carrying LPD_{WT} and LPD_{NADP} under both anaerobic (**Figure 3, B1-B4**) and oxygen-limited conditions (**Figure 3, C1-C4**), respectively. Moreover, *E. coli* Δ*lpd* Δ*pflB* Δ*sthA* Δ*ldhA* + $LPD_{low\ inhib}$ produced ethanol under both anaerobic and oxygen-limited conditions whereas *E. coli* Δ*lpd* Δ*pflB* Δ*sthA* Δ*ldhA* + LPD_{WT} did not. *E. coli* Δ*lpd* Δ*pflB* Δ*sthA* Δ*ldhA* + $LPD_{low\ inhib}$ produced 5.0 ± 0.7 mM ethanol anaerobically, and 35.4 ± 1.0 mM under oxygen-limited conditions. These results demonstrate that higher flux went through its PDH complex than in the strain carrying LPD_{WT}. The pyruvate dehydrogenase complex of *E. coli* was reported to exhibit low activity under anaerobic conditions due to its high sensitivity towards NADH (Hansen and Henning, 1966; Snoep *et al.*, 1993a; de Graef *et al.*, 1999). We previously described that introduction of the E354K mutation in the *lpd* gene only relieved a part of the NAD(P)H inhibition (Kim *et al.*, 2008) therefore the enzyme is still subjected to some inhibition.

Inhibition does not seem to be the only cause for the impaired growth of the strains under anaerobic conditions. Expression of the genes encoding the PDH complex might have been low or repressed under anaerobic conditions as reported previously (Smith and Neidhardt, 1983; Quail *et al.*, 1994; Cunningham *et al.*, 1998). This hypothesis is supported by the results obtained during oxygen-limited conditions.

5.3.3.4. Oxygen-limited fermentations

Introduction of 10.5 mL of oxygen to the cultures resulted in an increase in both biomass formation (**Figure 3, 1-B.4** and **C1-C4**) and specific growth rate (**Table 8**) for all strains.

Both *E. coli* Δ*lpd* Δ*pflB* Δ*sthA* Δ*ldhA* strains carrying an NAD^+-dependent LPD exhibited specific growth rates close to the ones obtained aerobically (**Table 8**). *E. coli* Δ*lpd* Δ*pflB* Δ*sthA* Δ*ldhA* + LPD_{WT} showed a 2.6-times increase in OD_{600nm} while *E. coli* Δ*lpd* Δ*pflB* Δ*sthA* Δ*ldhA* + $LPD_{low\ inhib}$ reached OD_{600nm} comparable to the ones obtained during anaerobic cultivation of *E. coli* Δ*lpd* Δ*pflB* Δ*sthA* + $LPD_{low\ inhib}$ (**Figure 2, B2** and **Figure 3, C2**).

Table 9. Fluxes through the PDH complex of *E. coli* Δ*lpd* Δ*pflB* Δ*sthA* Δ*ldhA* strains carrying an LPD variant on a plasmid during oxygen-limited cultivations. Absolute flux through PDH (J_{PDH}) and the fraction of the flux through PDH compared to the total maximum flux (J_{PDH}/J_{max}) are displayed in the table. The values correspond to the average of fluxes calculated from biological duplicates with standard deviations.

Strains	J_{PDH} (mM pyruvate/h)	J_{PDH}/J_{max} (%)
E. coli Δ*lpd* Δ*pflB* Δ*sthA* Δ*ldhA* + LPD_{WT}	0.25 ± 0.03	16.2 ± 2.8
E. coli Δ*lpd* Δ*pflB* Δ*sthA* Δ*ldhA* + $LPD_{low\ inhib}$	1.85 ± 0.20	57.0 ± 3.0
E. coli Δ*lpd* Δ*pflB* Δ*sthA* Δ*ldhA* + LPD_{NADP}	0.30 ± 0.19	29.9 ± 19.9
E. coli Δ*lpd* Δ*pflB* Δ*sthA* Δ*ldhA* + $LPD_{NADP+low\ inhib}$	0.15 ± 0.00	18.3 ± 3.4

Unlike strains carrying an NAD^+-dependent LPD, introduction of oxygen to the anaerobic cultures did not increase significantly growth of *E. coli* Δ*lpd* Δ*pflB* Δ*sthA* Δ*ldhA* + LPD_{NADP} and *E. coli* Δ*lpd* Δ*pflB* Δ*sthA* Δ*ldhA* + $LPD_{NADP+low\ inhib}$ (**Figure 3, C3-C4**). In addition, the growth rates exhibited by the strains as well as their metabolite profiles were close to the ones determined under strict anaerobic conditions (**Table 8**). Although *E. coli* Δ*lpd* Δ*pflB* Δ*sthA* Δ*ldhA* + LPD_{WT} and *E. coli* Δ*lpd* Δ*pflB* Δ*sthA* Δ*ldhA* + $LPD_{low\ inhib}$ displayed an intermediate behavior between aerobic and anaerobic when cultivated under oxygen-limited conditions, *E. coli* Δ*lpd* Δ*pflB* Δ*sthA* Δ*ldhA* + LPD_{NADP} behaved as cultivated under strict anaerobic conditions. As PDH_{NADP} showed higher

NAD(P)H tolerance than PDH_{WT} (Chapter 3, Figure 3), NAD(P)H inhibition and anaerobic expression of PDH do not seem to be the only cause for the strains' behavior. In fact, NADPH reoxidation seems to also be a bottleneck for the cells under anaerobic conditions.

The absence of NADPH reoxidation can result from low or no activity and/or expression of PntAB under anaerobic conditions or from an insufficient NADPH/NADP$^+$ ratio in the cells. Transcription of PntAB or STH was reported not to be regulated by the actual intracellular concentration of NADPH or the cultivation conditions but rather by the NADPH demand and the redox state of the cells (Haverkorn van Rijsewijk *et al.*, 2016). Indeed, PntAB transcription was shown to be repressed at low growth rate – mimicking low NADPH demand for anabolic reactions – due to cAMP-Crp. Thus, PntAB might not have been transcribed or active anaerobically as the strains presented very low growth rates (**Figure 3, B1-B4** and **C3-C4**). Aerobically, PntAB seemed to be active and used for NADPH reoxidation, which would be supported by the relatively high growth rates exhibited by *E. coli* Δ*lpd* Δ*pflB* Δ*sthA* Δ*ldhA* strains carrying an NADP$^+$-dependent LPD (**Figure 3, A3-A4**). On the other hand, the apparent inability of the strains exhibiting an NADP$^+$-LPD to reoxidize NADPH anaerobically – by the reverse action of PntAB – might have also arisen from the insufficient production of NADPH. A low expression and/or activity of the PDH complex would only lead to small amount of NADPH, thereby preventing the cells to reach the necessary NADPH/NADP$^+$ ratio required to compensate for the proton-motive force formed during the reaction catalyzed by PntAB.

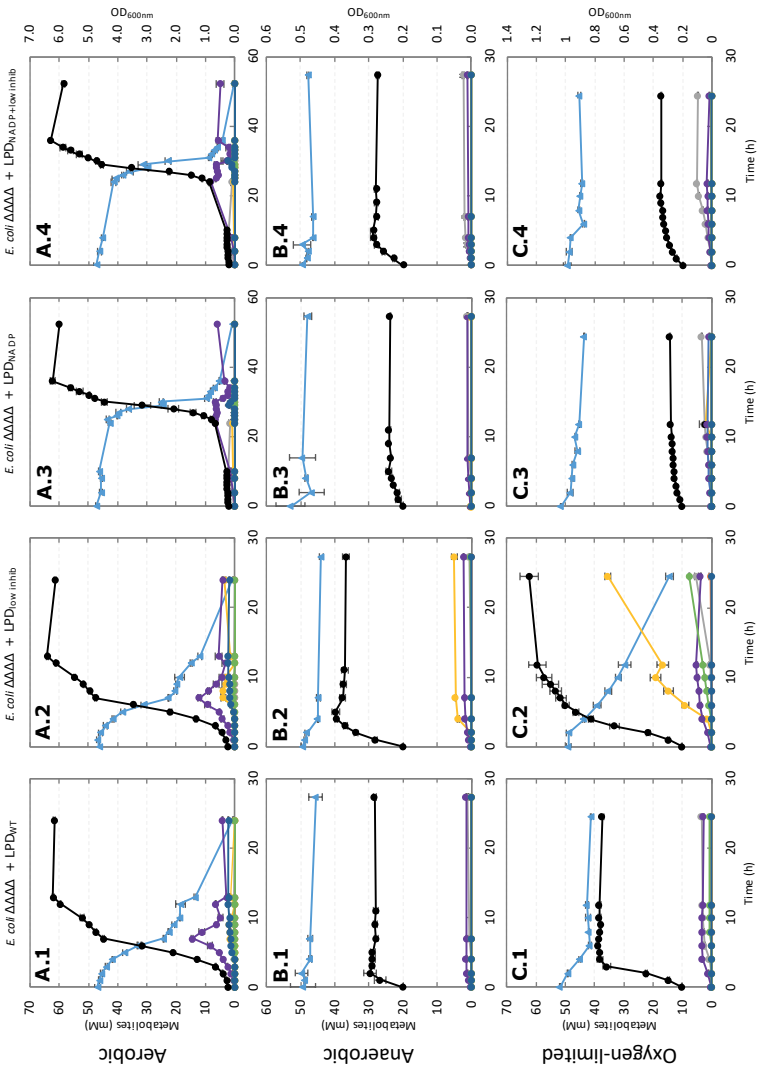

Figure 3. Growth and metabolite profiles of *E. coli* Δ*pflB* Δ*sthA* Δ*lpd* Δ*ldhA* strains carrying an LPD variants under three different cultivations conditions. The values presented represent the average of biological triplicates with standard deviations for aerobic and anaerobic cultivations and duplicates with standard deviations for oxygen-limited conditions. Legend: glucose, lactate, pyruvate, ethanol, acetate, succinate, formate and biomass.

5.4. Conclusion

In this study, a strategy was proposed to reoxidize NADPH using the membrane-bound transhydrogenase PntAB in an NADPH-overproducing strain. The proposed approach includes creation of a proton-motive force during the conversion of NADPH and NAD^+ to NADP+ and NADH, which could be subsequently used for additional energy generation. This is of particular interest for anaerobic fermentations where energy is scarce.

The *sthA* gene encoding STH was knocked out to force the regeneration of $NADP^+$ through the PntAB. Disruption of *sthA* did not give clear conclusion as the results obtained in this study were similar to the ones obtained previously for *E. coli* Δ*lpd* Δ*pflB* (Chapter 4). This indicates that the STH activity was low and was not competing with PntAB.

The membrane-bound transhydrogenase PntAB seems to be active during aerobic growth of *E. coli* Δ*lpd* Δ*pflB* Δ*sthA* Δ*ldhA* strains carrying an $NADP^+$-dependent LPD. Nevertheless, the enzyme does not seem to regenerate $NADP^+$ under anaerobic and oxygen-limited conditions. We hypothesized that a combination of NAD(P)H inhibition and poor expression of the genes encoding PDH led to low activity of the complexes. Consequently, the NADPH/$NADP^+$ ratio required for the reverse action of PntAB was not reached, and the cells exhibited poor growth. To test this hypothesis, the *aceE-aceF -lpd* genes encoding the PDH complex should be overexpressed using a strong promoter whose expression will not be affected by anaerobic conditions.

Regeneration of the excess NADPH can also be achieved by respiration if a mutation occurred in one of the genes encoding the Complex I of the electron transport chain. Therefore, the genes encoding NADH dehydrogenase I, and especially the *nuoF* gene, should be sequenced.

Additionally, we cannot rule out the possibility that anaerobic expression or activity of PntAB was not a bottleneck in the strains carrying an $NADP^+$-LPD. Therefore, the *pntA* and *pntB* genes encoding the two subunits of the

membrane-bound transhydrogenase should be overexpressed or knocked out to fully understand where the problem lies. The use of an inducible promoter would be ideal to test both conditions. Overexpression of *sthA* should also be tested since STH is known to reversibly catalyze the conversion of NADPH and NAD^+ to $NADP^+$ and NADH and is not coupled to a proton-motive force and could, as such, function as a control strain.

5.5. Supplementary material

Table S1. Enzymes predicted to contribute to NADH, NADPH and ATP metabolism when maximizing for ATP maintenance requirement (ATPM). The values are expressed in mmol/g_{DW}/h. The reversible reactions are indicated with <=> and the reversible reactions are indicated with –>. *, DHAPT reaction was knocked out in the model.

Reactions ID	Enzymes	Reactions	*E. coli* ΔΔΔ + LPD_{NADP}				*E. coli* ΔΔΔΔ + LPD_{NADP}			
			Aerobic*		Anaerobic		Aerobic		Anaerobic*	
			%	Flux	%	Flux	%	Flux	%	Flux
NADPH producing reactions										
AKGDH	2-oxoglutarate dehydrogenase (NADP)	2-oxoglutarate + CoA + NADP --> succinyl-CoA + CO_2 + NADPH	33.3	20	NA[a]	NA[a]	33.3	20	NA[a]	NA[a]
ICDHyr	Isocitrate dehydrogenase	isocitrate + NADP <=> 2-oxoglutarate + CO_2 + NADPH	33.3	20	NA[a]	NA[a]	33.3	20	NA[a]	NA[a]
PDH	Pyruvate dehydrogenase (NADP)	pyruvate + CoA + NADP --> acetyl-CoA + CO_2 + NADPH	33.3	20	100	20	33.3	20	100	20
NADPH consuming reactions										
NADTRHD	Soluble transhydrogenase (STH)	NAD + NADPH <=> NADH + NADP	100	60	100	20	NA[a]	NA[a]	NA[a]	NA[a]
THD2pp	Membrane-bound transhydrogenase (PntAB)	NADH + NADP + H^+_{out} <=> NAD + NADPH + H^+_{in}	NA[a]	NA[a]	NA[a]	NA[a]	100	60	100	20
NADH producing reactions										
NADTRHD	Soluble transhydrogenase (STH)	NAD + NADPH <=> NADH + NADP	60	60	50	20	NA[a]	NA[a]	NA[a]	NA[a]
MDH	Malate dehydrogenase	L-malate + NAD <=> oxaloacetate + NADH + H^+	20	20	NA[a]	NA[a]	20	20	NA[a]	NA[a]
GAPD	Glyceraldehyde-3-phosphate dehydrogenase	G3P + Pi + NAD <=> 1,3-bisphosphoglycerate + NADH + H^+	20	20	50	20	20	20	50	20
THD2pp	Membrane-bound transhydrogenase (PntAB)	NADH + NADP + H^+_{out} <=> NAD + NADPH + H^+_{in}	NA[a]	NA[a]	NA[a]	NA[a]	60	60	50	20
NADH consuming reactions										
NADH17pp	NADH dehydrogenase (menaquinone-8 & $3H^+$)	menaquinone-8 + NADH + 4 H^+_{in} --> menaquinol-8 + NAD + 3 H^+_{out}	100	100	NA[a]	NA[a]	100	100	NA[a]	NA[a]
ACALD	Acetaldehyde dehydrogenase (acetylating)	acetaldehyde + CoA + NAD <=> acetyl-CoA + NADH + H^+	NA[a]	NA[a]	50	20	NA[a]	NA[a]	50	20
ALCD2x	Alcohol dehydrogenase (ethanol)	ethanol + NAD <=> acetaldehyde + NADH + H^+	NA[a]	NA[a]	50	20	NA[a]	NA[a]	50	20
ATP producing reactions										
ATPS4rpp	ATP synthase (four protons for one ATP)	ADP + Pi + 4 H^+_{out} <=> ATP + H_2O + 3 H^+_{in}	79.6	195	NA[a]	NA[a]	80.8	210	14.3	5
SUCOAS	Succinyl-CoA synthetase (ADP-forming)	succinate + CoA + ATP <=> succinyl-CoA + ADP + Pi	8.2	20	NA[a]	NA[a]	7.7	20	NA[a]	NA[a]
PGK	Phosphoglycerate kinase	3-phosphoglycerate + ATP <=> 1,3-bisphosphoglycerate + ADP	8.2	20	66.7	20	7.7	20	57.1	20
PYK	Pyruvate kinase	phosphoenolpyruvate + ADP + H^+ --> pyruvate + ATP	4.1	10	NA[a]	NA[a]	NA[a]	NA[a]	NA[a]	NA[a]
NDPK4	Nucleoside-diphosphate kinase (ATP:dTDP)	ATP + dTDP <=> ADP + dTTP	NA[a]	NA[a]	33.3	10	NA[a]	NA[a]	28.6	10
NDPK1	Nucleoside-diphosphate kinase (ATP:GDP)	ATP + GDP <=> ADP + GTP	NA[a]	NA[a]	NA[a]	NA[a]	3.8	10	NA[a]	NA[a]
ATP consuming reactions										
ATPM	ATP maintenance requirement	ATP + H_2O --> ADP + Pi + H^+	95.9	235	66.7	20	96.2	250	71.4	25
PFK	Phosphofructokinase	D-fructose 6-phosphate + ATP <=> D-fructose 1,6-bisphosphate + ADP + H^+	4.1	10	NA[a]	NA[a]	NA[a]	NA[a]	28.6	10
PFK_3	Phosphofructokinase (s7p)	ATP + sedoheptulose 7-phosphate <=> ADP + sedoheptulose 1,7-bisphosphate + H^+	NA[a]	NA[a]	33.3	10	3.8	10	NA[a]	NA[a]

[a]NA, Not applicable. The enzymes are not predicted to contribute to the production or consumption of either NADH, NADPH or ATP.

Table S2. All enzymes predicted by the modified iML1515 GEM to contribute to NADH, NADPH and ATP metabolism when maximizing for biomass formation. The values are expressed in mmol/gDW/h. The reversible reactions are indicated with <=> and the reversible reactions are indicated with -->. *, DHAPT reaction was knocked out in the model.

Reactions ID	Enzymes	Reactions	*E. coli* ΔΔΔ + LPD_{NADP}				*E. coli* ΔΔΔΔ + LPD_{NADP}			
			Aerobic		Anaerobic		Aerobic*		Anaerobic*	
			%	Flux	%	Flux	%	Flux	%	Flux
NADPH producing reactions										
PDH	Pyruvate dehydrogenase (NADP)	pyruvate + CoA + NADP –> acetyl-CoA + CO_2 + NADPH	40.9	10.5	100	18.2	41.1	10.4	100	17.6
ICDHyr	Isocitrate dehydrogenase	isocitrate + NADP <=> 2-oxoglutarate + CO_2 + NADPH	29.7	7.6	NA[a]	NA[a]	29.6	7.5	NA[a]	NA[a]
AKGDH	2-oxoglutarate dehydrogenase (NADP)	2-oxoglutarate + CoA + NADP --> succinyl-CoA + CO_2 + NADPH	26	6.7	NA[a]	NA[a]	25.8	6.5	NA[a]	NA[a]
MTHFD	Methylenetetrahydrofolate dehydrogenase (NADP)	5,10-methyleneTHF + NADP <=> 5,10-methenylTHF + NADPH	3.4	0.9	NA[a]	NA[a]	3.5	0.9	NA[a]	NA[a]
NADPH consuming reactions										
NADTRHD	Soluble transhydrogenase (STH)	NAD + NADPH --> NADH + NADP	43.4	11.2	88.1	16	NA[a]	NA[a]	NA[a]	NA[a]
THD2pp	Membrane-bound transhydrogenase (PntAB)	NADH + NADP + H^+_{out} --> NAD + NADPH + H+in	NA[a]	NA[a]	NA[a]	NA[a]	49.3	12.5	88.9	15.7
GLUDy	Glutamate dehydrogenase (NADP)	L-glutamate + H_2O + NADP <=> 2-oxoglutarate + NH_4^+ + NADPH	29.3	7.5	7.9	1.4	30.2	7.6	7.7	1.4
FADRx2	FAD reductase	FAD + NADPH + H^+ --> $FADH_2$ + NADP	7.5	1.9	1.5	0.3	NA[a]	NA[a]	NA[a]	NA[a]
ASAD	Aspartate-semialdehyde dehydrogenase	L-aspartate 4-semialdehyde + NADP + Pi <=> 4-phospho-L-aspartate + NADPH + H^+	3.7	0.9	NA[a]	NA[a]	3.8	1	NA[a]	NA[a]
KARA1	Ketol-acid reductoisomerase (2,3-dihydroxy-3-methylbutanoate)	(R)-2,3-dihydroxy-3-methylbutanoate + NADP <=> (S)-2-acetolactate + NADPH + H^+	3	0.8	NA[a]	NA[a]	3.1	0.8	NA[a]	NA[a]
SULR	Sulfite reductase (NADPH2)	5 H^+ + 3 NADPH + SO_3 --> 3 H_2O + 3 NADP + H_2S	2.5	0.7	NA[a]	NA[a]	2.6	0.7	NA[a]	NA[a]
HSDy	Homoserine dehydrogenase (NADPH)	L-homoserine + NADP <=> L-aspartate 4-semialdehyde + NADPH + H^+	2.4	0.6	NA[a]	NA[a]	2.5	0.6	NA[a]	NA[a]
SHK3Dr	Shikimate dehydrogenase	3-dehydroshikimate + NADPH + H^+ <=> shikimate + NADP	1.3	0.3	NA[a]	NA[a]	1.3	0.3	NA[a]	NA[a]
DHDPRy	Dihydrodipicolinate reductase (NADPH)	2,3-dihydrodipicolinate + NADPH + H^+ <=> 2,3,4,5-tetrahydrodipicolinate + NADP	1.3	0.3	NA[a]	NA[a]	1.3	0.3	NA[a]	NA[a]
GTHOr	Glutathione oxidoreductase	oxidized glutathione + H^+ + NADPH <=> 2 reduced glutathione + NADP	1.2	0.3	NA[a]	NA[a]	NA[a]	NA[a]	NA[a]	NA[a]
AGPR	N-acetyl-g-glutamyl-phosphate reductase	N-acetyl-L-glutamate 5-semialdehyde + Pi + NADP <=> N-acetyl-L-glutamyl 5-phosphate + NADPH + H^+	1	0.3	NA[a]	NA[a]	1	0.3	NA[a]	NA[a]
KARA2	Ketol-acid reductoisomerase (2-Acetolactate)	(S)-2-aceto-2-hydroxybutanoate + NADPH + H^+ <=> (R)-2,3-dihydroxy-3-methylpentanoate + NADP	1	0.3	NA[a]	NA[a]	1	0.3	NA[a]	NA[a]
G5SD	Glutamate-5-semialdehyde dehydrogenase	L-glutamate 5-phosphate + NADPH + H^+ --> L-glutamate semialdehyde + Pi + NADP	0.8	0.2	NA[a]	NA[a]	0.8	0.2	NA[a]	NA[a]
P5CR	Pyrroline-5-carboxylate reductase	1-pyrroline-5-carboxylate + 2 H^+ + NADPH --> L-proline + NADP	0.8	0.2	NA[a]	NA[a]	0.8	0.2	NA[a]	NA[a]
G3PD2	Glycerol-3-phosphate dehydrogenase (NADP)	glycerol 3-phosphate + NADP <=> DHAP + NADPH + H^+	0.5	0.1	NA[a]	NA[a]	NA	NA	NA[a]	NA[a]
TRDR	Thioredoxin reductase (NADPH)	oxidized thioredoxin + NADPH + H^+ --> reduced thioredoxin + NADP	NA[a]	NA[a]	NA[a]	NA[a]	1.2	0.3	NA[a]	NA[a]
NADH producing reactions										
GAPD	Glyceraldehyde-3-phosphate dehydrogenase	glyceraldehyde 3-phosphate + Pi + NAD <=> 3-phospho-D-glyceroylphosphate + NADH + H^+	46.3	17.9	54.9	19.7	45	17.9	55.2	19.6
NADTRHD	Soluble transhydrogenase (STH)	NAD + NADPH --> NADH + NADP	29	11.2	44.5	16	NA[a]	NA[a]	NA[a]	NA[a]
THD2pp	Membrane-bound transhydrogenase (PntAB)	NADH + NADP + H^+_{out} --> NAD + NADPH + $H+_{in}$	NA[a]	NA[a]	NA[a]	NA[a]	31.4	12.5	44.1	15.7
MDH	Malate dehydrogenase	L-malate + NAD <=> oxaloacetate + NADH + H^+	19.7	7.6	NA[a]	NA[a]	18.8	7.4	NA[a]	NA[a]
PGCD	Phosphoglycerate dehydrogenase	3-phospho-D-glycerate + NAD --> 3-phosphohydroxypyruvate + NADH + H^+	3.9	1.5	0.6	0.2	3.9	1.5	0.8	0.3
IPMD	3-isopropylmalate dehydrogenase	3-carboxy-2-hydroxy-4-methylpentanoate + NAD --> 3-carboxy-4-hydroxy-2-oxopentanoate + NADH + H^+	1	0.4	NA[a]	NA[a]	1	0.4	NA[a]	NA[a]

NADH consuming reactions									
NADH17pp	NADH dehydrogenase (menaquinone-8 & $3H^+$)	menaquinone-8 + NADH + 4 H^+_{in} --> menaquinol-8 + NAD + $3H^+_{out}$	95.7	36.9	1.3	0.5	90.9	36.1	NA[a]	NA[a]
ACALD	Acetaldehyde dehydrogenase (acetylating)	acetaldehyde + CoA + NAD <=> acetyl-CoA + NADH + H^+	NA[a]	NA[a]	49.1	17.6	NA[a]	NA[a]	47.6	16.9
ALCD2x	Alcohol dehydrogenase (ethanol)	ethanol + NAD <=> acetaldehyde + NADH + H^+	NA[a]	NA[a]	49.1	17.6	NA[a]	NA[a]	47.6	16.9
FADRx	FAD reductase	FAD + NADH + H^+ --> $FADH_2$ + NAD	NA[a]	NA[a]	NA[a]	NA[a]	4.9	2	1	0.3
NADH18pp	NADH dehydrogenase (demethylmenaquinone-8 & $3H^+$)	demethylmenaquinone-8 + NADH + 4 H^+_{in} --> demethylmenaquinol-8 + NAD + 3 H^+_{out}	NA[a]	NA[a]	NA[a]	NA[a]	NA[a]	NA[a]	1.8	0.6
MDH	Malate dehydrogenase	L-malate + NAD <=> oxaloacetate + NADH + H^+	NA[a]	NA[a]	NA[a]	NA[a]	NA[a]	NA[a]	1.4	0.5
ATP producing reactions										
ATPS4rpp	ATP synthase (four protons for one ATP)	ADP + Pi + 4 H^+_{out} <=> ATP + H_2O + 3 H^+_{in}	72.5	69.3	NA[a]	NA[a]	73	70.7	11.6	3.6
PGK	Phosphoglycerate kinase	3-phosphoglycerate + ATP <=> 1,3-bisphosphoglycerate + ADP	18.7	17.9	70.9	19.7	18.4	17.9	62.7	19.6
SUCOAS	Succinyl-CoA synthetase (ADP-forming)	succinate + CoA + ATP <=> succinyl-CoA + ADP + Pi	6.5	6.2	NA[a]	NA[a]	6.2	6	NA[a]	NA[a]
NDPK3	Nucleoside-diphosphate kinase (ATP:CDP)	ATP + CDP <=> ADP + CTP	2.3	2.2	NA[a]	NA[a]	NA[a]	NA[a]	NA[a]	NA[a]
NDPK4	Nucleoside-diphosphate kinase (ATP:dTDP)	ATP + dTDP <=> ADP + dTTP	NA[a]	NA[a]	29.1	8.1	NA[a]	NA[a]	25.8	8.1
NDPK1	Nucleoside-diphosphate kinase (ATP:GDP)	ATP + GDP <=> ADP + GTP	NA[a]	NA[a]	NA[a]	NA[a]	2.3	2.3	NA[a]	NA[a]
ATP consuming reactions										
BIOMASS	Biomass	0.000223 10fthf_c + 2.6e-05 2fe2s_c + 0.000223...	69.6	66.5	33.3	9.3	69.6	67.5	38.4	12
PFK	Phosphofructokinase	fructose-6-phosphate + ATP –> fructose-1,6-bisphosphate + ADP + H^+	9.7	9.2	NA[a]	NA[a]	9.5	9.2	31.5	9.9
ATPM	ATP maintenance requirement	ATP + H_2O –> ADP + Pi + H^+	7.2	6.9	24.7	6.9	7.1	6.9	21.9	6.9
ADK1	Adenylate kinase	AMP + ATP <=> 2 ADP	1.6	1.5	NA[a]	NA[a]	2.4	2.3	1.7	0.5
GLNS	Glutamine synthetase	L-glutamate + NH_4^+ + ATP –> L-glutamine ATP + Pi + H^+	1.4	1.4	NA[a]	NA[a]	1.4	1.4	0.8	0.2
ASPK	Aspartate kinase	aspartate + ATP <=> 4-phospho-L-aspartate + ADP	1	0.9	NA[a]	NA[a]	1	1	NA[a]	NA[a]
R15BPK	Ribose-1,5-bisphosphokinase	ribose 1,5-bisphosphate + ATP --> 5-phosphoribosyl pyrophosphate + ADP	0.9	0.8	NA[a]	NA[a]	NA[a]	NA[a]	NA[a]	NA[a]
R1PK	Ribose 1-phosphokinase	ribose 1-phosphate + ATP --> ribose 1,5-bisposphate + ADP + H^+	0.9	0.8	NA[a]	NA[a]	NA[a]	NA[a]	NA[a]	NA[a]
PFK3	Phosphofructokinase (s7p)	sedoheptulose 7-phosphate + ATP <=> sedoheptulose 1,7-bisphosphate + ADP + H^+	NA[a]	NA[a]	35.6	9.9	NA[a]	NA[a]	NA[a]	NA[a]
ATPS4rpp	ATP synthase (four protons for one ATP)	ADP + Pi + 4 H^+_{out} <=> ATP + H_2O + 3 H^+_{in}	NA[a]	NA[a]	0.8	0.2	NA[a]	NA[a]	NA[a]	NA[a]
PRPPS	Phosphoribosylpyrophosphate synthetase	ribose 5-phosphate + ATP <=> phosphoribosyl pyrophosphate + AMP + H^+	NA[a]	NA[a]	NA[a]	NA[a]	0.9	0.8	NA[a]	NA[a]

[a]NA, Not applicable. The enzymes are not predicted to contribute to the production or consumption of either NADH, NADPH or ATP.

Table S3. Carbon recovery calculated during anaerobic growth of *E. coli* Δ*pflB* Δ*sthA* and *E. coli* Δ*pflB* Δ*sthA* Δ*lpd* carrying the different LPD variants. The values are expressed in C-mmol and correspond to the average of biological triplicates with standard deviations.

Time (h)	Δ*pflB* Δ*sthA*	ΔΔΔ + LPD_{WT}	ΔΔΔ + $LPD_{low\ inhib}$	ΔΔΔ + LPD_{NADP}	ΔΔΔ + $LPD_{NADP+low\ inhib}$
0	298.3 ± 3.5	302.1 ± 0.3	301.0 ± 0.6	300.9 ± 2.9	301.4 ± 0.7
2	295.9 ± 2.7	295.4 ± 0.2	297.2 ± 0.1	ND[a]	296.6 ± 0.2
4	ND[a]	296.9 ± 0.8	303.1 ± 0.7	291.6 ± 3.8	291.5 ± 3.0
6	294.4 ± 2.5	293.9 ± 0.9	293.0 ± 0.5	ND[a]	293.1 ± 0.4
8	289.6 ± 4.1	290.7 ± 0.5	292.5 ± 0.7	294.7 ± 0.4	293.4 ± 0.1
10	291.0 ± 2.9	291.1 ± 2.1	289.4 ± 0.4	ND[a]	290.6 ± 0.6
12	288.9 ± 1.5	289.3 ± 0.6	291.9 ± 0.7	295.0 ± 0.2	290.8 ± 0.6
24	289.9 ± 2.0	288.0 ± 0.7	289.9 ± 1.0	289.5 ± 0.6	285.3 ± 0.7

Table S4. Yields of fermentation products on glucose during aerobic cultivation on M9 medium supplemented with 50mM glucose. The yields were calculated at the end of cultivations and expressed in mol product formed per mol glucose consumed. The values displayed represent the average of biological triplicates (or duplicates for *E. coli ΔpflB*) with standard deviations.

Strains	Lactate	Pyruvate	Ethanol	Acetate	Succinate	Formate	Biomass
E. coli Δ*pflB*	0.02 ± 0.00	0.00 ± 0.00	0.05 ± 0.00	0.14 ± 0.01	0.02 ± 0.00	0.05 ± 0.00	1.81 ± 0.04
E. coli Δ*pflB* Δ*sthA*	0.00 ± 0.00	0.00 ± 0.00	0.00 ± 0.00	0.21 ± 0.02	0.00 ± 0.00	0.06 ± 0.00	1.34 ± 0.01
E. coli Δ*lpd* Δ*pflB* Δ*sthA* + LPD_{WT}	0.00 ± 0.00	0.00 ± 0.00	0.00 ± 0.00	0.05 ± 0.00	0.00 ± 0.00	0.00 ± 0.00	1.46 ± 0.01
E. coli Δ*lpd* Δ*pflB* Δ*sthA* + $LPD_{low\ inhib}$	0.00 ± 0.00	0.00 ± 0.00	0.06 ± 0.01	0.04 ± 0.00	0.00 ± 0.00	0.00 ± 0.00	1.20 ± 0.18
E. coli Δ*lpd* Δ*pflB* Δ*sthA* + LPD_{NADP}	0.01 ± 0.01	0.01 ± 0.00	0.00 ± 0.00	0.07 ± 0.01	0.00 ± 0.00	0.00 ± 0.00	2.08 ± 0.09
E. coli Δ*lpd* Δ*pflB* Δ*sthA* + $LPD_{NADP+low\ inhib}$	0.00 ± 0.00	0.00 ± 0.00	0.02 ± 0.02	0.81 ± 0.12	0.00 ± 0.00	0.03 ± 0.02	1.04 ± 0.01

Table S5. Yields of product formed on glucose (mol/mol) during anaerobic fermentation on M9 medium. The yields were determined at the end of the cultivations. The values shown correspond to the average of biological triplicates with standard deviations.

Strains	Lactate	Pyruvate	Ethanol	Acetate	Succinate	Formate	Biomass	CO_2
E. coli Δ*pflB*	1.65 ± 0.01	0.00 ± 0.00	0.08 ± 0.01	0.03 ± 0.00	0.03 ± 0.00	0.00 ± 0.00	0.31 ± 0.01	0.09 ± 0.01
E. coli Δ*pflB* Δ*sthA*	1.72 ± 0.02	0.01 ± 0.00	0.08 ± 0.00	0.03 ± 0.00	0.02 ± 0.00	0.00 ± 0.00	0.25 ± 0.02	0.00 ± 0.00
E. coli Δ*lpd* Δ*pflB* Δ*sthA* + LPD_{WT}	1.64 ± 0.01	0.00 ± 0.00	0.14 ± 0.01	0.02 ± 0.01	0.02 ± 0.00	0.00 ± 0.00	0.26 ± 0.00	0.14 ± 0.01
E. coli Δ*lpd* Δ*pflB* Δ*sthA* + $LPD_{low\ inhib}$	1.39 ± 0.01	0.00 ± 0.00	0.37 ± 0.01	0.04 ± 0.00	0.03 ± 0.00	0.00 ± 0.00	0.30 ± 0.01	0.38 ± 0.01
E. coli Δ*lpd* Δ*pflB* Δ*sthA* + LPD_{NADP}	1.73 ± 0.03	0.08 ± 0.00	0.00 ± 0.00	0.00 ± 0.01	0.00 ± 0.00	0.00 ± 0.00	0.14 ± 0.00	0.00 ± 0.01
E. coli Δ*lpd* Δ*pflB* Δ*sthA* + $LPD_{NADP+low\ inhib}$	1.79 ± 0.01	0.05 ± 0.00	0.00 ± 0.00	0.00 ± 0.00	0.00 ± 0.00	0.00 ± 0.00	0.11 ± 0.01	0.00 ± 0.00

Table S6. Carbon recovery of E. coli ΔpflB ΔsthA ΔldhA Δlpd carrying the LPD variants during anaerobic cultivations on M9 medium. The values are expressed in C-mmol present in the system and correspond to the average of three biological replicates with standard deviations.

Time (h)	ΔΔΔΔ + LPD_{WT}	ΔΔΔΔ + $LPD_{low\ inhib}$	ΔΔΔΔ + LPD_{NADP}	ΔΔΔΔ + $LPD_{NADP+low\ inhib}$
0	299.3 ± 21.6	287.2 ± 18.2	321.3 ± 25.6	301.9 ± 0.5
1	298.5 ± 2.4	298.6 ± 1.4	ND[a]	294.5 ± 0.9
2	306.7 ± 10.9	297.5 ± 3.8	285.8 ± 21.9	294.5 ± 1.1
3	ND[a]	ND[a]	ND[a]	307.6 ± 15.8
4	292.8 ± 2.4	292.8 ± 1.1	296.5 ± 1.6	289.9 ± 1.6
7	293.3 ± 3.6	294.5 ± 2.9	306.3 ± 23.5	291.4 ± 1.0
24.33	286.3 ± 10.4	311.1 ± 24.9	ND[a]	ND[a]
28.25	ND[a]	ND[a]	298.3 ± 7.6	301.4 ± 2.9

[a]ND, Not determined.

Table S7. Carbon recovery of *E. coli* Δ*pflB* Δ*ldhA* Δ*sthA* Δ*lpd* carrying the different LPD variants determined during oxygen-limited fermentations. The values are expressed in C-mmol present in the system and correspond to the average of three biological replicates with standard deviations.

Time (h)	ΔΔΔΔ + LPD_{WT}	ΔΔΔΔ + $LPD_{low\ inhib}$	ΔΔΔΔ + LPD_{NADP}	ΔΔΔΔ + $LPD_{NADP+low\ inhib}$
0	314.3 ± 0.5	297.1 ± 5.5	313.1 ± 1.6	300.3 ± 8.0
2	305.4 ± 1.1	303.3 ± 4.2	297.1 ± 2.9	299.5 ± 6.0
4	293.4 ± 3.0	288.4 ± 5.9	294.6 ± 2.0	301.7 ± 1.4
6	278.2 ± 2.3	290.7 ± 3.4	294.5 ± 1.4	278.5 ± 2.5
8	283.2 ± 0.3	290.3 ± 0.0	287.2 ± 5.1	292.2 ± 2.4
10	284.6 ± 4.8	288.1 ± 2.0	294.7 ± 0.6	293.6 ± 1.0
11.83	286.7 ± 4.7	271.6 ± 3.8	293.9 ± 7.8	292.5 ± 2.1
24.5	278.9 ± 1.8	262.2 ± 7.5	279.5 ± 1.0	294.3 ± 3.1

Table S8. Yields of fermentation products on glucose (mol/mol) during aerobic cultivations on M9 medium. The yields were determined at the end of the experiments. The values displayed represent the average of biological triplicates with standard deviations.

Strains	Lactate	Pyruvate	Ethanol	Acetate	Succinate	Formate	Biomass
E. coli Δ*lpd* Δ*pflB* Δ*sth*A Δ*ldhA* + LPD_{WT}	0.00 ± 0.00	0.00 ± 0.00	0.00 ± 0.00	0.12 ± 0.04	0.00 ± 0.00	0.05 ± 0.00	1.93 ± 0.04
E. coli Δ*lpd* Δ*pflB* Δ*sth*A Δ*ldhA* + $LPD_{low\ inhib}$	0.00 ± 0.00	0.00 ± 0.00	0.08 ± 0.01	0.09 ± 0.01	0.00 ± 0.00	0.04 ± 0.00	1.94 ± 0.01
E. coli Δ*lpd* Δ*pflB* Δ*sth*A Δ*ldhA* + LPD_{NADP}	0.00 ± 0.00	0.00 ± 0.00	0.00 ± 0.00	0.13 ± 0.00	0.00 ± 0.00	0.00 ± 0.00	1.87 ± 0.02
E. coli Δ*lpd* Δ*pflB* Δ*sth*A Δ*ldhA* + $LPD_{NADP+low\ inhib}$	0.00 ± 0.00	0.00 ± 0.00	0.00 ± 0.00	0.11 ± 0.03	0.00 ± 0.00	0.00 ± 0.00	1.80 ± 0.04

Table S9. Yields of product formed on glucose (mol/mol) during anaerobic fermentation on M9 medium. The yields were calculated at the end of the experiments and represent the average of biological triplicates with standard deviations.

Strains	Lactate	Pyruvate	Ethanol	Acetate	Succinate	Formate	Biomass	CO_2
E. coli Δ*lpd* Δ*pflB* Δ*sthA* Δ*ldhA* + PDH_{WT}	0.00 ± 0.00	0.50 ± 0.36	0.00 ± 0.00	0.55 ± 0.41	0.00 ± 0.00	0.00 ± 0.00	0.55 ± 0.34	0.55 ± 0.41
E. coli Δ*lpd* Δ*pflB* Δ*sthA* Δ*ldhA* + $PDH_{low\ inhib}$	0.00 ± 0.00	0.12 ± 0.03	0.78 ± 0.23	0.38 ± 0.04	0.02 ± 0.03	0.00 ± 0.00	0.48 ± 0.07	1.14 ± 0.25
E. coli Δ*lpd* Δ*pflB* Δ*sthA* Δ*ldhA* + PDH_{NADP}	0.00 ± 0.00	1.76 ± 2.05	0.00 ± 0.00	1.48 ± 1.72	0.00 ± 0.00	0.00 ± 0.00	0.80 ± 0.92	1.48 ± 1.72
E. coli Δ*lpd* Δ*pflB* Δ*sthA* Δ*ldhA* + $PDH_{NADP+low\ inhib}$	0.00 ± 0.00	1.26 ± 0.45	0.00 ± 0.00	0.57 ± 0.21	0.00 ± 0.00	0.00 ± 0.00	0.66 ± 0.20	0.57 ± 0.21

Table S10. Yields of product formed on glucose (mol/mol) during oxygen-limited fermentation on M9 medium. The yields were calculated at the end of the experiments and represent the average of biological triplicates with standard deviations.

Strains	Lactate	Pyruvate	Ethanol	Acetate	Succinate	Formate	Biomass	CO_2
E. coli Δ*lpd* Δ*pflB* Δ*sthA* Δ*ldhA* + PDH_{WT}	0.00 ± 0.00	0.31 ± 0.01	0.00 ± 0.00	0.2 ± 0.00	0.06 ± 0.00	0.00 ± 0.00	0.78 ± 0.04	0.19 ± 0.00
E. coli Δ*lpd* Δ*pflB* Δ*sthA* Δ*ldhA* + $PDH_{low\ inhib}$	0.01 ± 0.01	0.15 ± 0.01	1.03 ± 0.09	0.10 ± 0.01	0.2 ± 0.02	0.00 ± 0.00	0.47 ± 0.01	0.92 ± 0.09
E. coli Δ*lpd* Δ*pflB* Δ*sthA* Δ*ldhA* + PDH_{NADP}	0.00 ± 0.00	0.43 ± 0.03	0.00 ± 0.00	0.09 ± 0.00	0.00 ± 0.00	0.00 ± 0.00	0.16 ± 0.01	0.09 ± 0.00
E. coli Δ*lpd* Δ*pflB* Δ*sthA* Δ*ldhA* + $PDH_{NADP+low\ inhib}$	0.00 ± 0.00	1.19 ± 0.23	0.00 ± 0.00	0.18 ± 0.04	0.00 ± 0.00	0.00 ± 0.00	0.57 ± 0.12	0.18 ± 0.04

Chapter 6

Applying non-canonical redox cofactors in fermentation processes

This chapter has been published as:

Weusthuis, R.A., Folch P.L., Pozo-Rodríguez A. & Paul C.E. (2020). Applying non-canonical redox cofactors in fermentation processes. *iScience, 23*(9).

Summary

Fermentation processes are used to sustainably produce chemicals and as such contribute to the transition to a circular economy. The maximum theoretical yield of a conversion can only be approached if all electrons present in the substrate end up in the product. Control over the electrons is therefore crucial. However, electron transfer *via* redox cofactors results in a diffuse distribution of electrons over metabolism. To overcome this challenge, we propose to apply non-canonical redox cofactors (NRCs) in metabolic networks: cofactors that channel electrons exclusively from substrate to product, forming orthogonal circuits for electron transfer.

Keywords

Microbial cell factories, redox cofactors, electron transfer, metabolic networks, genome editing, *in vitro* and *in vivo* biocatalysis

6.1. Microbial cell factories as enabling technologies

Microbial cell factories are one of the enabling technologies to produce chemicals efficiently and sustainably. The catalytic power of the whole metabolic network, consisting of thousands of enzymes, can be used to realize the desired conversion. Genome-editing techniques make it more and more possible to engineer the metabolism of microorganisms to optimize product formation (Brouns *et al.*, 2008; Mohanraju *et al.*, 2016; Mougiakos *et al.*, 2018; Wu *et al.*, 2018). Metabolism is however a very complex network of reactions, with a high degree of entanglement and tight regulation. Product formation is therefore prone to be affected by other metabolic processes and *vice versa*. This complicates the thorough understanding of metabolic processes and makes it difficult to realize an efficient design. A trend to reduce the entanglement of product formation with other metabolic processes is to use synthetic biology to establish orthogonal pathways: growth-independent pathways optimized for the production of a target molecule, characterized by the minimization of interactions between the chemical-producing pathways and the biomass-producing pathways (Martin *et al.*, 2003; Chinen *et al.*, 2007; Hanai *et al.*, 2007; Prather and Martin, 2008).

6.2. Maximizing yield

Microbial cell factories are designed to achieve high yield (g product/g substrate). This is especially important for the production of bulk chemicals, because they have to compete with chemicals derived from low-cost fossil-based resources. The yield shows how efficient the substrate is converted into the product. The design target for yield is the maximal theoretical yield, which can be calculated using the degree of reduction of both substrate and product. This degree reflects the ability of molecules to donate or accept electrons in chemical reactions and therefore depends on their elemental composition. In organic molecules, C atoms can donate four electrons and H atoms one electron, whereas N atoms can accept three electrons and O atoms two

electrons (Weusthuis *et al.*, 2011). The degree of reduction of glucose ($C_6H_{12}O_6$) is 24 (6 × 4 + 12 × 1 + 6 × -2), that of lactic acid ($C_3H_6O_3$) = 12 (3 × 4 + 6 × 1 + 3 × -2), so the maximum theoretical yield of the conversion of glucose into lactic acid is 24/12 = 2 mol/mol.

The most straightforward approach for cell factory engineering to optimize the yield is therefore to design a metabolic network that enforces complete transfer of electrons present in the substrate to the final product. This requires strict control of electron transfer and redox reactions. However, redox couples that are spread over the metabolic network transfer electrons to each other, causing a diffuse distribution of electrons over metabolism. A good example is the utilization of glucose by *Escherichia coli*. The latter is able to transfer electrons *via* nicotinamide adenine dinucleotide NAD^+/NADH to terminal electron acceptors such as oxygen and nitrate – in a process called respiration – or to metabolic intermediates, forming products like ethanol, acetate, formate, succinate and lactate – in a process called fermentation. *E. coli* also transfers electrons *via* $NADP^+$/NADPH to reduce intermediates used in biomass production. If *E. coli* would be used as a microbial cell factory for the production of a certain chemical, all electrons from the substrate should end up in the product to approach the maximal theoretical yield, and not be diffusely diverted to other reactions. A strict control over the fate of electrons is therefore evidently important.

6.3. Redox cofactors

Electron transfer is mediated by specialized redox couples: redox cofactors. Three distinct families are operational in metabolism.

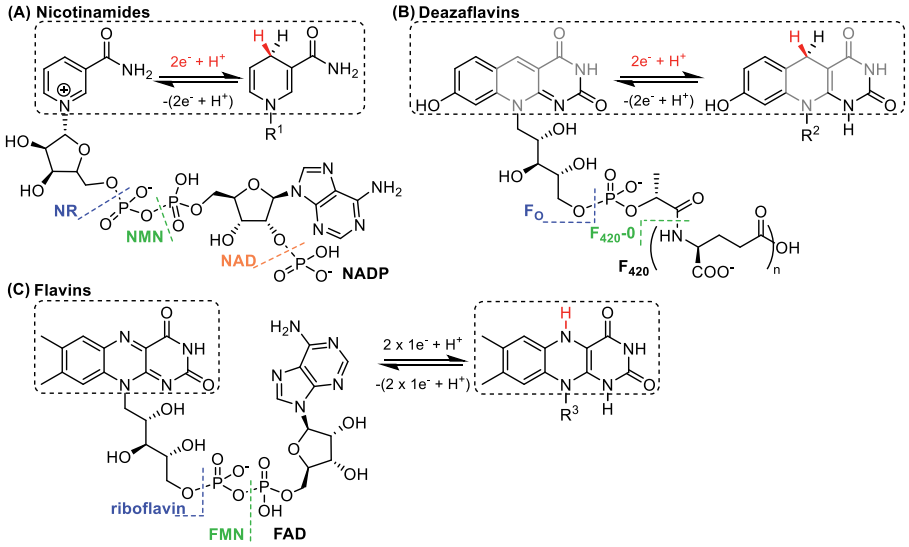

Figure 1. Chemical structures of selected redox cofactors. (A) Nicotinamide cofactors (reduced form) transfer two electrons in a one-step hydride transfer and become oxidized. NR = nicotinamide ribose; NMN = nicotinamide mononucleotide, NAD = nicotinamide adenine dinucleotide, NADP = nicotinamide adenine dinucleotide phosphate, AD = adenosine diphosphoribose. **(B)** Deazaflavin cofactors are nicotinamide cofactors (light grey highlights the nicotinamide structure, one-step hydride transfer) structurally disguised as flavins. **(C)** Flavin cofactors can transfer two electrons in a two-step one-electron transfer mechanism. FMN = flavin mononucleotide, FAD = flavin adenine dinucleotide.

6.3.1. Nicotinamide cofactors

Nicotinamide adenine dinucleotide cofactor NAD^+ and its phosphorylated form $NADP^+$ (**Figure 1A**) display an E_0' of -320 mV. Their actual redox potentials differ due to different ratios of the reduced and oxidized pools. NAD^+/NADH is kept in the oxidized state by transferring electrons to the electron transport chain, alcohols/aldehydes, 2-oxo carboxylic acids/amino acids and the reduction of carbon-carbon double bonds. NAD^+/NADH is used in oxidation reactions in both assimilation and dissimilation, whereas $NADP^+$/NADPH is kept in its reduced form by accepting electrons from the oxidation of aldehydes to carboxylic acids, and through oxidative decarboxylations.

6.3.2. Deazaflavin cofactors

The deazaflavin cofactor 8-hydroxy-5-deazaflavin (F_{420}, **Figure 1B**) and its truncated versions (F_O, F_{420}-0) resembles the structure of flavins and reactivity of NAD (in grey **Figure 1B** *vs* 1A) and displays a similar redox potential of -340 mV. This cofactor plays a role in primary and secondary metabolism in various archaea and bacteria. Its low-potential hydride transfer allows the mediation of various redox reactions involved in pathways such as antibiotic biosynthesis (Bashiri *et al.*, 2019). As the natural biosynthesis of F_{420} does not exist in *E. coli*, recent efforts afforded its heterologous production by recombinant expression in *E. coli* (Bashiri *et al.*, 2019), making this cofactor a good candidate for an orthogonal pathway.

6.3.3. Flavin cofactors

Flavin mononucleotide (FMN) and flavin adenine dinucleotide (FAD, **Figure 1C**) have a redox couple of -220 mV. Usually FAD and FMN are found as a prosthetic group in enzymes, shifting the E_0' to neutral values. They accept electrons from NAD(P)H and iron-sulfur clusters. Understanding electron flow through electron carrier proteins and their cofactors is key to engineer orthogonal pathways.

The redox cofactor NAD^+/NADH and its phosphorylated form $NADP^+$/NADPH are most relevant for product formation by microbial cell factories. The Kyoto Encyclopedia of Genes and Genomes (KEGG) database (www.genome.jp/kegg/) reports 983 NADH-dependent reactions and 1051 NADPH-dependent reactions, most of which are redox reactions. The iML1515 genome-scale constraint-based metabolic model (GSCBMM) of *E. coli* (Monk *et al.*, 2017) lists 127 reactions using NAD^+/NADH and 113 reactions using $NADP^+$/NADPH. These values indicate that the electrons are diffusely distributed over the whole metabolic network. The current trend to design true orthogonal pathways for product formation to diminish entanglement and regulation is therefore futile, if these pathways are dependent on NAD^+/NADH and $NADP^+$/NADPH. True orthogonal pathways can only be realized when also

the redox cofactor involved can be isolated as much as possible from other metabolic activities. The term “non-canonical redox cofactors” (NRCs) was used to describe such cofactors (Black *et al.*, 2020). To date, NRCs have especially been studied *in vitro* as cofactor biomimetics for enzymatic reactions and are only beginning to be applied *in vivo*.

6.4. Application of non-canonical redox cofactors in *in vitro* biocatalysis

When performing *in vitro* biocatalytic processes, several factors such as cost, solubility, instability or restricted activity of cofactors may impede further development of enzymes (Paul *et al.*, 2014; Paul and Hollmann, 2016; Guarneri *et al.*, 2019). Shorter versions of NADH, varying substituents on the dihydropyridine ring and nitrogen (**Figure 2A**), were synthesized and used as cofactor biomimetics with oxidoreductase enzymes to catalyze the reduction of carbon-carbon double bonds (Paul *et al.*, 2013; Knaus *et al.*, 2016; Löw *et al.*, 2016; Falcone *et al.*, 2019), the hydroxylation of benzoates (Ryan *et al.*, 2008; Guarneri *et al.*, 2020), or the oxidation of glucose (Nowak *et al.*, 2017; Huang *et al.*, 2019). These nicotinamide cofactor biomimetics allow for an orthogonal system when using enzymes as cell free extracts for the reduction of carbon-carbon double bonds: activity by other oxidoreductases such as alcohol dehydrogenases was excluded, as these enzymes do not function with those truncated cofactors (Paul *et al.*, 2013; Josa-Culleré *et al.*, 2019).

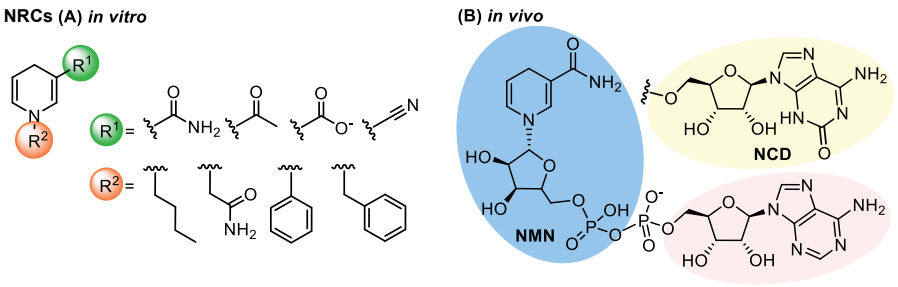

Figure 2. Chemical structures of selected NRCs. (A) NRCs used *in vitro*. These structures are examples of synthetic nicotinamide cofactor biomimetics successfully used with oxidoreductases. **(B)** NRCs used *in vivo*. NADH structure, the moiety highlighted in pink, adenosine, is modifiable to cytosine, above in yellow. In blue NMN = nicotinamide mononucleotide; in yellow NCD = nicotinamide cytosine dinucleotide.

Stability and activity

Modification of substituents on the NADH cofactor led to changes in redox properties as well as stability. The half-life of each cofactor depended on pH, temperature and the presence of other chemical components such as phosphate buffer (Norris and Stewart, 1977; Wu *et al.*, 1986). Further studies with synthetic cofactors displayed varying reaction rates depending on the substituted dihydropyridine ring for reduction and oxidation reactions (Knaus *et al.*, 2016; Guarneri *et al.*, 2020). These short synthetic analogues currently lack an efficient enzymatic recycling system (Nowak *et al.*, 2017; Zachos *et al.*, 2019). In parallel, NRCs recently used *in vivo*, NMN and nicotinamide cytosine dinucleotide (NCD, **Figure 1B**), rely on the natural structural backbone of NADH due to the difficulty in engineering dehydrogenase enzyme towards the shorter truncated versions used *in vitro* (Nowak *et al.*, 2017; Huang *et al.*, 2019).

Table 1. Prerequisites necessary for the successful application of NRCs in cell factories and fermentation processes.

#	Title	Description
Prerequisites for NRCs application in cell factories		
1	Redox potential	The redox couple donating electrons should have a lower redox potential than the NRC, the redox couple accepting the electrons a higher redox potential.
2	Specificity	Strict control over the electrons necessitates that the NRC should only transfer electrons between the objective donating and receiving redox couple. Transfer of these electrons should therefore be catalyzed by enzymes with a high specificity for the NRC. Also, native enzymes should not be able to use the NRC and non-enzymatic transfer of electrons from the NRC to other redox cofactors should be avoided.
3	Location	Although many NRCs have been applied in enzymatic conversions, they are not all suitable in microbial cell factories. This namely requires the intracellular action of the NRC. Microbial cell factories should therefore be able to biosynthesize the NRC, either *de novo* or *via* salvation pathways, or being able to take it up from the medium.
4	Regulation	Many enzyme activities depend on regulation by NAD/NADH and/or NADP/NADPH concentration ratios. The NRC should not interfere with this regulation.
Additional prerequisite for application of NRCs in fermentation processes		
5	Dissimilation vs assimilation	The NRC should only be used for (ATP-generating) dissimilation and not for assimilation.

6.5. Application of non-canonical redox cofactors *in vivo*

Applying these NRCs in microbial cell factories would provide an orthogonal circuit for electron transfer. It would increase the control over the fate of electrons and could therefore be used to improve bioprocesses. Although NRCs have been applied successfully in enzymatic conversions, additional

prerequisites regarding redox potential, specificity, location and regulation need to be fulfilled in order to function truly orthogonally *in vivo* (**Table 1**). Application of NRCs in microbial cell factories is a recent development, so far only two examples have been published. In the first example, nicotinamide cytosine dinucleotide (NCD^+/NCDH) (**Figure 2B**) was applied as an NRC for the production of malate by *E. coli* (**Figure 3A**) (Wang *et al.*, 2017), where phosphite/phosphate was used as electron donor. The NAD^+/NADH-dependent phosphite dehydrogenase and malic enzyme were modified in such a way that they accepted NCD^+/NCDH as redox cofactor. NCD^+ was supplemented to the growth medium and taken up by *E. coli*. The low redox potential of phosphite/phosphate (E_0' = -650 mV, (Claassens *et al.*, 2018) in combination with the high initial [phosphite]/[phosphate] ratio reversed the reaction catalyzed by malic enzyme, converting pyruvate and CO_2 into malate. This resulted in an overall increase in malate yield from 0.11 g/g to 0.15 g/g.

In the second example, nicotinamide mononucleotide (NMN^+/NMNH) (**Figure 2B**) was used as an NRC for the conversion of ketoisophorone, which was added to the medium, to levodione ((Black *et al.*, 2020), **Figure 3B**). This process comprised an ene reductase enzyme to catalyze the reduction of the ketoisophorone carbon-carbon double bond, whose redox potential is near 0 V. Because the nicotinamide moiety of $NAD(P)^+$ is responsible for electron transfer, the redox potential of NMN^+/NMNH is expected to be close to –320 mV. Its intracellular availability was enhanced by providing nicotinamide as nutrient, by overexpression of genes involved in NMN biosynthesis (*nadE* and *nadV*) and knocking out genes involved in NMN breakdown (*nadR* and *pnnC*). A glucose dehydrogenase (GDH), modified to accept NMN^+/NMNH as redox cofactor, and ene reductase (XenA) were introduced. These enzymes formed an orthogonal circuit for the transfer of electrons. Strains were created that had to rely on the activity of both enzymes for growth by knocking out key enzymes of the Embden-Meyerhoff-Parnas (EMP) pathway (*pgi*) and pentose phosphate (PP)-pathway (*zwf* and *gnd*). Only strains that harboured both enzymes were able to

grow, indicating that the two enzymes successfully established the new electrical circuit.

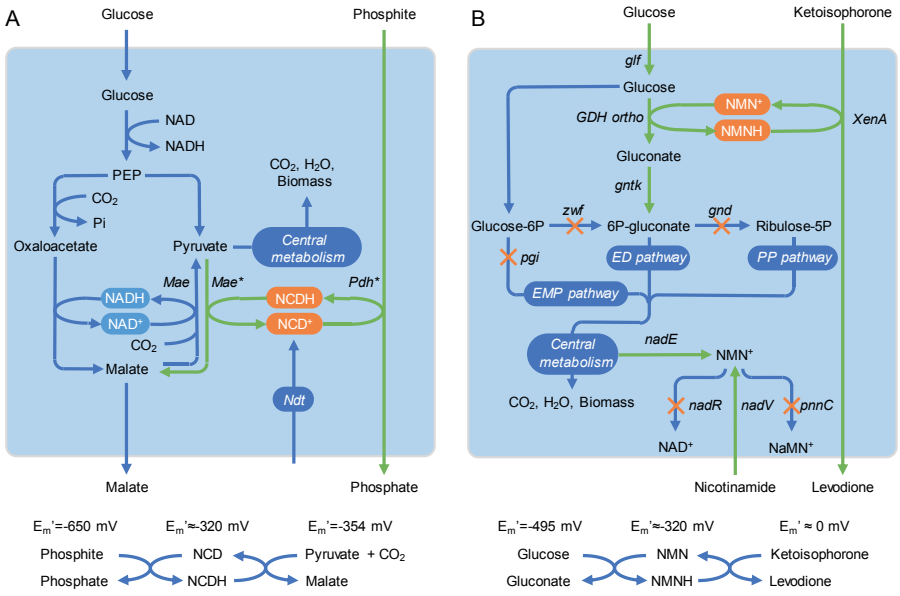

Figure 3. Examples of applying non-canonical redox cofactors in microbial cell factories. (A) Transferring electrons from phosphite/phosphate to malate/pyruvate + CO_2 via NCD^+/NCDH. Modified malic enzyme (Mae*) and phosphite dehydrogenase (Pdh*) were introduced. Adapted from Wang *et al.* (2017). **(B)** Transferring electrons from glucose/gluconate to ketoisophorone/levodione with NMN^+/NMNH as non-canonical cofactor. An NMN^+-dependent glucose dehydrogenase (GDH ortho) and ene reductase (XenA) were introduced. NMN^+ availability was enhanced by adding nicotinamide to the medium, knocking out the genes *nadR* and *pnnC* and overexpressing the genes *nadE* and *nadV*. The glycolytic flux was forced over glucose dehydrogenase by knocking out the genes *pgi*, *zwf* and *gnd*. Blue lines: native pathways. Green lines: introduced or overexpressed gene/enzyme; **x**: deleted gene/enzyme. Adapted from Black *et al.* (2020).

6.6. Modifying the cofactor dependency of dehydrogenases

To enable the application of NRCs it is required to change the cofactor specificity of oxidoreductases from the native redox cofactor to the NRC. In recent years, several methods have been developed to switch the cofactor dependency of dehydrogenases from NAD^+ to $NADP^+$, and *vice versa*. In particular, a web tool

named CSR-SALAD (Cofactor Specificity Reversal-Structural Analysis & Library Design) can assist, through a structure-guided and semi-rational approach, in the modification of the cofactor dependency of dehydrogenases (Cahn *et al.*, 2017). Engineering this cofactor dependency is now a commonly used strategy in the optimization of redox metabolism, and is starting to be applied for cofactor analogues, such as NRCs (Liu *et al.*, 2018). For example, in the case of NCD, Liu *et al.* (2020) identified three residues in the cofactor-binding pocket of LDH from *Lactobacillus helveticus* that may be hotspots for cofactor preference. Located in close proximity to the AD moiety of NAD, they are mostly conserved across NAD^+-dependent LDHs. Different combinations of the mutations V152R, I177K, N213E and N213I enabled the switch from NAD to NCD dependency. Moreover, V152 is positioned at the N-terminus of the conserved GX(X)GXXG sequence in the Rossmann fold motif and is present in other dehydrogenases, varying in some of them to L or I. With the malic enzyme (ME) from *E. coli*, the L310 residue (corresponding to V152 in LDH), was changed to an arginine to obtain an NCD-dependent ME (Ji *et al.*, 2011), therefore confirming the potential of modifying cofactor specificity to NCD by reproducing the mutations of these hotspot residues.

Recently, Black *et al.* (2020) incorporated four mutations in the GDH from *Bacillus subtilis*, switching from NADP to NMN preference. The mutations I195R and Y39Q were meant to form hydrogen bonds with the phosphate of NMN. Additionally, A93K was predicted to facilitate the interaction of Y39Q with NMN and S17E to promote the exclusion of NADP. The identification of these residues in other dehydrogenases can be challenging because protein-cofactor interactions are variable in $NADP^+$-dependent enzymes (Carugo and Argos, 1997a; Carugo and Argos, 1997b), and might be unsuitable for NAD^+-dependent enzymes. Alternatively, introducing other mutations for the hotspot residues identified in LDH for NCD specificity could enable the switch to NMN.

In conclusion, cooperative mutations can change the cofactor dependency of dehydrogenases. Targeting residues scattered over a relatively broad range of gene sequence will make the reversal of all mutations unlikely. However,

omitting only one of these mutations can already diminish the enzyme activity towards the NRC. The extent of this reduction and thereby the stability of the modifications, will depend on the contribution of the reversed mutation to the switch of cofactor dependency.

6.7. Application of non-canonical redox cofactors in fermentation processes

These results show that in these examples, the four prerequisites for application in microbial cell factories (**Table 1**) were met, which opens up the possibility to use NRCs in fermentation applications.

6.7.1. Challenges in fermentation processes

In fermentation processes, the substrate is converted into oxidized intermediates, which are reduced to principle: ethanol and lactate production. The yields obtained for these two processes approach the maximal theoretical yield (for recent reviews see Aditiya *et al.* (2016) and Alves de Oliveira *et al.* (2018)). With respect to the production of bulk chemicals, this is the mode of choice. The design of metabolic networks for new fermentation processes is however challenging. By-product formation is difficult to prevent and even if the ΔG' of the conversions is sufficiently negative, it often proves difficult to realize net ATP production. Application of NRCs in fermentation processes could remedy this matter. NRCs have not been applied in fermentation processes yet. Recently the development of an NCD-dependent lactate dehydrogenase (LDH) was described, which could be a prelude to such a development aiming at the production of lactate (Liu *et al.*, 2020).

6.7.2. Metabolic engineering with NRCs

The redox potential of redox couples and the chemical structure of NRCs are leading factors in the design of NRC-dependent metabolic networks for product formation, because they determine the thermodynamic feasibility of the

conversion. To remain close to wild-type situations it seems reasonable to focus initially on NRCs with redox potentials close to those of NAD^+/NADH and $NADP^+$/NADPH. $F_{420}/F_{420}H_2$ and nicotinamide derivatives such as NCD^+/NCDH and NMN^+/NMNH are in the suitable range.

Application of an NRC requires a change in cofactor dependency of at least two enzymes: one reducing the NRC, the other oxidizing it. **Figure 4** gives an overview of the redox reactions and their potentials involved in the dissimilation of glucose.

Only few reactions transfer electrons to NAD^+/NADH and $NADP^+$/NADPH. These reactions can be categorized into two groups: those involving the conversion of aldehydes into organic acids, and oxidative decarboxylations (**Figure 4**). The associated redox couples have a redox potential lower than that of $NAD(P)^+$/NAD(P)H. These redox couples are good candidates to reduce NRC^+/NRCH. GAPDH, both phosphorylating and non-phosphorylating, is the only enzyme involved in all pathways and therefore an obvious candidate.

In wild-type fermentation situations the electrons are transferred from $NAD(P)^+$/NAD(P)H to redox couples with higher redox potentials. These reactions can be categorized into three groups: the reduction of aldehydes to alcohols, the reductive amination of 2-oxoacids with NH_3 to amino acids, and the reduction of carbon-carbon double bounds (**Figure 4**). When designing an NRC-dependent network suitable for fermentative product formation it is therefore necessary to include such an NRC-dependent reaction.

The redox potentials of both NAD^+/NADH and $NADP^+$/NADPH are fixed within certain boundaries by cellular regulation, NAD^+/NADH more oxidized and $NADP^+$/NADPH more reduced. The NRCs offer more flexibility to fine tune their redox potentials, by varying the ratio of the NRC^+ and NRCH concentrations, between those of the cofactor reducing and oxidizing reactions because they only depend on two enzyme activities. This may have benefits, especially for

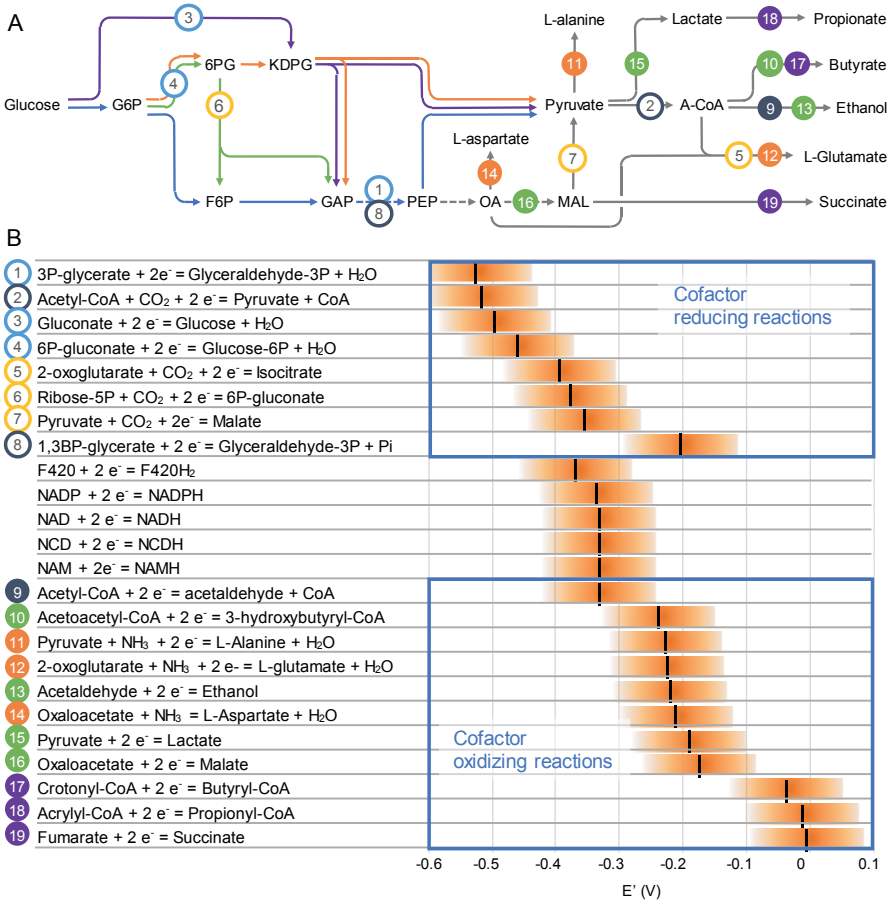

Figure 4. An overview of the redox reactions and their potential involved in the dissimilation of glucose. (A) The glycolytic pathways and the redox reactions involved. Embden-Meyerhof-Parnas pathway (blue arrows), Entner-Doudoroff pathway (orange arrows), semi-phosphorylating Entner-Doudoroff pathway (purple arrows), pentose phosphate pathway (green arrows), fermentation pathways (gray arrows). **(B)** The redox potentials of relevant redox couples. | = Em' (the redox potential at pH 7, at 1 mM concentrations of the redox couple components (Flamholz *et al.*, 2012). The orange band indicates the range of the E' between 1-99% oxidation. The redox reactions in the glycolytic pathways have a low redox potential, the redox reaction in the fermentation pathway a high redox potential. Aldehydes/organic acids (blue circles); oxidative decarboxylations (orange circles); alcohols/aldehydes (green circles); reduction of carbon-carbon double bonds (purple circles); other (gray circles). Interrupted lines depict a number of reactions. G6P = glucose-6-phosphate; 6PG = 6-phosphogluconate; KDPG = 2-dehydro-3-deoxy-phosphogluconate; F6P = fructose-6-phosphate; PEP = phosphoenolpyruvate; GAP = glyceraldehyde-3-phosphate; OA = oxaloacetate; MAL = malate; A-CoA = acetyl-CoA.

the functioning of GAPDH, which operates on the edge of thermodynamic feasibility with NAD^+/NADH as cofactor (**Figure 4**).

The synthesis of some compounds requires more than one oxidation and reduction reaction. Examples are the production of succinate (Meng *et al.*, 2016), L-glutamate (Chinen *et al.*, 2007) and 1,4-butanediol (Burgard *et al.*, 2016). In these cases, it would be interesting to investigate whether it is required to make all involved dehydrogenases NRC-dependent, or if it is possible to restrict this system to GAPDH as cofactor reducing enzyme, and a limited number of cofactor-oxidizing dehydrogenases able to regenerate NRCs.

6.7.3. GSCBMM model predictions

We used GSCBMM iML1515 of *E. coli* to illustrate how NRCs can be applied and which challenges will be encountered, aiming at lactate production using NRC-dependent GAPDH and LDH (**Figure 5**).

GAPDH is applied for both dissimilation and assimilation purposes. In wild-type situations (**Figure 5A**) GAPDH transfers electrons *via* NAD^+/NADH. The NAD^+ reduced in dissimilation is completely regenerated by the synthesis of fermentation products. This also generates the ATP required for growth and maintenance purposes. The model, when maximizing ATP production, predicts a mixture of ethanol, acetate and formate. The NAD^+ used in assimilation cannot be regenerated by producing the same dissimilatory fermentation products. Instead, it can be regenerated by a transhydrogenase transferring electrons from NAD^+/NADH to $NADP^+$/NADPH, which is required for assimilation, or by producing a by-product whose formation requires net NADH input (e.g. succinate or glycerol). Indeed, the model, when maximizing growth, predicts that the NAD^+ used by GAPDH for assimilation purposes is regenerated by action of the transhydrogenase STH.

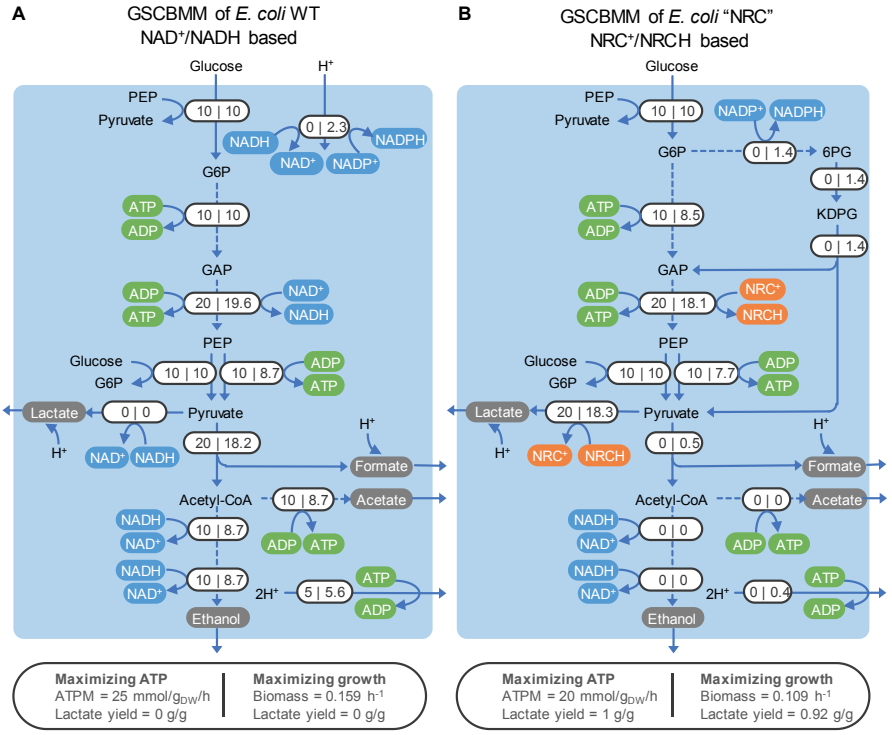

Figure 5. Carbon flux distributions predicted by a modified version of GSCBMM iML1515. Carbon flux distribution in **(A)** wild-type *E. coli* and **(B)** *E. coli* "NRC" carrying non-canonical redox cofactor "NRC"-dependent glyceraldehyde-3-phosphate dehydrogenase (NRC-GAPDH) and lactate dehydrogenase (NRC-LDH) under anaerobic conditions. A modified iML1515 genome-scale metabolic model of *E. coli* was used to predict the effect of introducing NRC-dependent enzymes in *E. coli* under anaerobic conditions on ATP maintenance requirement (ATPM) and biomass formation (growth rate). For more information about the model and the modifications introduced, see **Supplementary Information**.

We introduced a new redox couple in the model named NRC^+/NRCH and changed the cofactor specificity of GAPDH and LDH accordingly. The predictions are shown in **Figure 5B**. The dissimilatory flux was redirected from ethanol/acetate/formate to lactate only. Lactate synthesis was responsible for ATP production and resulted in complete cofactor regeneration when the model maximized for ATP production. Using the EMP pathway as single glycolytic pathway for assimilation would result in incomplete regeneration of NRC^+. The model used the Entner-Doudoroff (ED) pathway instead. This pathway converts glucose into GAP and pyruvate, partially bypassing GAPDH. This resulted in

two glycolytic fluxes: a dissimilatory one using the NRC *via* a combination of the EMP and ED pathways, and an assimilatory one using NAD(P) exclusively *via* the ED pathway. This indicates that a fifth prerequisite for the successful usage of NRCs in fermentation processes applies: the NRC should only be used for (ATP-generating) dissimilation and not for assimilation (**Table 1**). In the case of an NRC-dependent GAPDH, this can be realized by using the ED pathway.

6.7.4. Adaptive laboratory evolution (ALE)

ALE is a powerful technique for the improvement of microbial traits that are advantageous for growth or survival of the microorganism (Dragosits and Mattanovich, 2013). We did not ask the model to redirect the fluxes to lactate, or to implement the NRC-dependent enzymes, but to optimize for either ATP or biomass production, with high lactate production as result. This indicates that ALE can be applied to improve the flux over the NRC-dependent enzymes provided they are able to carry sufficient flux to fulfil maintenance requirements. It cannot be excluded, however, that the application of ALE will result in reversion of the NRC-dependent enzymes to their original cofactor dependency.

6.7.5. Aerobic NRC application

As indicated above, when respiration is applied, it is impossible to reach the maximum theoretical yield. This problem is significantly reduced when dissimilation depends on NRC-depending enzymes because reduced NRC is not a substrate for NADH dehydrogenase. This indicates that NRCs can also be applied for the synthesis of fermentation products under aerobic conditions. This opens the opportunity to use NRCs in strict aerobic microorganisms that rely on the availability of oxygen for the synthesis of biomass buildings blocks. It would also enable NAD^+ used in assimilatory pathways (approximately 8% of the total flux in the lactate case) to be regenerated by respiration, at the expense of a somewhat lower yield. An additional advantage could be additional ATP synthesis *via* respiration that could support metabolic networks that generate too little ATP. We tried to simulate aerobic application in the GSCBMM by making oxygen available. We expected that the NRC would support the

dissimilatory flux to lactate, and that the NAD(P)$^+$ used by assimilation would be regenerated by respiration. The model indeed produced lactate using the NRC-dependent enzymes, but subsequently converted lactate by an ubiquinol-dependent LDH back to pyruvate, which was used for further cellular processes. Knocking out this enzyme resulted in a situation in which a circular EMP/ED pathway was used, as described for *P. putida* (Nikel *et al.*, 2015), in which the NRC-dependent GAPDH was completely bypassed. The ED produced NADPH instead of NADH. The model used STH to convert NADPH into NADH which was subsequently used in respiration. Knocking out the gene encoding STH (*sthA*) could prevent this, forcing the flux over the NRC-dependent GAPDH, but the model kept finding new combinations of reactions that together acted as a transhydrogenase. These predictions are largely possible due to the exceptional flexibility of GSCBMMs. In real life many of the reactions required to bypass NRC-dependent GAPDH are not switched on due to regulation, e.g. by catabolite repression in presence of glucose. Aerobic application of NRCs could therefore be successful. Nevertheless, these model predictions indicate that mutations which open alternative routes, bypassing the application of the NRCs, will be very advantageous for growth under aerobic conditions. This may trigger the appearance of mutated strains that do not rely on the NRC for product formation.

6.8. Concluding remarks and future perspectives

NRCs have successfully been applied in microbial cell factories, providing an orthogonal circuit for electron transfer, making it possible to have full control over the fate of electrons.

Fermentation processes are being developed to enable the sustainable production of chemicals. To approach the maximum theoretical yield, it is required to transfer all electrons from the substrate to the product. This is not straightforward as electrons are diffusely distributed over metabolism by redox cofactors.

6.8.1. Highlights

In this paper, we have shown that application of NRCs could prevent the wide diffusion of electrons over the metabolism. Using NRCs in fermentation processes has the potential to tremendously impact the design and application of fermentation processes. It will maximize the transfer of electrons from substrate to product, and as such, making it possible to approach the maximal theoretical yield. Consequently, it will minimize by-product formation. Product formation will also result in ATP production. The whole metabolic network can therefore be optimized using ALE. Moreover, it may be applied under aerobic conditions, broadening the scope of application to aerobic microorganisms.

6.8.2. Remaining questions

NRCs have not been applied in fermentation processes yet. Several questions remain to be addressed before this system can be applied successfully.

- Making dissimilation dependent on an NRC is a tremendous interference in cellular metabolism. How will this affect cellular functioning?
- NRC application may often result in less ATP synthesis, being detrimental for growth and maintenance. Will NRC-independent mutant strains appear and outcompete NRC-dependent strains? Will these mutants revert to the original cofactor dependency, or will they bypass the NRC-dependent enzymes? What can be done to prevent the appearance of such strains?
- In this paper, the application of NRC for the production of lactate was worked out as an example, using NRC-dependent GAPDH and LDH. Other options for electron-donating and electron-receiving reactions are possible and have to be investigated.
- Using NRCs should be limited to dissimilatory fluxes, indicating that NRC-independent assimilation pathways have to be constructed. We have identified the ED pathway as option in combination with GAPDH. What other options are possible?
- The cofactor dependency of a few enzymes has been changed from $NAD(P)^+$ to NCD^+ and NMN^+ by changing three and four amino acids,

respectively. Is it possible to apply this strategy to other oxidoreductases as well?

- Other redox cofactors are applied in fermentation processes (Box 1), such as ferredoxin and F_{420}. Will ferredoxin- and F_{420}-based NRCs also be beneficial for product formation and, if so, how can this be realized?
- Microbial cell factories have been constructed that are able to synthesize sufficient NMN^+/NMNH and NCD^+/NCDH *de novo* or by salvation pathways. Is this also sufficient to sustain the high fluxes required for fermentation processes?

6.8.3. Limitations of the study

To predict the effect of applying NRCs in fermentation processes, especially with respect to assimilation, we have used a genome-scale constraint-based metabolic model of *E. coli* (iML1515). More elaborate metabolic models are available (e.g. enzyme-constrained models), whose application may give different results.

6.8.4. Data and code availability

All data and code required to repeat the model predictions are available in the Supplemental Information section.

6.9. Supplementary material

Transparent Methods

The iML1515 genome-scale metabolic model from *Monk et al.* (2017) was modified to predict the effect of non-canonical redox cofactor "NRC"-dependent glyceraldehyde-3-phosphate dehydrogenase and lactate dehydrogenase on the anaerobic metabolism of *E. coli*. The models can be found in SBML format/scripts in the supplementary files "*E. coli* WT.ipynb", "*E. coli* WT.xml", "*E. coli* NRC-GAPDH and NRC-LDH.ipynb" and "*E. coli* NRC-GAPDH and NRC-LDH. xml".

To introduce the NRC-dependent enzymes, the native reactions catalyzed by glyceraldehyde-3- phosphate dehydrogenase (GAPD) and D-lactate dehydrogenase (LDH_D) were first knocked out by setting the upper and lower bounds of the reactions to 0. The two new cofactors – non-canonical redox cofactor oxidized (NRCox) and reduced (NRCred) – were added to the model as new metabolites. Then, the reactions catalyzed by the NRC-dependent glyceraldehyde-3-phosphate dehydrogenase (GAPD_NRC) and NRC-dependent D-lactate dehydrogenase (LDH_D_NRC) were added to the model. The upper and lower bounds of the reactions were set at the same values than the native enzyme ([-1000; 1000]).

Additional modifications were performed in the models for both *E. coli* WT and *E. coli* carrying NRC-dependent glyceraldehyde-3-phosphate dehydrogenase and D-lactate dehydrogenase regardless of the objective to maximize used.

The reaction catalyzed by the membrane-bound transhydrogenase PntAB (THD2pp) was modified to allow the translocation of one proton instead of two. The reactions catalyzed by dihydroxyacetone phosphotransferase (DHAPT) and pyruvate dehydrogenase complex (PDH) were knocked out by setting the upper and lower bounds of the reactions to [0; 0].

The direction of the reaction catalyzed by acyl-CoA dehydrogenase (butanoyl-CoA) (ACOAD1fr) was reversed by modifying the bounds of the reaction from [0; 1000] to [-1000; 0].

Finally, anaerobic conditions were enabled by setting the upper and lower bounds of the oxygen exchange (EX_o2_e) reaction to [0; 0].

The models were run using 10 mmol/g_{DW}/h glucose as carbon source. Biomass (BIOMASS_Ec_iML1515_core_75p37M) and ATP maintenance requirement (ATPM) were used as objectives to maximize in the modified iML1515 genome-scale metabolic models. Gurobi was used as solver.

Supplementary files

The models can be found in SBML format/scripts in the supplementary files "*E. coli* WT.ipynb", "*E. coli* WT.xml", "*E. coli* NRC-GAPDH and NRC-LDH.ipynb" and "*E. coli* NRC-GAPDH and NRC-LDH. xml". Supplementary files can be found online at https://doi.org/10.1016/j.isci.2020.101471.

6.10. Glossary

Adaptive laboratory evolution. Adaptive laboratory evolution is a frequent method in biological studies to gain insights into the basic mechanisms of molecular evolution and adaptive changes that accumulate in microbial populations during long-term selection under specified growth conditions (Dragosits and Mattanovich, 2013).

Assimilation and dissimilation. Assimilation is the energy-requiring metabolic process that converts a substrate into biomass. Dissimilation is the metabolic process that converts a substrate into products, concomitantly producing the energy required for assimilation and maintenance.

Biocatalysis. Use of biological systems such as whole cells (*in vivo*) or isolated enzymes (*in vitro*) to catalyze reactions. Enzymes can catalyze chemical reactions with exquisite regio-, stereo- and/or chemoselectivity, with high rates of reactions depending on the type of reaction, and the substrates used.

Cofactors. Non-protein organic molecules (coenzymes) or metal ions required by an enzyme to assist during a catalytic reaction. Most common coenzymes for oxidoreductases are redox cofactors: nicotinamide adenine dinucleotide NAD(P), flavin adenine dinucleotide FAD and flavin mononucleotide FMN, and heme. Coenzymes can be covalently or tightly bound as a prosthetic group to a protein, or only transiently bound and used as co-substrate. Inorganic cofactors, such as Zn, Mg, Co, Mo and iron-sulfur (Fe-S) clusters, can play both functional and structural roles. An enzyme without its cofactor is an inactive apoenzyme.

Fermentation process. A metabolic process that releases energy from a sugar or other organic compound without requiring an external electron acceptor.

Genome editing. The modification of the genome within a living cell through the insertion, deletion, or replacement of one or more segments of DNA (Fang *et al.*, 2019).

Genome-scale constraint-based metabolic model (GSCBMM). A stoichiometric model of metabolism of a certain (micro)organism, including all enzymes annotated based on its genome and associated reactions and metabolites. The model can predict fluxes through the metabolic model within certain pre-set flux constraints.

Metabolic engineering. The practice of optimizing genetic and regulatory processes within cells to increase the cells' production of a certain substance. These processes are chemical networks that use a series of biochemical reactions and enzymes that allow cells to convert raw materials into molecules necessary for the cell's survival. Metabolic engineering specifically seeks to mathematically model these networks, calculates a yield of useful products, and pinpoints parts of the network that constrain the formation of these products (Yang *et al.*, 1998).

Microbial cell factories. Use of microbial cells as a means to produce targeted chemicals. Optimization of the process relies mostly on metabolic engineering.

Oxidoreductases. One of the seven classes of enzymes, they catalyze reduction (gain of electrons) and oxidation (loss of electrons) reactions. Approximately 80% of known oxidoreductases require the nicotinamide adenine dinucleotide cofactor.

Orthogonal pathways. Growth-independent pathways optimized for the production of a target chemical. These pathways are characterized by the minimization of interactions between the chemical-producing pathways and the biomass-producing pathways (Pandit *et al.*, 2017).

Synthetic biology. Applying the engineering paradigm of systems design to biological systems in order to produce predictable and robust systems with novel functionalities that do not exist in nature (The European Commission, 2005).

Chapter 7

Thesis summary and General discussion

Thesis summary

Microbial cell factories are widely used as platform for the production of pharmaceutical compounds, food ingredients and bulk chemicals. However, microbial production of low-cost chemicals requires high titer, rate and, most importantly, yield to compete with petrochemical-based processes. The maximum theoretical yield can be approached when all electrons from the substrate end up in the product of interest. The process should therefore not be based on respiration, as this involves the transfer of electrons to terminal electron acceptors. Instead, the process has to be based on fermentation, in which the metabolic pathways involved in product formation are redox-neutral and generate sufficient metabolic energy to fulfil the cells energetic requirements (maintenance, biomass formation), as described in **Chapter 1**. The development of omics, synthetic biology and genome editing tools allowed to design more efficient microbial cell factories carrying such redox-neutral product-forming pathways. Yet, the energy available during fermentative conversion of substrates into products is mostly dissipated, and only a small part is used to generate metabolic energy for the cells. Conserving additional metabolic energy during microbial processes would allow microorganisms to grow under more inhibitory conditions, reach higher biomass yields and produce higher amounts of product. Nevertheless, capturing additional metabolic energy during product formation is not straightforward.

In this thesis, we attempted to implement a strategy to increase the energy efficiency of *E. coli* during fermentation growth on glucose. We focused on conserving extra energy in the central carbon metabolism by using the energy difference of the redox cofactor couples NAD^+/NADH and $NADP^+$/NADPH.

Prior to designing a strategy to enhance the energetic efficiency of *E. coli*, we first reviewed the existing mechanisms found in microorganisms to conserve energy as well as options to reduce undesired energy expenditure during fermentative growth on carbohydrates (**Chapter 2**). Application and suitability of these systems during fermentative product formation were discussed.

Microorganisms can either produce energy directly in the form of ATP by substrate-level phosphorylation (SLP) or indirectly by generating an ion-motive force (IMF), depending on the energy available in a chemical reaction. Although all reactions involved in the conversion of substrate into product contributes to the overall Gibbs free energy, only a few have a sufficiently low Gibbs free energy to harvest it as metabolic energy. Generation of an ion-motive force requires around 20-30 kJ/mol whereas direct ATP synthesis requires around 40 kJ/mol. SLP leads to direct ATP formation by using the energy released from energy-rich bonds such as thioester of phosphate bonds to phosphorylate ADP. This mechanism is limited to a few reactions that are mainly product-specific and therefore cannot be applied to a wide range of product. However, some of the enzymes contributing to SLP have a broad substrate specificity. Protein engineering would therefore allow scientists to couple energy generation via SLP to the production of other chemicals. Nevertheless, we proposed that not all hydrolyses of energy-rich molecules contribute to SLP based on thermodynamics. When the energy available is insufficient to directly synthetize ATP, energy can be captured by generating an ion-motive force. This mode of energy conservation is driven by reduction of carbon-carbon double bonds, decarboxylation reactions and electron transfer between redox cofactors. We also reflected on how the redox potentials of redox couples affect SLP and IMF generation and provided a reference that can be used to design metabolic pathways for product formation with increased energy conservation. During the design of an energetically efficient microbial cell factory, energy-conserving mechanisms are often overlooked. However, they can have a strong positive impact on the availability of metabolic energy for the cells. This review provides a list of energy-saving systems present in microorganisms that could be implemented to increase energy availability. In this review, we distinguished between product-specific and generally applicable methods to conserve energy. The latter can be applied to a wider range of products and are therefore the most desirable option.

After evaluating potential targets for energy conservation, the reaction catalyzed by the pyruvate dehydrogenase complex (PDH) was selected due to its high negative Gibbs free energy (**Chapter 1**). This reaction is a key step in the carbon metabolism and conserving energy at this step could benefit the production of a wide range of compounds. Energy conservation can be realized by transferring electrons from “low redox potential” NADPH produced during conversion of pyruvate to acetyl-CoA by PDH to the “higher redox potential” NAD^+. The energy difference between the two redox couples can then be used by the membrane-bound transhydrogenase PntAB to create an electrochemical gradient over the membrane (proton-motive force) which can subsequently be utilized by the ATP synthase to phosphorylate ADP to ATP. This strategy – if successfully implemented in *E. coli* – would allow the synthesis of an additional 0.5 mol ATP per mol glucose. In this work, we realized a step-by-step approach trying to not only increase the energy efficiency of *E. coli* but also to understand the impact of the modifications on metabolism. To realize this scenario, several steps are required: 1) change the cofactor specificity of the pyruvate dehydrogenase complex from NAD^+ to $NADP^+$, 2) lower the NADH sensitivity of the PDH complex as it was proven to inhibit the enzyme under anaerobic conditions, 3) ensure that PDH is the sole enzyme catalyzing the anaerobic conversion of pyruvate to acetyl-CoA by knocking out the *pflB* gene encoding pyruvate formate-lyase (anaerobic counterpart of PDH), 4) ensure that NADPH reoxidation occurs only via the membrane-bound transhydrogenase PntAB by knocking out the *sthA* gene encoding the soluble transhydrogenase and 5) knock out any by-product formation. The steps necessary to achieve this strategy correspond to the different chapters of this thesis.

Chapter 3 describes the creation of an $NADP^+$-dependent pyruvate dehydrogenase in *E. coli*. The PDH complex is encoded by three genes *aceE*, *aceF* and *lpd*, and the latter is responsible for the NAD(H) binding site. Introduction of seven amino acids mutations in the *lpd* gene resulted in a change of cofactor specificity from NAD^+ to $NADP^+$. The modifications resulted in a 7.6-fold higher apparent activity of the PDH complex with $NADP^+$ than NAD^+. In

addition, it also changed the cofactor dependency of the 2-oxoglutarate dehydrogenase (ODH), which was only able to function with $NADP^+$ (data not shown in this thesis). Nevertheless, the PDH complexes showed to be subjected to NAD(P)H inhibition. Introduction of an additional amino acid mutation in the *lpd* gene successfully lowered the sensitivity towards both NADH and NADPH. The effect of an $NADP^+$-dependent LPD on the metabolism of *E. coli* was then assessed by knocking out the genomic *lpd* gene and introducing the different LPD variants on a medium copy plasmid. Aerobically, *E. coli* strains carrying an $NADP^+$-dependent LPD exhibited significantly reduced specific growth rates and accumulated pyruvate, the substrate of PDH. Introduction of an $NADP^+$-LPD most likely resulted in the production of high amount of NADPH in the cells during the reactions catalyzed by the PDH and ODH complexes. Accumulation of pyruvate and the decreased specific growth rate observed show that reoxidation of the surplus of NADPH is a challenge for the cells and that the transhydrogenase (STH and PntAB) activity was insufficient. Conversely, the change of cofactor dependency of the PDH complex did not have consequences on the anaerobic metabolism of *E. coli* as pyruvate formate-lyase (PFL) – the anaerobic counterpart of the PDH complex – bypassed PDH to convert pyruvate to acetyl-CoA.

In **Chapter 4**, the anaerobic activity of the PDH complex was investigated in an *E. coli* strain lacking a functional pyruvate formate-lyase. Both *lpd* and *pflB* genes were disrupted and the LPD variants were introduced on a plasmid. The strains relying solely on the PDH complex for the anaerobic conversion of pyruvate to acetyl-CoA grew under fermentative conditions, demonstrating that PDH alone can support anaerobic growth of *E. coli* on minimal medium. These results are in accordance with the observations made in Chapter 3 where disruption of *lpd* in wild-type *E. coli* resulted in lower specific growth rates, thereby indicating that the PDH complex is carrying flux – although limited – under anaerobic conditions. Although deletion of *pflB* led to an increased flux through the PDH complexes, it was limited due to the formation of lactate. Lactate formation allows regeneration of the NADH produced in glycolysis while

the NADPH produced during the reaction catalyzed by PDH is used for biomass formation. Accumulation of pyruvate and lactate under aerobic and anaerobic conditions respectively revealed that a bottleneck was present at the pyruvate node in *E. coli* Δ*pflB* carrying an $NADP^+$-dependent PDH. The cells cannot reoxidize the intracellular surplus of NADPH produced during the conversion of pyruvate to acetyl-CoA. Nonetheless, the strain exhibiting an $NADP^+$-PDH with reduced sensitivity towards NAD(P)H produced 2.5 ± 0.6 mM ethanol, demonstrating that part of the NADPH produced was converted into NADH by one of the transhydrogenases. As hypothesized in Chapter 3, the activity of the transhydrogenases is insufficient to transfer the surplus of $NADP^+$ to NADH under both cultivation conditions. Finally, a genome-scale metabolic model was used to predict the behavior of *E. coli* exhibiting an $NADP^+$-dependent PDH under both aerobic and anaerobic conditions using biomass as objective to maximize. Under both conditions, the model predicted a slight increase in specific growth rate for the strain carrying an $NADP^+$-dependent PDH which was not observed experimentally. Simulation of pyruvate accumulation under aerobic conditions revealed that it had a negative impact on growth since it diverted flux from assimilation, which is in accordance with the experimental data previously obtained. Anaerobically, the model predicted the formation of lactate as main fermentation product regardless the cofactor specificity of the PDH complex. However, the presence of an $NADP^+$-dependent PDH was expected to redirect part of the flux from lactate towards ethanol production, which was experimentally observed for *E. coli* Δ*lpd* Δ*pflB* + $PDH_{NADP+low\ inhib}$.

Lactate formation limits the carbon flux towards the PDH complex and masked the potential of the enzyme to convert pyruvate to acetyl-CoA anaerobically. In **Chapter 5**, we set out to implement the last steps required to realize the strategy described in Chapter 1 to increase the energetic efficiency of *E. coli* during fermentative growth on glucose. First, a genome-scale metabolic model was used to predict the behavior of an *E. coli* strains carrying all the modifications necessary to achieve the goal strategy. The objectives maximized were either ATP or biomass formation. Maximizing for ATP formation allows to determine

the maximum theoretical yield of ATP formation whereas maximizing for biomass allows to predict the effect on the strain metabolism. Replacement of STH by PntAB for NADPH reoxidation was predicted to increase ATP formation by 6.4% and 25% under aerobic and anaerobic conditions, respectively. It should also lead to an increase in growth rate or biomass formation of 1.4% and 30.3%, respectively. Therefore, capturing additional metabolic energy via our strategy should be more visible under anaerobic conditions. To achieve the goal strategy, both *sthA* and *ldhA* genes were disrupted in *E. coli* Δ*lpd* Δ*pflB* carrying the different LPD variants. This was realized as a step-wise approach to gain insights in the role of STH on the metabolism of the strains carrying an $NADP^+$-dependent PDH. We showed that STH was most likely not active and therefore did not contribute to NADPH reoxidation in the previous chapters as its disruption did not have a significant impact on growth and product formation of the strains. During aerobic fermentations, the final strain carrying an $NADP^+$-dependent PDH did not produce any fermentation products (and did not accumulate pyruvate) and used glucose almost solely for growth purposes. The membrane-bound PntAB was most likely active and regenerated the excess NADPH produced during the conversions of both pyruvate and 2-oxoglutarate catalyzed by PDH and ODH complexes, respectively. Nonetheless, we cannot rule out the possibility that NADPH regeneration was realized by respiration. Anaerobically, disruption of lactate formation resulted in poor growth of the strains regardless the cofactor specificity of the PDH complex showing that PDH activity was limited. Introduction of small amount of oxygen increased biomass formation for strains carrying an NAD^+-dependent PDH demonstrating that anaerobic expression of PDH was not the only culprit for poor anaerobic growth but NADPH reoxidation was also a bottleneck. Therefore, $NADP^+$ regeneration could not be achieved in the cells due to the insufficient activities of PntAB or PDH under anaerobic conditions.

The capture of extra metabolic energy using the strategy described in this thesis is promising. Nevertheless, it relies on the use of the redox cofactors NAD(H) and NADP(H) which are involved in a multitude of reactions across metabolic

pathways. The unwanted diffusion of electrons from these redox cofactors to other reactions might prevent use from reaching the maximum theoretical yield of product formation. In **Chapter 6**, we propose to apply non-canonical redox cofactors (NRCs) to increase product formation in microbial processes. Microbial cells factories allow to produce chemicals in an efficient and sustainable way as they are designed to reach high product yield. Achieving the maximum theoretical yield of product formation requires a tight control over the electrons. However, the use of redox cofactors in metabolic networks allows electrons to diffuse over these pathways and divert them from the product, thereby lowering the overall yield. Non-canonical redox cofactors can be applied to fermentation processes to increase product formation by diminishing the entanglement of electrons to the metabolic networks. However, they also need to fulfil some prerequisites to successfully apply them in microbial cell factories. We distinguished three classes of redox cofactors found in microorganisms: nicotinamide cofactors (NAD(H) and NADP(H)), deazaflavin cofactors (F420) and flavin cofactors (FMN and FAD). To date, however, they have been mostly used *in vitro* as cofactor biomimetics for enzymatic reactions and their *in vivo* application has just begun. Their application in microbial cell factories would provide a tighter control over the electrons fate by creating an orthogonal circuit for electron transfer. Several examples of successful applications of NRCs *in vivo* are described in this opinion paper. However, application of NRCs in microbial processes requires to change the cofactor specificity of oxidoreductases from the native cofactor to the NRC. This can be achieved by insertion cooperative mutations as discussed in the chapter. Application of NRCs in microbial fermentations is discussed including their potential benefit on the processes and considerations regarding metabolic engineering and NRCs properties. A genome-scale metabolic model was used to predict the effect of using NRC on lactate production in *E. coli*. By changing the cofactor specificity of both glyceraldehyde-3-phosphate dehydrogenase and lactate dehydrogenase to accept NRC, an orthogonal circuit for electron transfer was created which allowed homofermentative production of lactate. Applying NRC in microbial cell factories is therefore a very promising option to increase product

yield in microbial fermentation processes and compete with petrochemical-based processes.

Chapter 7 summarizes the work performed in this thesis and places the research in a broader context. Further engineering steps required to successfully achieve the strategy proposed in this thesis are discussed based on the results obtained in Chapters 3, 4 and 5. Finally, we propose several options to tackle the current challenges currently hindering microbial processes to reach product yield close or equal to the maximum theoretical yield of product formation.

General discussion

7.1. Towards conservation of additional energy during fermentative growth of *E. coli* on glucose

7.1.1. Thermodynamic feasibility of the strategy

The approach designed in this thesis to harness additional metabolic energy during fermentative growth on glucose of *E. coli* relies on the creation of a proton-motive force by the membrane-bound transhydrogenase PntAB (**Chapter 1**). *E. coli* is one of the few microorganisms possessing two transhydrogenases: STH and PntAB (Clarke and Bragg, 1985a; Clarke *et al.*, 1986; Boonstra *et al.*, 1999). Both transhydrogenases catalyze *in vitro* the reversible transfer of electrons between $NADP^+$/NADPH and NAD^+/NADH (Sweetman and Griffiths, 1971; Van de Stadt *et al.*, 1971; Hanson, 1979; Clarke and Bragg, 1985b; Boonstra *et al.*, 1999). However, they seem to have divergent functions *in vivo*: STH is a cytosolic enzyme that catalyzes the reaction in an energy-independent manner (Boonstra *et al.*, 1999) and it is vital for growth under cultivation conditions leading to NADPH overproduction (Canonaco *et al.*, 2001; Sauer *et al.*, 2004) while PntAB was shown to be the main enzyme responsible for NADPH production during aerobic growth of *E. coli* on glucose (Sauer *et al.*, 2004). PntAB drives the transfer of electrons from NADH to $NADP^+$ using an electrochemical proton gradient (Sweetman and Griffiths, 1971; Jackson, 2003) and one proton is translocated across the membrane per hydride transferred from NADH to $NADP^+$ (Bizouarn *et al.*, 1996). Although some previous work suggested that PntAB might be able to regenerate $NADP^+$ *in vivo* (Jan *et al.*, 2013), the reversibility of the reaction remains controversial (Van de Stadt *et al.*, 1971; Hanson, 1979; Clarke and Bragg, 1985b; Pedersen *et al.*, 2008). The *in vivo* reversal of the reaction catalyzed by PntAB entails a difference in redox potential between NAD^+/NADH and $NADP^+$/NADPH larger than the membrane potential. Therefore, the Gibbs free energy released from

NADPH reoxidation should be sufficient to pump a proton out, against the proton-motive force.

Values reported for $NADP^+$/NADPH and NAD^+/NADH ratios vary between 0.017 to 0.95 and 3.74 to 1820, respectively (Spaans *et al.*, 2015). The difference in redox potential between the cofactors is 149 mV, which is theoretically sufficient for the creation of a proton-motive force. To reach this ratio, the $NADP^+$-dependent PDH complex must be highly active under anaerobic conditions. This entails high expression of the genes encoding the complex and low to no inhibition by NADPH and NADH.

7.1.2. Was the proton-motive force with us?

The strategy designed in this thesis would theoretically lead to 1.4% and 25% increase in metabolic energy available for the cells grown on glucose under aerobic and anaerobic conditions, respectively. Under the conditions employed, this additional energy would result in 1.4% and 25% higher biomass yields, assuming the biomass composition does not change.

Aerobically, *E. coli* Δ*lpd* Δ*pflB* Δ*sthA* + LPD_{NADP} reached a biomass yield of 2.08 ± 0.18 mol/mol, whereas the strain carrying LPD_{WT} reached a biomass yield of 1.46 ± 0.02 mol/mol (**Chapter 5, Table S4**). This represents an increase of 42 %. This difference is much higher than the expected 1.4%, indicating that the suitability of the methods used to determine the biomass yields requires a critical evaluation. The biomass yield is based on the amount of glucose consumed and the optical density reached. Especially the technique used to assess biomass formation (OD_{600nm}) is not suitable to determine the biomass concentration accurately as it not only depends on the biomass concentration but also on cell morphology. Dry weight measurements would be more suitable, but it will still be very hard to accurately determine a difference of 1.4%. So, whether our strategy to increase energy conservation was successful under aerobic conditions was not proven nor invalidated.

Realization of the strategy designed in this thesis should be more easily assessed anaerobically since 25% additional metabolic energy can be conserved under this condition. Here, successful implementation of the scenario will not only affect cell growth (visible as an increase in specific growth rate or cell concentrations) but will also lead to homofermentative ethanol production. Ethanol production can be easily quantified using analytical methods such as HPLC or GC. In **Chapter 4**, *E. coli* Δ*lpd* Δ*pflB* carrying an $NADP^+$-dependent LPD grew anaerobically by producing lactate as main fermentation product. Lactate production was therefore disrupted to ensure higher carbon flux over the modified PDH (**Chapter 5**), and a shift from lactate towards ethanol production was expected. Nevertheless, *E. coli* Δ*lpd* Δ*pflB* Δ*sthA* Δ*ldhA* strains carrying an $NADP^+$-dependent LPD barely grew under both anaerobic and oxygen-limited conditions and did not produce any ethanol. Several hypotheses were proposed regarding the potential bottlenecks preventing the implementation of the strategy under anaerobic conditions.

7.1.3. Identification of the bottlenecks preventing the conservation of additional metabolic energy

The results obtained in **Chapter 5** did not allow us to clearly identify the cause(s) preventing anaerobic growth of the cells on glucose. However, several potential bottlenecks were proposed: 1) insufficient NADPH production due to either low expression of PDH or low activity of PDH due to NADPH inhibition, 2) low expression or activity of PntAB and 3) inability of PntAB to reoxidize the surplus of NADPH in the cells. In order to implement the strategy to conserve additional metabolic energy during fermentative growth of *E. coli* on glucose the bottlenecks should be first identified. Expression of the genes encoding PntAB and PDH should be assessed during anaerobic growth on glucose. Several methods can be used such as a qPCR, transcriptomics or fluorescent reporter molecule. Nonetheless, gene expression does not always lead to high protein production as some regulation on translation might occur. Consequently, the amount of PDH and PntAB produced in the cells during fermentation should also be determined, for example using enzymatic activity assays, SDS-PAGE or

Western blot. To determine whether NADPH inhibition is a bottleneck, the intracellular concentrations of NAD^+, $NADP^+$ and their reduced forms should be measured. Accurate measurement of these redox cofactors concentrations *in vivo* is however challenging as they have high turnover rates and their concentrations are very low. Finally, the reversibility of PntAB for $NADP^+$ regeneration should be tested. *In vitro* enzymatic assays could be performed however they might not reflect the situation *in vivo*. Overexpression of the energy-independent soluble transhydrogenase STH is a suitable option. STH catalyzes the energy-independent conversion of NADPH and NAD^+ into $NADP^+$ and NADH. Overexpression of *sthA* under anaerobic conditions will increase STH activity and allow the reoxidation of the excess NADPH produced by the $NADP^+$-dependent PDH. As a consequence, the strains could grow anaerobically by producing ethanol although no additional energy would be conserved.

7.1.4. Anaerobic activity of PntAB

Low anaerobic expression of *pntAB* genes would lead to low activity of the membrane-bound transhydrogenase PntAB. Accordingly, the enzyme would not be able to regenerate the excess NADPH produced during the conversion of pyruvate to acetyl-CoA catalyzed by the $NADP^+$-dependent PDH, which will lead to cofactor unbalance and ultimately cell death. To tackle this challenge, the genes encoding PntAB should be overexpressed. This can be achieved by expressing the genes on a plasmid or by changing the promoter of the genes on a genomic level.

Expressing the *pntAB* genes on a high copy plasmid under the control of a strong promoter is a suitable and straightforward approach. Nevertheless, maintenance of such a plasmid (size and expression level) might have negative consequences on the cells. Cells require energy to maintain the plasmid, which might be challenging under anaerobic conditions where energy is scarce. In addition, the use of a strong promoter can impair growth and product formation as the cells will spend a lot of energy on producing this particular protein. The development of genetic engineering tools such as Lambda-Red recombination

(Datsenko and Wanner, 2000; Baba *et al.*, 2006) or CRISPR-Cas9 (Jiang *et al.*, 2015) allow fast and efficient genomic modifications of *E. coli*. Replacing the native promoter of the *pntAB* genes on *E. coli* genome could be a better alternative to plasmid-based expression. Several promoters should be tested to ensure anaerobic expression of PntAB without negative impact on cell growth.

We selected three promoters to express *pntAB* anaerobically: an anaerobically induced promoter (P_{ldhA}), a constitutively expressed (P_{gapAp1}) and an inducible promoter (P_{trc}). The first promoter P_{ldhA} regulates the expression of the native lactate dehydrogenase. Although present aerobically, LDH is induced during anaerobic growth on carbohydrates (Mat-Jan *et al.*, 1989; Bunch *et al.*, 1997; Jiang *et al.*, 2001a). In this thesis, we showed that *E. coli* carrying an $NADP^+$-dependent PDH formed lactate as main fermentation product therefore the P_{ldhA} is a viable option for anaerobic expression of the *pntAB* genes. The second promoter tested is the first promoter of the *gapA* gene encoding glyceraldehyde-3-phosphate dehydrogenase (Seta *et al.*, 1997). This glycolytic enzyme is expressed in *E. coli* under various cultivation conditions as its transcription is controlled by multiple promoters (Charpentier and Branlant, 1994; Charpentier *et al.*, 1998; Riehle *et al.*, 2003; Thouvenot *et al.*, 2004). The *gapAp1* promoter is mostly active during the cell's growth phase and the beginning of the stationary phase (Charpentier and Branlant, 1994; Thouvenot *et al.*, 2004) and therefore suited for our approach. Finally, we selected the synthetic promoter P_{trc}. This promoter is a hybrid of the *lacUV5* and *trp* promoters and presents a stronger expression compared to the *lac* promoter (Brosius *et al.*, 1985; Mulligan *et al.*, 1985). It is inducible by IPTG and has been previously used for expression of STH in *E. coli* (Canonaco *et al.*, 2001). The use of an inducible promoter allows us to have an on/off situation and therefore better determine the effect of *pntAB* expression on *E. coli* metabolism. *E. coli* Δ*lpd* Δ*pflB* Δ*sthA* Δ*ldhA* + $LPD_{NADP+low\ inhib}$ (with *pntAB* genes under the control of their native promoter) was used as control strain.

Aerobically, no significant differences in growth or metabolite profiles were observed between the control strain (**Figure 1A**) and the P_{gapAp1}-*pntAB* strain

(**Figure 1B**). Both strains exhibited similar specific growth rates and reached similar final OD_{600nm} and produced up to 13mM acetate. Conversely, the uninduced P_{trc}-*pntAB* strain exhibited similar growth and fermentation profiles (**Figure 1D**) to the ones obtained in Chapters 3 and 4. The strain presented a very long lag phase and produced high amount of pyruvate (up to 60 mM) during exponential growth which was then converted into acetate. These results support our conclusion from Chapter 5 that PntAB is able to regenerate the excess of NADPH produced by PDH under aerobic conditions. The P_{ldhA}-*pntAB* strain showed an intermediate profile between the control strain and the P_{trc}-*pntAB* strain. It reached lower apparent cell densities than the control and P_{gapAp1}-*pntAB* strains (**Figure 1C**). In addition, the strain accumulated up 26 mM pyruvate, which was subsequently converted into acetate during stationary phase. Lactate dehydrogenase is expressed aerobically but it is fully induced anaerobically (Mat-Jan *et al.*, 1989; Bunch *et al.*, 1997; Jiang *et al.*, 2001a). Therefore, we inferred that the *pntAB* genes were not active at the beginning of the fermentation and got induced later as the conditions became more oxygen-limited.

Anaerobically, none of the strains grew or consumed glucose regardless the promoter used for expressing PntAB (**Figure 1E-H**). The *ldhA* promoter was shown to be highly active in our strains as they produced lactate as main fermentation product (**Chapters 4** and **5**). The lack of growth of P_{ldhA}-*pntAB* strongly suggests that anaerobic expression of PntAB is not the bottleneck preventing us from realizing the scenario proposed in this thesis. Insufficient anaerobic expression of PDH and low activity of the complex due to NADPH inhibition seem to be the most probable causes preventing anaerobic growth. This would lead to a low NADPH concentration which is not sufficient to reverse the reaction catalyzed by PntAB.

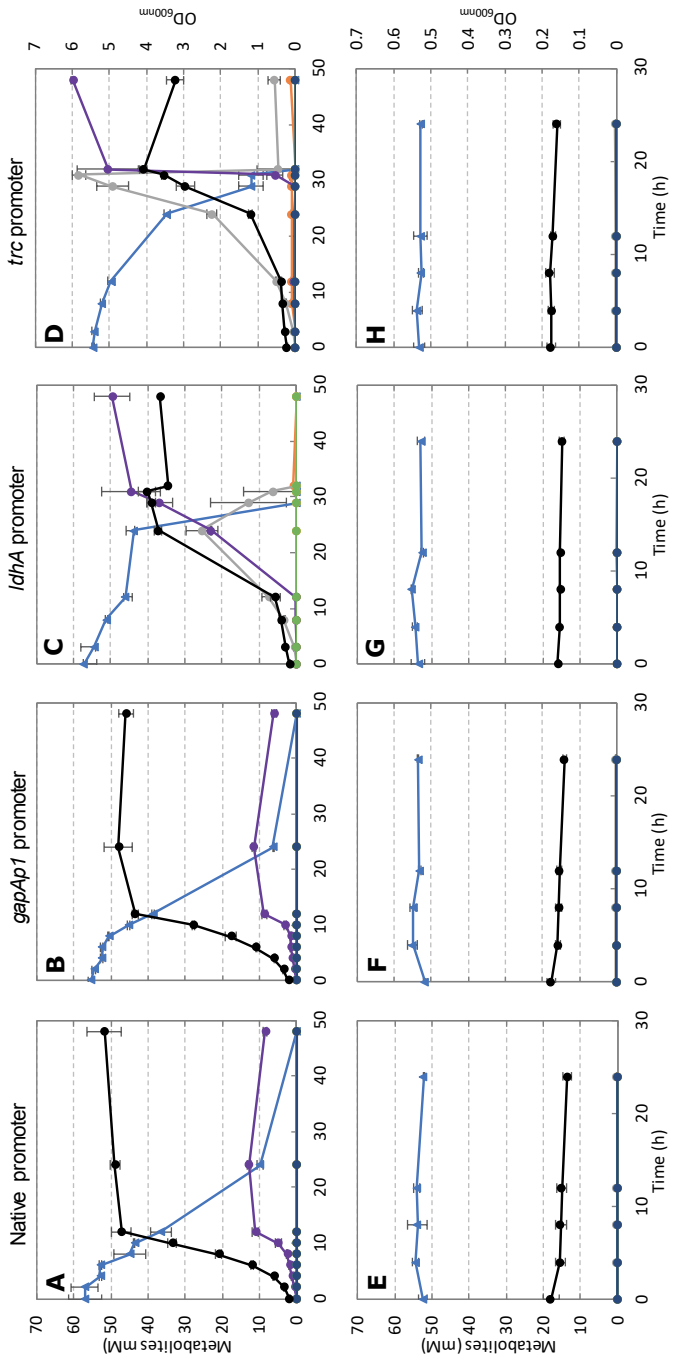

Figure 1. Aerobic (A-D) and anaerobic (E-H) fermentations of *E. coli* Δ*lpd* Δ*pflB* Δ*sthA* Δ*ldhA* + $LPD_{NADP+low\ inhib}$ on M9 medium supplemented with 50 mM glucose. **A** and **E**, *pntAB* genes expressed under their native promoter; **B** and **F**, *pntAB* genes expressed under *gapAp1* promoter; **C** and **G**, *pntAB* genes expressed under *ldhA* promoter and **D** and **H**, *pntAB* genes expressed under the inducible *trc* promoter. The *trc* promoter was not induced. The values represent the average of biological triplicates with standard deviations. Legend: glucose, lactate, pyruvate, ethanol, acetate, succinate, formate and biomass.

Overexpression of the membrane-bound transhydrogenase PntAB could prevent NADPH inhibition of the $NADP^+$-dependent PDH. Insufficient expression and activity of PntAB in an NADPH over-producing strain will result in NADPH accumulation thereby creating an imbalance in the cells. Increased activity of PntAB under anaerobic conditions would allow the cells to convert the excess NADPH faster thereby lowering the intracellular NADPH pool. This decrease in NADPH concentration would hopefully result in higher PDH activity as NADPH inhibition would be partially or totally alleviated.

Additionally, PntAB activity could be enhanced by modifying the catalytic parameters of the enzyme. In *E. coli* the K_m of PntAB for NADH is 10-times higher than the one for NADPH (Meuller *et al.*, 1997). Decreasing the K_m for NADPH would increase the affinity of PntAB for this compound and increase the catalytic efficiency of the reverse reaction. Protein engineering has been successfully used to decrease K_m and increase k_{cat}, which resulted in an overall increased catalytic efficiency (Wilkinson *et al.*, 1984; Dozier *et al.*, 2014). These modifications can be realized by introducing point mutations in the gene encoding the cofactor binding site of NADPH.

7.1.5. Anaerobic activity of the $NADP^+$-dependent PDH complex

The lack of growth observed under anaerobic conditions in **Chapter 5** can also be explained by poor expression or activity of the $NADP^+$-dependent PDH complex. The PDH complex is a central enzyme of the aerobic carbon metabolism of *E. coli*. However, PFL takes over the conversion of pyruvate to acetyl-CoA under anaerobic conditions (Knappe *et al.*, 1974; Clark, 1989; Sawers and Böck, 1989; Knappe and Sawers, 1990; Sawers and Suppmann, 1992) as PDH is subjected to NADH inhibition and exhibits very low or undetectable activity (Smith and Neidhardt, 1983; Snoep *et al.*, 1993a; de Graef *et al.*, 1999). In **Chapter 3**, we successfully changed the cofactor specificity of LPD and lowered its inhibition by both NADH and NADPH. Nevertheless, the sensitivity was only partially alleviated making PDH still subjected to NAD(P)H

inhibition at high concentrations of NADH and NADPH. Furthermore, PDH sustained anaerobic growth of an *E. coli* lacking a functional PFL but the strain formed lactate as main fermentation product, reaching a lactate yield on glucose close to the maximum theoretical yield of 2 mol/mol glucose. Therefore, only a fraction of the carbon flux went through the $NADP^+$-dependent PDH complex and small amount of NADPH was therefore produced. Disruption of *ldhA* in the final strains forced the carbon flux through the PDH complexes (**Chapter 5**). Consequently, it is possible that high NADH and NADPH concentrations were reached under anaerobic conditions thereby inhibiting the NAD^+-dependent and $NADP^+$-dependent PDH complexes, respectively.

7.1.5.1. Lowering NAD(P)H inhibition

If NAD(P)H inhibition indeed represses the anaerobic activity of PDH in the final *E. coli* strains, further engineering should be performed. NAD(P)H inhibition resides in the LPD subunit of the PDH complex (Schmincke-Ott and Bisswanger, 1981; Wilkinson and Williams, 1981; Sahlman and Williams, 1989). In this thesis, we introduced one amino acid mutation (E354K) on the *lpd* gene to drastically reduce the inhibition. This amino acid mutation, as well as H322Y, has been previously shown to reduce the K_i of the PDH complex 10-fold (Kim *et al.*, 2008). However, other amino acids changes could be introduced in the *lpd* gene to further alleviate the inhibition. For instance, Sun *et al.* (2012) systematically replaced the L-glutamate in position 354 by all other amino acids. The K_i was decreased by approximately 20-fold when L-glutamate was replaced by glycine, proline and tryptophan. In addition, these changes in amino acid at position 354 restored anaerobic growth of an *E. coli* strain lacking both *pflB* and *ldhA*.

The increased availability of enzyme crystal structures and the development of prediction software in the last decades allow relatively fast and easy modifications of proteins (Yuan *et al.*, 2005). As the crystal structure of *E. coli* PDH complex is available (Fuller *et al.*, 1979; Arjunan *et al.*, 2002; Arjunan *et al.*, 2006; Chandrasekhar *et al.*, 2006; Kale *et al.*, 2007; Arjunan *et al.*, 2014;

Wang *et al.*, 2014; Dadinova *et al.*, 2016), protein engineering is a viable option to further reduce NADH and NADPH inhibition of the PDH complex.

7.1.5.2. Overexpressing of the native NADP$^+$-dependent PDH

Low activity of the NADP$^+$-dependent PDH complex under anaerobic conditions can result from low expression of the genes encoding PDH. In *E. coli*, the PDH complex is composed of several copies of three enzymatic components: pyruvate dehydrogenase, dihydrolipoyllysine-residue acetyltransferase and lipoamide dehydrogenase. These subunits are encoded by *aceE*, *aceF* and *lpd*, respectively (Guest *et al.*, 1989; Quail *et al.*, 1994). These genes are part of the *pdhR-aceE-aceF-lpd* operon, which forms two distinct transcripts: *pdhR-aceEF-lpd* and *lpd*. *pdhR* encodes the pyruvate dehydrogenase regulator which represses transcription of the genes controlled by P_{pdh} (Quail *et al.*, 1994; Quail and Guest, 1995). In the presence of pyruvate, PdhR is inactivated allowing transcription of the genes encoding PDH. Disruption of *pdhR* in *E. coli* led to an increased PDH activity under oxygen-limited conditions (Maeda *et al.*, 2017). Consequently, *pdhR* knock-out is a potential target to increase the anaerobic PDH activity in our strains. Nevertheless, transcription of the genes encoding PDH are subjected to additional regulations. Transcription factors such as FNR or ArcA repress the initiation of *aceEF* and *lpd* transcription by binding on the promoters of the PDH operon (Iuchi and Lin, 1988; Quail *et al.*, 1994; Cunningham *et al.*, 1998; Cunningham and Guest, 1998; Kang *et al.*, 2005). Disruption of the genes encoding the transcription factors repressing anaerobic transcription of the PDH operon is however not a viable option as they regulate numerous genes and enzymes in the cells. On the other hand, replacing both P_{pdh} and P_{lpd} promoters is a good approach to suppress repression of transcription and increase anaerobic activity of the PDH complex. In this work, the genomic *lpd* gene was knocked out and the variants were expressed on the medium copy plasmid pBbA2k under their native promoter. Plasmid-based expression of *lpd* resulted in an 8-fold increase in expression under aerobic conditions (data not shown). However, transcription regulators might still repress its expression anaerobically thereby leading to low or no expression. In

addition, the *aceEF* genes are still subjected to the native regulation. Therefore, expression of *aceEF* – as well as expression of *lpd* – might be the major bottleneck preventing the strain to grow anaerobically. To ensure anaerobic transcription and expression of the genes encoding the PDH complex, the selected promoters should not be subjected to the same repression as P_{pdh} and P_{lpd}. For instance, the P_{gapAp1} promoter is an interesting candidate as it is expressed regardless the presence of oxygen (Charpentier and Branlant, 1994; Thouvenot *et al.*, 2004). The use of an inducible promoter should however be avoided as constitutive expression of PDH would require the constant use of an inducer and strong expression of this system might lead to inclusion bodies or negatively affect *E. coli* metabolism. Expression of *aceEF* and *lpd* genes under new promoters can be realized on a plasmid or on the genome. If the latter approach is selected, point mutations need to be introduced in the *lpd* gene to ensure the change of cofactor specificity and to lower NADPH inhibition.

7.1.5.3. Expressing a heterologous PDH complex active under anaerobic conditions

Some microorganisms use PDH to convert pyruvate to acetyl-CoA under fermentative conditions (Inui *et al.*, 1984b; Ctrnacta *et al.*, 2006; Sawada *et al.*, 2009). For instance, the Gram-positive bacterium *Enterococcus faecalis* can use both PFL and PDH to convert pyruvate to acetyl-CoA anaerobically (Snoep *et al.*, 1990). The flux distribution between the two enzymes depends on the redox potential of the redox couple NAD^+/NADH (Snoep *et al.*, 1991). PDH contribution was found to be positively correlated with an increased redox potential of NADH/NAD^+, suggesting that PDH is active when NADH/NAD^+ is mostly in the oxidized form. This finding tends to suggest that the PDH of *E. faecalis* is subjected to NADH inhibition. Enzymatic assays performed on the purified PDH complex as well as individual subunits revealed that LPD is indeed subjected to NADH inhibition (Snoep *et al.*, 1992). Nevertheless, the PDH of *E. faecalis* is active at NADH/NAD^+ ratios shown to inhibit *E. coli* PDH complex (Snoep *et al.*, 1993b). Therefore, heterologous expression of the PDH complex of *E. faecalis* in our *E. coli* strain would be an interesting approach to tackle

NADH inhibition. Nonetheless, the cofactor dependency remains to be changed in order to realize the designed strategy for energy conservation. The change of cofactor dependency could be achieved using protein and genetic engineering. The increased availability of enzymes crystal structures and the emergence of predicting software such as CSR SALAD can facilitate the modification of the cofactor dependency (Cahn *et al.*, 2017).

Another example of microorganisms able to use the PDH anaerobically is the freshwater alga *Euglena gracilis*. Contrary to *E. faecalis*, it uses an oxygen-sensitive $NADP^+$-dependent PDH complex (Inui *et al.*, 1984b; Inui *et al.*, 1987; Inui *et al.*, 1989). The enzyme is located in the mitochondria and is involved in fatty acid synthesis (Inui *et al.*, 1987). To our knowledge, NADPH and NADH were not proven to inhibit the complex in this strain. Heterologous expression of this $NADP^+$-dependent PDH in *E. coli* could therefore be a viable solution to solve NAD(P)H inhibition and the change of cofactor dependency. Expression of heterologous enzymes is a powerful tool to transfer desirable traits from one organism to another. However, the optimal conditions for pH, temperature, codon usage, etc differ between organisms, which can limit the expression and activity of the heterologous enzyme (Rosano and Ceccarelli, 2014). These parameters need to be carefully considered for the choice of the donor organism. In addition, the foreign genes should be codon optimized or codon harmonized to avoid the formation of inclusion bodies, which result in low or no activity (Angov *et al.*, 2008). For instance, the $NADP^+$-dependent PDH complex of *E. gracilis* functions optimally at 40°C and pH 7.5 (Inui *et al.*, 1987), which are close from the optimal values of *E. coli*.

7.1.6. Adaptive laboratory evolution (ALE)

Implementation of the recommendations mentioned above might still not allow us to realize the proposed strategy. Adaptive laboratory evolution (ALE) is a powerful tool to improve traits beneficial for microbial growth and survival (Dragosits and Mattanovich, 2013). ALE has been applied in a wide range of microbial strains to improve growth, product formation as well as to remove inhibition (Reyes *et al.*, 2014; LaCroix *et al.*, 2015; Oide *et al.*, 2015; Mundhada

et al., 2017; Pereira *et al.*, 2019; Perli *et al.*, 2020). For instance, Weusthuis *et al.* (2017) subjected *Monascus ruber* to ALE to remove inhibition of glucose consumption by lactic acid. The evolved strain showed a significant increase in both lactate yield and productivity. ALE could therefore be applied to the final strains created in this thesis to increase the flux over the $NADP^+$-dependent PDH. The strains should be cultivated in minimal medium supplemented with glucose under oxygen-limited conditions and transferred sequentially into fresh medium with increase anoxic conditions.

7.2. NADPH overproduction for microbial production of NADPH-requiring compounds

Biosynthesis of numerous industrially relevant compounds such as amino acids, terpenoids or lipids necessitates the input of NADPH (Kabus *et al.*, 2007; Park *et al.*, 2014; Kim *et al.*, 2015). The efficiency of microbial production of such compounds depends on the availability of cofactors and precursors. The capacity of anabolic NADPH regeneration is however low compared to the catabolic capacity of the cells to reduce NAD^+. As a result, increasing NADPH availability in microbial cell factories has gained interest for the production of NADPH-requiring compounds (Lee *et al.*, 2013; Wang *et al.*, 2013c; Spaans *et al.*, 2015; Han and Liang, 2018). Several groups have successfully augmented NADPH formation in microorganisms by either engineering enzymes involved in cofactor regeneration and synthesis (Canonaco *et al.*, 2001; Kabus *et al.*, 2007; Li *et al.*, 2009; Lee *et al.*, 2010; Bastian *et al.*, 2011) or by modifying the cofactor specificity of enzymes involved in the product pathways from NAD^+ to $NADP^+$ (Martínez *et al.*, 2008; Wang *et al.*, 2013a).

In this thesis, the cofactor specificity of LPD was modified from NAD^+ to $NADP^+$ which resulted in the creation of $NADP^+$-dependent PDH and ODH complexes. Both PDH and ODH are highly expressed under aerobic conditions as they catalyze key reactions of the central carbon metabolism of *E. coli*, providing

acetyl-CoA and succinyl-CoA, respectively. Nevertheless, the cells accumulated pyruvate due to a lack of electron sink for NADPH (**Chapter 3** and **Chapter 4**). Introduction of an NADPH-consuming enzyme or pathways would provide such an electron sink for NADPH and restore the cofactor balance in the cells. Such a system can be used in microbial cell factories to produce industrially relevant NADPH-requiring compounds such as terpenoids or amino acids under both aerobic and anaerobic conditions.

7.3. Genome-scale metabolic models

A genome-scale metabolic model (GEM) of *E. coli* (Monk *et al.*, 2017) was modified and used in this thesis to predict the impact of the genetic modifications on the strains' metabolisms. GEMs consist of stoichiometry-based, mass-balanced metabolic reactions that allow the prediction of metabolic fluxes across a metabolic network using optimization methods such as flux balance analysis (FBA) (Orth *et al.*, 2010). These models, in combination with programming tools such as OptKnock (Burgard *et al.*, 2003), RobustKnock (Tepper and Shlomi, 2009) or Gap Filling (Orth and Palsson, 2010; Thiele *et al.*, 2014), benefit the design of novel microbial cell factories by identifying of reactions to be knocked out or knocked in to achieve a specific objective such as production of a target compound (Ko *et al.*, 2020). Nevertheless, GEMs are limited as they are stoichiometry-based and assume a steady state inside the cells which does not allow the accumulation of intermediates. Fluxes over metabolic reactions are – in reality – limited by kinetic parameters such as K_m, k_{cat}, and inhibition. Kinetic models can therefore be used to predict more accurately the *in vivo* metabolic situation by increasing the level of complexity of the model. Such models already exist for well-described organisms like *E. coli* (Chassagnole *et al.*, 2002; Khodayari and Maranas, 2016; Millard *et al.*, 2017; Kurata and Sugimoto, 2018) however they are not always available for non-model organisms since they require multi-omics data. GEMs, kinetic models and fermentation models are constantly improving and allow the prediction of microbial behavior with

increased degree of complexity and accuracy. These models can be used to design new microbial cell factories and to improve microbial process by reducing the costs of wet work.

7.4. Towards improvement of microbial *chassis* for the production of chemicals

7.4.1. Applying non-canonical redox cofactors to the strategy

The strategy presented in this thesis to conserve additional metabolic energy relies on the transfer of electrons between the two redox couples $NADP^+$/NADPH and NAD^+/NADH. These redox cofactors are widely used in the metabolic network and electrons are therefore diffusing over the metabolism. Applying non-canonical redox cofactors (NRCs) is an elegant solution to overcome this challenge as they allow a tight control over the electrons fate. In **Chapter 6**, we described several NRCs and how their application in fermentation processes can be used to achieve practical yields close the maximum theoretical yields.

Non-canonical redox cofactors such as NMN^+/NMNH and NCD^+/NCDH are a suitable option to replace $NADP^+$/NADPH in our scenario. These NRCs are biomimetic nicotinamide analogues that rely on the natural structure of NAD(P)H. As such they are non-toxic for the cells and have similar redox potentials than $NAD(P)^+$/NAD(P)H. Both NMN^+/NMNH and NCD^+/NCDH have been successfully applied *in vivo* for the production of malate (Wang *et al.*, 2017) and levodione (Black *et al.*, 2020).

To enable implementation of NRCs in the scenario proposed in this thesis, the cofactor dependency of both PDH and PntAB enzymes must be modified to accept the NRC. The modifications should also ensure that both enzymes are not able to accept $NADP^+$/NADPH. Nowadays, cofactor engineering is a widely used approach to optimize redox metabolism and to increase product yield in

microbial processes (Wang *et al.*, 2013c; Liu *et al.*, 2018). Several methods and tools are available to change the cofactor specificity of enzymes, and it starts to be applied to cofactor analogues such as NRCs (Liu *et al.*, 2018). Furthermore, the cells should be able to synthetize the NRC. Although Wang *et al.* (2017) supplied NCD^+ to the medium, Black *et al.* (2020) overexpressed the genes involved in NMN synthesis and knocked out the genes involved in NMN breakdown. As a result, the strain was able to synthetize the NRC used for levodione synthesis. Therefore, due to the proof of *in vivo* NMN^+/NMNH synthesis, this redox couple would be the best candidate to replace $NADP^+$/NADPH in our approach.

Protein engineering for NRC application in combination with adaptive laboratory evolution can streamline the metabolic flux in the *chassis* through the newly engineered NRC-dependent enzymes. This strategy will result in the creation of an orthogonal (and therefore independent) pathway for redox cofactor and energy generation. The field of synthetic biology would therefore benefit tremendously from such an approach as this is a generally applicable method that can improve the synthesis of acetyl-CoA-based compounds formed from carbohydrates.

7.4.2. Impact on the fields of synthetic biology and metabolic engineering for the design of new microbial cell factories

Microbial cells factories are commonly used for the production of a wide range of non-natural compounds (Lee *et al.*, 2012; Davy *et al.*, 2017; Chi *et al.*, 2018; Park *et al.*, 2018; Yuan and Alper, 2019). At first, their design focused on growth-coupled production of chemicals as the target compound is an obligatory by-product of biomass formation. The engineered strains usually exhibit slower growth due to metabolic burden. Laboratory evolution is a popular strategy to improve further bioproduction of these chemicals (Lu *et al.*, 2012; Reyes *et al.*, 2014; Mans *et al.*, 2018; Wang *et al.*, 2020). Nonetheless, growth-coupled production prevents to reach high product yield as the substrate is used for both

biomass formation (and maintenance purposes) and product formation. To achieve high TRY, decoupling product synthesis from biomass formation is a promising approach. In this respect, implementation of orthogonal pathways optimized for product synthesis holds potential (Mampel *et al.*, 2013; Pandit *et al.*, 2017). These pathways are designed to ensure minimal to no interactions between the product-forming and biomass-forming pathways. Several groups have reported successful implementation of orthogonal pathways to increase product formation (Eriksen *et al.*, 2015; Cheng *et al.*, 2019; Ignea *et al.*, 2019).

Synthetic biology focuses on creating microbial cell factories with reduced energy cost to maximize the production of target chemicals via synthetic pathways. A heterotrophic cell factory can be regarded as a *chassis* powered by an engine module where assimilation (e.g. microbial biomass and cost-associated maintenance) is driven by ATP synthetized during dissimilation of the substrate (e.g. catabolism). In order to approach the maximum theoretical yield of product formation, the engine module should be independent from the regulation occurring within the *chassis*, However, this is challenging from an ATP point of view since assimilation and dissimilation are interconnected.

The strategy proposed in this thesis together with the use of non-canonical redox cofactors (NRCs) are a promising step towards achieving orthogonality of the engine to chassis. Since NRCs are not naturally used by the cells, this strategy results in the creation of an independent redox circuit within the *chassis* and allows the conservation of additional metabolic energy.

In synthetic biology, independence between co-existing modules is defined as orthogonality (de Lorenzo, 2011). This can be realized at several levels such as transcription/translation, cofactors or metabolic pathway. An orthogonal metabolic flux can be achieved when a synthetic product-forming pathway shares a precursor with a native pathway. At the level of metabolic currency, an example of orthogonality is given by NRCs. Protein engineering allows the creation of NRC-dependent enzymes and therefore orthogonal redox circuits which are independent from the endogenous cofactor network.

Implementation of an orthogonal NRC-dependent strategy circuit can be therefore applied to the production of acetyl-CoA-derived chemicals. Expression of NRC-dependent enzymes PDH and PntAB using synthetic promoters would ensure that both enzymes are not subjected to endogenous regulation on both genetic and metabolic levels and as such be orthogonal to the native pathway. However, one might argue that the strategy is not orthogonal to assimilation as the cells require the action of PDH to supply acetyl-CoA for biomass formation.

The combination of an NRC-dependent redox circuit together with control over the flux from acetyl-CoA towards product formation is key for achieving independence between growth and production. Redirecting the pool of acetyl-CoA from biomass formation towards product biosynthesis can be triggered by metabolic switches. These switches can be realized by 1) applying nutrient limitations, 2) knocking out or 3) silencing genes involved in biomass formation. Nutrient limitation has been successfully applied in fermentation processes to increase the production of several industrially relevant compounds (Bahl *et al.*, 1982; Liu *et al.*, 2015; Willrodt *et al.*, 2016; Yang *et al.*, 2016). During limitation, the resting cells would use the substrate solely to produce the chemical of interest thereby increasing product yield. The choice of the nutrient to limit needs to be carefully considered depending on the target chemical. Nutrient limitation is an easily applicable method to limit biomass production however it can result in undesired secondary effect on the cell metabolism and negatively affect product formation. Disruption of genes involved in biomass formation can also be used to stop cell growth and increase product formation. Nevertheless, this approach does not allow to reach high cell densities which are needed to achieve high titer and productivity. On the other hand, silencing the genes involved in biomass synthesis is a very elegant solution to switch the flux towards product formation. Unlike gene knock outs, gene silencing can be triggered at a desired time and can be achieved adding inhibitors (Li *et al.*, 2016), using small RNAs (Nakashima *et al.*, 2006; Na *et al.*, 2013) or CRISPR interference (Li *et al.*, 2020). For instance, dCas9 can be engineered to silence specific genes involved in biomass formation by blocking their transcription (Li

et al., 2020). As biomass formation is stopped, the intermediate – in our case acetyl-CoA – will be used to produce the target compound since it cannot be accumulated inside the cells.

Generally, redirecting the flux from biomass towards product formation should be realized after reaching a cell density that allows to achieve high titer and productivity. The methods described above can be regarded as metabolic switches which result in orthogonality of the production pathway to the biomass-forming pathway. Control over these metabolic switches is time-dependent raising the following statement: orthogonality can be seen as a time-related process. Redistribution of the metabolic fluxes mediated by changes in either gene expression or protein activity can be defined as dynamic metabolic control (Burg *et al.*, 2016). The ability to control cellular growth via external or internal stimuli can be coupled to a two-stage microbial fermentation processes to increase product yield further (Burg *et al.*, 2016). The first phase focuses on biomass formation allowing to reach a desired cell density. In the second phase, biomass formation is stopped thereby allocating all substrate to product formation. Two-stage fermentation using a chassis with an orthogonal engine is a powerful method to reach high TRY.

Implementation of NRCs in the strategy proposed in this thesis can be used for the production of acetyl-CoA-derived compounds. This strategy also allows conservation of additional energy that can benefit the production of energy-requiring chemicals and fulfil the maintenance requirements of microbial cell factories whose engine is orthogonal to assimilation. Other strategies can be implemented to create an orthogonal engine to the chassis to maximize the yield of other target chemicals. Nevertheless, the engine should provide sufficient metabolic energy to fulfil the maintenance requirement of the cells, and to produce the desired chemicals if the product pathway requires ATP. The knowledge acquired in **Chapter 2** to harness extra energy in product pathways can be used to design such synthetic pathways.

References

Abdel-Rahman, M.A., Tashiro, Y., and Sonomoto, K. (2013) Recent advances in lactic acid production by microbial fermentation processes. *Biotechnology Advances* **31**: 877-902.

Aditiya, H.B., Mahlia, T.M.I., Chong, W.T., Nur, H., and Sebayang, A.H. (2016) Second generation bioethanol production: a critical review. *Renewable and Sustainable Energy Reviews* **66**: 631-653.

Alves de Oliveira, R., Komesu, A., Vaz Rossell, C.E., and Maciel Filho, R. (2018) Challenges and opportunities in lactic acid bioprocess design — From economic to production aspects. *Biochemical Engineering Journal* **133**: 219-239.

Amador-Noguez, D., Brasg, I.A., Feng, X.-J., Roquet, N., and Rabinowitz, J.D. (2011) Metabolome remodeling during the acidogenic-solventogenic transition in *Clostridium acetobutylicum*. *Applied and environmental microbiology* **77**: 7984-7997.

Amarasingham, C.R., and Davis, B.D. (1965) Regulation of α-ketoglutarate dehydrogenase formation in *Escherichia coli*. *Journal of Biological Chemistry* **240**: 3664-3668.

Andersen, K.B., and von Meyenburg, K. (1977) Charges of nicotinamide adenine nucleotides and adenylate energy charge as regulatory parameters of the metabolism in *Escherichia coli*. *Journal of Biological Chemistry* **252**: 4151-4156.

Angov, E., Hillier, C.J., Kincaid, R.L., and Lyon, J.A. (2008) Heterologous protein expression is enhanced by harmonizing the codon usage frequencies of the target gene with those of the expression host. *PLOS ONE* **3**: e2189.

Arechaga, I., Butler, P.J.G., and Walker, J.E. (2002) Self-assembly of ATP synthase subunit c rings. *FEBS Letters* **515**: 189-193.

Arjunan, P., Nemeria, N., Brunskill, A., Chandrasekhar, K., Sax, M., Yan, et al. (2002) Structure of the pyruvate dehydrogenase multienzyme complex E1 component from *Escherichia coli* at 1.85 Å resolution. *Biochemistry* **41**: 5213-5221.

Arjunan, P., Sax, M., Brunskill, A., Chandrasekhar, K., Nemeria, N., Zhang, S., et al. (2006) A thiamin-bound, pre-decarboxylation reaction intermediate analogue in the pyruvate dehydrogenase E1 subunit induces large scale disorder-to-order transformations in the enzyme and reveals novel structural features in the covalently bound adduct. *Journal of Biological Chemistry* **281**: 15296-15303.

Arjunan, P., Wang, J., Nemeria, N.S., Reynolds, S., Brown, I., Chandrasekhar, K., et al. (2014) Novel binding motif and new flexibility revealed by structural analyses of a pyruvate dehydrogenase-dihydrolipoyl acetyltransferase subcomplex from the *Escherichia coli* pyruvate dehydrogenase multienzyme complex. *The Journal of Biological Chemistry* **289**: 30161-30176.

Atsumi, S., Cann, A.F., Connor, M.R., Shen, C.R., Smith, K.M., Brynildsen, M.P., et al. (2008) Metabolic engineering of *Escherichia coli* for 1-butanol production. *Metabolic Engineering* **10**: 305-311.

Auriol, C., Bestel-Corre, G., Claude, J.-B., Soucaille, P., and Meynial-Salles, I. (2011) Stress-induced evolution of *Escherichia coli* points to original concepts in respiratory

cofactor selectivity. *Proceedings of the National Academy of Sciences of the United States of America* **108**: 1278-1283.

Baba, T., Ara, T., Hasegawa, M., Takai, Y., Okumura, Y., Baba, M., et al. (2006) Construction of *Escherichia coli* K-12 in-frame, single-gene knockout mutants: the Keio collection. *Molecular Systems Biology* **2**: 2006.0008.

Bahl, H., Andersch, W., and Gottschalk, G. (1982) Continuous production of acetone and butanol by *Clostridium acetobutylicum* in a two-stage phosphate limited chemostat. *European journal of applied microbiology and biotechnology* **15**: 201-205.

Baldwin, R.L., and Milligan, L.P. (1964) Electron transport in *Peptostreptococcus elsdenii*. *Biochimica et Biophysica Acta (BBA) - Specialized Section on Enzymological Subjects* **92**: 421-432.

Bar-Even, A., Flamholz, A., Noor, E., and Milo, R. (2012) Thermodynamic constraints shape the structure of carbon fixation pathways. *Biochimica et Biophysica Acta (BBA) - Bioenergetics* **1817**: 1646-1659.

Barrett, M.P., Walmsleyt, A.R., and Gould, G.W. (1999) Structure and function of facultative sugar transporters. *Current Opinion in Cell Biology* **11**: 496-502.

Bashiri, G., Antoney, J., Jirgis, E.N.M., Shah, M.V., Ney, B., Copp, J., et al. (2019) A revised biosynthetic pathway for the cofactor F_{420} in prokaryotes. *Nature Communications* **10**: 1558.

Bastian, S., Liu, X., Meyerowitz, J.T., Snow, C.D., Chen, M.M.Y., and Arnold, F.H. (2011) Engineered ketol-acid reductoisomerase and alcohol dehydrogenase enable anaerobic 2-methylpropan-1-ol production at theoretical yield in *Escherichia coli*. *Metabolic Engineering* **13**: 345-352.

Beatrix, B., Bendrat, K., Rospert, S., and Buckel, W. (1990) The biotin-dependent sodium ion pump glutaconyl-CoA decarboxylase from *Fusobacterium nucleatum* (subsp. *nucleatum*). Comparison with the glutaconyl-CoA decarboxylases from gram-positive bacteria. *Archives of Microbiology* **154**: 362-369.

Bechthold, I., Bretz, K., Kabasci, S., Kopitzky, R., and Springer, A. (2008) Succinic acid: a new platform chemical for biobased polymers from renewable resources. *Chemical Engineering & Technology* **31**: 647-654.

Bendrat, K., and Buckel, W. (1993) Cloning, sequencing and expression of the gene encoding the carboxytransferase subunit of the biotin-dependent Na^+ pump glutaconyl-CoA decarboxylase from *Acidaminococcus fermentans* in *Escherichia coli*. *European Journal of Biochemistry* **211**: 697-702.

Bennett, B.D., Kimball, E.H., Gao, M., Osterhout, R., Van Dien, S.J., and Rabinowitz, J.D. (2009) Absolute metabolite concentrations and implied enzyme active site occupancy in *Escherichia coli*. *Nature Chemical Biology* **5**: 593-599.

Bennett, G.N., and San, K.Y. (2001) Microbial formation, biotechnological production and applications of 1,2-propanediol. *Applied Microbiology and Biotechnology* **55**: 1-9.

Benning, M.M., Haller, T., Gerlt, J.A., and Holden, H.M. (2000) New reactions in the crotonase superfamily: structure of methylmalonyl coa decarboxylase from *Escherichia coli*. *Biochemistry* **39**: 4630-4639.

Berg, M., and Dimroth, P. (1998) The biotin protein MadF of the malonate decarboxylase from *Malonomonas rubra*. *Archives of Microbiology* **170**: 464-468.

Berg, M., Hilbi, H., and Dimroth, P. (1996) The acyl carrier protein of malonate decarboxylase of *Malonomonas rubra* contains 2'-(5''-phosphoribosyl)-3'-dephosphocoenzyme A as a prosthetic group. *Biochemistry* **35**: 4689-4696.

Berg, M., Hilbi, H., and Dimroth, P. (1997) Sequence of a gene cluster from *Malonomonas rubra* encoding components of the malonate decarboxylase Na^+ pump and evidence for their function. *European Journal of Biochemistry* **245**: 103-115.

Bertsch, J., Parthasarathy, A., Buckel, W., and Müller, V. (2013) An electron-bifurcating caffeyl-CoA reductase. *Journal of Biological Chemistry* **288**: 11304-11311.

Beyenbach, K.W., and Wieczorek, H. (2006) The V-type H^+ ATPase: molecular structure and function, physiological roles and regulation. *Journal of Experimental Biology* **209**: 577-589.

Biegel, E., and Müller, V. (2011) A Na^+-translocating pyrophosphatase in the acetogenic bacterium *Acetobacterium woodii*. *Journal of Biological Chemistry* **286**: 6080-6084.

Bielen, A.A.M., Willquist, K., Engman, J., Van Der Oost, J., Van Niel, E.W.J., and Kengen, S.W.M. (2010) Pyrophosphate as a central energy carrier in the hydrogen-producing extremely thermophilic *Caldicellulosiruptor saccharolyticus*. *FEMS Microbiology Letters* **307**: 48-54.

Bizouarn, T., Fjellström, O., Meuller, J., Axelsson, M., Bergkvist, A., Johansson, C., et al. (2000) Proton translocating nicotinamide nucleotide transhydrogenase from *E. coli*. Mechanism of action deduced from its structural and catalytic properties. *Biochimica et Biophysica Acta (BBA) - Bioenergetics* **1457**: 211-228.

Bizouarn, T., Sazanov, L.A., Aubourg, S., and Baz Jackson, J. (1996) Estimation of the H^+/H^- ratio of the reaction catalysed by the nicotinamide nucleotide transhydrogenase in chromatophores from over-expressing strains of *Rhodospirillum rubrum* and in liposomes inlaid with the purified bovine enzyme. *Biochimica et Biophysica Acta (BBA) - Bioenergetics* **1273**: 4-12.

Black, W.B., Zhang, L., Mak, W.S., Maxel, S., Cui, Y., King, E., et al. (2020) Engineering a nicotinamide mononucleotide redox cofactor system for biocatalysis. *Nature Chemical Biology* **16**: 87-94.

Bocanegra, J.A., Scrutton, N.S., and Perham, R.N. (1993) Creation of an NADP-dependent pyruvate dehydrogenase multienzyme complex by protein engineering. *Biochemistry* **32**: 2737-2740.

Bogachev, A.V., Murtazina, R.A., and Skulachev, V.P. (1996) H^+/e^- stoichiometry for NADH dehydrogenase I and dimethyl sulfoxide reductase in anaerobically grown *Escherichia coli* cells. *Journal of Bacteriology* **178**: 6233-6237.

Bogorad, I.W., Lin, T.-S., and Liao, J.C. (2013) Synthetic non-oxidative glycolysis enables complete carbon conservation. *Nature* **502**: 693-697.

Boiangiu, C.D., Jayamani, E., Brügel, D., Herrmann, G., Kim, J., Forzi, L., et al. (2005) Sodium ion pumps and hydrogen production in glutamate fermenting anaerobic bacteria. *Journal of Molecular Microbiology and Biotechnology* **10**: 105-119.

Boonstra, B., French, C.E., Wainwright, I., and Bruce, N.C. (1999) The *udhA* gene of *Escherichia coli* encodes a soluble pyridine nucleotide transhydrogenase. *Journal of Bacteriology* **181**: 1030-1034.

Boonstra, B., Rathbone, D.A., French, C.E., Walker, E.H., and Bruce, N.C. (2000) Cofactor regeneration by a soluble pyridine nucleotide transhydrogenase for biological production of hydromorphone. *Applied and Environmental Microbiology* **66**: 5161-5166.

Bott, M., Pfister, K., Burda, P., Kalbermatter, O., Woehlke, G., and Dimroth, P. (1997) Methylmalonyl-CoA decarboxylase from *Propionigenium modestum*. *European Journal of Biochemistry* **250**: 590-599.

Braune, A., Bendrat, K., Rospert, S., and Buckel, W. (1999) The sodium ion translocating glutaconyl-CoA decarboxylase from *Acidaminococcus fermentans*: cloning and function of the genes forming a second operon. *Molecular Microbiology* **31**: 473-487.

Brosius, J., Erfle, M., and Storella, J. (1985) Spacing of the -10 and -35 regions in the *tac* promoter. Effect on its *in vivo* activity. *Journal of Biological Chemistry* **260**: 3539-3541.

Brouns, S.J.J., Barends, T.R.M., Worm, P., Akerboom, J., Turnbull, A.P., Salmon, L., and van der Oost, J. (2008) Structural insight into substrate binding and catalysis of a novel 2-keto-3-deoxy-D-arabinonate dehydratase illustrates common mechanistic features of the FAH superfamily. *Journal of Molecular Biology* **379**: 357-371.

Buck, D., Spencer, M.E., and Guest, J.R. (1986) Cloning and expression of the succinyl-CoA synthetase genes of *Escherichia coli* K12. *Microbiology* **132**: 1753-1762.

Buckel, W. (2001) Sodium ion-translocating decarboxylases. *Biochimica et Biophysica Acta (BBA) - Bioenergetics* **1505**: 15-27.

Buckel, W., and Semmler, R. (1982) A biotin-dependent sodium pump: glutaconyl-CoA decarboxylase from *Acidaminococcus fermentans*. *FEBS Letters* **148**: 35-38.

Buckel, W., and Semmler, R. (1983) Purification, characterisation and reconstitution of glutaconyl-CoA decarboxylase, a biotin-dependent sodium pump from anaerobic bacteria. *European Journal of Biochemistry* **136**: 427-434.

Buckel, W., and Thauer, R.K. (2013) Energy conservation via electron bifurcating ferredoxin reduction and proton/Na^+ translocating ferredoxin oxidation. *Biochimica et Biophysica Acta (BBA) - Bioenergetics* **1827**: 94-113.

Buckel, W., and Thauer, R.K. (2018a) Flavin-based electron bifurcation, a new mechanism of biological energy coupling. *Chemical Reviews* **118**: 3862-3886.

Buckel, W., and Thauer, R.K. (2018b) Flavin-Based electron bifurcation, ferredoxin, flavodoxin, and anaerobic respiration with protons (Ech) or NAD^+ (Rnf) as electron acceptors: a historical review. *Frontiers in Microbiology* **9**.

Bühler, B., Bollhalder, I., Hauer, B., Witholt, B., and Schmid, A. (2003) Use of the two-liquid phase concept to exploit kinetically controlled multistep biocatalysis. *Biotechnology and Bioengineering* **81**: 683-694.

Bühler, B., Witholt, B., Hauer, B., and Schmid, A. (2002) Characterization and application of xylene monooxygenase for multistep biocatalysis. *Applied and Environmental Microbiology* **68**: 560-568.

Bunch, P.K., Mat-Jan, F., Lee, N., and Clark, D.P. (1997) The *IdhA* gene encoding the fermentative lactate dehydrogenase of *Escherichia coli*. *Microbiology* **143**: 187-195.

Burg, J.M., Cooper, C.B., Ye, Z., Reed, B.R., Moreb, E.A., and Lynch, M.D. (2016) Large-scale bioprocess competitiveness: the potential of dynamic metabolic control in two-stage fermentations. *Current Opinion in Chemical Engineering* **14**: 121-136.

Burgard, A., Burk, M.J., Osterhout, R., Van Dien, S., and Yim, H. (2016) Development of a commercial scale process for production of 1,4-butanediol from sugar. *Current Opinion in Biotechnology* **42**: 118-125.

Burgard, A.P., Pharkya, P., and Maranas, C.D. (2003) Optknock: a bilevel programming framework for identifying gene knockout strategies for microbial strain optimization. *Biotechnology and Bioengineering* **84**: 647-657.

Burgstaller, W. (1997) Transport of small ions and molecules through the plasma membrane of filamentous fungi. *Critical Reviews in Microbiology* **23**: 1-46.

Burma, D.P., and Horecker, B.L. (1958) Pentose fermentation by *Lactobacillus plantarum*: III. Ribulokinase. *Journal of Biological Chemistry* **231**: 1039-1051.

Cahn, J.K.B., Werlang, C.A., Baumschlager, A., Brinkmann-Chen, S., Mayo, S.L., and Arnold, F.H. (2017) A general tool for engineering the NAD/NADP cofactor preference of oxidoreductases. *ACS Synthetic Biology* **6**: 326-333.

Canonaco, F., Hess, T.A., Heri, S., Wang, T., Szyperski, T., and Sauer, U. (2001) Metabolic flux response to phosphoglucose isomerase knock-out in *Escherichia coli* and impact of overexpression of the soluble transhydrogenase UdhA. *FEMS Microbiology Letters* **204**: 247-252.

Carugo, O., and Argos, P. (1997a) NADP-dependent enzymes. I: Conserved stereochemistry of cofactor binding. *Proteins: Structure, Function and Genetics* **28**: 10-28.

Carugo, O., and Argos, P. (1997b) NADP-dependent enzymes. II: Evolution of the mono- and dinucleotide binding domains. *Proteins: Structure, Function and Genetics* **28**: 29-40.

Chandrasekhar, K., Arjunan, P., Sax, M., Nemeria, N., Jordan, F., and Furey, W. (2006) Active-site changes in the pyruvate dehydrogenase multienzyme complex E1 apoenzyme component from *Escherichia coli* observed at 2.32 Å resolution. *Acta Crystallographica Section D Biological Crystallography* **62**: 1382-1386.

Chang, Y.-J., Pukall, R., Saunders, E., Lapidus, A., Copeland, A., Nolan, M., et al. (2010) Complete genome sequence of *Acidaminococcus fermentans* type strain (VR4). *Standards in Genomic Sciences* **3**: 1-14.

Chang, Y.-Y., Wang, A.-Y., and Cronan Jr, J.E. (1994) Expression of *Escherichia coli* pyruvate oxidase (PoxB) depends on the sigma factor encoded by the *rpoS*(*katF*) gene. *Molecular Microbiology* **11**: 1019-1028.

Charpentier, B., Bardey, V., Robas, N., and Branlant, C. (1998) The EII^{Glc} protein is involved in glucose-mediated activation of *Escherichia coli gapA* and *gapB-pgk* transcription. *Journal of Bacteriology* **180**: 6476-6483.

Charpentier, B., and Branlant, C. (1994) The *Escherichia coli gapA* gene is transcribed by the vegetative RNA polymerase holoenzyme $E\sigma^{70}$ and by the heat shock RNA polymerase $E\sigma^{32}$. *Journal of Bacteriology* **176**: 830-839.

Chassagnole, C., Noisommit-Rizzi, N., Schmid, J.W., Mauch, K., and Reuss, M. (2002) Dynamic modeling of the central carbon metabolism of *Escherichia coli*. *Biotechnology and Bioengineering* **79**: 53-73.

Chemler, J.A., Fowler, Z.L., McHugh, K.P., and Koffas, M.A.G. (2010) Improving NADPH availability for natural product biosynthesis in *Escherichia coli* by metabolic engineering. *Metabolic Engineering* **12**: 96-104.

Chen, J., Li, W., Zhang, Z.-Z., Tan, T.-W., and Li, Z.-J. (2018) Metabolic engineering of *Escherichia coli* for the synthesis of polyhydroxyalkanoates using acetate as a main carbon source. *Microbial Cell Factories* **17**: 102.

Cheng, S., Liu, X., Jiang, G., Wu, J., Zhang, J.-l., Lei, D., et al. (2019) Orthogonal engineering of biosynthetic pathway for efficient production of limonene in *Saccharomyces cerevisiae*. *ACS Synthetic Biology* **8**: 968-975.

Chi, H., Wang, X., Shao, Y., Qin, Y., Deng, Z., Wang, L., and Chen, S. (2018) Engineering and modification of microbial chassis for systems and synthetic biology. *Synthetic and Systems Biotechnology* **4**: 25-33.

Chinen, A., Kozlov, Y.I., Hara, Y., Izui, H., and Yasueda, H. (2007) Innovative metabolic pathway design for efficient L-glutamate production by suppressing CO_2 emission. *Journal of Bioscience and Bioengineering* **103**: 262-269.

Chou, H.-H., Marx, C.J., and Sauer, U. (2015) Transhydrogenase promotes the robustness and evolvability of *E. coli* deficient in NADPH production. *PLoS Genetics* **11**: e1005007.

Chowdhury, N.P., Klomann, K., Seubert, A., and Buckel, W. (2016) Reduction of flavodoxin by electron bifurcation and sodium ion-dependent reoxidation by NAD^+ catalyzed by ferredoxin-NAD^+ reductase (Rnf). *The Journal of Biological Chemistry* **291**: 11993-12002.

Claassens, N.J., Sánchez-Andrea, I., Sousa, D.Z., and Bar-Even, A. (2018) Towards sustainable feedstocks: a guide to electron donors for microbial carbon fixation. *Current Opinion in Biotechnology* **50**: 195-205.

Clark, D.P. (1989) The fermentation pathways of *Escherichia coli*. *FEMS Microbiology Letters* **63**: 223-234.

Clarke, D.M., and Bragg, P.D. (1985a) Cloning and expression of the transhydrogenase gene of *Escherichia coli*. *Journal of Bacteriology* **162**: 367-373.

Clarke, D.M., and Bragg, P.D. (1985b) Purification and properties of reconstitutively active nicotinamide nucleotide transhydrogenase of *Escherichia coli*. *European Journal of Biochemistry* **149**: 517-523.

Clarke, D.M., Loo, T.W., Gillam, S., and Bragg, P.D. (1986) Nucleotide sequence of the *pntA* and *pntB* genes encoding the pyridine nucleotide transhydrogenase of *Escherichia coli*. *European Journal of Biochemistry* **158**: 647-653.

Conway, T. (1992) The Entner-Doudoroff pathway: history, physiology and molecular biology. *FEMS Microbiology Reviews* **9**: 1-27.

Ctrnacta, V., Ault, J.G., Stejskal, F., and Keithly, J.S. (2006) Localization of pyruvate:$NADP^+$ oxidoreductase in sporozoites of *Cryptosporidium parvum*. *Journal of Eukaryotic Microbiology* **53**: 225-231.

Cueto-Rojas, H.F., van Maris, A.J.A., Wahl, S.A., and Heijnen, J.J. (2015) Thermodynamics-based design of microbial cell factories for anaerobic product formation. *Trends in Biotechnology* **33**: 534-546.

Cui, J., Maloney, M.I., Olson, D.G., and Lynd, L.R. (2020) Conversion of phosphoenolpyruvate to pyruvate in *Thermoanaerobacterium saccharolyticum*. *Metabolic Engineering Communications* **10**: e00122.

Cunningham, L., Georgellis, D., Green, J., and Guest, J.R. (1998) Co-regulation of lipoamide dehydrogenase and 2-oxoglutarate dehydrogenase synthesis in *Escherichia coli*: characterisation of an ArcA binding site in the *lpd* promoter. *FEMS Microbiology Letters* **169**: 403-408.

Cunningham, L., and Guest, J.R. (1998) Transcription and transcript processing in the *sdhCDAB-sucABCD* operon of *Escherichia coli*. *Microbiology* **144**: 2113-2123.

Curthoys, N.P., Straus, L.D.A., and Rabinowitz, J.C. (1972) Formyltetrahydrofolate synthetase. Substrate binding to monomeric subunits. *Biochemistry* **11**: 345-349.

Cyert, M.S., and Philpott, C.C. (2013) Regulation of cation balance in *Saccharomyces cerevisiae*. *Genetics* **193**: 677-713.

Dadinova, L.A., Rodina, E.V., Vorobyeva, N.N., Kurilova, S.A., Nazarova, T.I., and Shtykova, E.V. (2016) Structural investigations of *E. coli* dihydrolipoamide dehydrogenase in solution: small-angle X-ray scattering and molecular docking. *Crystallography Reports* **61**: 414-420.

Datsenko, K.A., and Wanner, B.L. (2000) One-step inactivation of chromosomal genes in *Escherichia coli* K-12 using PCR products. *Proceedings of the National Academy of Sciences of the United States of America* **97**: 6640-6645.

Davy, A.M., Kildegaard, H.F., and Andersen, M.R. (2017) Cell factory engineering. *Cell Systems* **4**: 262-275.

de Anda, R., Lara, A.R., Hernández, V., Hernández-Montalvo, V., Gosset, G., Bolívar, F., and Ramírez, O.T. (2006) Replacement of the glucose phosphotransferase transport system by galactose permease reduces acetate accumulation and improves process performance of *Escherichia coli* for recombinant protein production without impairment of growth rate. *Metabolic Engineering* **8**: 281-290.

de Graef, M.R., Alexeeva, S., Snoep, J.L., and Teixeira de Mattos, M.J. (1999) The steady-state internal redox state (NADH/NAD) reflects the external redox state and is correlated with catabolic adaptation in *Escherichia coli*. *Journal of Bacteriology* **181**: 2351-2357.

de Kok, S., Yilmaz, D., Suir, E., Pronk, J.T., Daran, J.-M., and van Maris, A.J.A. (2011) Increasing free-energy (ATP) conservation in maltose-grown *Saccharomyces cerevisiae* by expression of a heterologous maltose phosphorylase. *Metabolic Engineering* **13**: 518-526.

de Lorenzo, V. (2011) Beware of metaphors: chasses and orthogonality in synthetic biology. *Bioengineered Bugs* **2**: 3-7.

de Vries, W., Gerbrandy, S.J., and Stouthamer, A.H. (1967) Carbohydrate metabolism in *Bifidobacterium bifidum*. *Biochimica et Biophysica Acta (BBA) - General Subjects* **136**: 415-425.

Decker, K., Jungermann, K., and Thauer, R.K. (1970) Energy production in anaerobic organisms. *Angewandte Chemie International Edition in English* **9**: 138-158.

Dehning, I., and Schink, B. (1989) *Malonomonas rubra* gen. nov. sp. nov., a microaerotolerant anaerobic bacterium growing by decarboxylation of malonate. *Archives of Microbiology* **151**: 427-433.

Dehning, I., Stieb, M., and Schink, B. (1989) *Sporomusa malonica* sp. nov., a homoacetogenic bacterium growing by decarboxylation of malonate or succinate. *Archives of Microbiology* **151**: 421-426.

Dellomonaco, C., Clomburg, J.M., Miller, E.N., and Gonzalez, R. (2011) Engineered reversal of the β-oxidation cycle for the synthesis of fuels and chemicals. *Nature* **476**: 355-359.

Deng, Y., Mao, Y., and Zhang, X. (2015) Driving carbon flux through exogenous butyryl-CoA: acetate CoA-transferase to produce butyric acid at high titer in *Thermobifida fusca*. *Journal of Biotechnology* **216**: 151-157.

Deprez, M.-A., Eskes, E., Wilms, T., Ludovico, P., and Winderickx, J. (2018) pH homeostasis links the nutrient sensing PKA/TORC1/Sch9 ménage-à-trois to stress tolerance and longevity. *Microbial Cell* **5**: 119-136.

Di Berardino, M., and Dimroth, P. (1996) Aspartate 203 of the oxaloacetate decarboxylase beta-subunit catalyses both the chemical and vectorial reaction of the Na^+ pump. *The EMBO journal* **15**: 1842-1849.

Dimroth, P. (1980) A new sodium-transport system energized by the decarboxylation of oxaloacetate. *FEBS Letters* **122**: 234-236.

Dimroth, P. (1981) Characterization of a membrane-bound biotin-containing enzyme: oxaloacetate decarboxylase from *Klebsiella aerogenes*. *European Journal of Biochemistry* **115**: 353-358.

Dimroth, P. (1982a) The generation of an electrochemical gradient of sodium ions upon decarboxylation of oxaloacetate by the membrane–bound and Na^+–activated oxaloacetate decarboxylase from *Klebsiella aerogenes*. *European Journal of Biochemistry* **121**: 443-449.

Dimroth, P. (1982b) The role of biotin and sodium in the decarboxylation of oxaloacetate by the membrane-bound oxaloacetate decarboxylase from *Klebsiella aerogenes*. *European Journal of Biochemistry* **121**: 435-441.

Dimroth, P. (1997) Primary sodium ion translocating enzymes. *Biochimica et Biophysica Acta (BBA) - Bioenergetics* **1318**: 11-51.

Dimroth, P., and Cook, G.M. (2004) Bacterial Na^+- or H^+-coupled ATP synthases operating at low electrochemical potential. In: *Advances in Microbial Physiology*: Academic Press. 175-218.

Dimroth, P., and Hilbi, H. (1997) Enzymic and genetic basis for bacterial growth on malonate. *Molecular Microbiology* **25**: 3-10.

Dimroth, P., Jockel, P., and Schmid, M. (2001) Coupling mechanism of the oxaloacetate decarboxylase Na^+ pump. *Biochimica et Biophysica Acta (BBA) - Bioenergetics* **1505**: 1-14.

Dimroth, P., Kaim, G., and Matthey, U. (2000) Crucial role of the membrane potential for ATP synthesis by F_1F_0 ATP synthases. *Journal of Experimental Biology* **203**: 51-59.

Dimroth, P., and Schink, B. (1998) Energy conservation in the decarboxylation of dicarboxylic acids by fermenting bacteria. *Archives of Microbiology* **170**: 69-77.

Dimroth, P., and von Ballmoos, C. (2007) ATP synthesis by decarboxylation phosphorylation. In: *Bioenergetics: Energy Conservation and Conversion*. Schäfer, G., and Penefsky, H.S. (eds). Berlin, Heidelberg: Springer Berlin Heidelberg. 153-184.

Dittrich, C.R., Bennett, G.N., and San, K.-Y. (2005) Characterization of the acetate-producing pathways in *Escherichia coli*. *Biotechnology Progress* **21**: 1062-1067.

Doebbe, A., Rupprecht, J., Beckmann, J., Mussgnug, J.H., Hallmann, A., Hankamer, B., and Kruse, O. (2007) Functional integration of the HUP1 hexose symporter gene into the genome of *C. reinhardtii*: Impacts on biological H_2 production. *Journal of Biotechnology* **131**: 27-33.

Dozier, J.K., Khatwani, S.L., Wollack, J.W., Wang, Y.-C., Schmidt-Dannert, C., and Distefano, M.D. (2014) Engineering protein farnesyltransferase for enzymatic protein labeling applications. *Bioconjugate Chemistry* **25**: 1203-1212.

Dragosits, M., and Mattanovich, D. (2013) Adaptive laboratory evolution – principles and applications for biotechnology. *Microbial Cell Factories* **12**: 64.

Du, T., Buenbrazo, N., Kell, L., Rahmani, S., Sim, L., Withers, S.G., et al. (2019) A bacterial expression platform for production of therapeutic proteins containing human-like O-linked glycans. *Cell Chemical Biology* **26**: 203-212.e205.

Dulermo, T., Lazar, Z., Dulermo, R., Rakicka, M., Haddouche, R., and Nicaud, J.-M. (2015) Analysis of ATP-citrate lyase and malic enzyme mutants of *Yarrowia lipolytica* points out the importance of mannitol metabolism in fatty acid synthesis. *Biochimica et Biophysica Acta (BBA) - Molecular and Cell Biology of Lipids* **1851**: 1107-1117.

Earle, S.R., and Fisher, R.R. (1980) Reconstitution of bovine heart mitochondrial transhydrogenase: a reversible proton pump. *Biochemistry* **19**: 561-569.

Eriksen, D.T., HamediRad, M., Yuan, Y., and Zhao, H. (2015) Orthogonal fatty acid biosynthetic pathway improves fatty acid ethyl ester production in *Saccharomyces cerevisiae*. *ACS Synthetic Biology* **4**: 808-814.

Falcone, N., She, Z., Syed, J., Lough, A., and Kraatz, H.-B. (2019) synthesis and biochemical evaluation of nicotinamide derivatives as NADH analogue coenzymes in ene reductase. *ChemBioChem* **20**: 838-845.

Fang, Y., Chen, X., and Godbey, W.T. (2019) Chapter 42 - Gene editing in regenerative medicine. In: *Principles of Regenerative Medicine (Third Edition)*. Atala, A., Lanza, R., Mikos, A.G., and Nerem, R. (eds). Boston: Academic Press. 741-759.

Flamholz, A., Noor, E., Bar-Even, A., and Milo, R. (2012) eQuilibrator--the biochemical thermodynamics calculator. *Nucleic Acids Research* **40**: D770-D775.

Floras, N., Xiao, J., Berry, A., Bolivar, F., and Valle, F. (1996) Pathway engineering for the production of aromatic compounds in *Escherichia coli*. *Nature Biotechnology* **14**: 620-623.

Folsom, J.P., and Carlson, R.P. (2015) Physiological, biomass elemental composition and proteomic analyses of *Escherichia coli* ammonium-limited chemostat growth, and comparison with iron- and glucose-limited chemostat growth. *Microbiology* **161**: 1659-1670.

Fuhrer, T., and Sauer, U. (2009) Different biochemical mechanisms ensure network-wide balancing of reducing equivalents in microbial metabolism. *Journal of Bacteriology* **191**: 2112-2121.

Fuller, C.C., Reed, L.J., Oliver, R.M., and Hackert, M.L. (1979) Crystallization of a dihydrolipoyl transacetylase-dihydrolipoyl dehydrogenase subcomplex and its implications regarding the subunit structure of the pyruvate dehydrogenase complex from *Escherichia coli*. *Biochemical and Biophysical Research Communications* **90**: 431-438.

Galivan, J.H., and Allen, S.H.G. (1968) Methylmalonyl-CoA decarboxylase: partial purification and enzymatic properties. *Archives of Biochemistry and Biophysics* **126**: 838-847.

Garcia-Ochoa, F., and Gomez, E. (2009) Bioreactor scale-up and oxygen transfer rate in microbial processes: An overview. *Biotechnology Advances* **27**: 153-176.

Grabe, M., Wang, H., and Oster, G. (2000) The mechanochemistry of V-ATPase proton pumps. *Biophysical Journal* **78**: 2798-2813.

Graf, M., Bokranz, M., Böcher, R., Friedl, P., and Kröger, A. (1985) Electron transport driven phosphorylation catalyzed by proteoliposomes containing hydrogenase, fumarate reductase and ATP synthase. *FEBS Letters* **184**: 100-103.

Gray, C.T., Wimpenny, J.W., and Mossman, M.R. (1966) Regulation of metabolism in facultative bacteria: II. Effects of aerobiosis, anaerobiosis and nutrition on the formation of Krebs cycle enzymes in *Escherichia coli*. *Biochimica et Biophysica Acta (BBA) - General Subjects* **117**: 33-41.

Gregory, J.D., and Robbins, P.W. (1960) Metabolism of sulfur compounds (sulfate metabolism) *Annual Review of Biochemistry* **29**: 347-364.

Grüber, G., Wieczorek, H., Harvey, W.R., and Müller, V. (2001) Structure–function relationships of A-, F- and V-ATPases. *Journal of Experimental Biology* **204**: 2597-2605.

Guadalupe-Medina, V., Wisselink, H.W., Luttik, M.A., de Hulster, E., Daran, J.-M., Pronk, J.T., and van Maris, A.J. (2013) Carbon dioxide fixation by Calvin-Cycle enzymes improves ethanol yield in yeast. *Biotechnology for biofuels* **6**: 125-125.

Guarneri, A., van Berkel, W.J.H., and Paul, C.E. (2019) Alternative coenzymes for biocatalysis. *Current Opinion in Biotechnology* **60**: 63-71.

Guarneri, A., Westphal, A.H., Leertouwer, J., Lunsonga, J., Franssen, M.C.R., Opperman, D.J., et al. (2020) Flavoenzyme-mediated regioselective aromatic hydroxylation with coenzyme biomimetics. *ChemCatChem* **12**: 1368-1375.

Guest, J.R., Angier, S.J., and Russell, G.C. (1989) Structure, expression, and protein engineering of the pyruvate dehydrogenase complex of *Escherichia coli*. *Annals of the New York Academy of Sciences* **573**: 76-99.

Guest, J.R., and Creaghan, I.T. (1973) Gene-protein relationships of the α-keto acid dehydrogenase complexes of *Escherichia coli* K12: isolation and characterization of lipoamide dehydrogenase mutants. *Microbiology* **75**: 197-210.

Guest, J.R., and Creaghan, I.T. (1972) Lipoamide dehydrogenase mutants of *Escherichia coli* K 12. *The Biochemical Journal* **130**: 8.

Guest, J.R., Russell, G.C., Stadtman, E.R., and Chock, P.B. (1992) Complexes and complexities of the citric acid cycle in *Escherichia coli*. In: *Current Topics in Cellular Regulation*: Academic Press. 231-247.

Gutiérrez-Luna, F.M., Hernández-Domínguez, E.E., Valencia-Turcotte, L.G., and Rodríguez-Sotres, R. (2018) Review: "Pyrophosphate and pyrophosphatases in plants, their involvement in stress responses and their possible relationship to secondary metabolism". *Plant Science* **267**: 11-19.

Ha, S.-J., Galazka, J.M., Joong Oh, E., Kordić, V., Kim, H., Jin, Y.-S., and Cate, J.H.D. (2013) Energetic benefits and rapid cellobiose fermentation by *Saccharomyces cerevisiae* expressing cellobiose phosphorylase and mutant cellodextrin transporters. *Metabolic Engineering* **15**: 134-143.

Han, L., and Liang, B. (2018) New approaches to NAD(P)H regeneration in the biosynthesis systems. *World Journal of Microbiology and Biotechnology* **34**: 141.

Hanai, T., Atsumi, S., and Liao, J.C. (2007) Engineered synthetic pathway for isopropanol production in *Escherichia coli*. *Applied and Environmental Microbiology* **73**: 7814-7818.

Hansen, B., Bokranz, M., Schönheit, P., and Kröger, A. (1988) ATP formation coupled to caffeate reduction by H_2 in *Acetobacterium woodii* NZva16. *Archives of Microbiology* **150**: 447-451.

Hansen, R.G., and Henning, U. (1966) Regulation of pyruvate dehydrogenase activity in *Escherichia coli* K12. *Biochimica et Biophysica Acta (BBA) - Enzymology and Biological Oxidation* **122**: 355-358.

Hanson, R.L. (1979) The kinetic mechanism of pyridine nucleotide transhydrogenase from *Escherichia* coli. *Journal of Biological Chemistry* **254**: 888-893.
Harold, F.M. (1986) The vital force: a study of bioenergetics. New York: W. H. Freeman.

Hartmanis, M.G. (1987) Butyrate kinase from *Clostridium acetobutylicum*. *Journal of Biological Chemistry* **262**: 617-621.

Harwood, C.S., and Canale-Parola, E. (1981a) Adenosine 5'-triphosphate- yielding pathways of branched-chain amino acid fermentation by a marine spirochete. *Journal of Bacteriology* **148**: 117-123.

Harwood, C.S., and Canale-Parola, E. (1981b) Branched-chain amino acid fermentation by a marine spirochete: strategy for starvation survival. *Journal of Bacteriology* **148**: 109-116.

Harwood, C.S., and Canale-Parola, E. (1982) Properties of acetate kinase isozymes and a branched-chain fatty acid kinase from a spirochete. *Journal of Bacteriology* **152**: 246-254.

Haverkorn van Rijsewijk, B.R.B., Kochanowski, K., Heinemann, M., and Sauer, U. (2016) Distinct transcriptional regulation of the two *Escherichia coli* transhydrogenases PntAB and UdhA. *Microbiology* **162**: 1672-1679.

Heath, E.C., Hurwitz, J., Horecker, B.L., and Ginsburg, A. (1958) Pentose fermentation by *Lactobacillus plantarum*: I. Cleavage of xylulose 5-phosphate by phosphoketolase. *Journal of Biological Chemistry* **231**: 1009-1029.

Hermann, T. (2003) Industrial production of amino acids by coryneform bacteria. *Journal of Biotechnology* **104**: 155-172.

Hernández-Montalvo, V., Martínez, A., Hernández-Chavez, G., Bolivar, F., Valle, F., and Gosset, G. (2003) Expression of *galP* and *glk* in a *Escherichia coli* PTS mutant restores glucose transport and increases glycolytic flux to fermentation products. *Biotechnology and Bioengineering.* **83**: 687-694.

Herrmann, G., Jayamani, E., Mai, G., and Buckel, W. (2008) Energy conservation via electron-transferring flavoprotein in anaerobic bacteria. *Journal of Bacteriology* **190**: 784-791.

Hess, V., González, J.M., Parthasarathy, A., Buckel, W., and Müller, V. (2013a) Caffeate respiration in the acetogenic bacterium *Acetobacterium woodii*: a coenzyme A loop saves energy for caffeate activation. *Applied and Environmental Microbiology* **79**: 1942-1947.

Hess, V., Schuchmann, K., and Müller, V. (2013b) The ferredoxin:NAD^+ Oxidoreductase (Rnf) from the acetogen *Acetobacterium woodii* requires Na^+ and is reversibly coupled to the membrane potential. *Journal of Biological Chemistry* **288**: 31496-31502.

Hess, V., Vitt, S., and Müller, V. (2011) A caffeyl-coenzyme A synthetase initiates caffeate activation prior to caffeate reduction in the acetogenic bacterium *Acetobacterium woodii*. *Journal of Bacteriology* **193**: 971-978.

Heßlinger, C., Fairhurst, S.A., and Sawers, G. (1998) Novel keto acid formate-lyase and propionate kinase enzymes are components of an anaerobic pathway in *Escherichia coli* that degrades L-threonine to propionate. *Molecular Microbiology* **27**: 477-492.

Hetzel, M., Brock, M., Selmer, T., Pierik, A.J., Golding, B.T., and Buckel, W. (2003) Acryloyl-CoA reductase from *Clostridium propionicum*. *European Journal of Biochemistry* **270**: 902-910.

Hilbi, H., Dehning, I., Schink, B., and Dimroth, P. (1992) Malonate decarboxylase of *Malonomonas rubra*, a novel type of biotin-containing acetyl enzyme. *European Journal of Biochemistry* **207**: 117-123.

Hilpert, W., and Dimroth, P. (1982) Conversion of the chemical energy of methylmalonyl-CoA decarboxylation into a Na^+ gradient. *Nature* **296**: 584-585.

Hilpert, W., and Dimroth, P. (1983) Purification and characterization of a new sodium-transport decarboxylase. *European Journal of Biochemistry* **132**: 579-587.

Hilpert, W., and Dimroth, P. (1991) On the mechanism of sodium ion translocation by methylmalonyl-CoA decarboxylase from *Veillonella alcalescens*. *European Journal of Biochemistry* **195**: 79-86.

Hilpert, W., Schink, B., and Dimroth, P. (1984) Life by a new decarboxylation-dependent energy conservation mechanism with Na^+ as coupling ion. *The EMBO Journal* **3**: 1665-1670.

Hirsch, C.A., Rasminsky, M., Davis, B.D., and Lin, E.C.C. (1963) A fumarate reductase in *Escherichia coli* distinct from succinate dehydrogenase. *Journal of Biological Chemistry* **238**: 3770-3774.

Hoek, P.v., Aristidou, A.A., Hahn, J.J., and Patist, A. (2003) Fermentation goes large-scale.

Huang, C., Jr., Lin, H., and Yang, X. (2012) Industrial production of recombinant therapeutics in *Escherichia coli* and its recent advancements. *Journal of Industrial Microbiology & Biotechnology* **39**: 383-399.

Huang, R., Chen, H., Upp, D.M., Lewis, J.C., and Zhang, Y.-H.P.J. (2019) A high-throughput method for directed evolution of NAD(P)$^+$-dependent dehydrogenases for the reduction of biomimetic nicotinamide analogues. *ACS Catalysis* **9**: 11709-11719.

Hurwitz, J. (1958) Pentose phosphate cleavage by *Leuconostoc mesenteroides*. *Biochimica et Biophysica Acta (BBA) - Bioenergetics* **28**: 599-602.

Ignea, C., Raadam, M.H., Motawia, M.S., Makris, A.M., Vickers, C.E., and Kampranis, S.C. (2019) Orthogonal monoterpenoid biosynthesis in yeast constructed on an isomeric substrate. *Nature Communications* **10**: 3799.

Inui, H., Miyatake, K., Nakano, Y., and Kitaoka, S. (1984a) Fatty acid synthesis in mitochondria of *Euglena gracilis*. *European Journal of Biochemistry* **142**: 121-126.

Inui, H., Miyatake, K., Nakano, Y., and Kitaoka, S. (1984b) Occurrence of oxygen-sensitive, NADP$^+$-dependent pyruvate dehydrogenase in mitochondria of *Euglena gracilis*. *The Journal of Biochemistry* **96**: 931-934.

Inui, H., Miyatake, K., Nakano, Y., and Kitaoka, S. (1989) Pyruvate:NADP$^+$ oxidoreductase from *Euglena gracilis*: the kinetic properties of the enzyme. *Archives of Biochemistry and Biophysics* **274**: 434-442.

Inui, H., Ono, K., Miyatake, K., Nakano, Y., and Kitaoka, S. (1987) Purification and characterization of pyruvate:NADP$^+$ oxidoreductase in *Euglena gracilis*. *Journal of Biological Chemistry* **262**: 9130-9135.

Iuchi, S., and Lin, E.C. (1988) *arcA* (dye), a global regulatory gene in *Escherichia coli* mediating repression of enzymes in aerobic pathways. *Proceedings of the National Academy of Sciences* **85**: 1888-1892.

Jackson, J.B. (2003) Proton translocation by transhydrogenase. *FEBS Letters* **545**: 18-24.

Jahreis, K., Pimentel-Schmitt, E.F., Brückner, R., and Titgemeyer, F. (2008) Ins and outs of glucose transport systems in eubacteria. *FEMS Microbiology Reviews* **32**: 891-907.

Jan, J., Martinez, I., Wang, Y., Bennett, G.N., and San, K.Y. (2013) Metabolic engineering and transhydrogenase effects on NADPH availability in *Escherichia coli*. *Biotechnology Progress* **29**: 1124-1130.

Jayamani, E., and Buckel, W. (2008) A unique way of energy conservation in glutamate fermenting clostridia. Philipps-Universität Marburg.

Jeckelmann, J.-M., and Erni, B. (2019) Carbohydrate transport by group translocation: the bacterial phosphoenolpyruvate: sugar phosphotransferase system. In: *Bacterial Cell Walls and Membranes*. Kuhn, A. (ed). Cham: Springer International Publishing. 223-274.

Ji, D., Wang, L., Hou, S., Liu, W., Wang, J., Wang, Q., and Zhao, Z.K. (2011) Creation of bioorthogonal redox systems depending on nicotinamide flucytosine dinucleotide. *Journal of the American Chemical Society* **133**: 20857-20862.

Jiang, G.R., Nikolova, S., and Clark, D.P. (2001a) Regulation of the *ldhA* gene, encoding the fermentative lactate dehydrogenase of *Escherichia coli*. *Microbiology* **147**: 2437-2446.

Jiang, W., Hermolin, J., and Fillingame, R.H. (2001b) The preferred stoichiometry of c subunits in the rotary motor sector of *Escherichia coli* ATP synthase is 10. *Proceedings of the National Academy of Sciences* **98**: 4966-4971.

Jiang, Y., Chen, B., Duan, C., Sun, B., Yang, J., and Yang, S. (2015) Multigene editing in the *Escherichia coli* genome via the CRISPR-Cas9 system. *Applied and Environmental Microbiology* **81**: 2506-2514.

Jin, R.Z., and Lin, E.C.C. (1984) An inducible phosphoenolpyruvate: dihydroxyacetone phosphotransferase system in *Escherichia coli*. *Microbiology* **130**: 83-88.

Jones, C.M., Hernández Lozada, N.J., and Pfleger, B.F. (2015) Efflux systems in bacteria and their metabolic engineering applications. *Applied Microbiology and Biotechnology* **99**: 9381-9393.

Jones, C.P., and Ingram-Smith, C. (2014) Biochemical and kinetic characterization of the recombinant ADP-forming acetyl coenzyme A synthetase from the amitochondriate protozoan *Entamoeba histolytica*. *Eukaryotic Cell* **13**: 1530-1537.

Josa-Culleré, L., Lahdenperä, A.S.K., Ribaucourt, A., Höfler, G.T., Gargiulo, S., Liu, Y.-Y., et al. (2019) Synthetic biomimetic coenzymes and alcohol dehydrogenases for asymmetric catalysis. *Catalysts* **9**.

Jung, Y.K., Kim, T.Y., Park, S.J., and Lee, S.Y. (2010) Metabolic engineering of *Escherichia coli* for the production of polylactic acid and its copolymers. *Biotechnology and Bioengineering.* **105**: 161-171.

Kabus, A., Georgi, T., Wendisch, V.F., and Bott, M. (2007) Expression of the *Escherichia coli pntAB* genes encoding a membrane-bound transhydrogenase in *Corynebacterium glutamicum* improves L-lysine formation. *Applied Microbiology and Biotechnology* **75**: 47-53.

Kale, S., Arjunan, P., Furey, W., and Jordan, F. (2007) A dynamic loop at the active center of the *Escherichia coli* pyruvate dehydrogenase complex E1 component modulates substrate utilization and chemical communication with the E2 component. *Journal of Biological Chemistry* **282**: 28106-28116.

Kang, Y., Weber, K.D., Qiu, Y., Kiley, P.J., and Blattner, F.R. (2005) Genome-wide expression analysis indicates that FNR of *Escherichia coli* K-12 regulates a large number of genes of unknown function. *Journal of Bacteriology* **187**: 1135-1160.

Kashket, E.R. (1983) Stoichiometry of the H^+-ATPase of *Escherichia coli* cells during anaerobic growth. *FEBS Letters* **154**: 343-346.

Kashket, E.R., and Wilson, T.H. (1974) Proton motive force in fermenting *Streptococcus lactis* 7962 in relation to sugar accumulation. *Biochemical and Biophysical Research Communications* **59**: 879-886.

Kawai, S., Mori, S., and Mukai, T. (2001) Molecular characterization of *Escherichia coli* NAD kinase. *Eur Journal of Biochemistry* **268**.

Keasling, J.D. (2010) Manufacturing molecules through metabolic engineering. *Science* **330**: 1355-1358.

Kell, D.B., Swainston, N., Pir, P., and Oliver, S.G. (2015) Membrane transporter engineering in industrial biotechnology and whole cell biocatalysis. *Trends in Biotechnology* **33**: 237-246.

Khodayari, A., and Maranas, C.D. (2016) A genome-scale *Escherichia coli* kinetic metabolic model k-ecoli457 satisfying flux data for multiple mutant strains. *Nature Communications* **7**: 13806.

Kim, S.Y., Lee, J., and Lee, S.Y. (2015) Metabolic engineering of *Corynebacterium glutamicum* for the production of L-ornithine. *Biotechnology and Bioengineering.* **112**: 416-421.

Kim, Y., Ingram, L.O., and Shanmugam, K.T. (2008) Dihydrolipoamide dehydrogenase mutation alters the nadh sensitivity of pyruvate dehydrogenase complex of *Escherichia coli* K-12. *Journal of Bacteriology* **190**: 3851-3858.

Knappe, J., and Blaschkowski, H.P. (1975) Pyruvate formate-lyase from *Escherichia coli* and its activation system. In: *Methods in Enzymology*: Academic Press. 508-518.

Knappe, J., Blaschkowski, H.P., Gröbner, P., and Schmitt, T. (1974) Pyruvate formate-lyase of *Escherichia coli*: the acetyl-enzyme intermediate. *European Journal of Biochemistry* **50**: 253-263.

Knappe, J., and Sawers, G. (1990) A radical-chemical route to acetyl-CoA: the anaerobically induced pyruvate formate-lyase system of *Escherichia coli*. *FEMS Microbiology Letters* **75**: 383-398.

Knaus, T., Paul, C.E., Levy, C.W., de Vries, S., Mutti, F.G., Hollmann, F., and Scrutton, N.S. (2016) Better than nature: nicotinamide biomimetics that outperform natural coenzymes. *Journal of the American Chemical Society* **138**: 1033-1039.

Ko, Y.-S., Kim, J.W., Lee, J.A., Han, T., Kim, G.B., Park, J.E., and Lee, S.Y. (2020) Tools and strategies of systems metabolic engineering for the development of microbial cell factories for chemical production. *Chemical Society Reviews* **49**: 4615-4636.

Komati Reddy, G., Lindner, S.N., and Wendisch, V.F. (2015) Metabolic engineering of an ATP-neutral Embden-Meyerhof-Parnas pathway in *Corynebacterium glutamicum*: growth restoration by an adaptive point mutation in NADH dehydrogenase. *Applied and Environmental Microbiology* **81**: 1996-2005.

Konings, W.N. (1985) Generation of metabolic energy by end-product efflux. *Trends in Biochemical Sciences* **10**: 317-319.

Kornberg, A. (1957) Pyrophosphorylases and phosphorylases in biosynthetic reactions. In: *Advances in Enzymology and Related Areas of Molecular Biology*. 191-240.

Krämer, M., and Cypionka, H. (1989) Sulfate formation via ATP sulfurylase in thiosulfate- and sulfite-disproportionating bacteria. *Archives of Microbiology* **151**: 232-237.

Kresge, N., Simoni, R.D., and Hill, R.L. (2005) Otto Fritz Meyerhof and the elucidation of the glycolytic pathway. *Journal of Biological Chemistry* **280**: e3.

Kröger, A. (1978) Fumarate as terminal acceptor of phosphorylative electron transport. *Biochimica et Biophysica Acta (BBA) - Reviews on Bioenergetics* **505**: 129-145.

Kruger, N.J., and von Schaewen, A. (2003) The oxidative pentose phosphate pathway: structure and organisation. *Current Opinion in Plant Biology* **6**: 236-246.

Kurata, H., and Sugimoto, Y. (2018) Improved kinetic model of *Escherichia coli* central carbon metabolism in batch and continuous cultures. *Journal of Bioscience and Bioengineering* **125**: 251-257.

Labes, A., and Schönheit, P. (2001) Sugar utilization in the hyperthermophilic, sulfate-reducing archaeon *Archaeoglobus fulgidus* strain 7324: starch degradation to acetate and CO_2 via a modified Embden-Meyerhof pathway and acetyl-CoA synthetase (ADP-forming). *Archives of Microbiology* **176**: 329-338.

LaCroix, R.A., Sandberg, T.E., O'Brien, E.J., Utrilla, J., Ebrahim, A., Guzman, G.I., et al. (2015) Use of adaptive laboratory evolution to discover key mutations enabling rapid growth of *Escherichia coli* K-12 MG1655 on glucose minimal medium. *Applied and Environmental Microbiology* **81**: 17-30.

Lambden, P.R., and Guest, J.R. (1976) Mutants of *Escherichia coli* K12 unable to use fumarate as an anaerobic electron acceptor. *Journal of General Microbiology* **97**: 145-160.

Laubinger, W., and Dimroth, P. (1988) Characterization of the ATP synthase of *Propionigenium modestum* as a primary sodium pump. *Biochemistry* **27**: 7531-7537.

Leandro, M.J., Sychrová, H., Prista, C., and Loureiro-Dias, M.C. (2011) The osmotolerant fructophilic yeast *Zygosaccharomyces rouxii* employs two plasma-membrane fructose uptake systems belonging to a new family of yeast sugar transporters. *Microbiology* **157**: 601-608.

Lee, H.C., Kim, J.S., Jang, W., and Kim, S.Y. (2010) High NADPH/$NADP^+$ ratio improves thymidine production by a metabolically engineered *Escherichia coli* strain. *Journal of Biotechnology* **149**: 24-32.

Lee, J., Jang, Y.-S., Choi, S.J., Im, J.A., Song, H., Cho, J.H., et al. (2012) Metabolic engineering of *Clostridium acetobutylicum* ATCC 824 for isopropanol-butanol-ethanol fermentation. *Applied and Environmental Microbiology* **78**: 1416-1423.

Lee, J.W., Kim, H.U., Choi, S., Yi, J., and Lee, S.Y. (2011) Microbial production of building block chemicals and polymers. *Current Opinion in Biotechnology* **22**: 758-767.

Lee, S., Mattanovich, D., and Villaverde, A. (2012) Systems metabolic engineering, industrial biotechnology and microbial cell factories. *Microbial Cell Factories* **11**: 156.

Lee, S.K., Chou, H., Ham, T.S., Lee, T.S., and Keasling, J.D. (2008) Metabolic engineering of microorganisms for biofuels production: from bugs to synthetic biology to fuels. *Current Opinion in Biotechnology* **19**: 556-563.

Lee, T.S., Krupa, R.A., Zhang, F., Hajimorad, M., Holtz, W.J., Prasad, N., et al. (2011) BglBrick vectors and datasheets: a synthetic biology platform for gene expression. *Journal of Biological Engineering* **5**: 12.

Lee, W.-H., Kim, M.-D., Jin, Y.-S., and Seo, J.-H. (2013) Engineering of NADPH regenerators in *Escherichia coli* for enhanced biotransformation. *Applied Microbiology and Biotechnology* **97**: 2761-2772.

Lee, W.-H., Park, J.-B., Park, K., Kim, M.-D., and Seo, J.-H. (2007) Enhanced production of ε-caprolactone by overexpression of NADPH-regenerating glucose 6-phosphate dehydrogenase in recombinant *Escherichia coli* harboring cyclohexanone monooxygenase gene. *Applied Microbiology and Biotechnology* **76**: 329-338.

Lee, W.-H., Pathanibul, P., Quarterman, J., Jo, J.-H., Han, N.S., Miller, M.J., et al. (2012) Whole cell biosynthesis of a functional oligosaccharide, 2′-fucosyllactose, using engineered *Escherichia coli*. *Microbial Cell Factories* **11**: 48.

Li, F., Hinderberger, J., Seedorf, H., Zhang, J., Buckel, W., and Thauer, R.K. (2008) Coupled ferredoxin and crotonyl coenzyme A (CoA) reduction with NADH catalyzed by the butyryl-CoA dehydrogenase/Etf complex from *Clostridium kluyveri*. *Journal of Bacteriology* **190**: 843-850.

Li, S., Jendresen, C.B., Landberg, J., Pedersen, L.E., Sonnenschein, N., Jensen, S.I., and Nielsen, A.T. (2020) Genome-wide CRISPRi-based identification of targets for decoupling growth from production. *ACS Synthetic Biology* **9**: 1030-1040.

Li, S., Jendresen, C.B., and Nielsen, A.T. (2016) Increasing production yield of tyrosine and mevalonate through inhibition of biomass formation. *Process Biochemistry* **51**: 1992-2000.

Li, Y., Lin, Z., Huang, C., Zhang, Y., Wang, Z., Tang, Y.J., et al. (2015) Metabolic engineering of *Escherichia* coli using CRISPR-Cas9 meditated genome editing. *Metabolic Engineering* **31**: 13-21.

Li, Z.J., Cai, L., Wu, Q., and Chen, G.Q. (2009) Overexpression of NAD kinase in recombinant *Escherichia coli* harboring the *phbCAB* operon improves poly(3-hydroxybutyrate) production. *Applied Microbiology and Biotechnology* **83**: 936-947.

Lim, S.-J., Jung, Y.-M., Shin, H.-D., and Lee, Y.-H. (2002) Amplification of the NADPH-related genes *zwf* and *gnd* for the oddball biosynthesis of PHB in an *E. coli* transformant harboring a cloned *phbCAB* operon. *Journal of Bioscience and Bioengineering* **93**: 543-549.

Lin, P.P., Jaeger, A.J., Wu, T.-Y., Xu, S.C., Lee, A.S., Gao, F., et al. (2018) Construction and evolution of an *Escherichia* coli strain relying on nonoxidative glycolysis for sugar catabolism. *Proceedings of the National Academy of Sciences* **115**: 3538-3546.

Lindberg, P., Park, S., and Melis, A. (2010) Engineering a platform for photosynthetic isoprene production in cyanobacteria, using *Synechocystis* as the model organism. *Metabolic Engineering* **12**: 70-79.

Lindner, S.N., Calzadiaz Ramirez, L., Krüsemann, J., Yishai, O., Belkhelfa, S., He, H., et al. (2018) NADPH-auxotrophic *E. coli*: a sensor strain for testing *in vivo* regeneration of NADPH. *ACS Synthetic Biology* **7**: 2742-2749.

Liu, J., Li, H., Zhao, G., Caiyin, Q., and Qiao, J. (2018) Redox cofactor engineering in industrial microorganisms: strategies, recent applications and future directions. *Journal of Industrial Microbiology and Biotechnology* **45**: 313-327.

Liu, W., Zheng, P., Yu, F., and Yang, Q. (2015) A two-stage process for succinate production using genetically engineered *Corynebacterium acetoacidophilum*. *Process Biochemistry* **50**: 1692-1700.

Liu, Y., Li, Q., Wang, L., Guo, X., Wang, J., Wang, Q., and Zhao, Z.K. (2020) Engineering D-lactate dehydrogenase to favor an non-natural cofactor nicotinamide cytosine dinucleotide. *ChemBioChem* **21**: 1972-1975.

Liu, Z., Gao, Y., Chen, J., Imanaka, T., Bao, J., and Hua, Q. (2013) Analysis of metabolic fluxes for better understanding of mechanisms related to lipid accumulation in oleaginous yeast *Trichosporon cutaneum*. *Bioresource Technology* **130**: 144-151.

Löw, S.A., Löw, I.M., Weissenborn, M.J., and Hauer, B. (2016) Enhanced ene-reductase activity through alteration of artificial nicotinamide cofactor substituents. *ChemCatChem* **8**: 911-915.

Lu, L., Wei, L., Zhu, K., Wei, D., and Hua, Q. (2012) Combining metabolic engineering and adaptive evolution to enhance the production of dihydroxyacetone from glycerol by *Gluconobacter oxydans* in a low-cost way. *Bioresource Technology* **117**: 317-324.

Maeda, S., Shimizu, K., Kihira, C., Iwabu, Y., Kato, R., Sugimoto, M., et al. (2017) Pyruvate dehydrogenase complex regulator (PdhR) gene deletion boosts glucose metabolism in *Escherichia coli* under oxygen-limited culture conditions. *Journal of Bioscience and Bioengineering* **123**: 437-443.

Mampel, J., Buescher, J.M., Meurer, G., and Eck, J. (2013) Coping with complexity in metabolic engineering. *Trends in Biotechnology* **31**: 52-60.

Mans, R., Daran, J.-M.G., and Pronk, J.T. (2018) Under pressure: evolutionary engineering of yeast strains for improved performance in fuels and chemicals production. *Current Opinion in Biotechnology* **50**: 47-56.

Mans, R., Hassing, E.-J., Wijsman, M., Giezekamp, A., Pronk, J.T., Daran, J.-M., and van Maris, A.J.A. (2017) A CRISPR/Cas9-based exploration into the elusive mechanism for lactate export in *Saccharomyces cerevisiae*. *FEMS Yeast Research* **17**.

Mans, R., van Rossum, H.M., Wijsman, M., Backx, A., Kuijpers, N.G.A., van den Broek, M., et al. (2015) CRISPR/Cas9: a molecular Swiss army knife for simultaneous introduction of multiple genetic modifications in *Saccharomyces cerevisiae*. *FEMS Yeast Research* **15**.

Marques, W.L., Mans, R., Henderson, R.K., Marella, E.R., Horst, J.t., Hulster, E.d., et al. (2018) Combined engineering of disaccharide transport and phosphorolysis for enhanced ATP yield from sucrose fermentation in *Saccharomyces cerevisiae*. *Metabolic Engineering* **45**: 121-133.

Martin, V.J.J., Piteral, D.J., Withers, S.T., Newman, J.D., and Keasling, J.D. (2003) Engineering a mevalonate pathway in *Escherichia coli* for production of terpenoids. *Nature Biotechnology* **21**: 796-802.

Martínez, I., Zhu, J., Lin, H., Bennett, G.N., and San, K.-Y. (2008) Replacing *Escherichia coli* NAD-dependent glyceraldehyde 3-phosphate dehydrogenase (GAPDH) with a NADP-dependent enzyme from *Clostridium acetobutylicum* facilitates NADPH dependent pathways. *Metabolic Engineering* **10**: 352-359.

Marty-Teysset, C., Posthuma, C., Lolkema, J.S., Schmitt, P., Divies, C., and Konings, W.N. (1996) Proton motive force generation by citrolactic fermentation in *Leuconostoc mesenteroides*. *Journal of Bacteriology* **178**: 2178-2185.

Mat-Jan, F., Alam, K.Y., and Clark, D.P. (1989) Mutants of *Escherichia coli* deficient in the fermentative lactate dehydrogenase. *Journal of Bacteriology* **171**: 342-348.

Matthies, C., and Schink, B. (1992a) Energy conservation in fermentative glutarate degradation by the bacterial strain WoGl3. *FEMS Microbiology Letters* **100**: 221-225.

Matthies, C., and Schink, B. (1992b) Fermentative degradation of glutarate via decarboxylation by newly isolated strictly anaerobic bacteria. *Archives of Microbiology* **157**: 290-296.

Matthies, C., Springer, N., Ludwig, W., and Schink, B. (2000) *Pelospora glutarica* gen. nov., sp. nov., a glutarate-fermenting, strictly anaerobic, spore-forming bacterium. *International Journal of Systematic and Evolutionary Microbiology* **50**: 645-648.

Meedel, T.H., and Pizer, L.I. (1974) Regulation of one-carbon biosynthesis and utilization in *Escherichia coli*. *Journal of Bacteriology* **118**: 905-910.

Mehrer, C.R., Incha, M.R., Politz, M.C., and Pfleger, B.F. (2018) Anaerobic production of medium-chain fatty alcohols via a β-reduction pathway. *Metabolic Engineering* **48**: 63-71.

Meng, J., Wang, B., Liu, D., Chen, T., Wang, Z., and Zhao, X. (2016) High-yield anaerobic succinate production by strategically regulating multiple metabolic pathways based on stoichiometric maximum in *Escherichia coli*. *Microbial Cell Factories* **15**: 141.

Meuller, J., Zhang, J., Hou, C., Bragg, P.D., and Rydström, J. (1997) Properties of a cysteine-free proton-pumping nicotinamide nucleotide transhydrogenase. *The Biochemical Journal* **324 (Pt 2)**: 681-687.

Millard, P., Smallbone, K., and Mendes, P. (2017) Metabolic regulation is sufficient for global and robust coordination of glucose uptake, catabolism, energy production and growth in *Escherichia coli*. *PLOS Computational Biology* **13**: e1005396.

Mohanraju, P., Makarova, K.S., Zetsche, B., Zhang, F., Koonin, E.V., and van der Oost, J. (2016) Diverse evolutionary roots and mechanistic variations of the CRISPR-Cas systems. *Science* **353**: aad5147.

Möller, D., Schauder, R., Fuchs, G., and Thauer, R.K. (1987) Acetate oxidation to CO_2 via a citric acid cycle involving an ATP-citrate lyase: a mechanism for the synthesis of ATP via substrate level phosphorylation in *Desulfobacter postgatei* growing on acetate and sulfate. *Archives of Microbiology* **148**: 202-207.

Monk, J.M., Lloyd, C.J., Brunk, E., Mih, N., Sastry, A., King, Z., et al. (2017) iML1515, a knowledgebase that computes *Escherichia coli* traits. *Nature Biotechnology* **35**: 904.

Mougiakos, I., Bosma, E.F., Ganguly, J., van der Oost, J., and van Kranenburg, R. (2018) Hijacking CRISPR-Cas for high-throughput bacterial metabolic engineering: advances and prospects. *Current Opinion in Biotechnology* **50**: 146-157.

Mulligan, M.E., Brosius, J., and McClure, W.R. (1985) Characterization *in vitro* of the effect of spacer length on the activity of *Escherichia coli* RNA polymerase at the TAC promoter. *Journal of Biological Chemistry* **260**: 3529-3538.

Mundhada, H., Seoane, J.M., Schneider, K., Koza, A., Christensen, H.B., Klein, T., et al. (2017) Increased production of L-serine in *Escherichia coli* through adaptive laboratory evolution. *Metabolic Engineering* **39**: 141-150.

Murarka, A., Clomburg, J.M., and Gonzalez, R. (2010) Metabolic flux analysis of wild-type *Escherichia coli* and mutants deficient in pyruvate-dissimilating enzymes during the fermentative metabolism of glucuronate. *Microbiology* **156**: 1860-1872.

Musfeldt, M., Selig, M., and Schönheit, P. (1999) Acetyl coenzyme A synthetase (ADP forming) from the hyperthermophilic archaeon *Pyrococcus furiosus*: identification, cloning, separate expression of the encoding genes, *acdAI* and *acdBI*, in *Escherichia coli*, and *in vitro* reconstitution of the active heterotetrameric enzyme from its recombinant subunits. *Journal of Bacteriology* **181**: 5885-5888.

Na, D., Yoo, S.M., Chung, H., Park, H., Park, J.H., and Lee, S.Y. (2013) Metabolic engineering of *Escherichia coli* using synthetic small regulatory RNAs. *Nature Biotechnology* **31**: 170-174.

Nakamura, C.E., and Whited, G.M. (2003) Metabolic engineering for the microbial production of 1,3-propanediol. *Current Opinion in Biotechnology* **14**: 454-459.

Nakashima, N., Tamura, T., and Good, L. (2006) Paired termini stabilize antisense RNAs and enhance conditional gene silencing in *Escherichia coli*. *Nucleic Acids Research* **34**: e138-e138.

Neupane, P., Bhuju, S., Thapa, N., and Bhattarai, H.K. (2019) ATP synthase: structure, function and inhibition. *Biomolecular Concepts* **10**: 1.

Ng, C.Y., Farasat, I., Maranas, C.D., and Salis, H.M. (2015) Rational design of a synthetic Entner–Doudoroff pathway for improved and controllable NADPH regeneration. *Metabolic Engineering* **29**: 86-96.

Nikel, P.I., Chavarría, M., Fuhrer, T., Sauer, U., and de Lorenzo, V. (2015) *Pseudomonas putida* KT2440 strain metabolizes glucose through a cycle formed by enzymes of the Entner-Doudoroff, Embden-Meyerhof-Parnas, and pentose phosphate pathways. *The Journal of Biological Chemistry* **290**: 25920-25932.

Noor, E., Bar-Even, A., Flamholz, A., Lubling, Y., Davidi, D., and Milo, R. (2012) An integrated open framework for thermodynamics of reactions that combines accuracy and coverage. *Bioinformatics* **28**: 2037-2044.

Noor, E., Bar-Even, A., Flamholz, A., Reznik, E., Liebermeister, W., and Milo, R. (2014) Pathway thermodynamics highlights kinetic obstacles in central metabolism. *PLOS Computational Biology* **10**: e1003483.

Noor, E., Haraldsdóttir, H.S., Milo, R., and Fleming, R.M.T. (2013) Consistent estimation of Gibbs energy using component contributions. *PLOS Computational Biology* **9**: e1003098.

Norris, D.J., and Stewart, R. (1977) The pyridinium–dihydropyridine system. I. Synthesis of a series of substituted pyridinium ions and their 1,4-dihydro reduction products and a determination of their stabilities in aqueous buffers. *Canadian Journal of Chemistry* **55**: 1687-1695.

Nowak, C., Pick, A., Lommes, P., and Sieber, V. (2017) Enzymatic reduction of nicotinamide biomimetic cofactors using an engineered glucose dehydrogenase: providing a regeneration system for artificial cofactors. *ACS Catalysis* **7**: 5202-5208.

Oide, S., Gunji, W., Moteki, Y., Yamamoto, S., Suda, M., Jojima, T., et al. (2015) Thermal and solvent stress cross-tolerance conferred to *Corynebacterium glutamicum* by adaptive laboratory evolution. *Applied and Environmental Microbiology* **81**: 2284-2298.

Orsi, W.D., Schink, B., Buckel, W., and Martin, W.F. (2020) Physiological limits to life in anoxic subseafloor sediment. *FEMS Microbiology Reviews* **44**: 219-231.

Orth, J.D., and Palsson, B.Ø. (2010) Systematizing the generation of missing metabolic knowledge. *Biotechnology and Bioengineering.* **107**: 403-412.

Orth, J.D., Thiele, I., and Palsson, B.Ø. (2010) What is flux balance analysis? *Nature Biotechnology* **28**: 245-248.

Otto, R., Lageveen, R.G., Veldkamp, H., and Konings, W.N. (1982) Lactate efflux-induced electrical potential in membrane vesicles of *Streptococcus cremoris*. *Journal of Bacteriology* **149**: 733-738.

Otto, R., Sonnenberg, A.S., Veldkamp, H., and Konings, W.N. (1980) Generation of an electrochemical proton gradient in *Streptococcus cremoris* by lactate efflux. *Proceedings of the National Academy of Sciences* **77**: 5502-5506.

Palmgren, M., and Morsomme, P. (2019) The plasma membrane H^+-ATPase, a simple polypeptide with a long history. *Yeast* **36**: 201-210.

Pandit, A.V., Srinivasan, S., and Mahadevan, R. (2017) Redesigning metabolism based on orthogonality principles. *Nature Communications* **8**: 15188.

Papagianni, M. (2007) Advances in citric acid fermentation by *Aspergillus niger*: biochemical aspects, membrane transport and modeling. *Biotechnology Advances* **25**: 244-263.

Park, S.H., Kim, H.U., Kim, T.Y., Park, J.S., Kim, S.-S., and Lee, S.Y. (2014) Metabolic engineering of *Corynebacterium glutamicum* for L-arginine production. *Nature Communications* **5**: 4618.

Park, S.Y., Yang, D., Ha, S.H., and Lee, S.Y. (2018) Metabolic engineering of microorganisms for the production of natural compounds. *Advanced Biosystems* **2**: 1700190.

Parker, C., Barnell, W.O., Snoep, J.L., Ingram, L.O., and Conway, T. (1995) Characterization of the *Zymomonas mobilis* glucose facilitator gene product (*glf*) in recombinant *Escherichia coli*: examination of transport mechanism, kinetics and the role of glucokinase in glucose transport. *Molecular Microbiology* **15**: 795-802.

Patzlaff, J.S., van der Heide, T., and Poolman, B. (2003) The ATP/substrate stoichiometry of the ATP-binding cassette (ABC) transporter OpuA. *Journal of Biological Chemistry* **278**: 29546-29551.

Paul, C.E., Arends, I.W.C.E., and Hollmann, F. (2014) Is simpler better? Synthetic nicotinamide cofactor analogues for redox chemistry. *ACS Catalysis* **4**: 788-797.

Paul, C.E., Gargiulo, S., Opperman, D.J., Lavandera, I., Gotor-Fernández, V., Gotor, V., et al. (2013) Mimicking nature: synthetic nicotinamide cofactors for C═C bioreduction using enoate reductases. *Organic Letters* **15**: 180-183.

Paul, C.E., and Hollmann, F. (2016) A survey of synthetic nicotinamide cofactors in enzymatic processes. *Applied Microbiology and Biotechnology* **100**: 4773-4778.

Pedersen, A., Karlsson, G.B., and Rydström, J. (2008) Proton-translocating transhydrogenase: an update of unsolved and controversial issues. *Journal of Bioenergetics and Biomembranes* **40**: 463.

Pel, H.J., de Winde, J.H., Archer, D.B., Dyer, P.S., Hofmann, G., Schaap, P.J., et al. (2007) Genome sequencing and analysis of the versatile cell factory *Aspergillus niger* CBS 513.88. *Nature Biotechnology* **25**: 221-231.

Pereira, R., Wei, Y., Mohamed, E., Radi, M., Malina, C., Herrgård, M.J., et al. (2019) Adaptive laboratory evolution of tolerance to dicarboxylic acids in *Saccharomyces cerevisiae*. *Metabolic Engineering* **56**: 130-141.

Pérez-García, F., and Wendisch, V.F. (2018) Transport and metabolic engineering of the cell factory *Corynebacterium glutamicum*. *FEMS Microbiology Letters* **365**.

Perli, T., Moonen, D.P.I., van den Broek, M., Pronk, J.T., and Daran, J.-M. (2020) Adaptive laboratory evolution and reverse engineering of single-vitamin prototrophies in *Saccharomyces cerevisiae*. *Applied and Environmental Microbiology* **86**: e00388-00320.

Petersen, J., Förster, K., Turina, P., and Gräber, P. (2012) Comparison of the H^+/ATP ratios of the H^+-ATP synthases from yeast and from chloroplast. *Proceedings of the National Academy of Sciences* **109**: 11150-11155.

Pettit, F.H., and Reed, L.J. (1967) Alpha-keto acid dehydrogenase complexes. 8. Comparison of dihydrolipoyl dehydrogenases from pyruvate and alpha-ketoglutarate dehydrogenase complexes of *Escherichia coli*. *Proceedings of the National Academy of Sciences* **58**: 1126-1130.

Pikis, A., Hess, S., Arnold, I., Erni, B., and Thompson, J. (2006) Genetic requirements for growth of *Escherichia coli* K12 on methyl-α-D-glucopyranoside and the five α-D-glucosyl-D-fructose isomers of sucrose. *Journal of Biological Chemistry* **281**: 17900-17908.

Pos, K.M., and Dimroth, P. (1996) Functional properties of the purified Na^+-dependent citrate carrier of *Klebsiella pneumoniae*: evidence for asymmetric orientation of the carrier protein in proteoliposomes. *Biochemistry* **35**: 1018-1026.

Prather, K.L.J., and Martin, C.H. (2008) *De novo* biosynthetic pathways: rational design of microbial chemical factories. *Current Opinion in Biotechnology* **19**: 468-474.

Puchart, V. (2015) Glycoside phosphorylases: structure, catalytic properties and biotechnological potential. *Biotechnology Advances* **33**: 261-276.

Qi, H., Li, S., Zhao, S., Huang, D., Xia, M., and Wen, J. (2014) Model-driven redox pathway manipulation for improved isobutanol production in *Bacillus subtilis* complemented with experimental validation and metabolic profiling analysis. *PLOS ONE* **9**: e93815.

Quail, M.A., and Guest, J.R. (1995) Purification, characterization and mode of action of PdhR, the transcriptional repressor of the *pdhR–aceEF–lpd* operon of *Escherichia coli*. *Molecular Microbiology* **15**: 519-529.

Quail, M.A., Haydon, D.J., and Guest, J.R. (1994) The *pdhR–aceEF–lpd* operon of *Escherichia coli* expresses the pyruvate dehydrogenase complex. *Molecular Microbiology* **12**: 95-104.

Reitzer, L. (2003) Nitrogen assimilation and global regulation in *Escherichia coli*. *Annual Review of Microbiology* **57**: 155-176.

Reitzer, L. (2004) Biosynthesis of glutamate, aspartate, asparagine, L-Alanine, and D-alanine. *EcoSal Plus* **1**.

Ren, Q., Henes, B., Fairhead, M., and Thöny-Meyer, L. (2013) High level production of tyrosinase in recombinant *Escherichia coli*. *BMC Biotechnology* **13**: 18-18.

Reyes, L.H., Gomez, J.M., and Kao, K.C. (2014) Improving carotenoids production in yeast via adaptive laboratory evolution. *Metabolic Engineering* **21**: 26-33.

Riehle, M.M., Bennett, A.F., Lenski, R.E., and Long, A.D. (2003) Evolutionary changes in heat-inducible gene expression in lines of *Escherichia coli* adapted to high temperature. *Physiological Genomics* **14**: 47-58.

Rosano, G.L., and Ceccarelli, E.A. (2014) Recombinant protein expression in *Escherichia coli*: advances and challenges. *Frontiers in Microbiology* **5**: 172.

Russnak, R., Konczal, D., and McIntire, S.L. (2001) A family of yeast proteins mediating bidirectional vacuolar amino acid transport. *Journal of Biological Chemistry* **276**: 23849-23857.

Ryan, J.D., Fish, R.H., and Clark, D.S. (2008) Engineering cytochrome P450 enzymes for improved activity towards biomimetic 1,4-NADH cofactors. *ChemBioChem* **9**: 2579-2582.

Sadie, C.J., Rose, S.H., den Haan, R., and van Zyl, W.H. (2011) Co-expression of a cellobiose phosphorylase and lactose permease enables intracellular cellobiose utilisation by *Saccharomyces cerevisiae*. *Applied Microbiology and Biotechnology* **90**: 1373-1380.

Sahdev, S., Khattar, S.K., and Saini, K.S. (2008) Production of active eukaryotic proteins through bacterial expression systems: a review of the existing biotechnology strategies. *Molecular and Cellular Biochemistry* **307**: 249-264.

Sahlman, L., and Williams, C.H. (1989) Lipoamide dehydrogenase from *Escherichia coli*. Steady-state kinetics of the physiological reaction. *Journal of Biological Chemistry* **264**: 8039-8045.

Saier, M.H., Jr. (1977) Bacterial phosphoenolpyruvate: sugar phosphotransferase systems: structural, functional, and evolutionary interrelationships. *Bacteriological Reviews* **41**: 856-871.

Sakamoto, N., Kotre, A.M., and Savageau, M.A. (1975) Glutamate dehydrogenase from *Escherichia coli*: purification and properties. *Journal of Bacteriology* **124**: 775-783.

Salema, M., Lolkema, J.S., San Romão, M.V., and Lourero Dias, M.C. (1996) The proton motive force generated in *Leuconostoc oenos* by L-malate fermentation. *Journal of Bacteriology* **178**: 3127-3132.

Sánchez, A.M., Bennett, G.N., and San, K.-Y. (2005) Novel pathway engineering design of the anaerobic central metabolic pathway in *Escherichia coli* to increase succinate yield and productivity. *Metabolic Engineering* **7**: 229-239.

Sato, K., Nishina, Y., Setoyama, C., Miura, R., and Shiga, K. (1999) Unusually high standard redox potential of acrylyl-CoA/propionyl-CoA Couple among enoyl-CoA/Acyl-CoA couples: a reason for the distinct metabolic pathway of propionyl-CoA from longer acyl-CoAs. *Journal of Biochemistry* **126**: 668-675.

Sauer, U., Canonaco, F., Heri, S., Perrenoud, A., and Fischer, E. (2004) The soluble and membrane-bound transhydrogenases UdhA and PntAB have divergent functions in NADPH metabolism of *Escherichia coli*. *Journal of Biological Chemistry* **279**: 6613-6619.

Sawada, K., Taki, A., Yamakawa, T., and Seki, M. (2009) Key role for transketolase activity in erythritol production by *Trichosporonoides megachiliensis* SN-G42. *Journal of Bioscience and Bioengineering* **108**: 385-390.

Sawers, G., and Böck, A. (1988) Anaerobic regulation of pyruvate formate-lyase from *Escherichia coli* K-12. *Journal of Bacteriology* **170**: 5330-5336.

Sawers, G., and Böck, A. (1989) Novel transcriptional control of the pyruvate formate-lyase gene: upstream regulatory sequences and multiple promoters regulate anaerobic expression. *Journal of Bacteriology* **171**: 2485-2498.

Sawers, G., and Suppmann, B. (1992) Anaerobic induction of pyruvate formate-lyase gene expression is mediated by the ArcA and FNR proteins. *Journal of Bacteriology* **174**: 3474-3478.

Schaffitzel, C., Berg, M., Dimroth, P., and Pos, K.M. (1998) Identification of an Na^+-dependent malonate transporter of *Malonomonas rubra* and its dependence on two separate genes. *Journal of Bacteriology* **180**: 2689-2693.

Schink, B., and Pfennig, N. (1982) *Propionigenium modestum* gen. nov. sp. nov. a new strictly anaerobic, nonsporing bacterium growing on succinate. *Archives of Microbiology* **133**: 209-216.

Schmincke-Ott, E., and Bisswanger, H. (1981) Dihydrolipoamide dehydrogenase component of the pyruvate dehydrogenase complex from *Escherichia coli* K12. *European Journal of Biochemistry* **114**: 413-420.

Schürmann, M., Wübbeler, J.H., Grote, J., and Steinbüchel, A. (2011) Novel reaction of succinyl coenzyme A (succinyl-CoA) synthetase: activation of 3-sulfinopropionate to 3-sulfinopropionyl-CoA in *Advenella mimigardefordensis* Strain DPN7^T during degradation of 3,3′-dithiodipropionic acid. *Journal of Bacteriology* **193**: 3078-3089.

Schwarz, E., Oesterhelt, D., Reinke, H., Beyreuther, K., and Dimroth, P. (1988) The sodium ion translocating oxalacetate decarboxylase of *Klebsiella pneumoniae*. Sequence of the biotin-containing alpha-subunit and relationship to other biotin-containing enzymes. *Journal of Biological Chemistry* **263**: 9640-9645.

Seedorf, H., Fricke, W.F., Veith, B., Brüggemann, H., Liesegang, H., Strittmatter, A., et al. (2008) The genome of *Clostridium kluyveri*, a strict anaerobe with unique metabolic features. *Proceedings of the National Academy of Sciences of the United States of America* **105**: 2128-2133.

Seeliger, S., Janssen, P.H., and Schink, B. (2002) Energetics and kinetics of lactate fermentation to acetate and propionate via methylmalonyl-CoA or acrylyl-CoA. *FEMS Microbiology Letters* **211**: 65-70.

Serrano, R. (1991) Transport across yeast vacuolar and plasma membranes. In: *The Molecular and Cellular Biology of the Yeast Saccharomyces. Volume 1: Genome Dynamics, Protein Synthesis and Energetics*. Broach JR, Pringle JR, and EW, J. (eds). New York: Cold Spring Harbor Laboratory Press. 523-585.

Seta, F.D., Boschi-Muller, S., Vignais, M.L., and Branlant, G. (1997) Characterization of *Escherichia coli* strains with *gapA* and *gapB* genes deleted. *Journal of Bacteriology* **179**: 5218-5221.

Shikata, K., Fukui, T., Atomi, H., and Imanaka, T. (2007) A novel ADP-forming succinyl-CoA synthetase in *Thermococcus kodakaraensis* structurally related to the archaeal nucleoside diphosphate-forming acetyl-CoA synthetases. *Journal of Biological Chemistry* **282**: 26963-26970.

Shin, W.-S., Lee, D., Lee, S.J., Chun, G.-T., Choi, S.-S., Kim, E.-S., and Kim, S. (2018) Characterization of a non-phosphotransferase system for *cis*,*cis*-muconic acid production in *Corynebacterium glutamicum*. *Biochemical and Biophysical Research Communications* **499**: 279-284.

Singh, A., Cher Soh, K., Hatzimanikatis, V., and Gill, R.T. (2011) Manipulating redox and ATP balancing for improved production of succinate in *E. coli*. *Metabolic Engineering* **13**: 76-81.

Smith, M.W., and Neidhardt, F.C. (1983) 2-oxoacid dehydrogenase complexes of *Escherichia coli*: cellular amounts and patterns of synthesis. *Journal of Bacteriology* **156**: 81-88.

Snoep, J.L., Arfman, N., Yomano, L.P., Fliege, R.K., Conway, T., and Ingram, L.O. (1994) Reconstruction of glucose uptake and phosphorylation in a glucose-negative mutant of *Escherichia coli* by using *Zymomonas mobilis* genes encoding the glucose facilitator protein and glucokinase. *Journal of Bacteriology* **176**: 2133-2135.

Snoep, J.L., de Graef, M.R., Westphal, A.H., de Kok, A., Joost Teixeira de Mattos, M., and Neijssel, O.M. (1993a) Differences in sensitivity to NADH of purified pyruvate dehydrogenase complexes of *Enterococcus faecalis*, *Lactococcus lactis*, *Azotobacter vinelandii* and *Escherichia coli*: implications for their activity *in vivo*. *FEMS Microbiology Letters* **114**: 279-283.

Snoep, J.L., Joost, M., de Mattos, T., and Neijssel, O.M. (1991) Effect of the energy source on the NADH/NAD ratio and on pyruvate catabolism in anaerobic chemostat cultures of *Enterococcus faecalis* NCTC 775. *FEMS Microbiology Letters* **81**: 63-66.

Snoep, J.L., Teixeira de Mattos, M.J., Postma, P.W., and Neijssel, O.M. (1990) Involvement of pyruvate dehydrogenase in product formation in pyruvate-limited anaerobic chemostat cultures of *Enterococcus faecalis* NCTC 775. *Archives of Microbiology* **154**: 50-55.

Snoep, J.L., van Bommel, M., Lubbers, F., Teixeira de Mattos, M.J., and Neijssel, O.M. (1993b) The role of lipoic acid in product formation by *Enterococcus faecalis* NCTC 775 and reconstitution *in vivo* and *in vitro* of the pyruvate dehydrogenase complex. *Microbiology* **139**: 1325-1329.

Snoep, J.L., Westphal, A.H., Benen, J.A.E., Teixeira de Mattos, M.J., Neijssel, O.M., and de Kok, A. (1992) Isolation and characterisation of the pyruvate dehydrogenase complex of anaerobically grown *Enterococcus faecalis* NCTC 775. *European Journal of Biochemistry* **203**: 245-250.

Song, H., and Lee, S.Y. (2006) Production of succinic acid by bacterial fermentation. *Enzyme and Microbial Technology* **39**: 352-361.

Spaans, S.K., Weusthuis, R.A., Van Der Oost, J., and Kengen, S.W.M. (2015) NADPH-generating systems in bacteria and archaea. *Frontiers in Microbiology* **6**: 742.

Spencer, M.E., and Guest, J.R. (1973) Isolation and properties of fumarate reductase mutants of *Escherichia coli*. *Journal of Bacteriology* **114**: 563-570.

Stahlberg, H., Müller, D.J., Suda, K., Fotiadis, D., Engel, A., Meier, T., et al. (2001) Bacterial Na^+-ATP synthase has an undecameric rotor. *EMBO Reports* **2**: 229-233.

Stauffer, L.T., Fogarty, S.J., and Stauffer, G.V. (1994) Characterization of the *Escherichia coli gcv* operon. *Gene* **142**: 17-22.

Steiert, P.S., Stauffer, L.T., and Stauffer, G.V. (1990) The *lpd* gene product functions as the L protein in the *Escherichia coli* glycine cleavage enzyme system. *Journal of Bacteriology* **172**: 6142-6144.

Steiger, M.G., Rassinger, A., Mattanovich, D., and Sauer, M. (2019) Engineering of the citrate exporter protein enables high citric acid production in *Aspergillus niger*. *Metabolic Engineering* **52**: 224-231.

Subtil, T., and Boles, E. (2011) Improving L-arabinose utilization of pentose fermenting *Saccharomyces cerevisiae* cells by heterologous expression of L-arabinose transporting sugar transporters. *Biotechnology for Biofuels* **4**: 38.

Sun, Z., Do, P.M., Rhee, M.S., Govindasamy, L., Wang, Q., Ingram, L.O., and Shanmugam, K.T. (2012) Amino acid substitutions at glutamate-354 in dihydrolipoamide dehydrogenase of *Escherichia coli* lower the sensitivity of pyruvate dehydrogenase to NADH. *Microbiology* **158**: 1350-1358.

Sweetman, A.J., and Griffiths, D.E. (1971) Studies on energy-linked reactions. Energy-linked transhydrogenase reaction in *Escherichia coli*. *Biochemical Journal* **121**: 125-130.

Swick, R.W., and Wood, H.G. (1960) The role of transcarboxylation in propionic acid fermentation. *Proceedings of the National Academy of Sciences* **46**: 28-41.

Tarmy, E.M., and Kaplan, N.O. (1968) Chemical characterization of D-lactate dehydrogenase from *Escherichia coli* B. *Journal of Biological Chemistry* **243**: 2579-2586.

ten Brink, B., Otto, R., Hansen, U.P., and Konings, W.N. (1985) Energy recycling by lactate efflux in growing and nongrowing cells of *Streptococcus cremoris*. *Journal of Bacteriology* **162**: 383-390.

Tepper, N., and Shlomi, T. (2009) Predicting metabolic engineering knockout strategies for chemical production: accounting for competing pathways. *Bioinformatics* **26**: 536-543.

Thakker, C., Martínez, I., San, K.-Y., and Bennett, G.N. (2012) Succinate production in *Escherichia coli*. *Biotechnology Journal* **7**: 213-224.

Thauer, R.K., Jungermann, K., and Decker, K. (1977) Energy conservation in chemotrophic anaerobic bacteria. *Bacteriological Reviews* **41**: 100-180.

Thiele, I., Vlassis, N., and Fleming, R.M.T. (2014) FASTGAPFILL: efficient gap filling in metabolic networks. *Bioinformatics* **30**: 2529-2531.

Thoden, J.B., Raushel, F.M., Wesenberg, G., and Holden, H.M. (1999) The binding of inosine monophosphate to *Escherichia coli* carbamoyl phosphate synthetase. *The Journal of Biological Chemistry* **274**: 22502-22507.

Thompson, J., Robrish, S.A., Immel, S., Lichtenthaler, F.W., Hall, B.G., and Pikis, A. (2001) Metabolism of sucrose and its five linkage-isomeric α-D-glucosyl-D-fructoses by *Klebsiella pneumoniae*: participation and properties of sucrose-6-phosphate hydrolase and phospho-α-glucosidase. *Journal of Biological Chemistry* **276**: 37415-37425.

Thouvenot, B., Charpentier, B., and Branlant, C. (2004) The strong efficiency of the *Escherichia coli gapA* P1 promoter depends on a complex combination of functional determinants. *The Biochemical Journal* **383**: 371-382.

Tomashek, J.J., and Brusilow, W.S.A. (2000) Stoichiometry of energy coupling by proton-translocating ATPases: a history of variability. *Journal of Bioenergetics and Biomembranes* **32**: 493-500.

Tran, Q.H., Bongaerts, J., Vlad, D., and Unden, G. (1997) Requirement for the proton-pumping NADH dehydrogenase I of *Escherichia coli* in Respiration of NADH to fumarate and its bioenergetic implications. *European Journal of Biochemistry* **244**: 155-160.

Tran, Q.H., and Unden, G. (1998) Changes in the proton potential and the cellular energetics of *Escherichia coli* during growth by aerobic and anaerobic respiration or by fermentation. *European Journal of Biochemistry* **251**: 538-543.

Trchounian, K., Blbulyan, S., and Trchounian, A. (2013) Hydrogenase activity and proton-motive force generation by *Escherichia coli* during glycerol fermentation. *Journal of Bioenergetics and Biomembranes* **45**: 253-260.

Tschech, A., and Pfennig, N. (1984) Growth yield increase linked to caffeate reduction in *Acetobacterium woodii*. *Archives of Microbiology* **137**: 163-167.

Twarog, R., and Wolfe, R.S. (1963) Role of butyryl phosphate in the energy metabolism of *Clostridium tetanomorphum*. *Journal of Bacteriology* **86**: 112-117.

Van de Stadt, R.J., Nieuwenhuis, F.J.R.M., and Van dam, K. (1971) On the reversibility of the energy-linked transhydrogenase. *Biochimica et Biophysica Acta (BBA) - Bioenergetics* **234**: 173-176.

van Maris, A.J.A., Konings, W.N., Dijken, J.P.v., and Pronk, J.T. (2004) Microbial export of lactic and 3-hydroxypropanoic acid: implications for industrial fermentation processes. *Metabolic Engineering* **6**: 245-255.

Vander Wauven, C., Simon, J.-P., Slos, P., and Stalon, V. (1986) Control of enzyme synthesis in the oxalurate catabolic pathway of *Streptococcus faecalis* ATCC 11700: evidence for the existence of a third carbamate kinase. *Archives of Microbiology* **145**: 386-390.

Vandock, K.P., Emerson, D.J., McLendon, K.E., and Rassman, A.A. (2011) Phospholipid dependence of the reversible, energy-linked, mitochondrial transhydrogenase in *Manduca sexta*. *The Journal of Membrane Biology* **242**: 89-94.

Varricchio, F. (1969) Control of glutamate dehydrogenase synthesis in *Escherichia coli*. *Biochimica et Biophysica Acta (BBA) - General Subjects* **177**: 560-564.

Vender, J., and Rickenberg, H.V. (1964) Ammonia metabolism in a mutant of *Escherichia coli* lacking glutamate dehydrogenase. *Biochimica et Biophysica Acta (BBA) - General Subjects* **90**: 218-220.

Veronese, F.M., Boccu, E., and Conventi, L. (1975) Glutamate dehydrogenase from *Escherichia coli*: Induction, purification and properties of the enzyme. *Biochimica et Biophysica Acta (BBA) - Enzymology* **377**: 217-228.

Voordouw, G., Vies, S.M., and Themmen, A.P.N. (1983) Why are two different types of pyridine nucleotide transhydrogenase found in living organisms? *European Journal of Biochemistry* **131**: 527-533.

Vuoristo, K.S., Mars, A.E., Sanders, J.P.M., Eggink, G., and Weusthuis, R.A. (2016) Metabolic engineering of TCA cycle for production of chemicals. *Trends in Biotechnology* **34**: 191-197.

Vuoristo, K.S., Mars, A.E., Sangra, J.V., Springer, J., Eggink, G., Sanders, J.P.M., and Weusthuis, R.A. (2014) Metabolic engineering of itaconate production in *Escherichia coli*. *Applied Microbiology and Biotechnology* **99**: 221-228.

Vuoristo, K.S., Mars, A.E., Sangra, J.V., Springer, J., Eggink, G., Sanders, J.P.M., and Weusthuis, R.A. (2015) Metabolic engineering of the mixed-acid fermentation pathway of *Escherichia coli* for anaerobic production of glutamate and itaconate. *Applied Microbiology and Biotechnology Express* **5**: 1-11.

Wagner, A.F., Frey, M., Neugebauer, F.A., Schäfer, W., and Knappe, J. (1992) The free radical in pyruvate formate-lyase is located on glycine-734. *Proceedings of the National Academy of Sciences* **89**: 996-1000.

Wang, C., Bao, X., Li, Y., Jiao, C., Hou, J., Zhang, Q., et al. (2015a) Cloning and characterization of heterologous transporters in *Saccharomyces cerevisiae* and identification of important amino acids for xylose utilization. *Metabolic Engineering* **30**: 79-88.

Wang, C., Liwei, M., Park, J.-B., Jeong, S.-H., Wei, G., Wang, Y., and Kim, S.-W. (2018) Microbial platform for terpenoid production: *Escherichia coli* and yeast. *Frontiers in Microbiology* **9**.

Wang, J., Lin, M., Xu, M., and Yang, S.-T. (2016) Anaerobic fermentation for production of carboxylic acids as bulk chemicals from renewable biomass. In: *Anaerobes in Biotechnology*. Hatti-Kaul, R., Mamo, G., and Mattiasson, B. (eds). Cham: Springer International Publishing. 323-361.

Wang, J., Nemeria, N.S., Chandrasekhar, K., Kumaran, S., Arjunan, P., Reynolds, S., et al. (2014) Structure and function of the catalytic domain of the dihydrolipoyl acetyltransferase component in *Escherichia coli* pyruvate dehydrogenase complex. *The Journal of Biological Chemistry* **289**: 15215-15230.

Wang, L., Ji, D., Liu, Y., Wang, Q., Wang, X., Zhou, Y.J., et al. (2017) Synthetic cofactor-linked metabolic circuits for selective energy transfer. *ACS Catalysis* **7**: 1977-1983.

Wang, S., Huang, H., Moll, J., and Thauer, R.K. (2010) $NADP^+$ reduction with reduced ferredoxin and $NADP^+$ reduction with nadh are coupled via an electron-bifurcating enzyme complex in *Clostridium kluyveri*. *Journal of Bacteriology* **192**: 5115-5123.

Wang, Y., Fan, L., Tuyishime, P., Liu, J., Zhang, K., Gao, N., et al. (2020) Adaptive laboratory evolution enhances methanol tolerance and conversion in engineered *Corynebacterium glutamicum*. *Communications Biology* **3**: 217.

Wang, Y., San, K.-Y., and Bennett, G. (2013a) Improvement of NADPH bioavailability in *Escherichia coli* by replacing NAD^+-dependent glyceraldehyde-3-phosphate dehydrogenase GapA with $NADP^+$-dependent GapB from *Bacillus subtilis* and addition of NAD kinase. *Journal of Industrial Microbiology & Biotechnology* **40**: 1449-1460.

Wang, Y., San, K.-Y., and Bennett, G. (2013b) Improvement of NADPH bioavailability in *Escherichia coli* through the use of phosphofructokinase deficient strains. *Applied Microbiology and Biotechnology* **97**: 6883-6893.

Wang, Y., San, K.-Y., and Bennett, G.N. (2013c) Cofactor engineering for advancing chemical biotechnology. *Current Opinion in Biotechnology* **24**: 994-999.

Wang, Z., Ammar, E.M., Zhang, A., Wang, L., Lin, M., and Yang, S.-T. (2015b) Engineering *Propionibacterium freudenreichii* subsp. *shermanii* for enhanced propionic acid fermentation: effects of overexpressing propionyl-CoA:succinate CoA transferase. *Metabolic Engineering* **27**: 46-56.

Weisser, P., Krämer, R., Sahm, H., and Sprenger, G.A. (1995) Functional expression of the glucose transporter of *Zymomonas mobilis* leads to restoration of glucose and fructose uptake in *Escherichia coli* mutants and provides evidence for its facilitator action. *Journal of Bacteriology* **177**: 3351-3354.

Weusthuis, R., Lamot, I., van der Oost, J., and Sanders, J. (2011) Microbial production of bulk chemicals: development of anaerobic processes. *Trends in Biotechnology* **29**: 153-158.

Weusthuis, R.A., Adams, H., Scheffers, W.A., and van Dijken, J.P. (1993) Energetics and kinetics of maltose transport in *Saccharomyces cerevisiae*: a continuous culture study. *Applied and Environmental Microbiology* **59**: 3102-3109.

Weusthuis, R.A., Folch, P.L., Pozo-Rodríguez, A., and Paul, C.E. (2020) Applying non-canonical redox cofactors in fermentation processes. *iScience* **23**.

Weusthuis, R.A., Mars, A.E., Springer, J., Wolbert, E.J.H., van der Wal, H., de Vrije, T.G., et al. (2017) *Monascus ruber* as cell factory for lactic acid production at low pH. *Metabolic Engineering* **42**: 66-73.

Wieczorke, R., Dlugai, S., Krampe, S., and Boles, E. (2003) Characterisation of mammalian GLUT glucose transporters in a heterologous yeast expression system. *Cellular Physiology and Biochemistry* **13**: 123-134.

Wifling, K., and Dimroth, P. (1989) Isolation and characterization of oxaloacetate decarboxylase of *Salmonella typhimurium*, a sodium ion pump. *Archives of Microbiology* **152**: 584-588.

Wikström, M., and Hummer, G. (2012) Stoichiometry of proton translocation by respiratory complex I and its mechanistic implications. *Proceedings of the National Academy of Sciences of the United States of America* **109**: 4431-4436.

Wilkinson, A.J., Fersht, A.R., Blow, D.M., Carter, P., and Winter, G. (1984) A large increase in enzyme–substrate affinity by protein engineering. *Nature* **307**: 187-188.

Wilkinson, K.D., and Williams, C.H. (1981) NADH inhibition and NAD activation of *Escherichia coli* lipoamide dehydrogenase catalyzing the NADH-lipoamide reaction. *Journal of Biological Chemistry* **256**: 2307-2314.

Willrodt, C., Hoschek, A., Bühler, B., Schmid, A., and Julsing, M.K. (2016) Decoupling production from growth by magnesium sulfate limitation boosts *de novo* limonene production. *Biotechnology and Bioengineering* **113**: 1305-1314.

Wissenbach, U., Kröger, A., and Unden, G. (1990) The specific functions of menaquinone and demethylmenaquinone in anaerobic respiration with fumarate, dimethylsulfoxide, trimethylamine N-oxide and nitrate by *Escherichia coli*. *Archives of Microbiology* **154**: 60-66.

Woehlke, G., and Dimroth, P. (1994) Anaerobic growth of *Salmonella typhimurium* on L(+)- and D(−)-tartrate involves an oxaloacetate decarboxylase Na^+ pump. *Archives of Microbiology* **162**: 233-237.

Woehlke, G., Wifling, K., and Dimroth, P. (1992) Sequence of the sodium ion pump oxaloacetate decarboxylase from *Salmonella typhimurium*. *Journal of Biological Chemistry* **267**: 22798-22803.

Wu, J.T., Wu, L.H., and Knight, J.A. (1986) Stability of NADPH: effect of various factors on the kinetics of degradation. *Clinical Chemistry* **32**: 314-319.

Wu, W.Y., Lebbink, J.H.G., Kanaar, R., Geijsen, N., and van der Oost, J. (2018) Genome editing by natural and engineered CRISPR-associated nucleases. *Nature Chemical Biology* **14**: 642-651.

Yang, B., Liang, S., Liu, H., Liu, J., Cui, Z., and Wen, J. (2018) Metabolic engineering of *Escherichia coli* for 1,3-propanediol biosynthesis from glycerol. *Bioresource Technology* **267**: 599-607.

Yang, P., Liu, W., Cheng, X., Wang, J., Wang, Q., and Qi, Q. (2016) A new strategy for production of 5-aminolevulinic acid in recombinant *Corynebacterium glutamicum* with high yield. *Applied and Environmental Microbiology* **82**: 2709-2717.

Yang, T.H., Kim, T.W., Kang, H.O., Lee, S.-H., Lee, E.J., Lim, S.-C., et al. (2010) Biosynthesis of polylactic acid and its copolymers using evolved propionate CoA transferase and PHA synthase. *Biotechnology and Bioengineering.* **105**: 150-160.

Yang, Y.-T., Bennett, G.N., and San, K.-Y. (1998) Genetic and metabolic engineering. *Electronic Journal of Biotechnology* **1**: 20-21.

Yim, H., Haselbeck, R., Niu, W., Pujol-Baxley, C., Burgard, A., Boldt, J., et al. (2011) Metabolic engineering of *Escherichia coli* for direct production of 1,4-butanediol. *Nature Chemical Biology* **7**: 445-452.

Young, E., Poucher, A., Comer, A., Bailey, A., and Alper, H. (2011) Functional survey for heterologous sugar transport proteins, using *Saccharomyces cerevisiae* as a host. *Applied and Environmental Microbiology* **77**: 3311-3319.

Yu, L., Zhao, J., Xu, M., Dong, J., Varghese, S., Yu, M., et al. (2015) Metabolic engineering of *Clostridium tyrobutyricum* for n-butanol production: effects of CoA transferase. *Applied Microbiology and Biotechnology* **99**: 4917-4930.

Yuan, L., Kurek, I., English, J., and Keenan, R. (2005) Laboratory-directed protein evolution. *Microbiology and Molecular Biology Reviews* **69**: 373-392.

Yuan, S.-F., and Alper, H.S. (2019) Metabolic engineering of microbial cell factories for production of nutraceuticals. *Microbial Cell Factories* **18**: 46.

Zachos, I., Nowak, C., and Sieber, V. (2019) Biomimetic cofactors and methods for their recycling. *Current Opinion in Chemical Biology* **49**: 59-66.

Zaslavskaia, L.A., Lippmeier, J.C., Shih, C., Ehrhardt, D., Grossman, A.R., and Apt, K.E. (2001) Trophic conversion of an obligate photoautotrophic organism through metabolic engineering. *Science* **292**: 2073-2075.

Zhang, K., Sawaya, M.R., Eisenberg, D.S., and Liao, J.C. (2008) Expanding metabolism for biosynthesis of nonnatural alcohols. *Proceedings of the National Academy of Sciences* **105**: 20653-20658.

Zhao, H., Wang, P., Huang, E., Ge, Y., and Zhu, G. (2008) Physiologic roles of soluble pyridine nucleotide transhydrogenase in *Escherichia coli* as determined by homologous recombination. *Annals of Microbiology* **58**: 275.

Zhao, J., Li, Q., Sun, T., Zhu, X., Xu, H., Tang, J., et al. (2013a) Engineering central metabolic modules of *Escherichia coli* for improving β-carotene production. *Metabolic Engineering* **17**: 42-50.

Zhao, J., Xu, L., Wang, Y., Zhao, X., Wang, J., Garza, E., et al. (2013b) Homofermentative production of optically pure L-lactic acid from xylose by genetically engineered *Escherichia coli* B. *Microbial Cell Factories* **12**: 57.

Acknowledgments

After more than 7 years, a lot of struggles, efforts and commitment, this thesis is finally completed. I believe that this journey could not have been possible without the support of many people.

Johan, **Harry**, **Ruud** and **Gerrit** thank you for giving me the opportunity to start my PhD thesis.

Ruud, there are not enough words to thank you for your unconditional support over the years. I still remember when I arrived in Wageningen and struggled for a long time to pronounce your name properly. For me, you were “Rude” Weusthuis. Our project had a tumultuous beginning and when the consortium dissolved, we decided to go for a more exciting project that could be generally applied in microbial fermentations. However, trying to achieve this new goal came with its challenges, and lots of them! Your support, motivation and kick in the butt from time to time allowed me to tackle these challenges and become a better scientist and person. When I faced hard times, you were always available for discussions. More than once, you proved that you genuinely care about your students and that makes you a great supervisor. Over the years, we created a great bond and I truly enjoyed working together with you. I will miss our discussions about science and life in general. I will always remember that I have to be careful as I am too direct even for Dutch people! I hope that our paths will cross again in the future.

Gerrit, I would like to thank you for all the nice discussions about my PhD. You were always supportive and gave very good suggestions. You always had useful insights and reminded me of the industrial perspectives of the project, something we tend to forget when working in the lab mainly focusing on our experiments. Through our discussions, you challenged me and reminded me the importance of always having the big picture in mind. The project came with its challenges and during our meetings you also made me realized that I already achieved a lot. I thank you for that. It was a great pleasure to be able to work with you.

Mark B., we met during my MSc thesis at IMB. We met once again when you arrived as assistant professor at BPE last year. We managed to write a nice

piece together and your input was really valuable. You had great insights on how to improve the review. I wish I would have stayed longer to work with you. All the best in your tenure track!

The completion of this thesis also relies on the hard work of the students I supervised over the years. **André**, **Adil**, **Anna**, **Lorena**, **Coen**, **Vivienne**, **Sten** and **Nanouk** I would like to thank you all for your hard work. Your projects came with their fair share of challenges, but you stayed motivated and showed resilience. I am very proud of you and I really enjoyed our time together. I am happy to have seen you develop on both a personal and professional level. I wish you great success in life and future careers.

I also would like to thank my colleagues at BPE without for their support over the years. **Miranda**, **Marina**, **Snezana**, **Wendy**, **Fred**, **Sebastiaan** and **Rick**, I would like to thank you for your help regarding administration, ordering and technical support over the years. **Snezana**, I am really happy that you joined BPE. As many say, you are the “mama” of BPE. Always available and always positive. I could always count on your support both professionally and personally. I will always remember our coffee breaks and your amazing cooking and baking skills!

I would like to thank the staff members of BPE: **René**, **Marian**, **Hans**, **Dirk**, **Antoinette**, **Maria**, **Corjan**, **Mark S.**, **Packo**, **Mathieu**, **Douwe**, **Rafa**, **Iago**, **Iulian**, **Marta**, **Michel**, **Arjen**, **Giuseppe**, **Marcel**, **Sarah** and **Iris**. I really enjoyed our times together during Christmas dinners, borrels and labuitjes. Although you were not directly involved in my project, I had nice discussions and suggestions from some of you. Thank you for the nice times.

My PhD life would not have been the same without my office mates: **Kiira**, **Tim**, **Xiao**, **Richard**, **Enrico**, **Stephanie**, **Anna** and **August**. I have to say that throughout the years, no matter who was in the office, I had a great time! In one way of another, I would say that all of you have a “crazy” part which helped me in relieving the everyday pressure of the PhD. It also resulted in so many laughs! I also cherish the work discussions we had and the suggestions. **Kiira**, **Tim** and

Xiao we moved together in Radix and took a commemorative picture of us. That was the beginning of a great time with you guys! **Kiira**, you are one of the best encounters of my PhD life. As soon as we became office mates, we also became friends. You are at the antipode of a “traditional Finnish” person and one of the craziest person I know. Without you, my PhD would have been very boring! I will still remember you making me do some weird yoga posture in the office… **Enrico**, you were my office mate and friend. You are one of the most chaotic persons I know and looking at your bench and desk drove me crazy. When I joined your project as research assistant, I was afraid I would go nuts, but I really enjoyed the time we worked together. It was very fun and interesting working on *Rhodobacter* with you. I really liked our conversations about work as well as your weird routine after lunch and other topics. Thanks to you, I have a whole new sets of expressions embedded in my brain and some that are ruined for life. You are always the life of the party, do not change one bit! The last part of my general discussion is a nod to you: a tribute to *chassis* and orthogonality! I hope you enjoy it. **Anna**, you were one of my first students and now you are almost done with your PhD. I am so happy that you decided to move to the “fun” office. You definitely made the workdays seem shorter and better. I especially love your “sunshine moments” in the lab. We could always count on each other in the lab, discussing experiments but also for emotional support. More than office mate, you became my friend, gym and drinking buddy! You also brought many of us to your parents’ place to discover Germany. These weekends were awesome, filled with laughs, snoring and alcohol. Thank you for all the good times and all the best in finishing your thesis! **August**, you were always the quiet one of the bunch but definitely not the last for fun. You are one of the hardest working persons I know at BPE. You were always trying to work while we were making jokes. I think we corrupted you… It was a great pleasure to have you in the office!

During my extended time at BPE, other colleagues and friends were very important for me and helped me to keep a healthy work-life balance. I would like to thank the “old” BPE Beers and Dinners crew **Youri**, **Iago**, **Catalina**, **Jeroen**,

Aziz, **Giulia**, **Rafa**, **Agi**, **Josue**, **Joao**, **Luci**, **Christina**, **Maria V**., **Ward**, **Guido**, **Edgar** and **Alex** for the numerous dinners, barbecues (even during raining days in November) and activities like paintball. **Youri**, we first met at BCH (now BCT) and moved together at BPE with Kiira. At first, I thought you were a scary guy but in fact you are a very sweet person. We had great times together like organizing the pink "BPE got talent" Christmas dinner where you dressed as a pig. I enjoyed working with you in the lab and I would like to thank for your support when I was feeling down during my PhD. **Alex, Jeroen**, **Catalina**, **Elisa** and **Kiira** we travelled together to different places: Canarias Islands, Slovenia, France and Ibiza. These trips were filled with fun, food and wine in other words simply good times! **Iago**, thank for the many cheerful, colorful and crazy conversations over the years. Our coffee breaks together with Snezana were essential for finishing this thesis and should therefore not be underestimated.

I also would like to thank the "new" BPE Dinners and Beers crew and colleagues **Calvin**, **Kylie**, **Jort**, **Guangyuan**, **Fabian**, **Narcis**, **Pieter**, **August**, **Chunzhe**, **Enrico**, **Anna**, **Barbara**, **Robin**, **Ana**, **Christian**, **Sebastian**, **Renske**, **Narcis**, **Fabian**, **Anna**, **Christian**, **Rafa Ca.**, **Stephanie** for the fun times and Friday evening drinks. **Narcis**, or should I say Narciiiiis, we had many dinners, brunches and game of photosynthesis. We had great times together. I also enjoyed hearing you talking about Cathars and Catalunya. I wish you all the best and good luck in finishing your PhD. **Ana**, you did not stay as long as other people in the department, but it was a pleasure to work with you. I really enjoyed biking with you in the national park trying to find the "purple flowers" that Narcis was so passionate about! It is sad that you left BPE, but I am very happy that you are now doing your PhD in Madrid. All the best for this adventure and hopefully we can meet again! **Fabian**, together with Enrico you were the life of the party. Always keeping your house "Casa del Popolo" open for friends. Thanks to you and your cocktails I had many hard Saturday mornings! **Jort**, you started as Aziz student and now you are doing your PhD at BPE. It is always fun to have you around joking. You always bring the fun touch at the department. **Chunzhe**, **August** and **Guangyuan** thanks a lot for the dumpling, barbecue and

movie nights. I never thought that one day we would fold more than 100 hundred dumplings for a simple dinner. Thanks to you I know now how to fold properly dumpling although you kept the secret on the filling recipe. **Chunzhe**, you kicked me out of my office and stole my desk on your first day as a PhD. You were shy at first, but it was all a cover. You always have a positive attitude and you always have a word to make people smile and laugh. I wish I would stay longer to work with you. Now, it is your duty to drive Ruud crazy since Kiira, Youri, Alex, Enrico and I are now gone, but I think you are on good tracks. Good luck in finishing your PhD. I would also like to thank **Lenneke**, **Anne**, **Lenny**, **Kim**, **Gerard**, **Ilse**, **Mitsue**, **Jorijn**, **Lukas**, **Malgorzata**, **Rocca**, **Sabine** and **Pedro** for the nice times at BPE.

I also want to thank some people from MIB. **Nico**, **Elleke** and **Jeroen**, it was great fun organizing the joint discussions between MIB and BPE. I think that these meetings allowed us to create stronger bonds between our two groups and helped in developing new genetic engineering methods at BPE. **Costas**, **Christos** and **Eric** we mostly met during the Microbial Biotechnology and Animal Cell Culture theme meetings. It was very nice to interact with you guys and learn about your projects. I wish you all the best in finishing your PhD.

Anna, **Stephanie** and **Kylie**, I would like to thank you for the girl nights we had. A lot of booze and nice conversations to balance our crazy work life. Those nights were truly necessary to disconnect and just enjoy so thank you!

Many thanks to my housemates **Valentina**, **Gloria**, **Olga**, **Patricia**, **Tom**, **Joao**, **Neus** and **Kelly** who provides a warm and cheerful home. When I arrived in Wageningen, I was alone and did not know anyone. The dinners, excursions and activities we had together made me feel like I was home from day 1. **Vale**, you are definitely my crazy person in the house! We went through so many things during our time together: fun moments, breakups, PhD challenges and a lot of wine and Aperol Spritz! Definitely, I could have not done this PhD without you. You are a radiant person, full of energy. Everyone that meet you cannot not love you! Proof of it is that you accompanied me to all BPE Christmas

dinners as my +1 and my colleagues were very fond of you. I know that Camilo "stole me from you" but you will always have a special place in my heart.

Of course, I could not have completed this journey without the support of my friends and family. **Alexia**, ma Bichette, we met 7 years ago in the toilet during the PhD week. What a long journey we have been on since then! I cannot imagine not having you in my life. I love the straightforward talks, our Franglais conversations and the good times we had around food and drinks! I am so happy that you are my paranymph and will seat next to me on this very special day. Love you Bichette! **Jan**, thank you for making ma Bichette happy and for all the fun we have when we are together. **Thibaut**, thank you for all the great dinners and barbecues over the years. You are one of the most chilled person I know, and it is always a pleasure to spend time with you. **Juliette**, ma Brenda, I have known you since the first year of university. No matter where we are and for how long we do not see each other, when we meet it is always like if we saw each other yesterday. I believe that I could not be here today finishing my PhD without your support over the years during university. I am looking forward to the day we meet again! **Jolanda** and **Robert**, we met during my MSc thesis in Delft at IMB. You definitely contributed to my love for the Netherlands and therefore me doing my PhD at Wageningen University & Research. Thank you for visiting me in Wageningen during my PhD, it was great to have you here with me and I enjoyed the good times we had together. **Jolanda**, I still remember when you were wondering where the hell is Wageningen and now, you are doing your PhD here. All the best to the both of you! Hopefully we will see each other again very soon.

Merci à toute ma famille et plus particulièrement **Corrine**, **Philippe**, **Audrey**, **Mathieu**, **Claudy**, **Evelyne**, **Maryse**, **Sandra** et **Anaïs** pour leur soutien durant ma thèse.

Lydie, **Fabrice**, **Anna-Rose** et **Joaquim**, vous m'avez soutenu au fil des années. A chaque visite en France, vous m'avez accueillie à bras ouverts avec de bons petits plats et de super conversations. **Lydie**, on s'est rencontrées

quand je venais tout juste de fêter mes 11 ans lors de ton stage en entreprise avec mon père. Depuis ce temps, tu es devenue une partie intégrante de la famille et je te considère comme la sœur que je n'ai jamais eue. Je veux aussi vous remercier pour avoir pris soin de mes parents durant ma thèse. Savoir que vous êtes là pour eux et qu'ils sont si bien entourés alors que je suis si loin a enlevé un poids de mes épaules. Cela m'a permis de me focaliser sur les challenges auxquels j'ai fait face pendant ma thèse. Merci pour tout !

Maman et **Papa**, il n'y a pas de mots assez forts pour vous remercier de votre soutien au fil des années. Vous avez toujours cru en moi et m'avez poussé à travailler dur. Vous m'avez encouragé à croire en moi et à découvrir le monde. C'est grâce à vous que j'en suis là et que je défends finalement ma thèse. Vous avez toujours fait de moi votre priorité absolue et je vous en serais éternellement reconnaissante. Je vous aime et je vous remercie d'avoir fait de moi la personne que je suis aujourd'hui.

Camilo, chaton, you are definitely the best discovery I made during my PhD. You have always been there for me, first as friend and now as partner. Doing a PhD can be very stressful with a lot of up and down moments. I do not think I would have made it without you. You always supported me and encouraged me to do better. I am so happy to have you in my life, I love you.

About the author

About the author

Pauline Ludivine Folch was born on January 11th, 1991 in Montauban (France). After obtaining her baccalaureate in Sciences and Techniques of Laboratory at Lycée Bourdelle in Montauban, she moved to La Rochelle to start a two-year diploma at the University Institute of Technology. She specialized in Food and Biological Industries and graduated in 2010.

In September 2010, she started her BSc in Biotechnology and Management in Food Industries at the University of La Rochelle. She performed her BSc thesis at the University of La Rochelle where she investigated how to inhibit biofilm formation of *Staphylococcus aureus* on various abiotic surfaces using lactic acid bacteria. Then, she continued with her MSc studies in Biotechnology and Management in Food Industries at La Rochelle University. In January 2013, she joined the Industrial Microbiology group (IMB) at TU Delft for her MSc thesis. There, she worked on characterizing the physiology and robustness of *Saccharomyces cerevisiae* during different growth phases.

On October 1st, 2013 Pauline started her PhD thesis at BPE under the supervision of prof. Ruud Weusthuis and prof. Gerrit Eggink. During this project, she worked on conserving additional metabolic energy to enhance microbial product formation in *E. coli*.

In April 2019, she started as a PostDoctoral researcher between Wageningen University & Research (BPE) and FrieslandCampina to optimize the microbial production of human milk oligosaccharides.

Pauline is now working as Fermentation Specialist at Corbion in the Sustainable Food Solutions group.

List of publications

Orsi, E., Folch P.L., Monje-López, V.T., Fernhout B.M., Turcato A., Kengen S.W., Eggink G. & Weusthuis R.A. (2019). Characterization of heterotrophic growth and sesquiterpene production by *Rhodobacter sphaeroides* on a defined medium. *Journal of Industrial Microbiology & Biotechnology, 46(*8), 1179-1190. DOI: 10.1007/s10295-019-02201-6.

Weusthuis, R.A., Folch P.L., Pozo-Rodríguez A. & Paul C.E.(2020). Applying non-canonical redox cofactors in fermentation processes. *iScience, 23*(9).

Folch, P.L., Bisschops M.M.M. & Weusthuis R.A. (2021). Metabolic energy conservation for fermentative product formation. *Microbial Biotechnology*

Overview of completed training activities

Discipline-specific activities

Courses

- Bioprocess Design (BDSL), The Netherlands (2014)
- Advanced course Microbial Physiology & Fermentation Technology (BDSL), The Netherlands (2015)
- Metabolic Engineering (VLAG), The Netherlands (2015)

Conferences

- Conference NBC-15, The Netherlands (2014)
- Conference Microbial Biotechnology 1.0, The Netherlands (2014)
- Conference Microbial Biotechnology 2.0, The Netherlands (2015)
- Conference NBC-16 “Next Level Biotechnology”, The Netherlands (2016)
- Microbiology Centennial symposium with poster presentation, The Netherlands (2017)
- Microbial Biotechnology 6.0, The Netherlands (2019)

General courses

- VLAG PhD week (VLAG), The Netherlands (2014)
- Project and Time Management (WGS), The Netherlands (2014)
- Workshop PhD carrousel, The Netherlands (2015 and 2016)
- Scientific Writing (WGS), The Netherlands (2016)
- Career Perspectives (WGS), The Netherlands (2017)

Optionals

- MIB-30806 Applied Molecular Microbiology, The Netherlands (2013)
- Writing Project Proposal, The Netherlands (2014)
- MIMOSA meetings, The Netherlands (2013-2015)
- BPE group meetings, The Netherlands (2013-2017)
- Metabolic Engineering Tools meetings, The Netherlands (2014-2017)
- Industrial Biotechnology theme meetings, The Netherlands (2016-2017)

The research described in this thesis was financially supported partly by Agentschap NL, Top Knowledge Institute Biobased Economy (TKIBE) and the Bioprocess Engineering group (Wageningen University & Research).

Financial support from Wageningen University for printing this thesis is gratefully acknowledged.

Cover design by Pauline Folch

Printed by Digiforce || ProefschriftMaken
302